Neurons and Astrocytes Respond Differentially to Ketogenic Diet and Ketone Body Exposure: Implications for the Treatment of Alzheimer's Disease.

By
© 2020
Scott Joshua Koppel
B.Sc., University of California - Irvine, 2011

Submitted to the graduate degree program in Neuroscience and the Graduate Faculty of the University of Kansas in partial fulfillment of the requirements for the degree of Doctor of Philosophy.

_____
Committee Chair: Russell Swerdlow, MD

_____
Doug Wright, PhD

_____
Tim Fields, MD, PhD

_____
Chad Slawson, PhD

_____
John Thyfault, PhD

Date Defended: 11 May 2020

The dissertation committee for Scott Koppel certifies that this is the approved version of the following dissertation:

Neurons and Astrocytes Respond Differentially to Ketogenic Diet and Ketone Body Exposure: Implications for the Treatment of Alzheimer's Disease.

_____

Chair: Russell Swerdlow, MD

_____

Graduate Director: Doug Wright, PhD

Date Approved: 28 May 2020

Abstract

Glucose hypometabolism and mitochondrial dysfunction are early deficits in Alzheimer's disease (AD) brains that precede cognitive decline. Rescuing bioenergetic failure by providing an alternative fuel substrate is an attractive therapeutic strategy that may be beneficial in treating neurodegenerative disease. The ketogenic diet (KD) has been suggested as a treatment for AD. The KD is theorized to support the brain through the generation of ketone bodies that serve as an alternative fuel to glucose and possibly through other unknown mechanisms. KD and related neuroketotherapeutics have been shown to demonstrate molecular signaling effects including activating histone acetylation, increased BDNF signaling, reducing reactive oxygen species formation, and inhibiting the NLRP3 inflammasome. Historically many studies examine CNS function as though it is a homogenous bioenergetic compartment and under value how different CNS cell populations may respond to metabolic interventions or contribute to disease.

In these collected works, we investigate the bioenergetic and molecular response of two primary CNS cell types, neurons and astrocytes, to ketogenic diet and ketone salt interventions both *in vivo* and *in vitro*. While neuronal response recapitulates many previously described effects *in vitro* by increasing mitochondrial respiration and histone acetylation, astrocytes exhibit no response to ketone body availability in these domains. Interestingly, neuronal response also was found to include reduced signaling through pro-growth PI3K-Akt-mTORC1 pathways indicating that ketone bodies concurrently support energy production while signaling nutrient scarcity and inducing cellular quiescence. We further expanded on these findings by performing cell type enrichment for neurons and astrocytes via magnetic assisted cell sorting and transcriptomic profiling of these cell populations following 90-day ketogenic diet intervention in 16-week-old C57BL6/N mice. RNAseq and KEGG pathway analysis revealed that neuronal

transcription was generally increased in response to ketogenic diet while astrocytic transcription was largely suppressed as compared to animals maintained on standard chow diet. Findings of KEGG pathway analysis indicated that the three most implicated pathways affected by KD in neurons by significance were Alzheimer's disease, Parkinson's disease, and Huntington's disease indicating KD may have important disease modifying properties regarding these neurodegenerative diseases. Finally, we sought to develop a new model to study the effects of persistent stable ketosis on brain health through the development of a new mouse model, the conditionally expressing malonyl-CoA insensitive carnitine-palmitoyl transferase 1A transgenic mouse. Early studies indicate that the CPT1A^{M593S} mouse exhibits increased hepatic ketone body levels when crossed to Albumin-Cre strains, but increased ketosis is not observed in the blood. Acetyl-CoA generated from increased fatty acid β-oxidation may be increasingly exported as citrate in these animals.

Taken together, these works have characterized that the bioenergetic and molecular responses of the CNS to ketone interventions may have important therapeutic effects for the treatment of brain aging and neurodegenerative disease, but the specific response is heavily modulated as a function of cell type. Understanding and appreciating the consequences of these effects, which are often antagonistic in nature, are critical for the development of an effective dietary mimetic of the ketogenic diet for the specific targeting of mechanisms of action not only by target, but also by target population.

Acknowledgements

I would like to begin by thanking my mentor, Dr. Russell Swerdlow, for all of the encouragement, guidance, and patience over these past five years. His ability to guide me through the early frustrations and foster my independence as a researcher has helped me to grow not just in my career but in my life. I cannot thank him enough for the endless patience he demonstrated for me, especially when I didn't have patience in myself. Learning from him has unquestionably been the highlight of my young academic career.

Secondly, I'd like to thank my co-mentor Dr. Hao Zhu and the members of my dissertation committee: Drs. Doug Wright, Tim Fields, John Thyfault, and Chad Slawson. Collectively all of you have given me such fantastic feedback on my dissertation projects and always delivered criticisms positively and warmly. Dr. Zhu always greeted me with such positivity and enthusiasm for my work, educated me on so many husbandry skills I didn't previously have, and was always considerate with offering tickets to the symphony or ballets when he had no obligation to. I'd like Dr. Fields for having the faith in me to accept me into the KUMC Physician Scientist Training Program and seeing potential in me even as I'm sure other applicants maybe had more stellar metrics. Your mentoring throughout the many phases of the MD-PhD program and advice regarding my personal life has been extremely valuable to me. Dr. Wright has been such a reliable ally and advocate for graduate students in the KUMC Neuroscience program in addition to his contributions as a committee member and I'll always remember the fun we all had during papers class and program happy hours. I'd like to thank Dr. Slawson for the mentoring he gave me both during my laboratory rotation in his lab and as a member of my committee. I'd also like to thank him for always providing an enjoyable escape from talking science and indulging me in conversations on basketball and pro-wrestling to

maintain my sanity. I'd like to thank Dr. Thyfault for all of his scientific insight and suggestions for my work and for all of his positive enthusiasm regarding updates on our transgenic mice even when I found the data disappointing.

I'd like to thank all of our collaborators in KUMC Core services without which this work would've never been completed. Specifically, I'd like to recognize Dr. Thom Yankee, Rich Hastings, Dr. Devin Koestler, Dong Pei, Clark Bloomer, Rose Skinner, Yafen Niu, Dr. Jay Vivian, Michelle Winter, Mary Kroh, and all other support staff in Laboratory Animal Resources.

I'd like to thank all of the members of the Swerdlow laboratory, especially Drs. Heather Wilkins and Ian Weidling who were along for the entire ride, for being my allies in the trenches and sharing in all of my successes and failures. I'd also like to take the opportunity to apologize for my endless rants and strange texts from things I found on the internet at 3 AM.

I'd like to thank Dr. Tim Fields, Dr. Brenda Rongish, Janice Fletcher, and the students of the KUMC Physician Scientist Training Program for supporting me both institutionally and personally over these past. . . 7 years? Oh god. Well what's a few more? You all understand.

I would like to thank my undergraduate research mentors Dr. Karina Cramer and Dr. Mathew Korn. Dr. Cramer was my first PI and gave me my first opportunity in a biomedical research lab and was the first person to encourage me to pursue a MD-PhD and told me she believed I could do it. Dr. Korn, at the time just Matt, put up with what I can only imagine to be considerable frustration coaching me up as his undergraduate trainee while he completed his own dissertation work and I will always be indebted to him for developing my foundational scientific lab skills.

I would like to thank all of my friends, too many to list here, both in Kansas City and from California for helping preserve my sanity and keep me afloat during difficult times.

I would like to thank Tritia Schostak and the rest of the Schostak family for the good times and years of support that she and they provided.

Finally, and certainly not least, I would like to thank my entire family, but especially my parents, Richard and Debra Koppel, and my sister Erin Koppel. Mom and Dad, you two always provided Erin and I with the best upbringing you were able to and always scrapped and sacrificed to provide anything we wanted (within reason I suppose). I would never have made it anywhere near this far without your encouragement, patience, teachings, and love. I love you both immensely. I couldn't have asked for better parents. Erin, as my older sister I've always looked up to you and am always so proud of your relentless pursuit of justice and desire to see others treated with respect and love. Your art and passion have always been a reminder to me to try and step back and see the beauty in my work and life when I'm getting buried in large p-values, wide error bars, and reviewer critiques. I can't tell you how much I respect you and love you.

The works contained herein were financially supported through KU ADC P30 (AG035982), NIA F30 AG058397-01A1, NICHD T32 HD057850, Paul G. Roofe Memorial Fellowship, Mabel A. Woodyard Memorial Fellowship, KU Endowment, Institute for Neurological Discovery, and the STOP Alzheimer's Now Fund.

Table of Contents

List of Figures

List of Tables

Chapter 1: Introduction

This work was previously published as a review article in Neurochemistry International and reprinted here with permission from the publisher and additional, never-before published text. Original article: Koppel SJ and Swerdlow RH. (2018) Neuroketotherapeutics: A modern review of a century-old therapy. *Neurochem Int*. 117: 114-125. Doi: 10.1016/j.neuint.2017.05.019. PMCID: PMC5711637

Ketogenic therapies include any intervention that intentionally shifts the body into a state of ketone body production. Termed ketogenesis or ketosis, achieving a state of heightened ketone production has been used to treat epilepsy for nearly a century. The efficacy of ketogenic therapies to improve functional outcomes in epilepsy have increased interest in their translational potential to treat other neurologic disorders, including Alzheimer's disease (AD) and stroke rehabilitation.

Ketogenesis can be achieved through multiple strategies including caloric restriction, administering medium chain triglycerides (MCT), strenuous exercise, and ketogenic diets (KD) which primarily feature fats and minimize carbohydrates (Gano, Patel, & Rho, 2014). These generally well-tolerated interventions produce limited adverse effects. Ketotherapeutics still meet a considerable amount of scrutiny based on the association of ketones with the pathologic state of ketoacidosis, a complication of type I diabetes. It is important to recognize that these interventions produce a mild ketonemia, to about 5 mM, whereas ketoacidosis occurs when blood ketones enter a range of 10-25 mM. Ketoacidosis has not been found to manifest within the central nervous system microenvironment (Al-Mudallal, LaManna, Lust, & Harik, 1996).

While ketones can confer neurologic benefits, the mechanisms that underlie these benefits remain elusive. Here, we review the history of ketotherapeutics, potential mechanisms for their effects, and their therapeutic potential.

History of Ketotherapeutics

Ketogenic medicine perhaps dates back to ancient Greece. Most of the earliest writings on epilepsy were collected in *On the Sacred Disease*, part of the Hippocratic collection of works (Temkin, 1994; Wheless, 2008). This text illustrates that due to fears of demonic forces, society ostracized community members that suffered from fits, which today we understand to be

epileptic seizures. Forced to fend for their meals in the wilderness, and being unequipped to accomplish this task, these persons would struggle to obtain adequate caloric intake. Interestingly, after undergoing forced prolonged fasts they experienced reduced seizure frequency and severity.

The Book of Matthew from the New Testament provides a similar account. In one passage, a father requested help from Jesus and his apostles in curing his son of fits. They advised him to pray and have the child fast, which resulted in the child's recovery. The lower register of Raphael's *The Transfiguration* depicts this story. This painting possibly represents the earliest graphical depiction of bioenergetic medicine in the historical record, even if that was not the intended purpose of the work.

Fasting therapies were more formally adopted for the treatment of epilepsy in 1911 by the French physicians Guelpa and Marie (Guelpa, 1911). Similar revivals were spearheaded in the United States by the physician Hugh Conklin and fitness celebrity Bernarr Macfadden (Wheless, 2008). H. Rawle Geyelin, an endocrinologist, was the first to report cognitive improvements occurred in patients adhering to fasting regimens (Geyelin, 1921). In the same year, fasting and low carbohydrate/high fat diets were found to increase levels of the ketone bodies β-hydroxybutyrate and acetoacetate in normal, healthy subjects and were suggested to mediate neurologic benefits in children (Wilder, 1921; Woodyatt, 1921). Later investigations into the efficacy of KDs to treat epilepsy in adults demonstrated seizures were completely controlled or improved in 56 of 100 patients (Barborka, 1928).

The KD remained a popular epilepsy treatment until the 1980's, although its use gradually diminished with the advent of pharmaceutical therapies such as diphenylhydantoin, phenobarbital, and valproic acid. The KD enjoyed a resurgence in popularity following release of

a made-for-TV movie, *First Do No Harm*, in 1997 and national media coverage on a television news program, *Dateline*, in 2000 (Wheless, 2008).

Increased popularity has expanded the number of ketogenic-related therapies. An increasing number of reports note the impact of ketotherapeutics on clinical phenotypes, cell physiology, and molecular physiology.

Molecular and Biochemical Ketone Biology

Ketogenesis

In mammals, ketosis results following prolonged periods of profound, reduced dietary intake. In this state, carbohydrate intake is low which results in decreased serum insulin and increased serum glucagon (Apfelbaum, Lacatis, Reinberg, & Assan, 1972). This hormonal shift promotes hepatic glycogenolysis and gluconeogenesis to maintain euglycemia (Garber, Menzel, Boden, & Owen, 1974; Rui, 2014). A decline in insulin also promotes increased white adipose tissue lipolysis, which increases fatty acid circulation and β-oxidation (Vazquez-Vela, Torres, & Tovar, 2008).

Avid fatty acid β-oxidation occurs in liver mitochondria, where it generates increased levels of acetyl-CoA as shown in **Figure 1-1** (Drysdale & Lardy, 1953; Randle, Garland, Hales, & Newsholme, 1963). Once the added acetyl-CoA surpasses the ability of the tricarboxylic acid (TCA) cycle to degrade it, it diverts to other needs such as cholesterol synthesis or ketogenesis (Baird, Heitzman, & Hibbitt, 1972; Garber et al., 1974). With ketogenesis, two molecules of acetyl-CoA are joined by thiolase to generate acetoacetyl-CoA (Middleton, 1972). A third molecule of acetyl-CoA is then added to produce β-hydroxy-β-methylglutaryl-CoA (HMG-CoA) in a reaction mediated by HMG-CoA synthase (Hegardt, 1999). This HMG-CoA synthase-catalyzed reaction represents the rate-limiting step of the ketogenesis pathway. HMG-CoA lyase

then liberates a two-carbon group to produce one molecule each of acetyl-CoA and acetoacetate. Acetoacetate, therefore, represents, the first ketone body produced in the pathway (Puisac et al., 2012). Acetoacetate is further reduced by a molecule of NADH in a reaction mediated by β-hydroxybutyrate dehydrogenase 1 (BHD1) (Lehninger, Sudduth, & Wise, 1960). This step produces the most abundant ketone found in circulation, β-hydroxybutyrate **Figure 1-2**.

Deficiencies in HMG-CoA lyase prevent ketogenesis and HMG-CoA lyase deficiency produces the pathologic state of hypoketotic hypoglycemia following periods of fasting. Interestingly, this condition also commonly associates with seizures (Fernandes et al., 2013; Fernandes et al., 2015).

Of minor note, a small portion of acetoacetate undergoes non-enzymatic decarboxylation to form acetone (Kalapos, 2003). Acetone, while toxic in large concentrations, undergoes liver conversion via the methylglyoxal pathway. As acetone is highly volatile, when acetone production rates exceed conversion rates it is readily excreted by the pulmonary system. As a result, it does not reach appreciable levels under states of fasting or nutritional ketosis.

The net reaction is the synthesis of the two primary ketone bodies, β-hydroxybutyrate and acetoacetate, from two molecules of acetyl-CoA and the oxidation of one molecule of nicotinamide adenine dinucleotide (NADH). While the liver is certainly the primary organ for total body ketogenesis, though, other sites also produce ketone bodies. Increasing evidence reveals astrocytes perform ketogenesis when treated with medium chain triglycerides *in vitro*, which could play a role in regulating food intake (Le Foll, Dunn-Meynell, & Levin, 2015; Le Foll, Dunn-Meynell, Miziorko, & Levin, 2014, 2015; Le Foll & Levin, 2016). Ketones produced by astrocytes in response to increased dietary fat mediate this feedback by acting on

ventromedial hypothalamic (VMH) neurons (Le Foll et al., 2014) that monitor nutrient status, including levels of glucose, lactate, and fatty acids.

Guzman and Blazquez proposed astrocyte-generated ketone bodies transfer to neurons (Guzman & Blazquez, 2001). Astrocytes are already known to perform a similar function, called the astrocyte-neuron lactate shuttle (ANLS), in which glucose is processed to lactate that then undergoes neuron consumption (Dienel, 2013). The possibility of an astrocyte-neuron ketone shuttle is certainly intriguing and underscores the need to investigate how metabolites influence distinct cell populations in the brain.

Ketolysis and bioenergetics

Once produced by the liver, monocarboxylic acid transporters mediate the export of ketone bodies to the blood. This renders them available for extrahepatic catabolism and energy production (Hugo et al., 2012). The brain, heart, and muscle utilize ketone bodies (Fukao et al., 1997). Upon crossing the blood brain barrier, ketones are transported across cell plasma membranes via MCTs 1 and 2 in astrocytes and neurons, respectively (Vijay & Morris, 2014). Ketones are subsequently trafficked through the cytoplasm to the mitochondria, which serves as the primary site of ketone catabolism. Ketone catabolism largely features the reverse reactions that occur in ketogenesis, although specific parts of these opposing cycles are unique (Fukao et al., 1997).

The first step of ketone body catabolism is the oxidation of β-hydroxybutyrate to acetoacetate, with the concurrent reduction of NAD^+ to produce NADH **(Figure 1-1)**. BDH1 mediates this reaction. Acetoacetate is then converted to acetoacetyl-CoA by succinyl-CoA:3-ketoacid transferase (SCOT), also known as 3-oxoacid CoA-transferase 1 (OXCT1). As the name of this enzyme suggests, a CoA group is requisitioned from succinyl-CoA, thereby

generating a molecule of succinate. The liver, which lacks SCOT, cannot consume ketones and this ensures its role as an exclusive ketone body producer. Lastly, acetoacetyl-CoA undergoes processing to two molecules of acetyl-CoA, which can then enter the tricarboxylic acid (TCA) cycle.

Ketones, upon contributing carbon to the TCA cycle, influence cell physiology in a number of ways. Forward progression through the TCA cycle generates the high-energy electron carriers NADH and flavin adenine dinucleotide ($FADH_2$), which serve as substrates for the electron transport chain (ETC) and are necessary for the production of ATP from ADP in oxidative phosphorylation. This allows for a greater degree of nervous system bioenergetic plasticity, as it reduces glucose dependence and shifts the cell towards aerobic respiration. Indeed, ketone bodies have been shown to reduce glycolysis flux (LaManna et al., 2009). This likely occurs as part of a glycolysis negative feedback effect that arises due to increased NADH production.

Additionally, by supplying carbon to the TCA cycle ketone bodies increase TCA cycle anaplerosis (Owen, Kalhan, & Hanson, 2002). This in turn affects neurotransmitter levels as several TCA cycle intermediates serve as substrates for neurotransmitter synthesis. For example, α-ketoglutarate can exit the TCA cycle and undergo conversion to the major excitatory neurotransmitter, glutamate, or undergo decarboxylation to form an inhibitory neurotransmitter, γ-amino butyric acid (GABA). Acetyl-CoA itself combines with choline in the mitochondrial matrix to synthesize acetylcholine. Introducing ketone bodies to the nervous system not only effects bioenergetics, but also neurotransmitter levels.

Ketone bodies and mitochondrial function

How ketones influence mitochondrial efficiency is worth considering. In one study, supplementing the diet of C57BL/6J mice with a β-hydroxybutyrate-(R)-1,3-butanediol monoester ketone ester (KE) for 1 month was sufficient to induce ketonemia. The mice demonstrated increased expression of electron transport chain proteins, uncoupling protein (UCP) 1, and mitochondrial biogenesis signaling pathways in brown adipose tissue (Srivastava et al., 2012). Increased UCP expression in turn has multiple effects on mitochondrial physiology. First, in brown fat it increases heat production by shifting electron transfer energy away from ATP production. Second, increasing proton leak into the matrix can attenuate the generation of reactive oxygen nitrogen species (RONS) by helping to avoid matrix hyperpolarization. Data suggests that even a modest increase in proton leak can reduce hydrogen peroxide (H_2O_2) generation by as much as 70% (Echtay, 2007; Hansford, Hogue, & Mildaziene, 1997; Votyakova & Reynolds, 2001).

A similar study examined the effects of a KE on the expression of brain UCPs 4 and 5 in Wistar rats. Brains of KE-supplemented rats exhibited a 1.5-fold increase in UCPs 4 and 5 (Kashiwaya et al., 2010). Further, caloric restriction increased UCP 4 expression in rat brain cells with neurons and astrocytes exhibiting the greatest and least expression of UCP4 respectively (D. Liu et al., 2006; Sullivan et al., 2004). Similarly, the KD upregulated expression of UCPs 2 and 4 in C3HeB/FeJ mouse brain with the greatest effect observed upon the dentate gyrus of the hippocampus (Sullivan et al., 2004). Upregulation of UCP 4 and 5 *in vitro* were also shown to protect against the complex I inhibitor 1-methyl-4-phenylpyridinium (MPP^+), and the complex II inhibitor 3-nitroproprionic acid (3-NP) (Chu et al., 2009; Ho et al., 2006; Kwok et al., 2010; Ramsden et al., 2012; Wei, Chigurupati, Bagsiyao, Henriquez, & Chan, 2009). It appears that

UCP-mediated neuroprotection requires signaling through the NF-κB pathway, and increased ATP production through increased complex II flux (J. W. Ho et al., 2012; P. W. Ho et al., 2012).

Ketotherapeutic-induced RONS attenuation extends beyond the upregulation of UCPs. Maintaining rats on a KD for 3 weeks increased levels of glutathione (GSH), a free radical scavenger. This increase was associated with an increase in glutamate cysteine ligase (GCL), the rate-limiting enzyme in GSH synthesis (Jarrett, Milder, Liang, & Patel, 2008). It appears that KD-related increases in oxidative stress infrastructures are activated by initial increases in RONS, which induce oxidative stress response pathways through activation of its master regulator, nuclear factor erythroid 2-related factor (Nrf2) (Milder, Liang, & Patel, 2010).

In rats, a KD increases brain expression of genes that accommodate oxidative phosphorylation and the TCA cycle including subunits of ATP synthase, cytochrome oxidase, cytochrome c, NADH dehydrogenase, succinate dehydrogenase, isocitrate dehydrogenase, and malate dehydrogenase. This was associated with an electron microscopy-demonstrated increase in the number of hippocampal dentate gyrus mitochondria (Bough et al., 2006). It was unclear from this study, though, whether increased mitochondrial mass was due to enhanced mitochondrial biogenesis, reduced mitophagy, or a combination of both.

Ketone bodies and post-translational modification of protein

Increasing evidence suggests ketone bodies influence cell physiology independently, or at least indirectly, of their bioenergetic effects. Specifically, metabolites produced during ketone catabolism influence intracellular signaling by inducing changes in protein post-translational modifications (PTMs) (Newman & Verdin, 2014a, 2014b).

This phenomenon was initially considered after it was recognized that butyrate, a short chain fatty acid whose structure differs from a ketone body only by the absence of a beta carbon

hydroxyl group, affects histone acetylation (Stilling et al., 2016). In HEK293 cells and rodent kidney, increasing β-hydroxybutyrate levels inhibits histone deacetylases (HDACs) 1, 3, and 4 and consequently increases acetylation of key histone residues. This acetylation enhances FOXO3A-mediated gene transcription. A subset of the effected genes includes those responsible for mitigating oxidative stress such as manganese superoxide dismutase (MnSOD) and catalase (Shimazu et al., 2013). Similarly, *in vitro* exposure to β-hydroxybutyrate promotes activity of the EP300 family of lysine acetyltransferases (KATs) (Marosi et al., 2016). Since ketones appear to modulate a number of enzymes that control the cycling of protein acetylation in the cytoplasm and nucleus, it is likely that ketones alter other compartments in a similar manner. Ketones could influence activity of Sirtuin 3, the major mitochondrial deacetylase, especially considering their recognized trafficking into the mitochondrial matrix (Rardin et al., 2013).

Another exciting recent development in the area of ketone body-PTM relationships is the discovery that β-hydroxybutyrate itself can modify lysine residues (Xie et al., 2016). β-hydroxybutyrylation of lysine has been demonstrated to occur on histones and produce changes in gene expression that are similar to those of histone acetylation. It may also be possible that TCA intermediates generated through anaplerosis from ketogenic metabolites could serve as substrates for epigenetic modification. Changes in protein succinylation status mediated by α-ketoglutarate dehydrogenase or other succinylation enzymes under ketotic conditions may be worth investigating (G. E. Gibson et al., 2015).

Ketone bodies as extracellular signaling ligands

In addition to its ability to influence intracellular signaling, β-hydroxybutyrate may also function as an extracellular receptor ligand. It has been demonstrated to have agonistic effects on hydrocarboxylic acid receptor 2 (HCA2), otherwise known as the niacin receptor or G-Coupled

Protein Receptor (GPR) 109A (Rahman et al., 2014). β-hydroxybutyrate is able to activate HCA2 with an EC_{50} near 700 μM, well below the approximately 5 mM concentrations observed in nutritional ketosis. HCA2 expression primarily occurs on the surface of cells derived from monocytes, including macrophages and microglia. Functioning as an inhibitory GPR, HCA2 activation suppresses cAMP levels, which ultimately reduces the production of pro-inflammatory cytokines. This suggests ketogenic therapies can produce a beneficial anti-inflammatory effect, a prediction that has been experimentally verified (Selfridge et al., 2015). Other authors provide a more comprehensive review of the effects of HCA2 activation (Offermanns & Schwaninger, 2015).

Outside of the CNS, β-hydroxybutyrate has ligand effects on GPR41, also known as free fatty acid receptor 3 (FFA3). GPR41 is a Gi/o receptor previously shown to respond to the short chain fatty acid butyrate (Stilling et al., 2016; Won, Lu, Puhl, & Ikeda, 2013). Its expression is primarily restricted to sympathetic chain ganglia. Upon exposure to β-hydroxybutyrate, GPR41 suppresses the activity of the sympathetic nervous system through the Gβγ-PLCβ-MAPK signaling pathway (Kimura et al., 2011). Through this mechanism, ketones are able to modulate body energy expenditure and metabolic homeostasis.

Ketone bodies and activation of signaling pathways

Exogenous administration of ketones and ketones produced through vigorous exercise increase the expression of brain derived neurotrophic factor (BDNF) (Marosi et al., 2016; Sleiman et al., 2016; Swerdlow, 2014b). BDNF acts as a ligand for TrkB family nerve growth factor (NGF) receptors and exhibits weak agonistic effects on the p75 receptor. Upon binding TrkB, BDNF activates protein kinase B (Akt), phospholipase C gamma (PLCγ), and cAMP response element binding protein (CREB) signaling pathways (Baydyuk & Xu, 2014).

Interestingly, BDNF expression increases following histone deacetylase inhibition in cortical neurons (I. Koppel & Timmusk, 2013). The deacetylase inhibition properties of ketones may in fact induce BDNF expression. The extent to which ketosis activates such pathways remains relatively understudied, and investigations into these interactions could potentially explain some ketotherapeutic effects.

Akt regulates cell growth through its downstream targets tuberous sclerosis (TSC) 1, TSC2, and mammalian target of rapamycin complex (mTORC) 1. It also enhances cell survival by inhibiting Bad, a pro-apoptotic factor. Akt interacts with the GABA receptor, ataxin-1, and the huntingtin protein (Manning & Cantley, 2007). Akt levels are typically low in the adult brain, but expression increases following injury in some models (Owada, Utsunomiya, Yoshimoto, & Kondo, 1997). Akt is protective in the setting of reduced trophic support, exposure to reactive oxygen species, and DNA damage (Chong, Kang, & Maiese, 2002, 2003; Chong, Li, & Maiese, 2005; Henry, Lynch, Eapen, & Quelle, 2001; Kang, Chong, & Maiese, 2003; Matsuzaki et al., 1999).

PLCγ activation by BDNF signaling generates inositol 1,4,5-triphosphate (IP3) and diacylglycerol (DAG). IP3 and DAG, respectively, mobilize internal calcium stores and activate protein kinase C (PKC). Activation of these pathways has multiple effects including modulation of cell proliferation, migration, neurite outgrowth, synaptic plasticity, and survival. PLCγ expression primarily occurs in the cortex and hippocampus (Jang et al., 2013; Suh et al., 2008). PLCγ regulates N-methyl-D-aspartate (NMDA) receptor biology through neuregulin 1 (NRG1) (Gu, Jiang, Fu, Ip, & Yan, 2005). PLCγ facilitates hippocampal long-term potentiation (LTP), a process that facilitates the acquisition and storage of information at the synapse (Kandel, 2001; Minichiello et al., 2002). Given the role of PLCγ in cell survival and molecular mechanisms of

learning, activation of PLCγ by ketone induced BDNF signaling represents an intriguing potential mediator of ketotherapeutic effects.

CREB, typically activated by increases in cytosolic calcium or cAMP, has a recognized role in the regulation of circadian rhythms and memory formation (A. J. Silva, Kogan, Frankland, & Kida, 1998). Disruption of CREB signaling pathways induces neurodegeneration of the hippocampus and dorsolateral striatum in mice lacking the related protein cAMP response element modulatory protein (CREM) (Mantamadiotis et al., 2002). Certain CREB isoforms are critical in learning and memory processes (A. J. Silva et al., 1998). For instance, on food preference tasks mice lacking CREBα show competent immediate memory but reduced memory at 24 hours (Kogan et al., 1997). Ketone-mediated modulation of CREB activity through BDNF could have important translational potential in age-related dementias.

It has recently been shown that BDNF is also able to induce the expression of inhibin β-A via its action on synaptic NMDA receptors and nuclear calcium signaling. Increased inhibin β-A expression inhibits calcium currents generated by extrasynaptic NMDA receptors that are known to inhibit mitochondrial function and induce cell death following glutamate excitotoxicity (Lau, Bengtson, Buchthal, & Bading, 2015). This neuroprotective signaling pathway would offer great benefit to diseases that feature reduced BDNF signaling such as Huntington's disease, Alzheimer's disease, or age-related neurodegeneration.

Relevance to Development and Neurologic Disease

Ketones in Development

Ketone bodies play a critical role during normal brain development (Cotter, d'Avignon, Wentz, Weber, & Crawford, 2011; S. C. Cunnane, Courchesne-Loyer, St-Pierre, et al., 2016). Oxidation of ketones by the brain begins during fetal development (Adam, Raiha, Rahiala, &

Kekomaki, 1975). Mammalian neonates are largely reliant on maternal breast milk as their primary nutrition source. Maternal milk is rich in dietary fats and has a high ketogenic ratio due to its abundance of medium chain fatty acids (Breckenridge & Kuksis, 1967; Hilditch, 1944; Insull & Ahrens, 1959; Nehlig, 1999). Unlike adult ketosis, neonatal ketosis occurs independently of whether or not the infant is in a fed state (Lindblad, Settergren, Feychting, & Persson, 1977). Despite the fact that long chain fatty acids do not freely diffuse into the brain, a robust amount of neonate brain energy production relies on ketone metabolism (Nehlig & Pereira de Vasconcelos, 1993). Blocking ketogenesis enhances seizure severity in rat pups (Minlebaev & Khazipov, 2011).

The importance of ketones to the developing brain extend well beyond their role in bioenergetics. Ketones serve as the primary substrate for lipid synthesis during periods of rapid brain growth (S. C. Cunnane & Crawford, 2003; Freemantle et al., 2006). Indeed, neonatal ketogenesis appears so essential to development that even the neonatal intestine is capable of ketogenesis (Bekesi & Williamson, 1990).

Epilepsy

Epilepsy involves the aberrant, synchronous depolarization of neurons in the central nervous system. It generally manifests as paroxysmal disruptions of awareness, consciousness, and motor activity. Epilepsy affects 1% of the United States population and up to as many as 50 million people globally (Hirtz et al., 2007; Kobau et al., 2008; McNally & Hartman, 2012). As described previously, epilepsy represents the first condition that intentionally utilized ketotherapeutics. A modern randomized clinical trial in humans demonstrated that the KD was able to reduce seizures in 75% of pediatric epileptics over a three-month period (Neal et al.,

2008). Despite their modern use extending back by as much as a century, its therapeutic mechanism remains a matter of much debate.

Anticonvulsant properties of acetoacetate were first demonstrated in rabbits administered thujone to produce seizures (Keith, 1935). Given that glutamate excitotoxicity represents one possible cause of neuronal damage from seizures, efforts were made to investigate whether ketotherapeutics worked by attenuating neuronal excitation by modulating neurotransmitter balance or release. There is some evidence to suggest that ketotherapies increase GABA. In rats, acetoacetate and β-hydroxybutyrate increased the accumulation of GABA in rat presynaptic vesicles (Erecinska, Nelson, Daikhin, & Yudkoff, 1996). Magnetic resonance spectroscopy of humans maintained on a KD also showed increased brain GABA levels (Z. J. Wang et al., 2003). Further, ketotic rats exhibit lower levels of glutamate in neurons but stable amounts of GABA. Since GABA is synthesized from glutamate, this indicates a greater proportion of glutamate may be converted to GABA, and thereby shift the total balance of these neurotransmitters towards inhibition (Melo, Nehlig, & Sonnewald, 2006).

Reducing glutamate release could also potentially reduce seizure-associated glutamate excitotoxicity. Acetoacetate reversibly inhibits glutamate release in mouse hippocampal slices and cultured rat neurons at high concentrations of 10 mM (Juge et al., 2010). Others have noted this effect may not have physiologic relevance as extracellular levels of β-hydroxybutyrate in the hippocampal microenvironment were determined to be between 40-50 μM following three weeks of KD (McNally & Hartman, 2012; Samala, Klein, & Borges, 2011). In light of this, the role of ketotherapeutics in modulating neurotransmitter balance remains speculative.

Ketotherapeutics may modulate neuronal excitability independent of influencing neurotransmitter levels. As previously discussed, following their entry into the TCA cycle

ketones enhance the production of ATP. ATP levels could influence the activity of membrane ion pumps and thus alter neuron membrane potential. In this regard, ATP-sensitive potassium (K_{ATP}) channels are of particular interest given their recognized activation upon changes in the ATP/ADP ratio, and their effects on membrane polarization. Tanner et al. demonstrated that β-hydroxybutyrate enhances K_{ATP} channel opening in cultured mouse hippocampal neurons (Tanner, Lutas, Martinez-Francois, & Yellen, 2011). Cultured GABAergic substantia nigra pars reticulata (SNpr) neurons exhibited reduced firing rates in the presence of either acetoacetate or β-hydroxybutyrate. However, this effect disappeared following knockout of the potassium inward rectifier channel Kir6.2 or in the presence of the K_{ATP} channel inhibitor tolbutamide (Deransart et al., 2003). Consequently, it is possible that neuroprotection from seizure events could be mediated through reduced cell firing rates that result from changes in neuron membrane potential, and not the suppression or alteration of total neurotransmitter concentrations.

Voltage sensitive potassium channel Kv1.1 knockout mice maintained on a KD exhibited increased nuclear localization of the peroxisome proliferator activated receptor-γ 2 (PPARγ2) splice variant. This was associated with a 70% reduction in seizure frequency. The PPARγ antagonist GW9662 eliminated this benefit. Further, the anti-seizure effects of the KD were mimicked in Kv1.1 KO mice when administered the PPARγ agonist pioglitazone (Simeone, Matthews, Samson, & Simeone, 2017). Modulation of PPARγ activity presents an attractive and readily available target for novel epilepsy therapeutics.

Alzheimer's Disease

AD is the most common form of dementia and involves progressive neurodegeneration that causes impaired memory and a reduced ability to perform activities of daily living. Theories vary regarding the underlying etiology of the overall disease process, but glucose

hypometabolism, mitochondrial dysfunction, extracellular amyloid-β (Aβ) plaque accumulation, and intracellular tau protein neurofibrillary tangles are recognized biochemical and histological hallmarks (Swerdlow, 2011, 2012a, 2012b).

Emerging evidence suggests defects in mitochondrial function and a consequential decline in respiratory chain function alter amyloid precursor protein (APP) processing to favor the production of the pathogenic Aβ fragment (Wilkins & Swerdlow, 2016a). Several groups have shown that both APP and Aβ co-localize with mitochondria, suggesting the possibility that mitochondrial function and APP biology interact (Devi, Prabhu, Galati, Avadhani, & Anandatheerthavarada, 2006; Hansson Petersen et al., 2008). Ketone bodies block mitochondrial amyloid entry and improve cognition (Yin et al., 2016). This ability would predictably ameliorate Aβ-mediated suppression of respiratory chain function and could perhaps to some rescue the bioenergetic hypometabolism observed in AD brains (Swerdlow, 2012c). Alternatively, improving mitochondrial performance outright could reduce the production of Aβ and increase the production of soluble APPα, a molecule with trophic properties capable of binding the BDNF receptor p75 to promote neurite growth (Hasebe et al., 2013).

Fluorodeoxyglucose positron emission tomography (FDG-PET) studies find asymptomatic individuals with an increased AD risk show less prefrontal cortex, posterior cingulate, entorhinal cortex, and hippocampal glucose uptake than normal-risk individuals (de Leon et al., 2001; Ishii et al., 1997; Mosconi et al., 2011; Mosconi, De Santi, Brys, et al., 2008; Mosconi, De Santi, Li, et al., 2008; Mosconi et al., 2009; Mosconi, Tsui, et al., 2008; O'Dwyer et al., 2011; Reiman et al., 2004; Rosenbloom et al., 2011; Spulber et al., 2010; Villain et al., 2010; Vlassenko et al., 2010). This reduction associates with the downregulation of the glucose transporter GLUT1 in the AD brain (Winkler et al., 2015). Further, increasing evidence suggests

that increased insulin resistance contributes to the development of sporadic AD (de la Monte, 2009).

Clinical studies suggest ketogenic therapies may benefit AD patients. Medium chain triglyceride and ketone ester supplements raised plasma ketone levels and improved cognition in AD subjects (Henderson, 2008; Newport, VanItallie, Kashiwaya, King, & Veech, 2015; Reger et al., 2004). This is in agreement with epidemiological studies that report positive associations between ketotherapeutic use and reduced AD risk (Henderson, 2008; Morris, 2005).

Preclinical studies performed using the triple transgenic mouse model of AD demonstrated reduced pathology following the administration of the ketogenic modulator 2-deoxy-D-glucose (2-DG), which inhibits glycolysis and increases cell reliance on respiratory chain oxidative phosphorylation (Yao, Chen, Mao, Cadenas, & Brinton, 2011; Yao, Rettberg, Klosinski, Cadenas, & Brinton, 2011). Further, PET studies using radiolabeled acetoacetate and β-hydroxybutyrate demonstrated single compartment kinetics of brain ketone body utilization, matching levels and uptake over a large range of concentrations (Blomqvist et al., 2002; Blomqvist et al., 1995). Importantly, brain uptake of acetoacetate did not significantly differ either globally or regionally in early stage AD patient brains, as compared to age-matched controls (Castellano et al., 2015). Of note, increased astrocyte metabolism appeared to mitigate Aβ-related impairment of memory function in day old chicks, which implies bioenergetic benefits require astrocyte function (Gibbs, Gibbs, & Hertz, 2009). It remains unclear if the brain's capacity to utilize ketones in general declines with age.

Catabolism of white matter lipids, with the purpose of providing substrate for astrocytic ketogenesis, may occur in the aging female brain (Klosinski et al., 2015). This could mitigate neurocognitive decline by compensating metabolism defects with ketolysis (Bartzokis, Lu, &

Mintz, 2004; Bartzokis, Sultzer, et al., 2004; Brinton, 2008; Carmichael et al., 2010; Kuczynski et al., 2010). While ketone compensation may delay the onset of clinical symptoms, this process could lead to white matter demyelination and its associated clinical consequences (Morris, 2005). It would be interesting to know if providing increased dietary fats sustains ketogenesis and reduces white matter scavenging in the aged brain, thereby extending the window of ketone compensation and delaying the onset of AD symptoms. In support of this possibility, rats fed a high-fat diet rich in lipoic acid reportedly improved their performance on a novel object recognition task (Rodriguez-Perdigon, Solas, Moreno-Aliaga, & Ramirez, 2016).

Stroke

Stroke typically refers to an acute interruption of blood flow to a region of the brain that results in cell injury and cell death. Stroke carries significant morbidity and societal impact, and it is currently the fourth leading cause of death in the United States (Ovbiagele & Nguyen-Huynh, 2011). The majority of approved therapies to prevent and treat stroke focus on the prevention and dissolution of blood clots to maintain patent blood vessels. Therapeutics that can improve biochemical plasticity and confer resistance to the sequelae of ischemia could provide a strategy for reducing injury during and improving rehabilitation after stroke.

Supplying an oxidative phosphorylation-promoting intermediate would seem unlikely to enhance energy production within the ischemic core of an infarct. However, as discussed, the physiologic role of ketones extends far beyond their direct role in bioenergetic pathways. Providing ketone bodies to the penumbra, the region of brain tissue lying directly adjacent to the ischemic core, may spare glucose for the core, thereby helping to sustain energy production in the absence of molecular oxygen (C. L. Gibson, Murphy, & Murphy, 2012).

Preclinical studies in mice demonstrated that the KD and BHB reduce total infarct volume induced by permanent middle cerebral artery occlusion (MCAO) (Puchowicz et al., 2008; Rahman et al., 2014). Interestingly, this effect does not occur in HCA2 knockout mice, which suggests this benefit may rely on anti-inflammation signaling pathways. A similar phenomenon was reported in rodent models of ischemic stroke treated with BHB, which led to reductions in infarct volume, reduced brain edema, and improvements in motor function (Suzuki et al., 2002; Suzuki et al., 2001). This study did not determine, though, whether HCA2 signaling mediated these effects.

Traumatic Brain Injury

Epidemiologic studies link traumatic brain injury (TBI) to AD, PD, ALS and the recently described condition of chronic traumatic encephalopathy (CTE) (Bruce et al., 2015). Current therapies for TBI primarily consist of behavioral therapy and the pharmaceutical treatment of associated symptoms such as depression. Therapies that can enhance TBI recovery, or can precondition high-risk individuals towards lesser injuries, are sorely needed.

In rats, post-TBI administration of β-hydroxybutyrate reduced contusion volume in an age-dependent manner (Prins, Fujima, & Hovda, 2005; Prins & Matsumoto, 2014). This associated with a reversal of injury-related ATP reduction (Prins, Lee, Fujima, & Hovda, 2004). Recently, activation of the Akt/GSK-3β/β-catenin signaling pathway was found to enhance neuron survival in a TBI rat model (S. Zhao et al., 2012). Ketone activation of Akt signaling, therefore, could offer a potential strategy for preserving neuron integrity.

It is important to note a study reported β-hydroxybutyrate increased blood-brain barrier permeability in a TBI rat model (Orhan et al., 2016). This may contribute to increased

inflammation due to the exposure of brain parenchyma to pro-inflammatory blood components. The cost-benefit utility of ketotherapeutics in TBI, therefore, requires careful consideration.

Amyotrophic Lateral Sclerosis

Amyotrophic lateral sclerosis (ALS), also known as Lou Gehrig's disease, is a neurodegenerative disorder that features the demise of upper and lower motor neurons (Ji, Zhang, Chen, & Huang, 2017). Disease progression manifests as progressive muscle weakness and paralysis. Once respiratory muscle involvement occurs, ventilation compromise ensues and ultimately the disease concludes in death. As is the case with AD, the majority of ALS cases are sporadic but a subset of familial cases arise from autosomal dominant mutations. One well-studied causal mutation occurs in the gene that encodes superoxide dismutase 1 (SOD1). Two ketogenic therapy studies, which evaluated a KD and an MCT, reported improved motor performance in SOD1-G93A transgenic mice. In both studies, ketotherapeutics reduced the loss of lower motor neurons in the spinal cord ventral horn. However, neither study appeared to benefit survival outcomes (W. Zhao et al., 2012; Zhao et al., 2006).

Another common feature of the disease, one that it shares with frontotemporal dementia (FTD), is a cytoplasmic accumulation of the ubiquitinated nuclear protein transactive response DNA-binding protein 43 (TDP-43). Recent studies demonstrate the toxic mechanism of TDP-43 requires its localization to mitochondria, where it reduces the expression of mitochondrial DNA-encoded proteins (W. Wang et al., 2016). As ketone bodies seem able to modify mitochondria-Aβ interactions, it would be interesting to see whether they similarly affect mitochondria-TDP43 interactions.

Huntington's Disease

Huntington's disease (HD) is an autosomal dominant neurodegenerative disorder that presents with involuntary choreiform movements, impaired cognition, and psychiatric symptoms. It effects 5 to 8 people per 100,000 in Europe and North America. Disease pathogenesis involves trinucleotide repeat expansion of CAG residues in the *huntingtin* gene. The resulting polyglutamine-expanded protein undergoes errors in protein folding and toxic accumulation that ultimately leads to impaired neuron function and cell death. It primarily affects structures in the basal ganglia, which manifests grossly as caudate atrophy (Ross & Tabrizi, 2011).

Lim et al. provided initial support for the therapeutic potential of ketone bodies in HD. The investigators administered subcutaneous BHB to 3-nitroproprionic acid (3-NP) toxin and R6/2 genetic mouse models of HD. BHB attenuated motor dysfunction in both models. BHB-treated R6/2 mice also saw an extension of lifespan, as well as increased striatal histone acetylation (Lim et al., 2011). Further investigation in PC12 cells demonstrated the increase in histone acetylation occurred independent of mitochondrial function or HDAC inhibition. Additional testing of ketogenic therapies in HD appears warranted.

Parkinson's Disease

Parkinson's disease (PD) affects between 100 to 200 people per 100,000 over the age of 40, and its incidence increases with age. Disease pathogenesis involves a progressive neurodegeneration of dopaminergic neurons in the substantia nigra pars compacta (SNpc). The loss of these neurons manifests as progressive bradykinesia, tremors, and rigidity. Late stages of disease often feature increasing cognitive dysfunction and dementia (Kalia & Lang, 2015).

Preclinical studies in the MPTP mouse model show that infusing BHB or a KD reduces dopaminergic neuron degeneration, improves motor deficits, reduces microglial activation, and

reduces expression of pro-inflammatory cytokines (Tieu et al., 2003; Yang & Cheng, 2010). Similarly, a KD reduces dopamine neuron loss in the 6-hydroxydopamine PD rat model (Cheng et al., 2009).

In a five-participant pilot study of PD patients, a 28-day KD improved unified Parkinson's disease rating scale (UPDRS) scores. The small size of this study and the lack of a control group, though, precludes conclusive inferences (Vanitallie et al., 2005).

Multiple Sclerosis

Multiple sclerosis (MS) features an autoimmune-associated demyelination of CNS axons. It most often presents in a relapsing-remitting fashion that can include varying involvement of optic, sensory, motor, or coordination systems. After trauma, MS is the next most common CNS-related cause of young adult permanent disability (Noseworthy, Lucchinetti, Rodriguez, & Weinshenker, 2000; Ramagopalan & Sadovnick, 2011).

Preclinical data from the mouse experimental autoimmune encephalomyelitis (EAE) multiple sclerosis model indicate a KD improves outcomes. In their 2012 study, Kim et al. demonstrated a KD reduced brain inflammation, mitigated motor disability, preserved CA1 long-term potentiation, and improved spatial learning and memory as assessed by the Morris water maze. The KD also induced a reduction in reactive oxygen species in conjunction with reduced pro-inflammatory cytokines (Kim et al., 2012). The anti-inflammatory properties of the KD are in line with suggested benefits as discussed previously. It would be interesting to know if the HCA2 pathway modulates these effects.

Conclusions

Fatty acid β-oxidation by hepatocytes and astrocytes generates the primary ketone bodies, β-hydroxybutyrate and acetoacetate. These ketones are taken up and catabolized by neurons and

help produce energy via oxidative phosphorylation. Recent work suggests that ketone bodies or interventions that serve to produce or introduce ketone bodies provide neurologic benefits that extend beyond their direct role in bioenergetic fluxes. Specifically, ketones affect protein post-translational modifications, attenuate RONS production, increase antioxidant stress response pathway expression, modulate GPR and BDNF signaling pathways, contribute to anaplerosis, and exhibit anti-inflammatory effects **(Figure 1-3)**.

Ketotherapeutic approaches, therefore, may influence the nervous system through a variety of mechanisms. Their potential for treating a variety of neurologic conditions warrants consideration. Further, ketogenic benefits may extend beyond pathologic states and could promote healthy aging in general. In doing so, ketotherapeutics would delay and prevent the development of age-dependent neurologic disease.

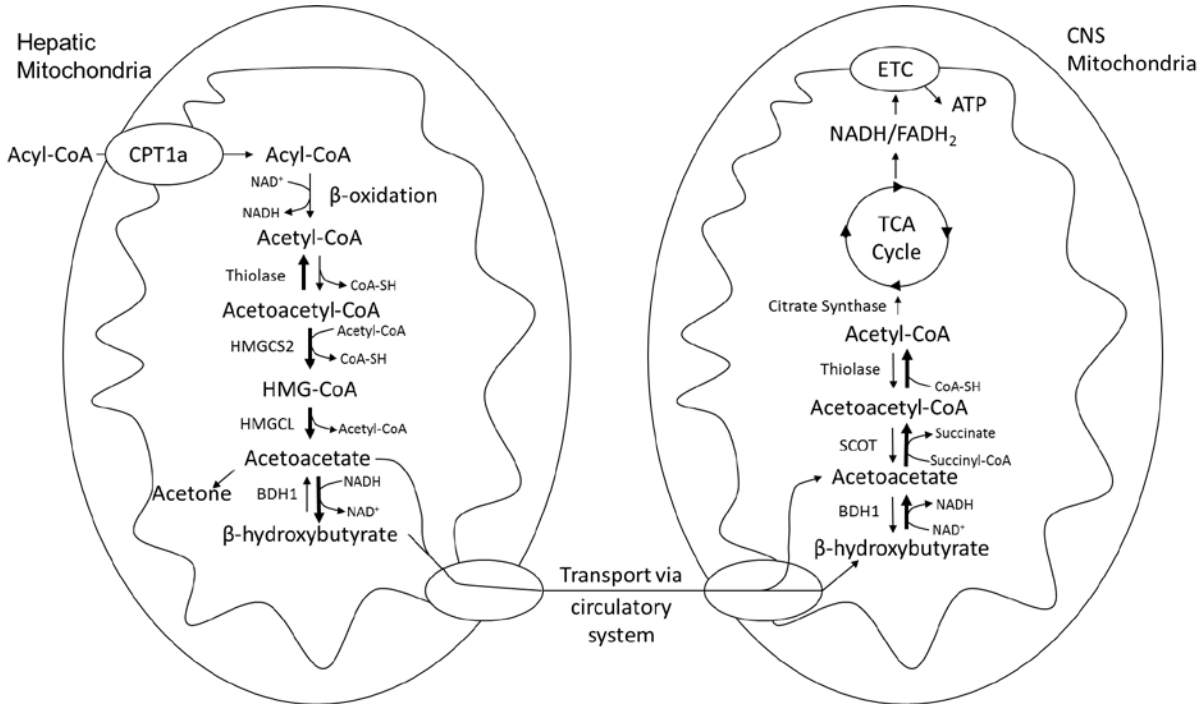
Hepatic
Mitochondria
Acyl-CoA
CPT1a
Acyl-CoA
NAD+
NADH
β-oxidation
Acetyl-CoA
Thiolase
CoA-SH
Acetoacetyl-CoA
HMGCS2
Acetyl-CoA
CoA-SH
HMG-CoA
HMGCL
Acetyl-CoA
Acetoacetate
Acetone
BDH1
NADH
NAD+
β-hydroxybutyrate
Transport via
circulatory
system
CNS
Mitochondria
ETC
ATP
NADH/FADH2
TCA
Cycle
Citrate Synthase
Acetyl-CoA
Thiolase
CoA-SH
Acetoacetyl-CoA
SCOT
Succinate
Succinyl-CoA
Acetoacetate
BDH1
NADH
NAD+
β-hydroxybutyrate

Figure 1-1: Ketogenesis and Ketolysis. Hepatic mitochondria serve as the primary site for the production of serum ketone bodies. Acetyl-CoA generated as a consequence of acyl-CoA β-oxidation is converted to HMG-CoA by the rate limiting enzyme HMGCS2. HMG-CoA is further processed to the primary ketone bodies acetoacetate and β-hydroxybutyrate which are excreted into circulation via MCTs 1 and 2. Ketone bodies enter the CNS via MCTs and are oxidized to acetyl-CoA through a series of reactions that require SCOT. Acetyl-CoA undergoes terminal oxidation through the TCA cycle to generate the high energy electron carriers NADH and $FADH_2$. Electrons enter the ETC leading to the generation of ATP through ATP synthase.

A

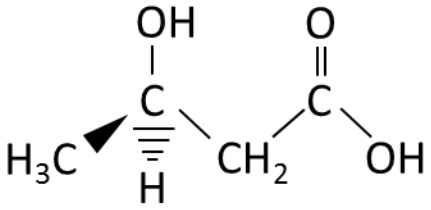

β-hydroxybutyrate

B

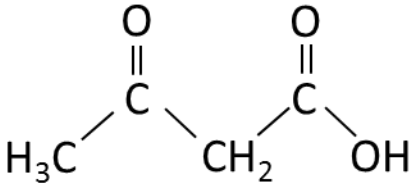

Acetoacetate

C

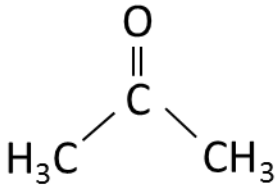

Acetone

Figure 1-2: Chemical Structures of Biologically Relevant Ketone Bodies. The physiologically relevant ketone bodies in order of decreasing serum concentrations are β-hydroxybutyrate (A), acetoacetate (B), and acetone (C). Acetone is highly volatile and is readily excreted via the pulmonary system and is not thought to contribute greatly to bioenergetic pathways.

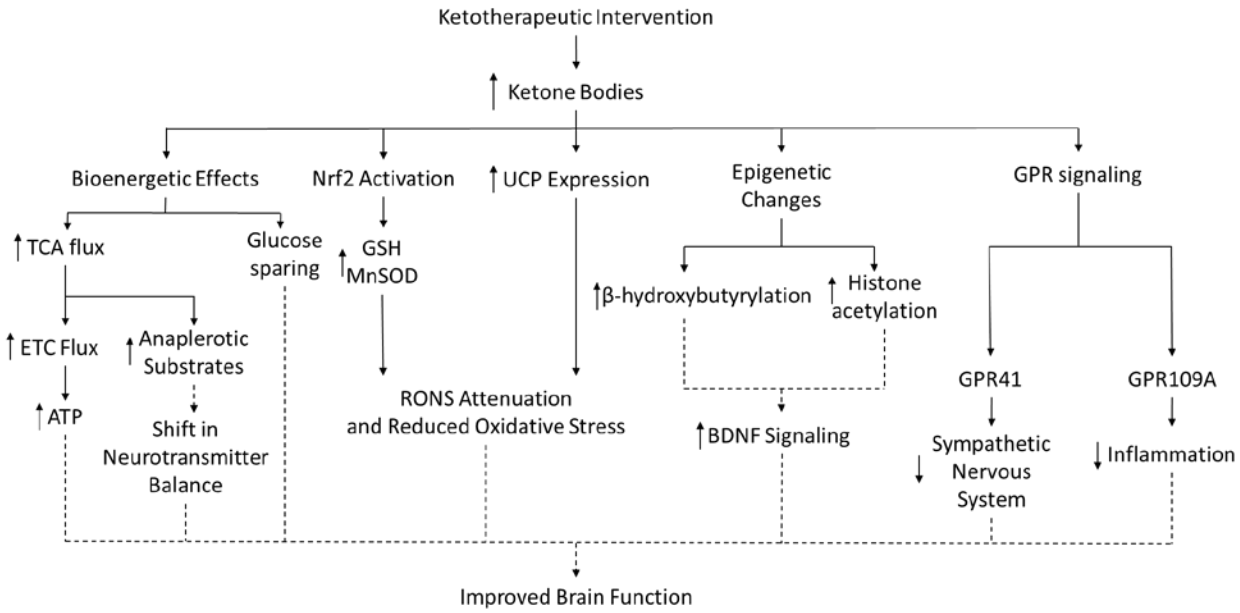
Ketotherapeutic Intervention
↑ Ketone Bodies
Bioenergetic Effects
Nrf2 Activation
↑ UCP Expression
Epigenetic Changes
GPR signaling
↑ TCA flux
Glucose sparing
↑ GSH
↑ MnSOD
↑ β-hydroxybutyrylation
↑ Histone acetylation
↑ ETC Flux
↑ Anaplerotic Substrates
↑ ATP
Shift in Neurotransmitter Balance
RONS Attenuation and Reduced Oxidative Stress
↑ BDNF Signaling
GPR41
GPR109A
↓ Sympathetic Nervous System
↓ Inflammation
Improved Brain Function

Figure 1-3: Pleiotropic Effects and Hypothesized Benefits of Ketotherapeutics. Multiple ketotherapeutics produce an increase in serum ketone bodies. Ketone bodies have been shown to increase oxidative metabolism, reduce oxidative stress, alter epigenetic protein post-translational modifications, increase BDNF signaling, and signal through GPRs in various model systems. Many of these effects require further study to determine the underlying mechanism of action and ultimate therapeutic value. Observed and hypothesized effects are indicated with solid and dashed lines respectively.

Chapter 2: β-hydroxybutyrate Enhances Mitochondrial Respiration While Signaling Nutrient Scarcity and Cellular Quiescence in Neurons but Not Astrocytes *In Vitro*

Introduction

Advancing age is the primary risk factor for the development of sporadic neurodegenerative disease including dementia and Alzheimer's disease (AD) (Guerreiro & Bras, 2015). Brain aging is associated with an accumulation of senescent cells and bioenergetic dysfunction (Bussian et al., 2018; Holtzman & Ulrich, 2019; Masaldan, Belaidi, Ayton, & Bush, 2019; Musi et al., 2018; Zhang et al., 2019). Senescence involves the irreversible exit from the cell cycle that is associated with increased inflammation known as the senescence associated secretory phenotype (SASP). Opposite to senescence, cells may become quiescent due to nutrient scarcity in the environment where they reversibly exit the cell cycle until the return of sufficient nutrition to stimulate growth. Entry into quiescence is generally thought to delay or prevent cellular senescence. Glucose hypometabolism and mitochondrial dysfunction both occur with advancing age and to a greater extent in AD (Castellano et al., 2015; S. Cunnane et al., 2011; Lezi & Swerdlow, 2012; Selfridge, E, Lu, & Swerdlow, 2013; D. F. Silva et al., 2012; D. F. Silva et al., 2013; Swerdlow, 2012a, 2012c, 2014a; Wilkins, Carl, Greenlief, Festoff, & Swerdlow, 2014; Wilkins & Swerdlow, 2016b). Reversing or preventing cellular aging through enhanced bioenergetic flux in addition to averting or clearing senescent cells, termed senolytic therapy, could have considerable therapeutic benefit in aging and age associated diseases of the central nervous system (CNS).

One approach to providing an alternative fuel is through the high-fat, low-carbohydrate ketogenic diet (KD) or other neuroketotherapeutics (Courchesne-Loyer et al., 2016; S. C. Cunnane, Courchesne-Loyer, Vandenberghe, et al., 2016; Hennebelle et al., 2016; S. J. Koppel & Swerdlow, 2018; M. K. Taylor, Swerdlow, & Sullivan, 2019). These methods commonly feature the induction of ketogenesis that raises circulating blood ketone levels to the point they are utilized by the brain for energy production via mitochondrial respiration and oxidative

phosphorylation. Ketogenesis is performed as a physiologic response to starvation to ensure that privileged organs such as the heart and brain have access to extra fuel while other tissues catabolize fats. The KD mimics starvation through the severe restriction of carbohydrate in the diet although caloric needs are being met.

While the biochemistry of ketolysis has been well established, a growing appreciation for the molecular effects of ketone bodies is emerging. Perhaps most notably, the primary ketone body, β-hydroxybutyrate (βOHB), has been shown to act as an inhibitor for histone deacetylases and induce increases transcription as a result of increased histone acetylation in HEK293 cells (Shimazu et al., 2013). Recently, βOHB has also been shown to prevent the accumulation of senescent cells in mouse vasculature through the quiescence regulator octamer-binding transcriptional factor 4 (Oct4, *POU5F1*) (Han et al., 2018). We have previously performed a retention and feasibility trial of 3-month KD intervention in patients with AD (Matthew K. Taylor, Sullivan, Mahnken, Burns, & Swerdlow, 2017; M. K. Taylor, Swerdlow, Burns, & Sullivan, 2019). In this study, completers of the diet demonstrated improvement on the Alzheimer's Disease Cognitive Assessment Scale-cognitive subscale while on the diet demonstrating the need to further study possible mechanisms of benefit of neuroketotherapeutics for the treatment of dementia. However, while many possible effects of ketone bodies have been suggested as being therapeutics, many of these hypotheses do not consider the multicellular composition of the brain.

The brain does not operate as a single homogenous compartment regarding its bioenergetics and metabolism. One well known model is the astrocyte neuron lactate shuttle (ANLS) where astrocytes refine glucose through glycolysis to pyruvate for export and consumption by neurons through the TCA cycle and electron transport chain (ETC) for energy

production (Bouzier-Sore, Serres, Canioni, & Merle, 2003; Dienel, 2013; L. Liu, MacKenzie, Putluri, Maletic-Savatic, & Bellen, 2017; Stobart & Anderson, 2013). It has been suggested that a similar compartmentalization may occur with ketone body metabolism (Guzman & Blazquez, 2001).

To improve our understanding of the effects of ketone bodies on the CNS, we conducted initial investigations into the effects of βOHB on mitochondrial function and nutrient sensing pathways in SH-SY5Y neuroblastoma cells. We further expanded our studies to primary rat neurons and astrocytes operating under our hypothesis that neurons would be more responsive to the presence of βOHB *in vitro* than astrocytes. We found that βOHB supported mitochondrial respiration and histone acetylation in both SH-SY5Y and primary neuronal cultures but not in astrocytic cultures. βOHB reduced activating phosphorylation of the nutrient sensing PI3K-Akt-mTOR pathway in SH-SY5Y's and neurons. βOHB was also able to increase transcription of Yamanaka factors in SH-SY5Y cells and increase protein level of Oct4 in primary neurons and astrocytes.

Materials and Methods

Culturing of SH-SY5Y Cells

All experiments utilizing timed pregnant rats described in this study were reviewed and authorized by the University of Kansas Medical Center Institutional Animal Care and Use Committee prior to any experimentation. SH-SY5Y cells are not currently recognized as a commonly misidentified cell by the International Cell Line Authentication Committee. Undifferentiated SH-SY5Y human neuroblastoma cells were cultured in DMEM (gibco #11966) supplemented with 10% fetal bovine serum (FBS) and 1% penicillin/streptomycin (P/S). D-glucose was supplemented to glucose free DMEM to achieve a final concentration of 1 g/L D-

glucose. Media was exchanged daily. Vehicle cells were supplemented with an additional 4 mM NaCl while β-hydroxybutyrate (βOHB) treated cells were cultured with freshly prepared media supplemented with 4 mM (R)-(-)-3-Hydroxybutyric acid sodium salt (Santa Cruz Biotechnology, Inc. sc-229050A). Cultures were considered chronically adapted to βOHB after being cultured for seven days or greater (≥ 7 DIV) in the presence of βOHB. Cultures were maintained at 37°C and 5% CO_2.

Isolation and Culturing of Primary Neurons and Astrocytes

All experiments involving vertebrate animals were reviewed and approved by the University of Kansas Medical Center Institutional Animal Care and Use Committee. Timed pregnant Sprague-Dawley rats (Charles River Laboratories, Wilmington, MA) were obtained on embryonic days 12-13 of gestation (E12-13). On day E16 pregnant rats were euthanized via CO_2 asphyxiation and secondary bilateral thoracotomy. E16 embryos were removed upon necropsy and cortices were obtained via dissection. Cortices were placed in digestion buffer consisting of 1-part TrypLE Express (gibco #12604-021) to 2-parts Neurobasal media (gibco #21104-049) and incubated for 5 minutes at 37°C. Digested cortices were processed to single cell suspension via trituration and passed through a 40 µm cell strainer. Cells were pelleted by centrifugation at 400 rcf for 3 minutes and washed in warmed neurobasal media to remove excess TypLE. The cell suspension was divided in half and pelleted again. Neurobasal media was removed and one pellet was resuspended in primary neuron culture media (Neurobasal media with 1x B27 supplement (gibco #17504-044), 25 µM L-glutamine, and 1% P/S) with the other resuspended in Astrocyte Growth Media (DMEM/F12 1:1 (gibco #11320-033) with 10% FBS and 1% P/S). Cells were plated on plastic cell culture plates pre-treated with poly-L-lysine and incubated at 37°C and 5% CO_2. The day following isolation neuronal media was replaced with media containing cytosine

arabinoside for 48 hours to arrest mitotically dividing cells and induce apoptosis of any cells other than post-mitotic neurons. Neuronal cultures were cultured for a minimum of 7 days prior to experimental investigation to allow for neurite extension and synapse formation between cells. Astrocyte cultures were grown to confluency in T75 flasks. Upon reaching confluency flasks were gently shaken for 1 hour at 37°C to remove non-astrocytic glia. Media was then removed and astrocytes were passaged using 0.05% Trypsin-EDTA and plated into new dishes for experimental investigation and allowed to grow to confluency. Both neuronal and astrocytic cultures were treated with vehicle or βOHB at previously discussed concentrations in their appropriate media. Purity of cultures were determined through immunocytochemical staining with antibodies targeting microtubule associated protein 2 (MAP2) (abcam #ab32454 1:500 dilution) and glial acidic fibrillary protein (GFAP) (abcam #ab7260 1:1000 dilution) for neurons and astrocytes respectively. Antibody labeling was visualized using AlexaFluor goat anti-rabbit 488 antibody (abcam ab#150077 1:2000) with Hoechst 33342 (Invitrogen #H1399) counterstain and imaged using an epifluorescent microscope.

Seahorse Extracellular Flux Analysis

Two days prior to assay 20,000 SH-SY5Y cells were seeded per well in a Seahorse XF96 cell culture plate (#101085-004). Primary neuron and astrocytes were plated at a density of 100,000 cells per well. Cells were seeded in 100 µL complete media, either vehicle or treatment media as appropriate, and allowed to stand for 1 hour at room temperature before being placed in a 37°C incubator at 5% CO_2. An additional 100 µL of media was added four hours later and cells were then returned to the incubator overnight. The following day media was exchanged to appropriate treatment medias and cells were allowed to incubate an additional night. The next day cell media was removed until 50 µL remained and cells were washed twice with 200 µL of

assay media (Seahorse XF Base Media supplemented with 1 g/L D-glucose and 2 mM L-glutamine). After the final wash assay media was added to a final well volume of 180 µL and the cell culture plate was placed in a de-gassing incubator at 37°C for 1 hour. For the mitochondrial stress test, 10x concentrated solutions of 10 µM oligomycin (Sigma #75351), FCCP (Sigma #C2920), and 5 µM rotenone (Sigma #R8875) with 5 µM antimycin A (Sigma #A8674) were added to ports A, B, and C respectively and injected sequentially during the assay run. Experiments were performed on the Seahorse XFe96 Analyzer (Agilent Technologies, Inc., Santa Clara, CA).

Measurement of ADP/ATP and NAD^+/NADH Ratios

ADP/ATP ratios were determined by the ADP/ATP Ratio Assay Kit (Sigma #MAK135) and performed according to manufacturer's instructions. Briefly SH-SY5Y cells were plated in 96-well plastic plates and treated as described in Seahorse Extracellular Flux Analysis. Two hours prior to assay media was freshly exchanged. To begin the assay culture media was removed and 90 µL of ATP reagent was added per well, mixed, and allowed to incubate for 1 minute. Luminescence due to ATP content was read. The plate was incubated for an additional 10 minutes and residual luminescence was read to determine residual background levels of ATP. 5 µL ADP reagent was added per well and mixed. After 1 minute, luminescence was read again. ADP/ATP ratio was calculated as (Read 3 – Read 2/Read1).

NAD^+/NADH ratios were determined using the NAD/NADH Glo Assay Kit (Promega #G9071). Cells were plated in white-walled flat bottom tissue culture plates and treated as described previously. Media was removed and 50 µL of PBS was added per well. An additional 50 µL of 0.2 NaOH with 1% DTAB was added per well and mixed to lyse cells. 50 µL was removed and placed into a new well for treatment with 25 µL of 0.4 N HCl. Plates were covered

and incubated for 15 minutes at 60°C then equilibrated back to room temperature over 10 minutes. 25 µL 0.5 M Tris base was added to acid treated wells and 50 µL of Tris-HCl was added to base-treated samples. 100 µL Detection Reagent was added per well and gently mixed. Plates were incubated at room temperature for 1 hour. Luminescence was measured with base treated samples used to determine NADH levels and acid treated samples measuring NAD^+ levels.

Measurement of Mitochondrial Membrane Potential

Mitochondrial membrane potential was determined through multiple methods. First, tetramethyl rhodamine ethyl ester (TMRE) (ThermoFisher #T669) staining with Hoechst 33342 nuclear staining was performed. SH-SY5Y cells were plated and treated as above. A subset of cells were treated with 20 µM FCCP for 1 hour as a positive control. Media was aspirated and fresh treatment media supplemented with 1 µM TMRE and 1 µg/mL Hoechst 33342 was added, and cells were returned to the incubator for 30 minutes. Media was aspirated and HBSS was added. Cells were immediately imaged at 20x magnification on the Biotek Cytation1 automated microscope. Images were analyzed for intensity of TMRE per cell using automated BioTek Gen5 software (Agilent Technologies, Inc., Santa Clara, CA).

JC-1 staining was also performed. 2 µM working concentration of JC-1 (ThermoFisher #T3168) was applied to SH-SY5Y cells in a 96 well plate in treatment media for 30 minutes at 37°C. Media was aspirated and replaced with HBSS. Fluorescence was measured at Excitation/Emission spectra o 490/590 nm and 490/529 nm for red and green fluorescence respectively and ratioed to determine dye incorporation into mitochondria.

Finally, nonyl acridine orange (NAO) staining was used (ThermoFisher #A1372). NAO incorporation has been shown recently to be sensitive to mitochondrial membrane potential

(Rodriguez et al., 2008). 100 nM working concentration was added in treatment media as described previously. Media was aspirated and NAO containing media was applied for 15 minutes at 37°C. Media was aspirated and cells detached from plates using 0.05% Trypsin-EDTA. Cells were collected and pelleted at 400 rcf for 3 minutes. Trypsin was aspirated and cells were washed in HBSS. Pelleting and resuspension were performed an additional time with cells resuspended in HBSS on ice. NAO intensity was measured by FACS analysis on a BD FACSAria II cytometer (BD Biosciences, San Jose, CA).

Autophagy Flux Assay

SH-SY5Y's were plated in 6 cm dishes and grown to confluency in treatment media. On day of assay, media was exchanged to media containing 100 nM Bafilomycin (Sigma #B1793) for 6 hours. Following treatment cells were washed in PBS and whole cell lysates were generated as described elsewhere. Ratios of LC3BII to LC3BI were evaluated by Western blot between bafilomycin treated and untreated samples to determine autophagy flux (Cell Signaling Technologies (CST) #3868 1:1000 dilution). Protein levels of NDP52, BNIP3, and Nix/BNIP3L were used to investigate mitophagy flux (CST #60732, 44060, and 12396 respectively, 1:1000 dilutions for all were used).

MTT Assay

Cellular metabolic activity was approximated via MTT assay. 60,000 SH-SY5Y cells were plated per well in 96-well flat bottom plastic plates and treated as described. On the day of assay 0.5 mg/mL thiazoyl blue tetrazolium bromide (MTT) reagent was prepared in treatment media and filter sterilized (Sigma #M2128). Media was aspirated from cells and 100 µL of MTT containing media was applied and mixed by gentle shaking. Cells were returned to 37°C

incubator for 3.5 hours. Media was carefully aspirated so as not to disturb the cell layer. 100 µL DMSO was added per well. Absorbance was measured per well at $\lambda = 540$ nm.

Cell Cycle and Growth Analysis

Cells that had been previously adapted to treatment conditions were passaged using 0.05% Trypsin-EDTA and seeded in 6-cm plastic dishes at a density of 100,000 cells/dish and were presumed to have uniform distribution with passage serving as timepoint t = 0. Cells were collected via gentle scraping in 200 µL ice-cold PBS following media aspiration at 24-hour intervals for 3 days. 20 µL of cell suspension was mixed with an equal volume of 0.4% trypan blue stain (ThermoFisher #T10282). Stained cells were loaded onto cell counting chamber slides and cell number per mL of solution was measured using Cell Countess automated cell counter (Invitrogen #C10227). Count per mL was multiplied by total volume of recovered cell suspension and used to approximate total cell count to the nearest 1,000 cells. Doubling time was estimated using Malthusian growth curve analysis performed in GraphPad Prism 8 software (GraphPad Software, San Diego, CA).

To determine effects of βOHB on cell cycle progression through cell synchronization at the G1/S checkpoint and release with propidium iodide staining. Adapted cells were passaged as described above. The next day media was exchanged to treatment media supplemented with 2.5 mM thymidine for 20 hours. Cells were washed with PBS and released into treatment media for 9 hours. A second 4-hour thymidine block was performed. Cells were then washed again and released and collected at 3-hour intervals for up to 24 hours. Collected cells were washed with ice-cold PBS and collected in 1 mL cold PBS. 2.5 mL of 90% ice-cold EtOH was added dropwise during gentle agitation to fix and permeabilize cells. Cells were washed and resuspended in cold PBS following centrifugation and stained in 1 mL PBS containing 50 µg/mL

propidium iodide (Sigma #P4864) and 1 mg/mL RNase A (ThermoFisher #EN0531). DNA content was measured by FACS analysis on a BD FACSAria II cytometer.

Cell Death Assay

Cell death was measured via TUNEL assay (Abcam #ab66108). Treated cells were washed with PBS and collected by gentle scraping. Following centrifugation cells were fixed in 1% paraformaldehyde on ice for 15 minutes and washed again before being resuspended in 500 µL PBS. Cell suspensions were added slowly to cold 70% EtOH and allowed to incubate on ice for 30 minutes. Cells were removed from EtOH following centrifugation and washed in TUNEL wash buffer before being suspended in TUNEL Stain Solution for 60 minutes at 37°C with agitation every 15 minutes. Cells were washed twice with rinse buffer before being suspended in 500 µL of PI/RNase A solution. Cells death was measured via FACS as mentioned previously within 3 hours of staining. Camptothecin treated and untreated HeLa cells were included as positive and negative controls for apoptosis-induced cell death respectively.

Generation of Whole Cell Lysates

Cells were seeded at similar concentrations in 6-well plates (Corning costar #3516). Following treatment and upon reaching confluency media was aspirated, cells were washed in phosphate buffered saline (PBS), and 100 µL of RIPA lysis buffer containing Thermo Halt Protease and Phosphate inhibitor cocktail (Thermo #1861284) was added per well. RIPA buffer contained 10 mM Tris-HCl (pH 8.0), 1 mM EDTA, 0.5 mM EGTA, 1% Triton X-100, 0.1% sodium deoxycholate, 0.1% SDS, and 140 mM NaCl. Cells were lysed by mechanical scraping and incubated on wet ice for 20 minutes. Lysates were then centrifuged for 10 minutes at 3,000 rcf at 4°C. Supernatant was transferred to a clean tube and stored at -80°C until ready for protein quantification. Protein concentration was determined via BCA Assay (Pierce #23225). 5 µL

lysate and 25 µL albumin standards were measured in duplicate in clear, flat bottom 96 well plates. Following addition of BCA working reagent plates were incubated for 30 minutes at 37°C. Absorbance was measured at λ = 562 nm. Lysates were diluted in laemmli buffer and water and subsequently boiled for 10 minutes at 95°C. Samples were stored at -20°C until use.

Western Blotting

Lysates were resolved by SDS-PAGE using pre-cast 4-12% criterion gels run at constant voltage of 100V in Tris/glycine/SDS running buffer (BioRad #1610772). 50 µg of protein was loaded per lane along with 5 µL protein ladder. Following SDS-PAGE protein was transferred to PVDF membrane activated by methanol (GE Amersham Hybond #10600023) in Tris/glycine buffer (BioRad #1610771) with 20% methanol. Protein transfer occurred at 400 mA for 1 hour on ice. Following transfer membranes were washed in Tris buffered saline with 0.1% tween (TBST) prior to blocking for 1 hour with 5% bovine serum albumin (BSA) in TBST (Boston BioProducts P-753). Blocked membranes were incubated at 4°C overnight on an orbital shaker incubating in primary antibody diluted in 5% BSA in TBST (pT308 Akt CST #2965 1:1000, pS473 Akt LifeTechnologies #700392 1:1000, Total Akt CST #4685 1:1000, Acetyl-H3K9 CST #9649 1:1000, pS79 ACC1 CST #3661 1:1000, Total ACC1 CST #3676 1:1000, β-tubulin CST #2146 1:1000, Total Histone 3 CST #4499 1:2000, Oct4 abcam #ab18976 1:1000, pT389 p70 S6 Kinase CST #9206 1:500, Total p70 S6 Kinase CST #2708 1:1000, pS293 PDHE1α abcam #ab177461 1:1000, Total PDHE1α abcam #ab92696 1:1000). The following day membranes were washed 3 times for 5 minutes in TBST followed by a 1-hour incubation at room temperature in appropriate secondary (Invitrogen Superclonal Secondary Antibody, HRP Conjugate #A28177 or #A27036), diluted 1:4000 in 5% condensed milk in TBST. Membranes were washed an additional 3 times for 5 minutes each prior to visualization of bands using

Supersignal West Femto Maximum Sensitivity Substrate (Thermo #34096) on a BioRad Chemidoc XRS+ imager. Densitometry was performed using Image Lab software (BioRad) with protein levels normalized to either β-tubulin or total protein content determined by amido black stain (Sigma #A8181).

RNA Isolation and RT-qPCR

RNA was isolated via phenol-chloroform extraction with TRI reagent (ThermoFisher #15596018). 1 µg of RNA template was used to generate cDNA with iScript reverse transcription Supermix (BioRad #1708841). cDNA target transcripts were measured by RT-qPCR using TaqMan Universal Master Mix II (ThermoFisher #4440038) and Taqman primers (*18S* Hs03003631_g1, *myc* Hs00153408_m1, *POU5F1* Hs00999634_gH, *Sox2* Hs04234836_s1). qPCR was performed according to master mix instructions on an Applied Biosystems StepOne Plus Real Time PCR system (96 well) using a 96 well plate (Applied Biosystems #4346906). Relative fold change was determined using the ΔΔCt method with *18S* acting as the housekeeping gene.

Lipid Droplet Staining, Triglyceride Assay, and Cholesterol Staining

Lipid droplets were identified through staining with BODIPY 493/503 (ThermoFisher #D3922). 1 mg/mL stock solution was used to create a 1:500 dilution in treatment media. Half of media was removed from cultured cells and 1:500 dilution was applied to achieve 1:1,000 dilution working concentration. Hoechst 33342 was added as a nuclear stain at a final concentration of 5 µg/mL. Cells were incubated for 30 minutes at 37°C prior and washed in PBS following staining. Cells were finally placed in PBS and imaged using a 20x objective on the Cytation1 automated microscope.

Triglyceride content was measured through use of the Triglyceride Quantification Assay Kit (Abcam #ab65336). Cells were collected in 5% NP-40 in water and heated to 80°C for 5 minutes. Cells lysates were cooled to room temp and this cycle of heating and cooling was repeated. Lysates were centrifuged at maximum speed for 2 minutes, supernatant was collected, and samples were diluted 10-fold with water. 50 µL of triglyceride standards and sample were loaded in duplicate onto a 96-well clear, flat bottom plate. 2 µL lipase enzyme was added per well and the plates were allowed to stand at room temperature for 20 minutes. Following this 50 µL of triglyceride reaction mix was loaded containing probe, enzyme mix and triglyceride assay buffer were added per well and plates were incubated for 60 minutes at room temperature in the dark. Absorbance was measured within two hours at $\lambda = 570$ nm. A remainder of lysate supernatant was then analyzed by BCA assay for normalization of triglyceride content to protein per sample.

Cholesterol content of cells was determined using the Cholesterol Assay Kit (Abcam #ab13316). SH-SY5Y cells were cultured in 96-well black walled flat bottom plates. Media was aspirated from cultured cells kit fixative solution was applied for 10 minutes. Cells were washed 3 times for 5 minutes each before the addition of 100 µL of working concentration filipin III stain. Cells were stained for 30 minutes in the dark. Cells were washed an additional two times for 5 minutes each. NucGreen 488 staining was performed following the final wash (ThermoFisher #R37109). Cells were imaged at 20x magnification on the Cytation1 instrument as mentioned previously.

mtDNA and Nuclear DNA Extraction

SH-SY5Y cells were seeded in 6 well dishes. Following treatment and upon confluency cells were washed once with ice-cold PBS and 1 mL PBS was added to each well. Cells were

gently scraped to lift cells into suspension and transferred to autoclaved 1.7 mL microcentrifuge tubes. Cells were pelleted at 600 rcf for 3 minutes and supernatant was removed. The cell pellet was resuspended in 300 µL ice-cold DNA lysis buffer (10 mM Tris-HCl, 0.1% SDS, 1 mM EDTA). 30 µL of 20 mg/mL proteinase K (Invitrogen #25530-015) was added to each sample. Samples were subsequently vortexed for 10 seconds to lyse cells. Lysed samples were incubated at 55°C overnight to allow for protein digestion. The following day 300 µL of phenol:chloroform:isoamyl alcohol (Sigma #77617) was added. Samples were inverted 10 times and centrifuged at 8,000 rcf for 15 minutes. 250 µL of supernatant was transferred to a clean microcentrifuge tube and an equal volume of chloroform was added. Samples were again mixed through inversion and centrifuged at 8,000 rcf for 15 minutes. 200 µL supernatant was transferred to a clean microcentrifuge tube. 220 µL isopropanol and 20 µL 3M sodium acetate were added and samples were incubated at -20°C overnight to precipitate DNA. The following day samples were centrifuged at 8,000 rcf for 15 minutes to pellet DNA. Pellets were washed twice in 70% EtOH. Pellets were air dried briefly prior to resuspension in 250 µL nuclease-free water. DNA concentration was determined and adjusted to a final concentration of 5 ng/µL by measuring A260/280 ratios.

mtDNA:Nuclear DNA Ratio Quantification via qPCR

2 µL of 5 ng/µL DNA were used per qPCR reaction. Total reaction mix included 2 µL template, 5 µL 2x Powerup SYBR Green Master Mix (Applied Biosystems #A25742), 1 µL forward primer, 1 µL reverse primer, and 1 µL nuclease free water for a total reaction volume of 10 µL. mtDNA levels were determined using primers targeting *MT-ND1* (Forward primer: 5'-CCA CCT CTA GCC TAG CCG TTT-3' ; reverse primer 5'-TGT TTG GGC TAC TGC TCG C-3'). Nuclear DNA content was measured using primers targeting *β2M* (Forward primer: 5'-

TGC TGT CTC CAT GTT TGA TGT ATC-3'; reverse primer: 5'-TCT CTG CTC CCC ACC TCT AAG T-3'). The run method included single incubation steps of 50°C for 2 minutes followed by 95 °C for 2 minutes. Next 40 cycles were performed of 95°C for 3 seconds and 60°C for 30 seconds. Finally, a melt curve was obtained by single incubations with a step and hold of 5 seconds of 95°C for 15 seconds, 60°C for 1 minute, and 95°C for 15 seconds. qPCR was performed as described previously.

Statistical Analysis

Initial power calculations were performed on preliminary data generated to measure statistical significance at 80% power with an α of 0.05 where 24-hour exposure of βOHB increased basal OCR in SH-SY5Y's by 15% compared to vehicle with a standard deviation of 16% indicating we would need an n of 18 per group. Since this time, our ability to normalize Seahorse data has improved greatly due to new technology in the lab, but we did not wish to reduce our n once experiments had begun. Therefore, unless otherwise stated, all experiments herein utilize groups where n = 18 per group where n is the number of independent cell culture preparations. Data were summarized as either means with standard deviations or means with standard errors. To compare means between two groups we used unpaired two-tailed Student's T-test. To compare means between three or more groups where only one variable was manipulated experimentally, we used one-way analysis of variance (ANOVA) to determine initial significance followed by Tukey's *post hoc* testing. To compare means between three or more groups where two variables were manipulated experimentally, we used two-way ANOVA with Tukey's multiple comparisons testing between groups. To estimate cell doubling time we used exponential (Malthusian) growth curves to determine best fit. A statistically significant outcome was determined where p-values were found to be less than 0.05. No randomization or

blinding was used to allocate or evaluate individual cell wells in this study. All statistical calculations were performed in GraphPad Prism 8 software.

Table 2-1: List of antibodies used in experiments

Antibody Name	Dilution	Source	Catalog #
GFAP	1:1000	abcam	#ab7620
MAP2	1:500	abcam	#ab32454
AlexaFluor Goat Anti-Rabbit 488	1:2000	abcam	#ab150077
NDP52	1:1000	Cell Signaling Technologies	#60732
BNIP3	1:1000	Cell Signaling Technologies	#44060
Nix/BNIP3L	1:1000	Cell Signaling Technologies	#12396
LC3B	1:1000	Cell Signaling Technologies	#3868
pT308 Akt	1:1000	Cell Signaling Technologies	#2965
pS473 Akt	1:1000	LifeTechnologies	#700392
Total Akt	1:1000	Cell Signaling Technologies	#4685
Acetylated Histone 3 Lysine 9	1:1000	Cell Signaling Technologies	#9649
pS79 ACC1	1:1000	Cell Signaling Technologies	#3661
Total ACC1	1:1000	Cell Signaling Technologies	#3676
β-tubulin	1:1000	Cell Signaling Technologies	#2146
Total Histone 3	1:2000	Cell Signaling Technologies	#4499
Oct4	1:1000	abcam	#ab18976
pT389 p70 S6 Kinase	1:500	Cell Signaling Technologies	#9206
Total p70 S6 Kinase	1:1000	Cell Signaling Technologies	#2708
pS293 PDHE1α	1:1000	abcam	#ab92696

Table 2-2: List of primers used in experiments.

Primer	Type/Sequence	Catalog
18S	Taqman	Hs03003631_g1
POU5F1	Taqman	Hs00999634_gH
myc	Taqman	Hs00153408_m1
Sox2	Taqman	Hs04234836_s1
MT-ND1 Forward	5’-CCA CCT CTA GCC TAG CCG TTT-3’	N/A
MT-ND1 Reverse	5’-TGT TTG GGC TAC TGC TCG C-3’	N/A
β2M Forward	5’-TGC TGT CTC CAT GTT TGA TGT ATC-3’	N/A
β2M Reverse	5’-TCT CTG CTC CCC ACC TCT AAG T-3’	N/A

Results

β-hydroxybutyrate enhances mitochondrial respiration while altering ADP/ATP and NAD^+/NADH ratios in SH-SY5Y cells.

To test the utility of SH-SY5Y neuroblastoma cells on studying the effects of ketone body metabolism *in vitro* we first wanted to confirm that SH-SY5Y cells utilize βOHB as a substrate for ketolysis that led to increased oxidative phosphorylation and mitochondrial respiration. For this, we performed a mitochondrial stress test using the Seahorse XFe96 Analyzer to assess mitochondrial function and how βOHB impacts multiple facets of cellular bioenergetics. βOHB significantly increased basal respiration when cells were exposed both acutely and chronically (**Fig. 2-1A-B** Vehicle 1.11 ± 0.13 pmol/min/1000 cells, 24-Hour βOHB 1.22 ± 0.11 pmol/min/1000 cells, Chronic βOHB 1.34 ± 0.12 pmol/min/1000 cells; mean ± SD, p = 0.0084 one-way ANOVA). Basal ECAR was only reduced with chronic exposure to βOHB (**Fig. 2-1A&C** Vehicle 2.70 ± 0.37 mpH/min/1000 cells, 24-Hour βOHB 2.67 ± 0.28 mpH/min/1000 cells, Chronic βOHB 2.54 ± 0.27 mpH/min/1000 cells; mean ± SD, p = 0.0151 one-way ANOVA). Increases in basal respiration were associated with increased OCR associated with ATP production rate (**Fig. 2-1D** Vehicle 0.19 ± 0.03 pmol/min/1000 cells, 24-Hour 0.31 ± 0.07 pmol/min/1000 cells, Chronic βOHB 0.39 ± 0.07 pmol/min/1000 cells; mean ± SD, p < 0.0001 one-way ANOVA) as well as an increased proton leak rate leading to a reduced coupling efficiency (**Fig. 2-1E** Vehicle 82.44 ± 3.38%, 24-Hour βOHB 74.68 ± 4.81%, Chronic βOHB 70.70 ± 5.21%; mean ± SD, p < 0.0001 one-way ANOVA). No differences in spare respiratory capacity or maximal respiratory capacity were observed in SH-SY5Y cells as these cells typically do not feature a spare capacity exceeding their basal respiration rate.

To further validate differences in respiration associated with ATP production rate we utilized a ADP/ATP ratio assay kit to determine if βOHB induced changes in the overall ratio of

these species. Indeed, we found that chronic, but not acute, treatment with βOHB reduced the ADP/ATP ratio in SH-SY5Y cells (**Fig. 2-2A** Vehicle 0.22 ± 0.02, 24-Hour βOHB 0.22 ± 0.01, Chronic βOHB 0.18 ± 0.02; mean ± SD, $p < 0.0001$ one-way ANOVA). Since we were providing an additional substrate for the TCA cycle, we also wished to verify if we were altering the balance of NAD^+/NADH species. We were able to demonstrate that this ratio was also increased under chronic, but not acute, conditions (**Fig. 2-2B** Vehicle 3.78 ± 0.86, 24-Hour βOHB 3.54 ± 0.85, Chronic βOHB 5.74 ± 2.19; mean ± SD, $p = 0.0011$ one-way ANOVA).

β-hydroxybutyrate reduces mitochondrial membrane potential (Ψ_m) in SH-SY5Y cells.

To further confirm the reduced coupling efficiency observed in mitochondrial stress test experiments we examined SH-SY5Y's cultured in the presence of βOHB using multiple dyes whose uptake is sensitive to mitochondrial membrane potential. Imaging with TMRE labeling indicated reduced Ψ_m with chronic βOHB (**Fig. 2-3A-B** Vehicle 100 ± 21.02%, 24-Hour βOHB 92.80 ± 9.74%, Chronic βOHB 71.49 ± 10.28%; mean ± SD, $p < 0.0001$ one-way ANOVA). FCCP was used as a positive control and was found to reduce Ψ_m to 38.34 ± 7.54% the intensity observed in Vehicle SH-SY5Y cells. JC1 dye showed reduced red/green ratio only in chronic βOHB samples when compared to vehicle (**Fig. 2-4** Vehicle 1.13 ± 0.15, 24-Hour βOHB 1.06 ± 0.14, Chronic βOHB 0.96 ± 0.15; mean ± SD, $p = 0.0010$ one-way ANOVA). Finally, uptake of nonyl acridine orange was reduced with both 24-hour and chronic βOHB treatment (**Fig. 2-5** Vehicle 100 ± 4.85%, 24-Hour βOHB 86.11 ± 12.92%, Chronic βOHB 77.03 ± 11.37%; mean ± SD, $p < 0.0001$ one-way ANOVA).

β-hydroxybutyrate increases autophagic capacity and increases mitochondrial mass in SH-SY5Y cells.

Reduced mitochondrial membrane potential can serve as a stress signal to initiate autophagy and, more specifically, mitophagy. To determine if this was the case an autophagy

flux assay was performed and relative amounts of autophagy and mitophagy components were measured via Western blotting. We measured an increase in the ratio of LC3BII/LC3BI in both bafilomycin untreated and treated samples when cells were cultured chronically in βOHB (**Fig. 2-6A-B** Vehicle w/o bafilomycin 100 ± 22.94%, 24-Hour βOHB w/o bafilomycin 98.56 ± 27.27%, Chronic βOHB w/o bafilomycin 156.60 ± 69.91%, Vehicle w/ bafilomycin 211.18 ± 96.70%, 24-Hour βOHB w/ bafilomycin 213.80 ± 91.36%, Chronic βOHB w/ bafilomycin 263.26 ± 121.41%; mean ± SD, p = 0.0093 by two-way ANOVA). We did not measure a difference in the delta between the two states when compared to vehicle autophagy flux delta (Vehicle +111.18 ± 116.43%, 24-Hour βOHB +103.66 ± 82.18%, Chronic βOHB +106.66 ± 110.42; mean ± SD). We noted a similar trend in the levels of mitophagy adaptor protein NDP52 (**Fig. 2-6C** Vehicle w/o bafilomycin 100 ± 27.59%, 24-Hour w/o bafilomycin 88.33 ± 27.65%, Chronic βOHB w/o bafilomycin 131.33 ± 38.82%, Vehicle w/ bafilomycin 170.23 ± 65.14%, 24-Hour βOHB w/ bafilomycin 198.44 ± 61.38%, Chronic βOHB w/ bafilomycin 256.98 ± 118.56%, p = 0.0045 two-way ANOVA). BNIP3, a regulator of Ψ_m for the purpose of initiating mitophagy, was increased by chronic βOHB treatment in bafilomycin treated cells (**Fig. 2-6D** Vehicle w/o bafilomycin 100 ± 45.37%, 24-Hour βOHB w/o bafilomycin 89.69 ± 39.73%, Chronic βOHB w/o bafilomycin 97.14 ± 34.68%, Vehicle w/ bafilomycin 423.58 ± 278.11%, 24-Hour βOHB w/ bafilomycin 461.70 ± 205.72%, Chronic βOHB w/ bafilomycin 1,679.07 ± 1,688.67%; mean ± SD, p = 0.0009 by two-way ANOVA). We detected not significant effect of βOHB on the related protein Nix/BNIP3L (**Fig. 2-6E** Vehicle w/o bafilomycin 100 ± 31.34%, 24-Hour βOHB w/o bafilomycin 64.13 ± 39.74%, Chronic βOHB w/o bafilomycin 198.82 ± 191.48%, Vehicle w/ bafilomycin 417.15 ± 85.99%, 24-Hour βOHB w/ bafilomycin 588.98 ± 241.17%, Chronic βOHB w/ bafilomycin 775.64 ± 868.62%; mean ± SD, p = 0.0608 by two-way

ANOVA). Although there was a difference between vehicle and chronically treated cells in the bafilomycin group following post-hoc analysis via Tukey's multiple comparisons test ($p = 0.0274$).

To approximate relative amounts of mitochondrial mass we isolated genomic DNA from SH-SY5Y cells and performed qPCR on mitochondrial DNA (mtDNA) and nuclear DNA (nDNA) targets for ΔΔCt analysis. Relative amounts of *MT-ND1* were referenced to *β2M* under different treatment conditions. We found that both 24-hour and chronic exposure to βOHB increased amounts of *MT-ND1* mtDNA relative to *β2M* nDNA (**Fig. 2-7** Vehicle 100 ± 19.98%, 24-Hour βOHB 154.50 ± 37.39%, Chronic βOHB 132.35 ± 23.83%; mean ± SD, $p = 0.0003$ by one-way ANOVA).

β-hydroxybutyrate slows metabolic activity and reduces cellular growth rate in SH-SY5Y cells without reducing viability.

Given that chronic βOHB increased mitochondrial respiration and shifted the ADP/ATP ratio in favor of ATP we hypothesized that the additional carbon source was enhancing metabolic activity and cell growth in SH-SY5Y cells. To test this, we performed the MTT assay to assess general metabolic activity. Both 24-hour and chronic βOHB limited the ability of SH-SY5Y cells to reduce the formazan dye relative to vehicle (**Fig. 2-8** Vehicle 100 ± 16.31%, 24-Hour βOHB 66.93 ± 6.34%, Chronic βOHB 40.32 ± 4.42%; mean ± SD, $p < 0.0001$ by one-way ANOVA). To ensure βOHB treatment was not lethal a TUNEL assay was performed and no significant difference in cell death was observed between treatment groups (**Fig. 2-9** Vehicle 967 ± 130, 24-Hour βOHB 1,105 ± 341, Chronic βOHB 936 ± 136; mean ± SD). All observed values were substantially lower than the positive control of camptothecin treated HeLa cells provided

by the kit manufacturer (mean 83,649 ± 4736, n = 3, p = 0.0045 one-way ANOVA) and were not significantly different from one another upon post-hoc analysis.

We next performed a cell growth assay to determine if reduced metabolic activity was associated with reduced division. No statistically significant difference was observed for the first two days post-split. On day 3, SH-SY5Y's chronically cultured in βOHB were significantly less numerous than cells grown in vehicle media (**Fig. 2-10** Vehicle 1,380,167 ± 310,354 cells, Chronic βOHB 698,300 ± 241,588 cells; mean ± SD, p = 0.000005 by unpaired t-test). This was estimated to result in an increase in cell doubling time from 17.40 hours to 30.22 hours by Malthusian growth best fit. To determine if the reduced cell growth was associated with a defect of progression through a specific portion of the cell cycle, we performed propidium iodide cell cycle analysis following double thymidine synchronization and release. The greatest difference was observed at 18-hours post release with an accumulation of cells in G0-G1 phase in chronically treated SH-SY5Y's (**Fig. 2-11** %G0-G1: Vehicle 58.47 ± 2.47%, Chronic βOHB 65.91 ± 1.54%, %S: Vehicle 24.94 ± 0.56%, Chronic βOHB 19.97 ± 0.87%, %G2-M: Vehicle 16.60 ± 2.86%, Chronic βOHB 14.12 ± 0.91%; mean ± SD, p < 0.0001 by two-way ANOVA).

β-hydroxybutyrate reduces activation of the PI3K-Akt-mTOR pathway and induces transcription of Yamanaka factors in SH-SY5Y cells.

As mTOR is a well-recognized regulator for the transition from G1 to S phase during mitotic division, we next sought to examine the activation status of the PI3K-Akt-mTOR pathway (**Fig. 2-12**). Chronic βOHB treatment was found to reduce Akt phosphorylation at both of its primary activation sites while increasing the total protein level of Akt in SH-SY5Y whole cell lysates (pT308/Total Akt: Vehicle 100 ± 74.33%, Chronic βOHB 16.76 ± 18.13%, pS473/Total Akt: Vehicle 100 ± 52.2%, Chronic βOHB 48.57 ± 25.67%, Total Akt: Vehicle 100

± 30.39%, Chronic βOHB 214.54 ± 160.46%; mean ± SD, p = 0.0002, 0.0009, and 0.008 respectively by unpaired t-test). The downstream target p70 S6 Kinase also demonstrated reduced phosphorylation at its T389 activation site when measured alone although significance is lost when adjusting for total p70 S6 Kinase (pT389/Total p70 S6 Kinase: Vehicle 100 ± 65.66%, Chronic βOHB 55.60 ± 46.80%; mean ± SD, p = 0.0710 by unpaired t-test).

Upon observing reduced metabolic activity, growth rate, and PI3K-Akt-mTOR activation, we hypothesized that βOHB was inducing cellular quiescence. With this, we first sought to determine if βOHB was capable of inducing histone acetylation in SH-SY5Y cells as had been previously reported in other cell types. βOHB did indeed increase histone 3 acetylation at lysine 9 but significance is lost when adjusting for total histone 3 levels (Acetyl-H3K9: Vehicle 100 ± 14.96%, Chronic βOHB 132.6 ± 22.25%, Acetyl-H3K9/Total H3 Vehicle 100 ± 38.21%, Chronic βOHB 123.3 ± 41.30%, mean ± SD, p = 0.0277 and 0.36 respectively). Given the increased acetylation when measured alone we next examined transcript levels of the quiescence regulating Yamanaka factors Oct4 (*POU5F1*), myc, Sox2, and Klf4 to determine if transcription was being activated to signal quiescence. Both 24-hour and chronic treatments with βOHB increased transcription of Oct4, myc, and Sox2 while we were unable to detect transcripts for Klf4 in any of the treatment groups (**Fig. 2-13** Oct4: Vehicle 100 ± 59.55%, 24-Hour βOHB 512.60 ± 320.12%, Chronic βOHB 595.83 ± 557.11%, myc: Vehicle 100 ± 58.34%, 24-Hour βOHB 134.60 ± 57.40%, Chronic βOHB 183.01 ± 77.82%, Sox2: Vehicle 100 ± 48.34%, 24-Hour βOHB 274.17 ± 192.06%, Chronic βOHB 325.21 ± 314.23%; mean ± SD, p = 0.0212, 0.0204, and 0.0598 respectively by one-way ANOVA).

β-hydroxybutyrate reduces AMPK activation, increases lipid droplet number, and reduces cellular triglyceride and cholesterol content in SH-SY5Y cells.

We next sought to determine if βOHB signaled nutrient scarcity through other pathways in addition to our observations of the PI3K-Akt-mTOR pathway. We investigated AMPK activation status through its downstream substrate ACC1. Chronic βOHB supplementation reduced S79 ACC1 phosphorylation indicating reduced AMPK activation (**Fig. 2-14** Vehicle 100 ± 45.67%, Chronic βOHB 56.43 ± 34.21%; mean ± SD, $p = 0.0190$ by unpaired t-test). As ACC1 serves as the rate-limiting step for de novo lipogenesis we next investigated if βOHB altered lipid content within SH-SY5Y cells through lipid droplet staining with BODIPY dye. βOHB increased the total number of lipid droplets per cell (**Fig. 2-15** Vehicle 1.39 ± 0.75, 24-Hour βOHB 2.27 ± 0.84, Chronic βOHB 3.30 ± 0.73; mean ± SD, $p < 0.0001$ by one-way ANOVA). We also measured cellular triglyceride content directly and found that chronic βOHB supplementation reduced triglyceride content (**Fig. 2-16** Vehicle 0.068 ± 0.010 nmol TG/μg protein, 24-Hour βOHB 0.068 ± 0.009 nmol TG/μg protein, Chronic βOHB 0.050 ± 0.005 nmol TG/μg protein; mean ± SD, $p < 0.0001$ by one-way ANOVA).

Since malonyl-CoA produced by ACC1 can also serve as a substrate for the synthesis of cholesterol, we examined if βOHB altered the amount of cholesterol in SH-SY5Y cells. βOHB reduced filipin III intensity at both 24-hours and when chronically administered (**Fig. 2-17** Vehicle 18,144 ± 4,407, 24-Hour βOHB 14,776 ± 2,660, Chronic βOHB 12,918 ± 2,494; mean ± SD, $p = 0.0003$ by one-way ANOVA). We also wished to further expand on possible alterations on carbon flux into the mitochondria by expanding on our earlier finding of reduced ECAR. We examined the phosphorylation status of the primary catalytic subunit of the pyruvate dehydrogenase complex PDHE1α modulated by pyruvate dehydrogenase kinase. We found that

βOHB increased levels of inhibitory phosphorylation of PDHE1α (**Fig. 2-18** Vehicle 100 ± 32.07%, Chronic βOHB 193.9 ± 112.8%, mean ± SD, p = 0.0029 by unpaired t-test).

β-hydroxybutyrate differentially effects the PI3K-Akt-mTOR pathway based upon cell type.

We followed up on our earlier observations in SH-SY5Y cells to determine if βOHB had a conserved effect to modulate cell signaling pathways in cell types more relevant to mammalian physiology: primary neurons and astrocytes (**Fig. 2-19**). Like SH-SY5Y cells, primary neurons exhibited reduced Akt phosphorylation at both regulation sites (**Fig. 2-20** pT308/Total Akt: Vehicle 100 ± 61.12%, Chronic βOHB 32.33 ± 31.41%; pS473/Total Akt: Vehicle 100 ± 48.32%, Chronic βOHB 54.57 ± 35.39%; mean ± SD, p = 0.0035 and 0.0161 by unpaired t-test respectively). Neurons also demonstrated increased histone 3 lysine 9 acetylation in response to βOHB (Vehicle 100 ± 20.80%, Chronic βOHB 159.10 ± 52.62%, mean ± SD, p = 0.0065 by unpaired t-test). Primary neurons also had increased protein level of Oct4 when cultured in the presence of βOHB (Vehicle 100 ± 33.00%, Chronic βOHB 157.57 ± 85.12%; mean ± SD, p = 0.0461 by unpaired t-test).

Unlike neurons, primary rat astrocytes had a non-significant increase in pT308 phosphorylation of Akt (**2-21** Vehicle 100 ± 116.76%, Chronic βOHB 242.95 ± 139.92%; mean ± SD, p = 0.1187 by unpaired t-test). While pS473 was reduced as in neurons (Vehicle 100 ± 108.91%, Chronic βOHB 28.19 ± 9.31%; mean ± SD, p = 0.0072 by unpaired t-test). Astrocytes did not increase histone acetylation in response to βOHB (Vehicle 100 ± 40.38%, Chronic βOHB 115.10 ± 41.97%, mean ± SD, p = 0.3781 by unpaired t-test). Astrocytes also exhibited only a single Oct4 band under vehicle conditions and a doublet when treated with βOHB (Vehicle 100 ± 21.89%, Chronic βOHB 180.72 ± 56.36%; mean ± SD, p = 0.0293).

β-hydroxybutyrate enhanced respiration in primary rat neurons in a manner similar to that observed in SH-SY5Y cells.

We expanded our observations in primary cells by performing mitochondrial stress tests on primary neurons and found that βOHB increased basal respiration as expected (**Fig. 2-22** Vehicle 2.54 ± 0.61 pmol/min/1000 cells, 24-Hour βOHB 3.25 ± 0.35 pmol/min/1000 cells, Chronic βOHB 4.34 ± 0.90 pmol/min/1000 cells; mean ± SD, $p < 0.0001$ by one-way ANOVA). Interestingly, unlike SH-SY5Y cells, primary neurons demonstrated an increased basal ECAR with chronic βOHB treatment (Vehicle 0.70 ± 0.07 mpH/min/1000 cells, 24-Hour βOHB 0.70 ± 0.06 mpH/min/1000 cells, Chronic βOHB 0.80 ± 0.16 mpH/min/1000 cells; mean ± SD, $p = 0.0064$ by one-way ANOVA). Chronic βOHB also induced an increased ATP production rate in primary neurons (Vehicle 1.55 ± 0.64 pmol/min/1000 cells, 24-Hour βOHB 1.41 ± 0.85, Chronic βOHB 3.08 ± 1.79 pmol/min/1000 cells; mean ± SD, $p = 0.0003$ by one-way ANOVA). βOHB had a preserved ability to increase leak rate in primary neurons (Vehicle 1.00 ± 0.64 pmol/min/1000 cells, 24-Hour βOHB 1.84 ± 0.89 pmol/min/1000 cells, Chronic βOHB 1.92 ± 1.00 pmol/min/1000 cells; mean ± SD, $p = 0.0054$ by one-way ANOVA). This increased leak rate did not associate with a significant reduction in coupling percentage (Vehicle 61.34 ± 21.47%, 24-Hour βOHB 43.68 ± 26.43%, Chronic βOHB 53.83 ± 25.75%; mean ± SD, $p = 0.1110$ by one-way ANOVA). βOHB increased maximum respiration at both 24-hour and chronic timepoints (Vehicle 3.35 ± 1.37 pmol/min/1000 cells, 24-Hour βOHB 5.73 ± 1.26 pmol/min/1000 cells, Chronic βOHB 5.69 ± 1.07 pmol/min/1000 cells; mean ± SD, $p < 0.0001$ by one-way ANOVA). Although this increase in maximum respiration was only associated with an increased spare capacity with 24-hour βOHB (Vehicle 0.81 ± 0.86 pmol/min/1000 cells, 24-Hour βOHB 2.49 ± 1.08 pmol/min/1000 cells, Chronic βOHB 1.07 ± 0.62 pmol/min/1000 cells; mean ± SD, $p < 0.0001$ by one-way ANOVA). Finally, both 24-hour and chronic exposure to

βOHB increased non-mitochondrial respiration in primary rat neurons (Vehicle 0.68 ± 0.20 pmol/min/1000 cells, 24-Hour βOHB 0.89 ± 0.22 pmol/min/1000 cells, Chronic βOHB 1.05 ± 0.30 pmol/min/1000 cells; mean ± SD, p = 0.0002 by one-way ANOVA).

β-hydroxybutyrate does not alter basal fluxes in primary rat astrocytes but does increase respiratory capacity and improves mitochondrial efficiency.

We next investigated if βOHB's effects are conserved across cell types in the CNS or if there exists a specialized response to metabolite availability as a function of cell type. For this, we performed a mitochondrial stress test on primary rat astrocytes to investigate the effects of βOHB on non-neuronal CNS cells. βOHB did not increase basal respiration in astrocytes unlike SH-SY5Y cells and primary neurons (**Fig. 2-23** Vehicle 2.93 ± 0.74 pmol/min/1000 cells, Chronic βOHB 2.85 ± 0.73 pmol/min/1000 cells; mean ± SD, p = 0.7309 by unpaired t-test). There was also no observed increase in basal ECAR (Vehicle 1.10 ± 0.20 mpH/min/1000 cells, Chronic βOHB 1.15 ± 0.29 mpH/min/1000 cells; mean ± SD, p = 0.5484 by unpaired t-test). There was an observed reduction in leak rate with βOHB treatment (Vehicle 0.71 ± 0.21 pmol/min/1000 cells, Chronic βOHB 0.53 ± 0.17 pmol/min/1000 cells; mean ± SD, p = 0.0071 by unpaired t-test). Reduced leak was associated with an increased coupling percentage (Vehicle 75.89 ± 2.48%, Chronic βOHB 81.34 ± 3.64%; mean ± SD, p < 0.0001 by unpaired t-test). βOHB did increase maximum and spare respiratory capacity in primary astrocytes (Maximum Capacity: Vehicle 8.93 ± 1.93 pmol/min/1000 cells, Chronic βOHB 10.65 ± 1.36 pmol/min/1000 cells; Spare Capacity: Vehicle 6.00 ± 1.21 pmol/min/1000 cells, Chronic βOHB 7.80 ± 1.12 pmol/min/1000 cells; mean ± SD, p = 0.0042 and <0.0001 respectively by unpaired t-test). There was no observed difference in non-mitochondrial respiration (Vehicle 1.65 ± 0.41 pmol/min/1000 cells, Chronic βOHB 1.57 ± 0.37 pmol/min/1000 cells; mean ± SD, p = 0.5297 by unpaired t-test).

Discussion

In the present study we investigated the ability of the primary ketone body, β-hydroxybutyrate, to support mitochondrial energy production and effect molecular signaling pathways important to cell growth and division in both neurons and astrocytes *in vitro*. βOHB increased respiration and induced uncoupling in both SH-SY5Y neuroblastoma cells and primary rat neurons but not in primary astrocytes. Increased maximal respiration and spare capacity in response to βOHB was only observed in primary cultures. Interestingly, only chronic exposure to βOHB was able to shift ratios of ADP/ATP and NAD^+/NADH. Reduced metabolic activity as measured by MTT assay points to a more oxidative intracellular environment in agreement with the shift in NAD^+/NADH ratios. We further showed that changes in mitochondrial leak rate were associated with mitochondrial membrane depolarization and increased mitochondrial mass despite indications of possibly increased autophagy and mitophagy.

The stark differences in mitochondrial response to βOHB between neurons and astrocytes are of considerable interest. On first impression neurons are behaving exactly as one would expect in response to the availability of a fuel source. Astrocytes however are peculiar in that they are not simply inert to βOHB, but they have a specific response separate from their own energy production. Expanded maximal respiration and spare capacity, to an extent far greater to that measured in our neuronal cultures, could be indicative of increased mitochondrial mass. It is possible that this increased mitochondrial mass could be serving an anabolic purpose in astrocytes and a catabolic purpose in neurons. Others have suggested and produced some data to suggest that astrocytes can perform ketogenesis as a means of regulating food intake in the ventromedial hypothalamus. (Le Foll, Dunn-Meynell, & Levin, 2015; Le Foll et al., 2014; Le Foll, Dunn-Meynell, Miziorko, et al., 2015; Le Foll & Levin, 2016). It's possible that ketones

themselves serve as a signal to upregulate mitochondrial mass in astrocytes so that they may have a greater capacity to perform ketogenesis themselves.

While increases in NAD^+/NADH ratio first appear to be incongruent with increased mitochondrial respiration it is important to consider several factors. The first being that we measured whole cell ratios and that the ratio found within the mitochondrial matrix may differ substantially. Secondly, this shift would be expected in a system where energy becomes derived via ketolysis while sparing glucose and reducing glycolytic flux. This is due to the stoichiometry of the reactions wherein ketolysis is known to produce one reduced equivalent of NADH while generating two molecules of Acetyl-CoA from βOHB while glycolysis produces two molecules of NADH for every molecule of glucose. Finally, one feature of aging is the reduction of total levels of NAD^+ (Johnson & Imai, 2018). This has led to the suggestion that therapeutic strategies to reverse this loss could have positive effects possibly through NAD^+ sensitive enzymes such as the sirtuin family of deacetylases or poly-ADP-ribose polymerases (PARPs) (Julien et al., 2009; Lutz, Milenkovic, Regelsberger, & Kovacs, 2014; Ng, Wijaya, & Tang, 2015).

Strikingly, the addition of βOHB was able to inhibit signaling through the PI3K-Akt-mTOR pathway despite serving as an additional carbon source and supporting energy production. This reduced signaling was associated with reduced growth rate of SH-SY5Y cells with a defect at transition from G1 to S phase. Suppression of the Akt system was conserved in primary neurons. Astrocytes appear to be suppressed as well as neurons but through a different mechanism. Where SH-SY5Y's and neurons reduce activating phosphorylation of Akt but increase total protein levels, astrocytes were observed to have markedly diminished amounts of total Akt. Reductions in PI3K-Akt-mTOR signaling align well with increased levels of

Yamanaka factors that would induce quiescent behavior. Our data further expands findings of βOHB's ability to induce Oct4 expression in cells other than vasculature (Han et al., 2018).

This ability to simultaneously support bioenergetics while signaling nutrient scarcity to activate stress response pathways could help to explain the ability to extend lifespan and preserve memory in aged mice (Newman et al., 2017). Previously, it had been considered that reduced mTOR activation on ketogenic diet was due to reduced insulin signaling secondary to carbohydrate restriction of the diet. However, here we demonstrate that the ketone body itself is capable of inducing these signaling effects independent to carbohydrate content of the cell culture medium.

Of note, not all nutrient sensing pathways indicated scarcity. AMPK appeared to be less active in conditions where βOHB was supplemented in media as measured by its downstream target ACC1. Increased ACC1 activation was associated with increased lipid droplet formation although triglycerides appeared to be decreased with chronic βOHB exposure. βOHB also reduced cellular cholesterol content in addition to reduced TGs. Taken together it is possible that ketone bodies have a general catabolic signaling effect to consume other sources of carbon to stave off possible starvation. If true, it is puzzling why AMPK would not inhibit ACC1 to prevent futile cycling between Acetyl-CoA and fats through *de novo* lipogenesis. One possibility could be that activation of too many stress pathways could act as a queue for the cell to commit to pro-apoptotic pathways and that the presence of βOHB alone is enough to inhibit such a commitment.

Finally, we would be remised to not acknowledge the limitations of the present study. We appreciated that immortalized, undifferentiated neuroblastoma cells have fundamentally different

metabolic profiles and behaviors to primary cells of the central nervous system and so we sought to expand our models used in the current study. So too must we acknowledge that primary cells derived from embryonic rat cortex fail to recapitulate not only the *in vivo* microenvironment in all its complexity, but they also fail to model any lifespan associated changes to gene expression or accumulated damage to mimic an aged cell. Future studies would benefit to devise a method to study the effects of long-term ketogenic diet intervention *in vivo* across multiple CNS cell types in a high throughput and unbiased manner. In so doing we can further define the relevant effects of the ketogenic diet and further work to develop effective dietary mimetics for the treatment of neurodegenerative disease and to promote healthy aging.

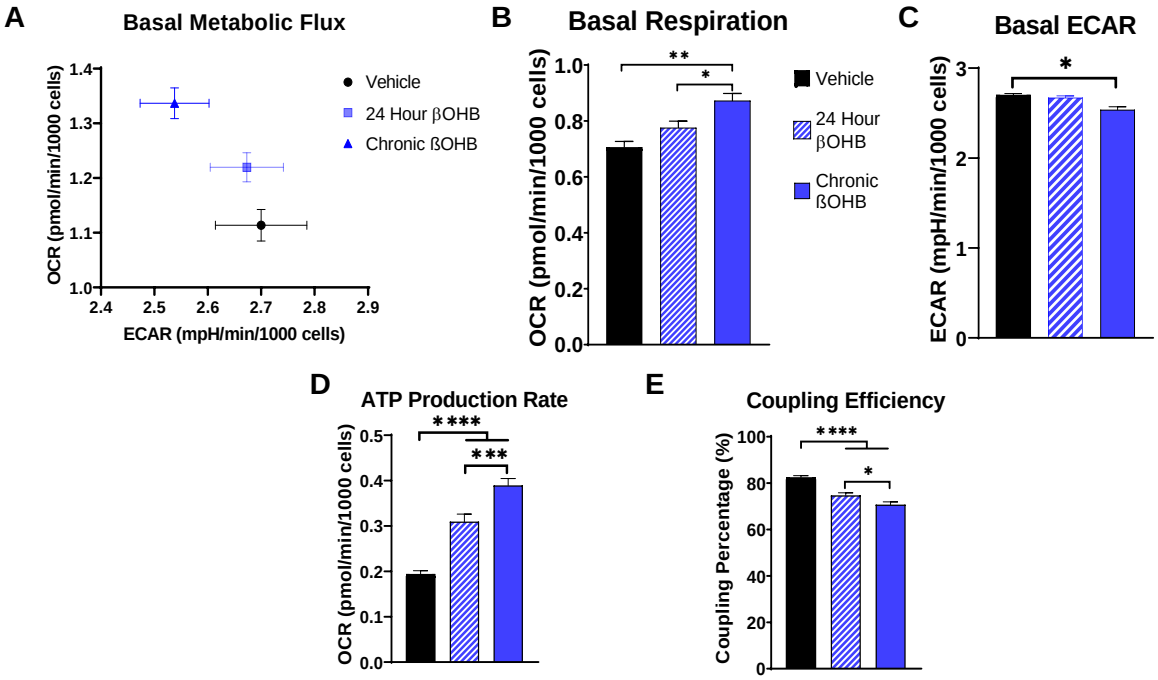
A
Basal Metabolic Flux
OCR (pmol/min/1000 cells)
ECAR (mpH/min/1000 cells)
Vehicle
24 Hour βOHB
Chronic ßOHB
B
Basal Respiration
OCR (pmol/min/1000 cells)
**
*
Vehicle
24 Hour βOHB
Chronic ßOHB
C
Basal ECAR
ECAR (mpH/min/1000 cells)
*
D
ATP Production Rate
OCR (pmol/min/1000 cells)
****
***
E
Coupling Efficiency
Coupling Percentage (%)
****
*

Figure 2-1: β-hydroxybutyrate increases basal respiration and reduces basal extracellular acidification rate in SH-SY5Y cells. A) Shifts in OCR and ECAR become more pronounced with longer exposure to βOHB *in vitro*. B) Both acute and chronic exposure to βOHB increased basal OCR. C) Chronic exposure to βOHB reduced basal ECAR. D) OCR associated with ATP production was increased both acutely and chronically with βOHB. E) Coupling efficiency was reduced by βOHB treatment. (n = 18 per group. *, **, ***, **** correspond to p-values < 0.05, 0.01, 0.001, and 0.0001 respectively. Error bars represent SEM).

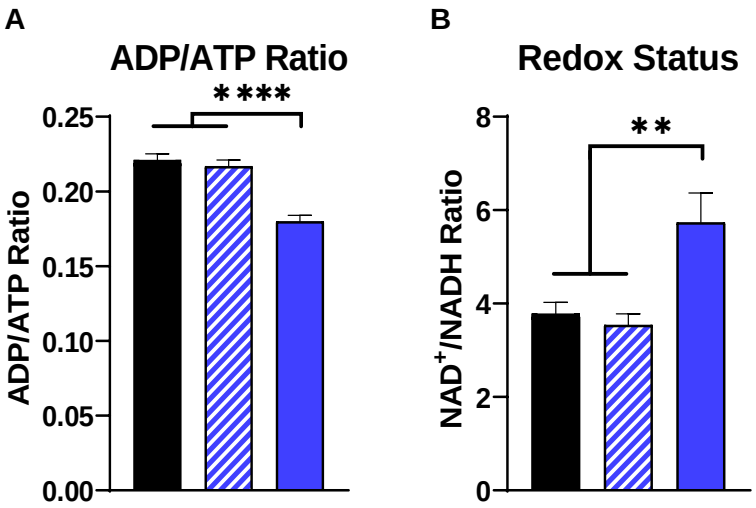
A
ADP/ATP Ratio
****
ADP/ATP Ratio
0.25
0.20
0.15
0.10
0.05
0.00
B
Redox Status
**
NAD+/NADH Ratio
8
6
4
2
0

Figure 2-2: β-hydroxybutyrate shifts ADP/ATP and NAD^+/NADH ratios chronically but not acutely in SH-SY5Y cells. A) ADP/ATP ratio was decreased with chronic exposure to βOHB. B) NAD^+/NADH ratio was increased with chronic βOHB treatment. (n = 18 per group. *, **, ***, **** correspond to p-values < 0.05, 0.01, 0.001, and 0.0001 respectively. Error bars represent SEM).

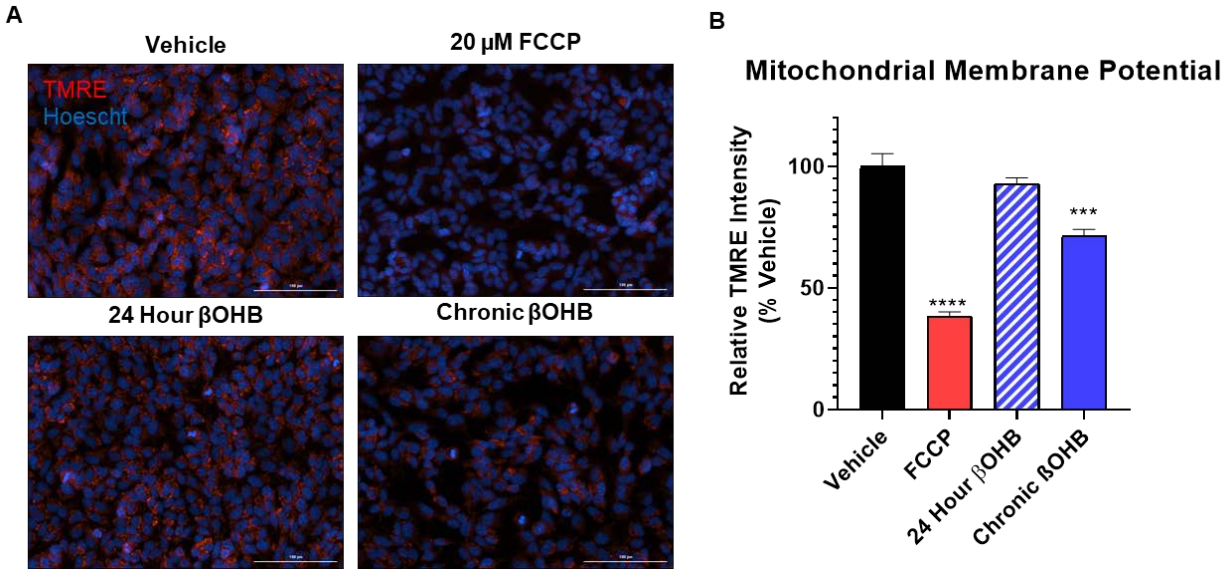
A
Vehicle
20 μM FCCP
TMRE
Hoescht
24 Hour βOHB
Chronic βOHB
B
Mitochondrial Membrane Potential
Relative TMRE Intensity (% Vehicle)
100
50
0
****
***
Vehicle
FCCP
24 Hour βOHB
Chronic βOHB

Figure 2-3: β-hydroxybutyrate reduces mitochondrial membrane potential in SH-SY5Y cells. A) Representative images of TMRE labeling of SH-SY5Y cells under different conditions with Hoechst nuclear stain. B) βOHB reduced mitochondrial membrane potential with chronic treatment as measured by TMRE intensity. (n = 18 per group. *, **, ***, **** correspond to p-values < 0.05, 0.01, 0.001, and 0.0001 respectively. Error bars represent SEM).

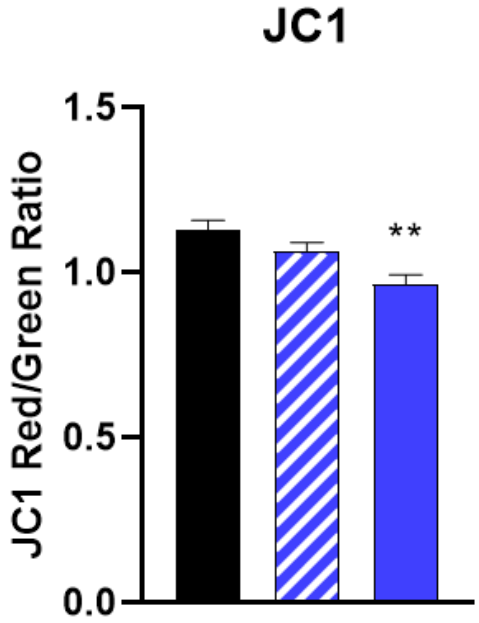
JC1
JC1 Red/Green Ratio
1.5
1.0
0.5
0.0
**

Figure 2-4: Chronic βOHB reduced JC1 measured mitochondrial membrane potential. (n = 18 per group. *, **, ***, **** correspond to p-values < 0.05, 0.01, 0.001, and 0.0001 respectively. Error bars represent SEM).

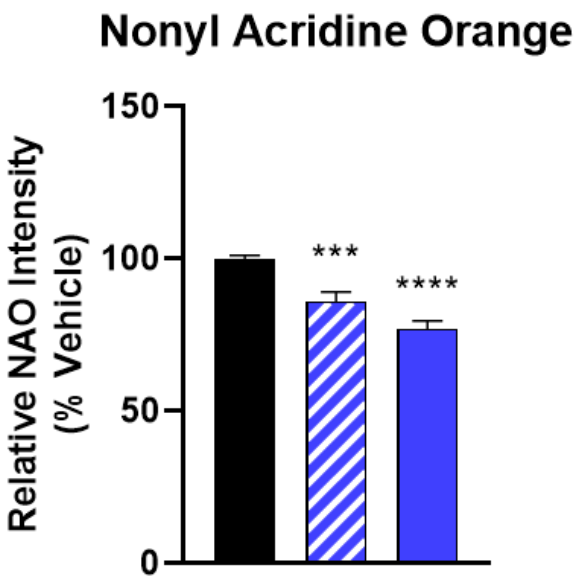
Nonyl Acridine Orange
Relative NAO Intensity
(% Vehicle)
150
100
50
0
***
****

Figure 2-5: Incorporation of NAO into mitochondria is reduced at 24 hours and chronically upon exposure to βOHB. (n = 18 per group. *, **, ***, **** correspond to p-values < 0.05, 0.01, 0.001, and 0.0001 respectively. Error bars represent SEM).

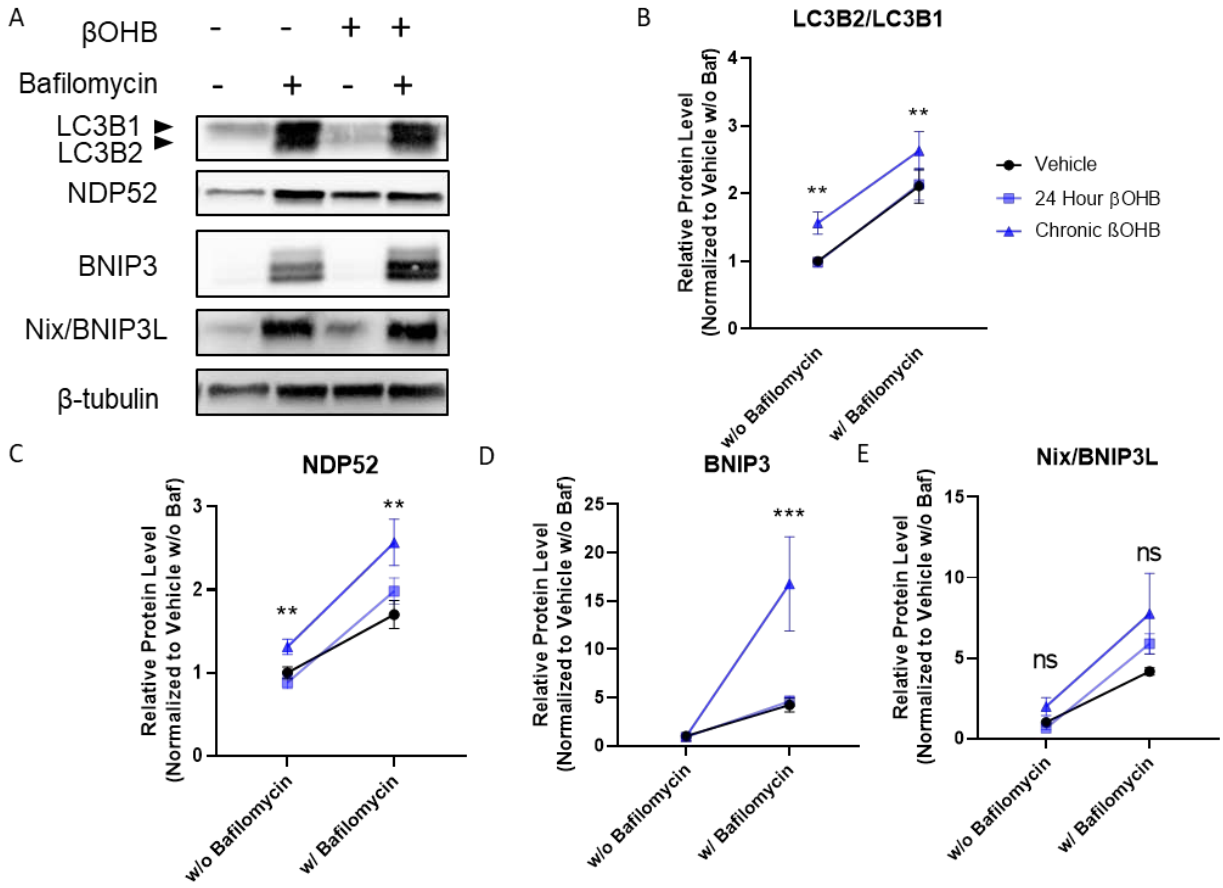
A
βOHB - - + +
Bafilomycin - + - +
LC3B1
LC3B2
NDP52
BNIP3
Nix/BNIP3L
β-tubulin
B
LC3B2/LC3B1
Relative Protein Level (Normalized to Vehicle w/o Baf)
Vehicle
24 Hour βOHB
Chronic ßOHB
w/o Bafilomycin
w/ Bafilomycin
C
NDP52
D
BNIP3
E
Nix/BNIP3L
ns

Figure 2-6: Chronic treatment with β-hydroxybutyrate increases autophagic capacity without altering flux and leads to increases in mitochondrial mass. A) Western blot images of autophagy flux samples from vehicle and chronic βOHB samples. B) βOHB increased the total amount of both LC3B lipidated and unlipidated forms under baseline and bafilomycin treated conditions but does not increase the delta compared to untreated samples. C) βOHB induced an increase in the mitophagy adaptor protein NDP52 that matched changes in LC3B. D) βOHB increased levels of mitophagy protein BNIP3 that was observable only with bafilomycin treatment. E) βOHB produced no significant change in the amount of mitophagy protein Nix/BNIP3L regardless of bafilomycin treatment. (n = 18 per group. * and ** correspond to p-values < 0.05 and 0.01 respectively. Error bars represent SEM).

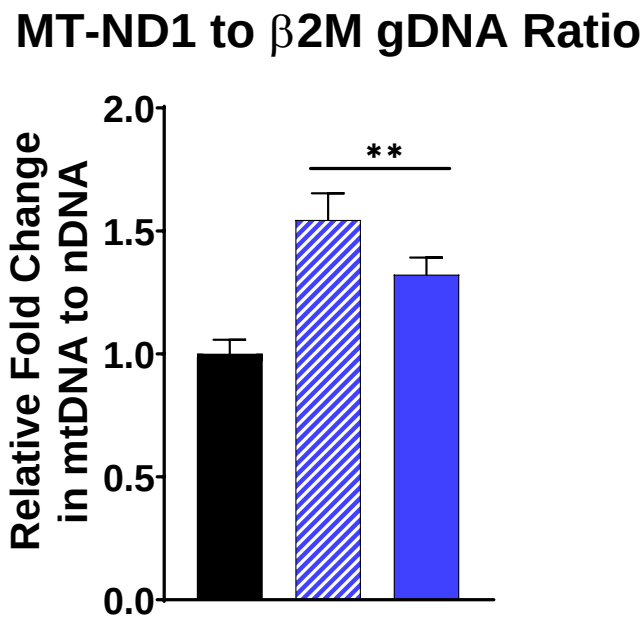
MT-ND1 to β2M gDNA Ratio
Relative Fold Change in mtDNA to nDNA
2.0
1.5
1.0
0.5
0.0
**

Figure 2-7: mtDNA copy number as measured by qPCR of fold change of copies of *MT-ND1* in isolated gDNA relative to nuclear encoded copies of *β2M*. (n = 18 per group. * and ** correspond to p-values < 0.05 and 0.01 respectively. Error bars represent SEM).

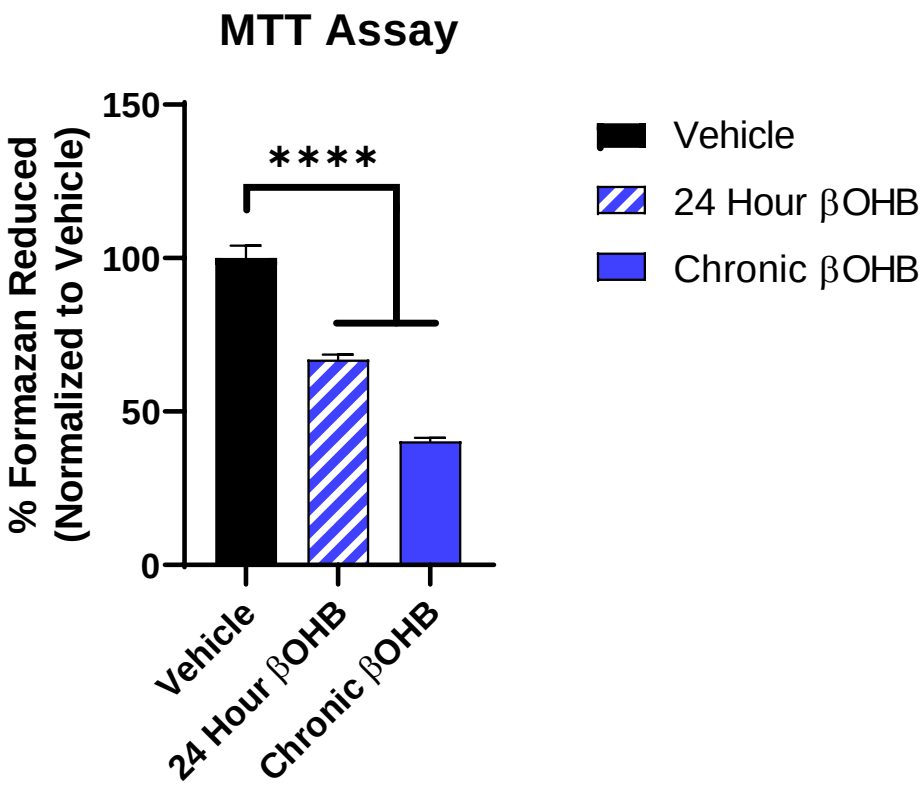
MTT Assay
% Formazan Reduced
(Normalized to Vehicle)
150
100
50
0
****
Vehicle
24 Hour βOHB
Chronic βOHB
Vehicle
24 Hour βOHB
Chronic βOHB

Figure 2-8: βOHB reduced cellular metabolic activity as measured by MTT assay at both 24-hour and chronic timepoints. (n = 18 per group. *, **, ***, **** correspond to p-values < 0.05, 0.01, 0.001, and 0.0001 respectively. Error bars represent SEM).

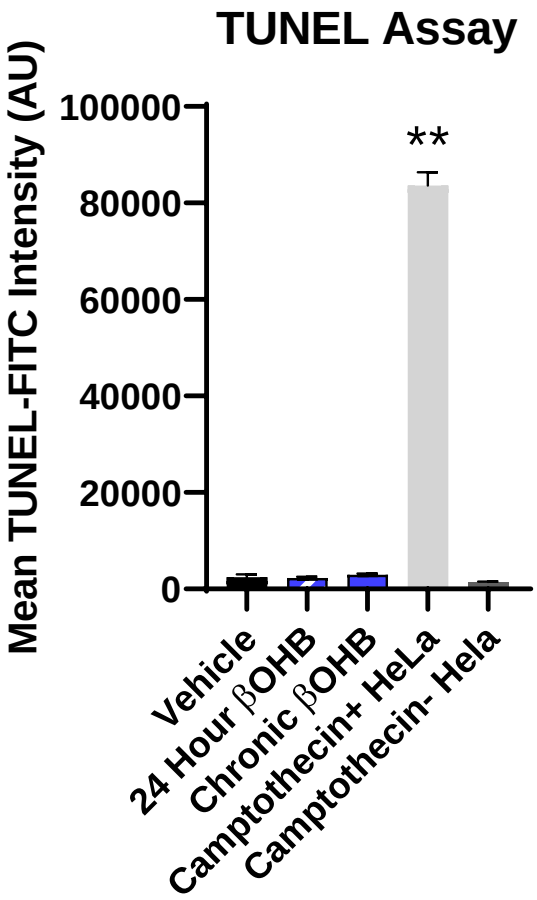
TUNEL Assay
Mean TUNEL-FITC Intensity (AU)
100000
80000
60000
40000
20000
0
**
Vehicle
24 Hour βOHB
Chronic βOHB
Camptothecin+ HeLa
Camptothecin- Hela

Figure 2-9: βOHB did not induce cell death in SH-SY5Y's at treatment concentrations. Camptothecin positive and negative HeLa cells were included as apoptosis positive and negative controls respectively. (n = 18 per group. *, **, ***, **** correspond to p-values < 0.05, 0.01, 0.001, and 0.0001 respectively. Error bars represent SEM).

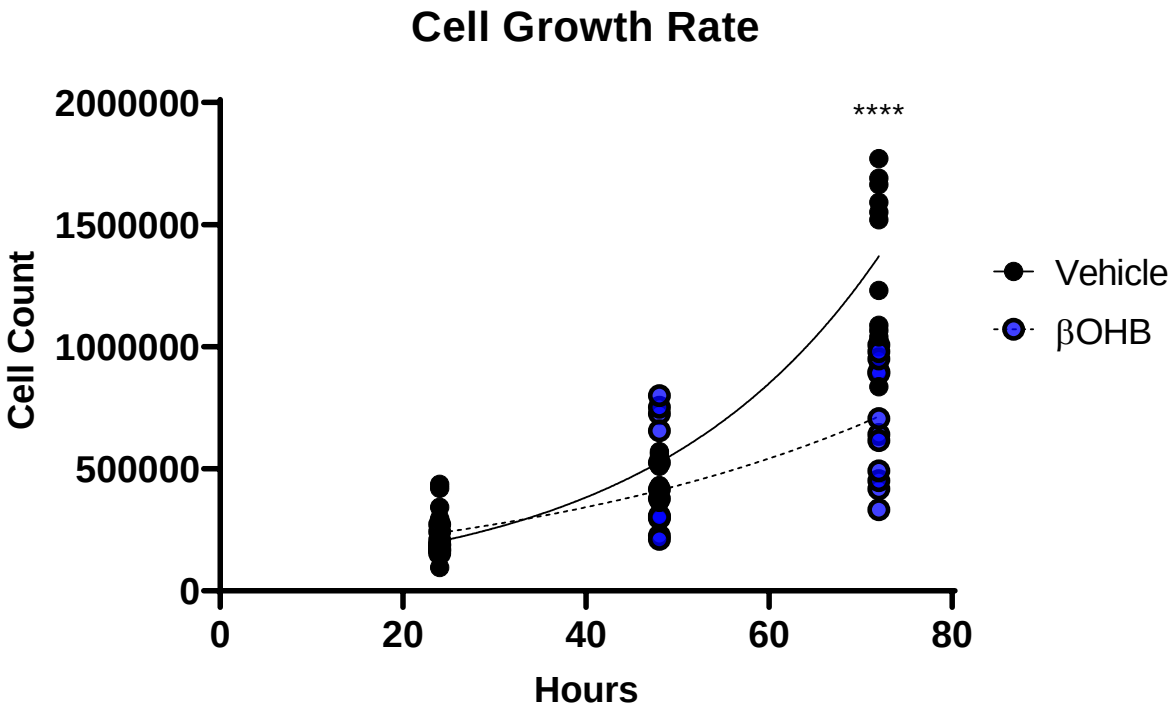
Cell Growth Rate
2000000
1500000
1000000
500000
0
Cell Count
****
0
20
40
60
80
Hours
Vehicle
βOHB

Figure 2-10: βOHB slowed cell growth rate that became readily apparent by 3 days following cell seeding. Doubling time increased from 17 hours to 33 hours. (n = 18 per group. *, **, ***, **** correspond to p-values < 0.05, 0.01, 0.001, and 0.0001 respectively. Error bars represent SEM).

A

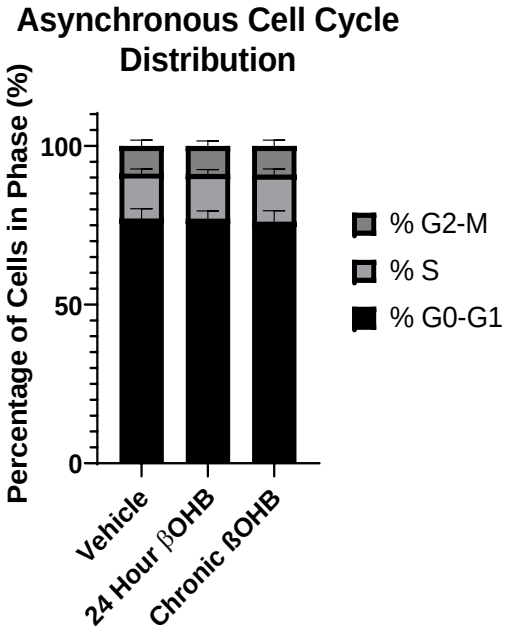
Asynchronous Cell Cycle Distribution
Percentage of Cells in Phase (%)
100
50
0
% G2-M
% S
% G0-G1
Vehicle
24 Hour βOHB
Chronic ßOHB

B

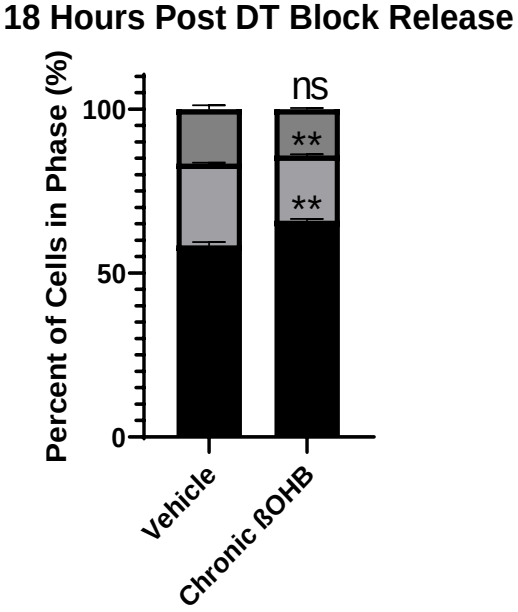
18 Hours Post DT Block Release
Percent of Cells in Phase (%)
100
50
0
ns
**
**
Vehicle
Chronic ßOHB

Figure 2-11: βOHB slows progression of SH-SY5Y cell progression through the G1/S transition in mitosis. A) Treatment with βOHB did not reveal a change in the distribution of cells in different phases of cell cycle under asynchronous growth conditions. B) Treatment with βOHB along with cell synchronization by double thymidine block and release revealed an accumulation of cells in G0-G1 phase indicating a defect in transition through G1-S phase at the 18-hour post release timepoint. (n = 18 per group. *, **, ***, **** correspond to p-values < 0.05, 0.01, 0.001, and 0.0001 respectively. Error bars represent SEM).

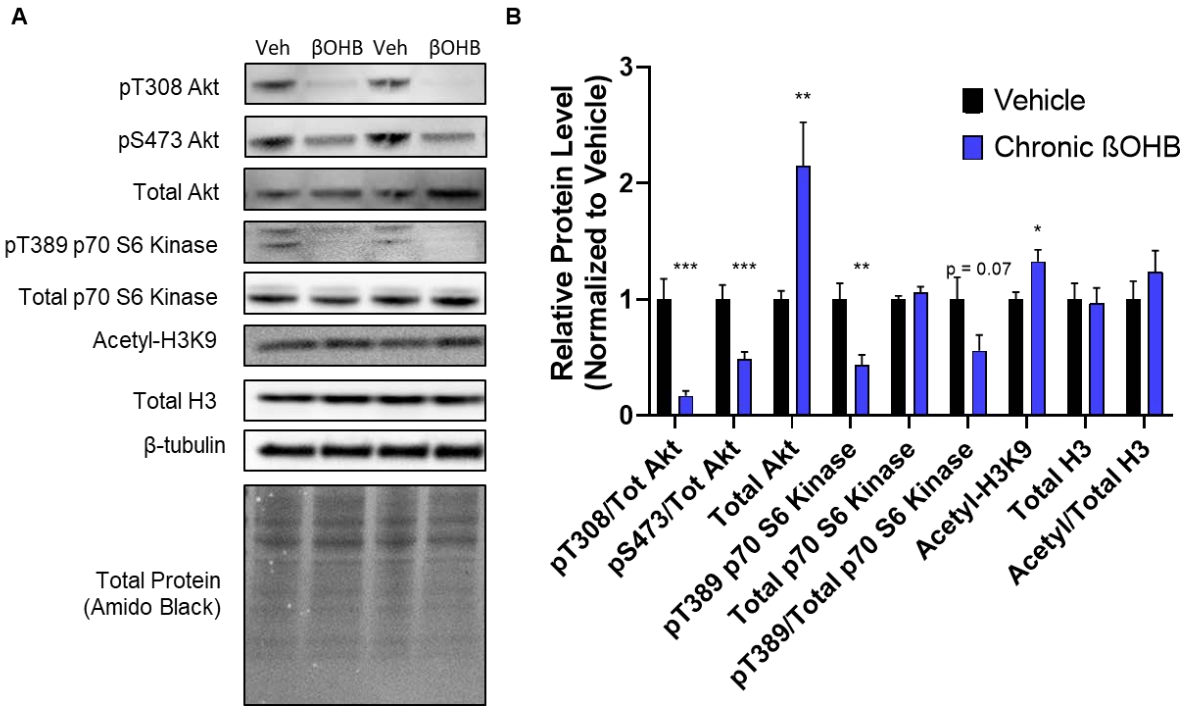
A
Veh
βOHB
Veh
βOHB
pT308 Akt
pS473 Akt
Total Akt
pT389 p70 S6 Kinase
Total p70 S6 Kinase
Acetyl-H3K9
Total H3
β-tubulin
Total Protein
(Amido Black)
B
Relative Protein Level
(Normalized to Vehicle)
Vehicle
Chronic ßOHB
***
***
**
**
p = 0.07
*
pT308/Tot Akt
pS473/Tot Akt
Total Akt
pT389 p70 S6 Kinase
Total p70 S6 Kinase
pT389/Total p70 S6 Kinase
Acetyl-H3K9
Total H3
Acetyl/Total H3

Figure 2-12: β-hydroxybutyrate reduces PI3K-Akt-mTOR pathway activation in SH-SY5Y cells. A) Western blot images of PI3K-Akt-mTOR pathway enzymes and their regulatory post-translational modification sites along with acetylation status of histone 3. B) Treatment with βOHB reduced Akt phosphorylation at both Ser473 and Thr308 activation sites as well as reduced phosphorylation of the downstream target p70 S6 Kinase at Thr389. Total protein levels of Akt were increased by βOHB treatment. Histone 3 acetylation was increased at lysine 9. (n = 18 per group. *, **, ***, **** correspond to p-values < 0.05, 0.01, 0.001, and 0.0001 respectively. Error bars represent SEM).

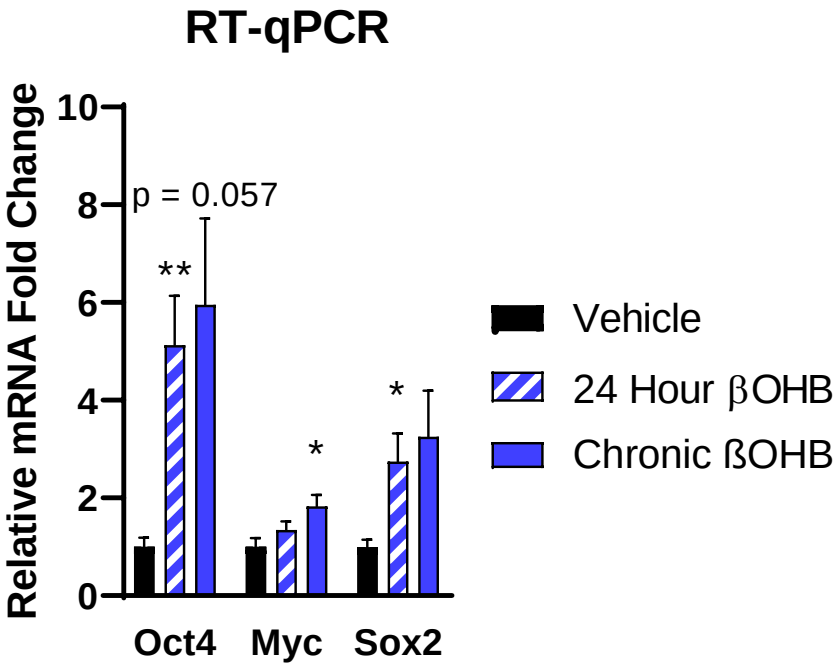
RT-qPCR
Relative mRNA Fold Change
10
8
6
4
2
0
p = 0.057
**
*
*
Oct4
Myc
Sox2
Vehicle
24 Hour βOHB
Chronic ßOHB

Figure 2-13: βOHB increased mRNA levels of Yamanaka factors *POU5F1* (Oct4), *Sox2*, and *myc*. No detectable levels of transcript for Klf4 were found in SH-SY5Y cells under any treatment condition. (n = 18 per group. *, **, ***, **** correspond to p-values < 0.05, 0.01, 0.001, and 0.0001 respectively. Error bars represent SEM).

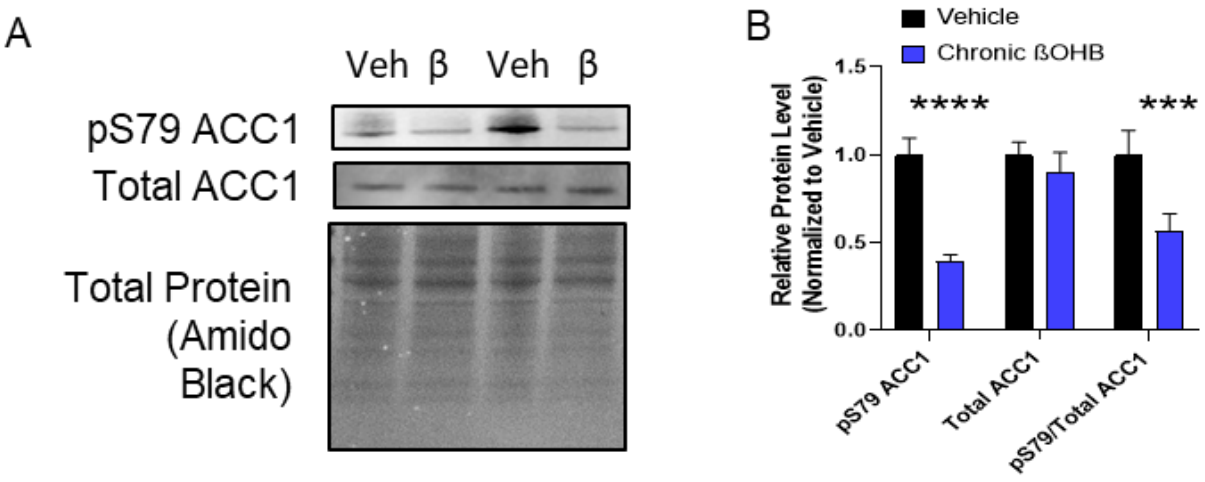
A
Veh β Veh β
pS79 ACC1
Total ACC1
Total Protein (Amido Black)
B
Vehicle
Chronic ßOHB
Relative Protein Level (Normalized to Vehicle)
1.5
1.0
0.5
0.0
****
***
pS79 ACC1
Total ACC1
pS79/Total ACC1

Figure 2-14: β-hydroxybutyrate reduced phosphorylation of the AMPK downstream target ACC1 A) Western blot images demonstrating changes in phosphorylation of ACC1 at Ser79. B) Chronic βOHB exposure reduced phosphorylation of ACC1 at the inhibitory Ser79 site regulated by activated AMPK. (n = 18 per group. *, **, ***, **** correspond to p-values < 0.05, 0.01, 0.001, and 0.0001 respectively. Error bars represent SEM).

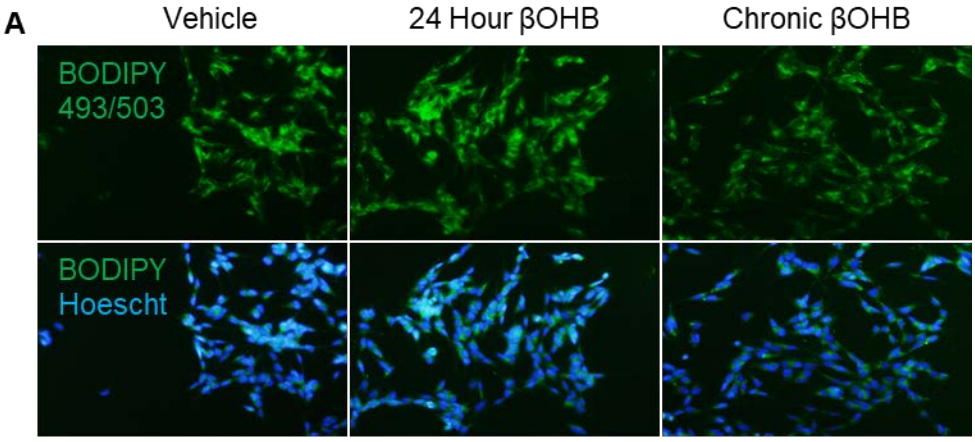
A
Vehicle
24 Hour βOHB
Chronic βOHB
BODIPY 493/503
BODIPY Hoescht

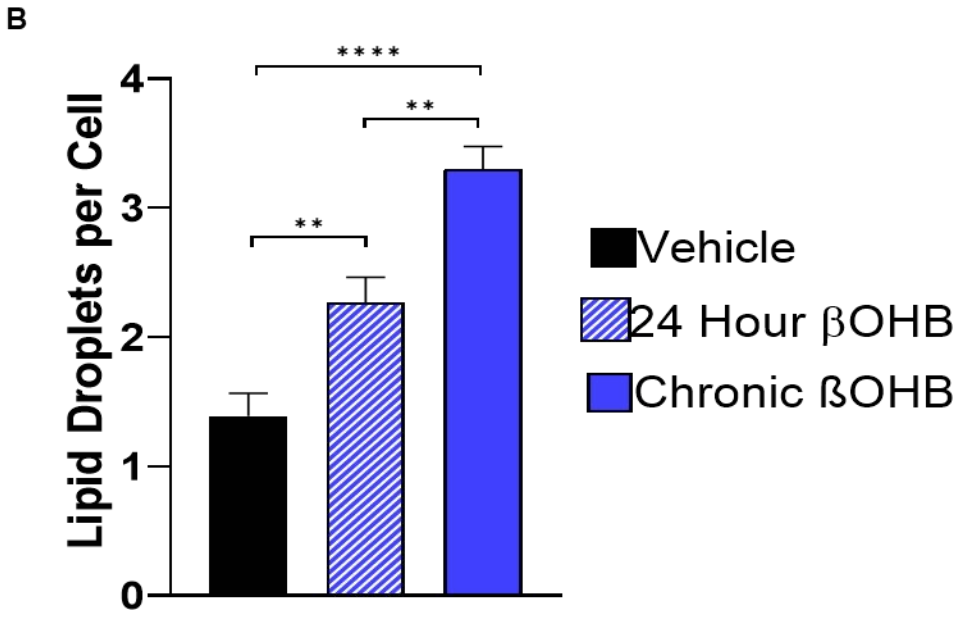
B
Lipid Droplets per Cell
0
1
2
3
4
****
**
**
Vehicle
24 Hour βOHB
Chronic ßOHB

Figure 2-15: β-hydroxybutyrate increased lipid droplet number in SH-SY5Y cells. A) Fluorescent imaging of green BODIPY 493/503 labeled lipid droplets at 20x magnification with Hoechst 33342 nuclear staining. B) Quantification of lipid droplet number per cell indicate βOHB treatment increased total number of lipid droplets. (n = 18 per group. *, **, ***, **** correspond to p-values < 0.05, 0.01, 0.001, and 0.0001 respectively. Error bars represent SEM).

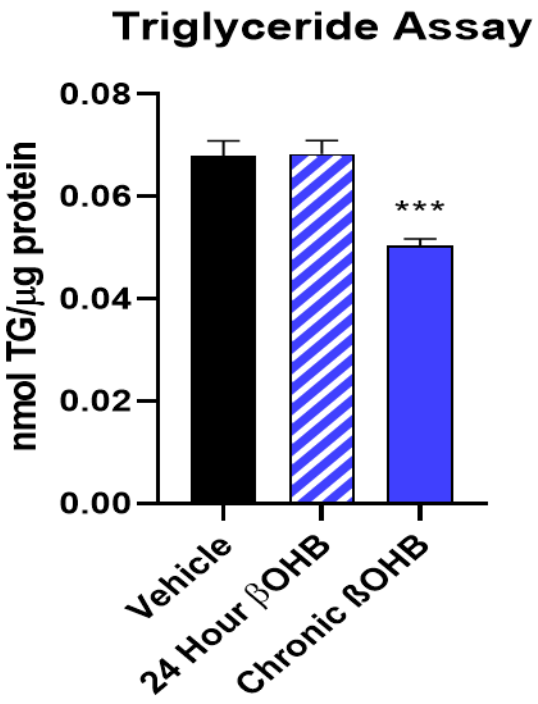
Triglyceride Assay
nmol TG/μg protein
0.08
0.06
0.04
0.02
0.00
***
Vehicle
24 Hour βOHB
Chronic ßOHB

Figure 2-16: β-hydroxybutyrate reduced cellular triglyceride content in SH-SY5Y cells.

Chronic exposure to βOHB reduced cellular triglyceride content. (n = 18 per group. *, **, ***, **** correspond to p-values < 0.05, 0.01, 0.001, and 0.0001 respectively. Error bars represent SEM).

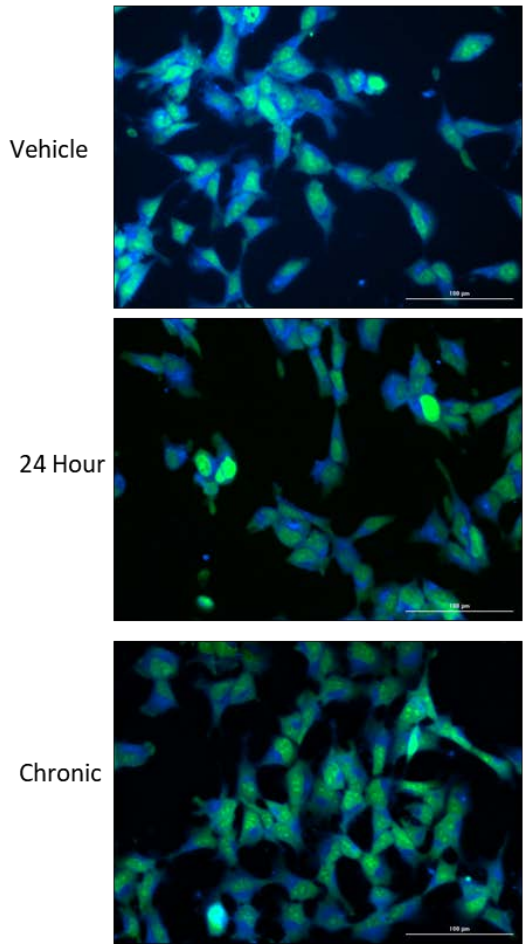
Vehicle
24 Hour
Chronic

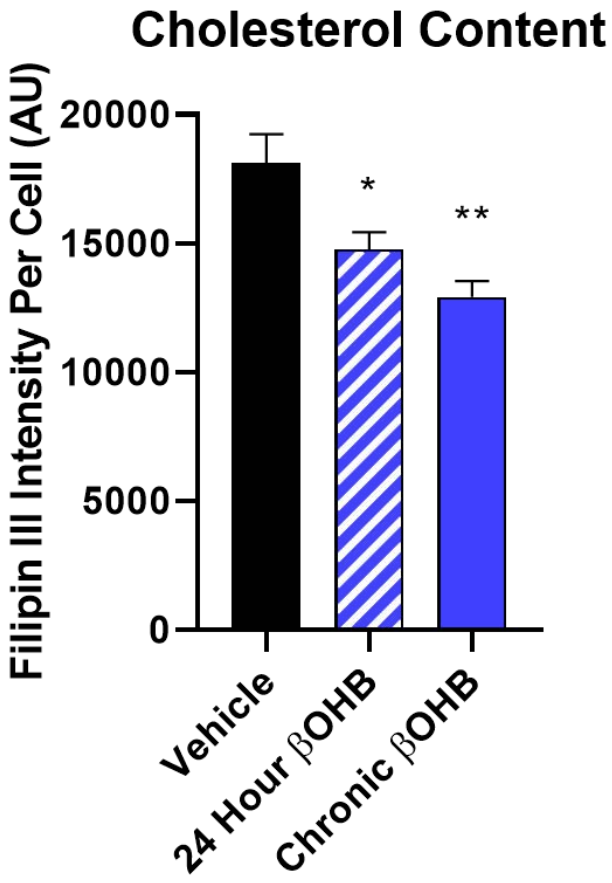
Cholesterol Content
Filipin III Intensity Per Cell (AU)
20000
15000
10000
5000
0
*
**
Vehicle
24 Hour βOHB
Chronic βOHB

Figure 2-17: β-hydroxybutyrate reduced cellular cholesterol content in SH-SY5Y cells. A) Fluorescent images of SH-SY5Y cells labeled with the cholesterol reporter filipin III in blue and nuclear stain NucGreen at 20x magnification. B) βOHB reduced cholesterol content in SH-SY5Y cells. (n = 18 per group. *, **, ***, **** correspond to p-values < 0.05, 0.01, 0.001, and 0.0001 respectively. Error bars represent SEM).

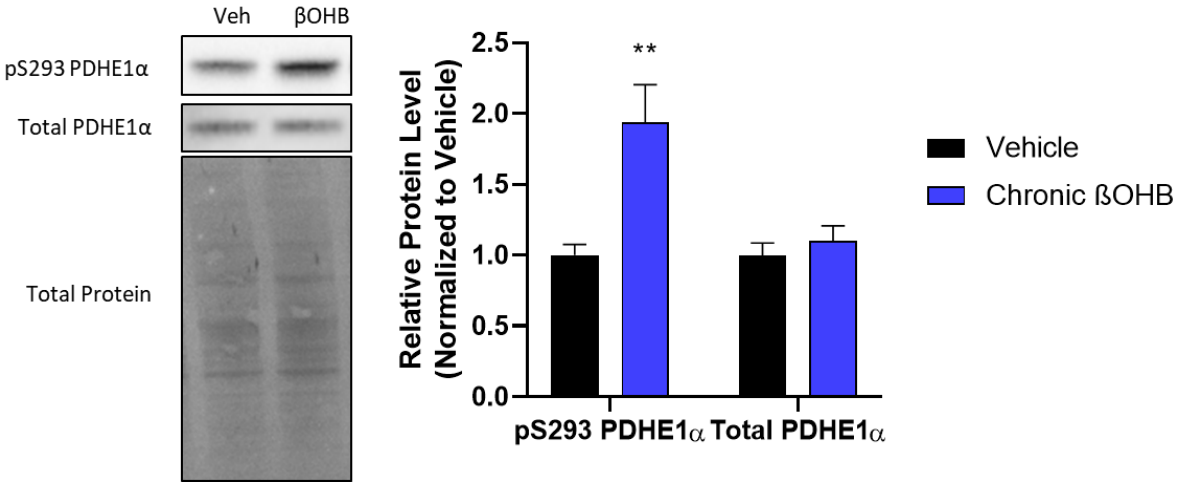
Veh
βOHB
pS293 PDHE1α
Total PDHE1α
Total Protein
Relative Protein Level
(Normalized to Vehicle)
2.5
2.0
1.5
1.0
0.5
0.0
**
pS293 PDHE1α
Total PDHE1α
Vehicle
Chronic ßOHB

Figure 2-18: β-hydroxybutyrate and increased inhibition of PDHE1α in SH-SY5Y cells. A) Western Blot images demonstrating changes in PDHE1α subunit phosphorylation. B) βOHB increases phosphorylation of PDHE1α at the inhibitory Ser293 site. (n = 18 per group. *, **, ***, **** correspond to p-values < 0.05, 0.01, 0.001, and 0.0001 respectively. Error bars represent SEM).

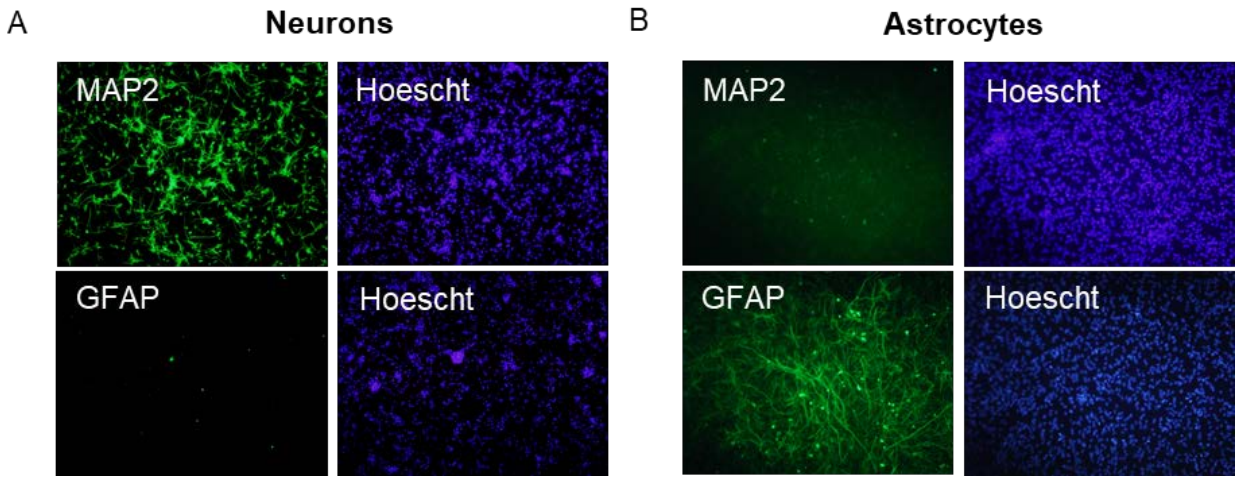
A
Neurons
MAP2
Hoescht
GFAP
Hoescht
B
Astrocytes
MAP2
Hoescht
GFAP
Hoescht

Figure 2-19: Enrichment for neurons and astrocytes by differing isolation and culture protocols as evidenced by fluorescent microscopy. A) Fluorescent imaging showing enrichment of primary rat neurons in culture. Neurons and astrocytes were labeled with MAP2 and GFAP respectively. Hoechst 33342 was used to visualize nuclei. B) Fluorescent imaging showing enrichment of primary rat astrocytes in culture.

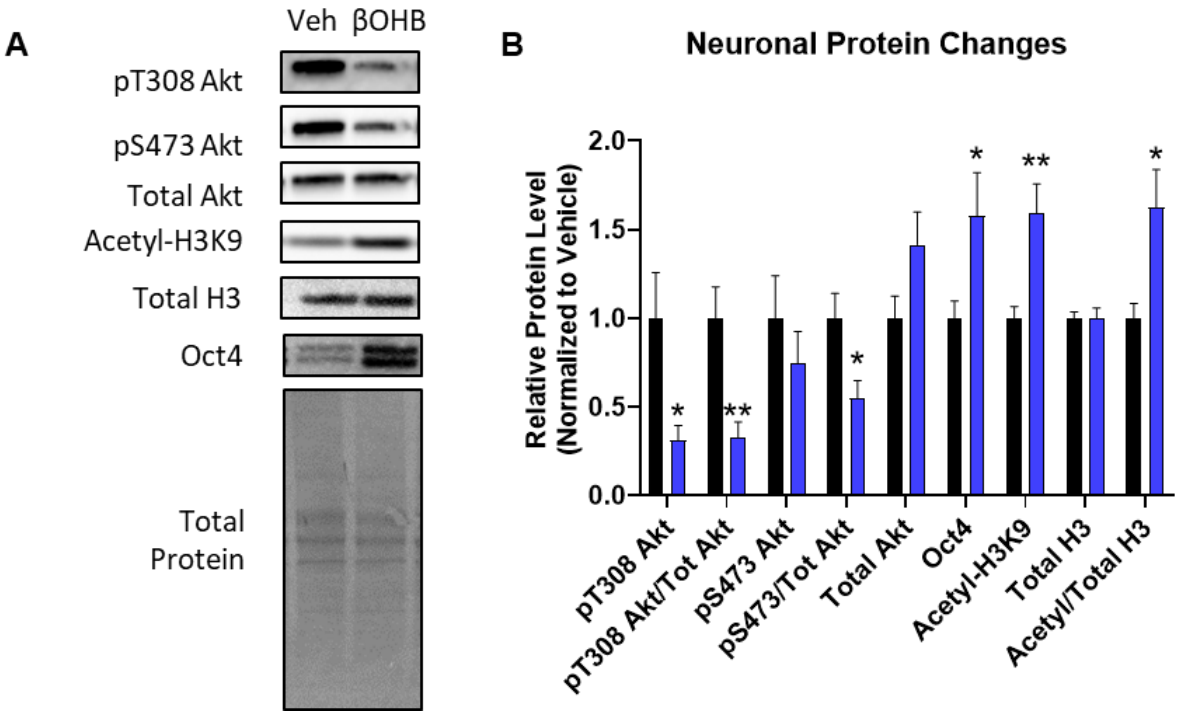
A
Veh
βOHB
pT308 Akt
pS473 Akt
Total Akt
Acetyl-H3K9
Total H3
Oct4
Total
Protein
B
Neuronal Protein Changes
Relative Protein Level
(Normalized to Vehicle)
2.0
1.5
1.0
0.5
0.0
*
**
*
*
**
*
pT308 Akt
pT308 Akt/Tot Akt
pS473 Akt
pS473/Tot Akt
Total Akt
Oct4
Acetyl-H3K9
Total H3
Acetyl/Total H3

Figure 2-20: β-hydroxybutyrate reduced PI3K-Akt-mTOR activation, increased histone acetylation, and increased protein levels of Oct4 in primary rat neurons. A) Western blot images of protein changes in primary rat neuron. B) βOHB reduced phosphorylation of Akt in a manner like those observed in SH-SY5Y cells while simultaneously increasing the amount of histone acetylation and Oct4 protein. (n = 18 per group. *, **, ***, **** correspond to p-values < 0.05, 0.01, 0.001, and 0.0001 respectively. Error bars represent SEM).

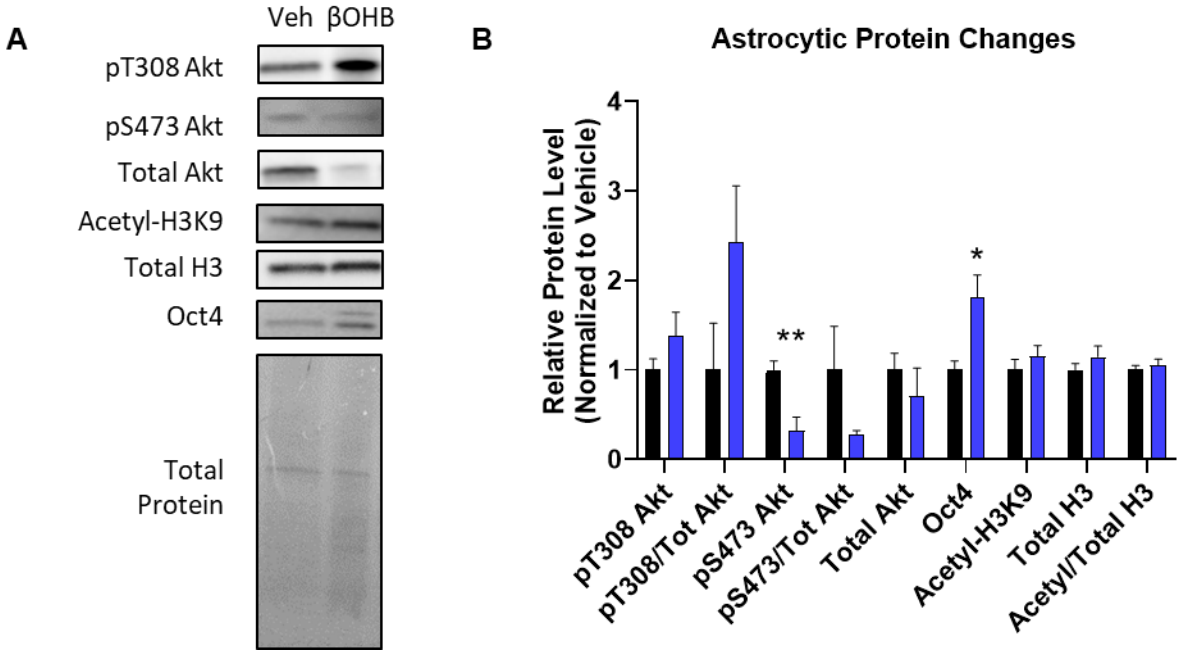
A
Veh
βOHB
pT308 Akt
pS473 Akt
Total Akt
Acetyl-H3K9
Total H3
Oct4
Total
Protein
B
Astrocytic Protein Changes
Relative Protein Level
(Normalized to Vehicle)
0
1
2
3
4
**
*
pT308 Akt
pT308/Tot Akt
pS473 Akt
pS473/Tot Akt
Total Akt
Oct4
Acetyl-H3K9
Total H3
Acetyl/Total H3

Figure 2-21: β-hydroxybutyrate did not influence primary rat astrocytes in the same manner as observed in neurons. A) Western blot images of protein changes in primary rat astrocyte whole cell lysates. F) βOHB reduced S473 Akt phosphorylation but only demonstrated non-significant trends for T308. βOHB did not increase histone acetylation as observed in SH-SY5Y and rat neurons. Vehicle treated rat astrocytes demonstrated only a single band of Oct4 protein whereas βOHB treated astrocytes showed an increased density of the original band plus a second band at a slightly higher molecular weight. (n = 18 per group. *, **, ***, **** correspond to p-values < 0.05, 0.01, 0.001, and 0.0001 respectively. Error bars represent SEM).

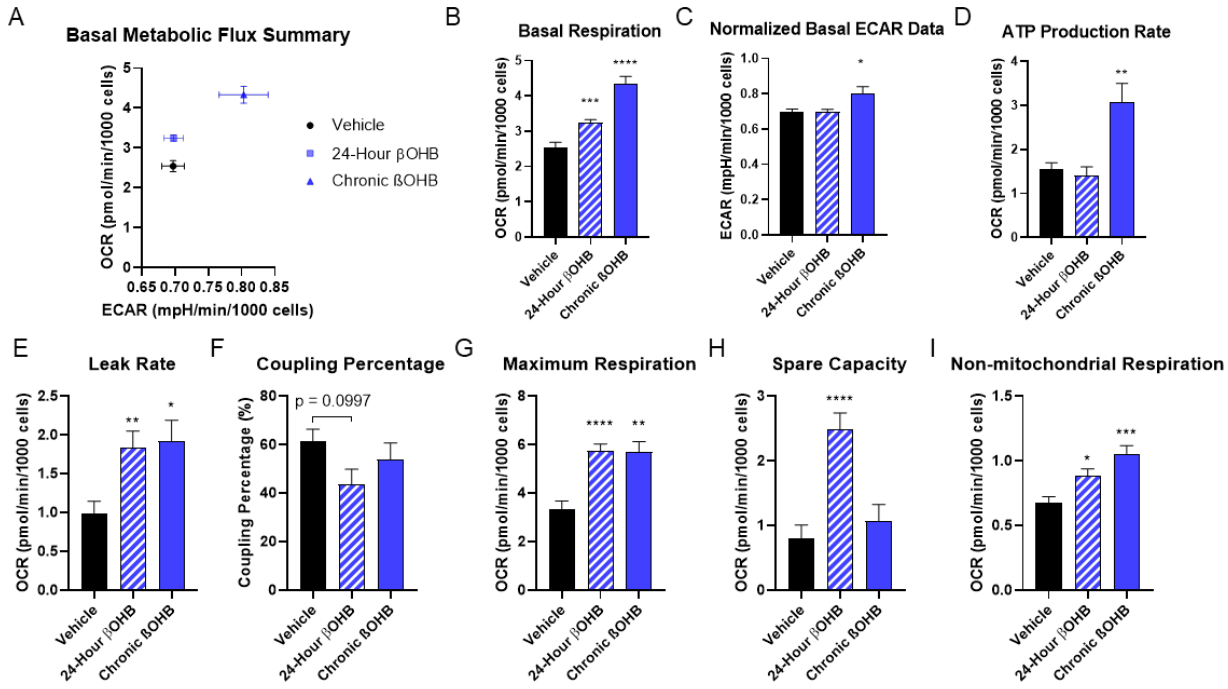
A
Basal Metabolic Flux Summary
OCR (pmol/min/1000 cells)
ECAR (mpH/min/1000 cells)
0.65 0.70 0.75 0.80 0.85
Vehicle
24-Hour βOHB
Chronic ßOHB
B
Basal Respiration
OCR (pmol/min/1000 cells)
C
Normalized Basal ECAR Data
ECAR (mpH/min/1000 cells)
D
ATP Production Rate
OCR (pmol/min/1000 cells)
E
Leak Rate
OCR (pmol/min/1000 cells)
F
Coupling Percentage
Coupling Percentage (%)
p = 0.0997
G
Maximum Respiration
OCR (pmol/min/1000 cells)
H
Spare Capacity
OCR (pmol/min/1000 cells)
I
Non-mitochondrial Respiration
OCR (pmol/min/1000 cells)
Vehicle
24-Hour βOHB
Chronic ßOHB

Figure 2-22: β-hydroxybutyrate increased respiration in primary rat neurons in a manner similar to its effects in SH-SY5Y cells. A-C) βOHB increased respiration with at both 24-hours and chronically. Unlike in SH-SY5Y cells, chronic administration of βOHB increased the basal ECAR. D) Chronic βOHB increased respiration associated with ATP production rate. E-F) OCR attributed to proton leak was increased by βOHB at both 24-hours and chronically, but any association with reduced coupling efficiency was not statistically significant. G-H) Maximal respiration was increased by βOHB at both timepoints, but spare capacity was only transiently enhanced at the 24-hour mark. I) Non-mitochondrial respiration was increased by βOHB. (n = 18 per group. *, **, ***, **** correspond to p-values < 0.05, 0.01, 0.001, and 0.0001 respectively. Error bars represent SEM).

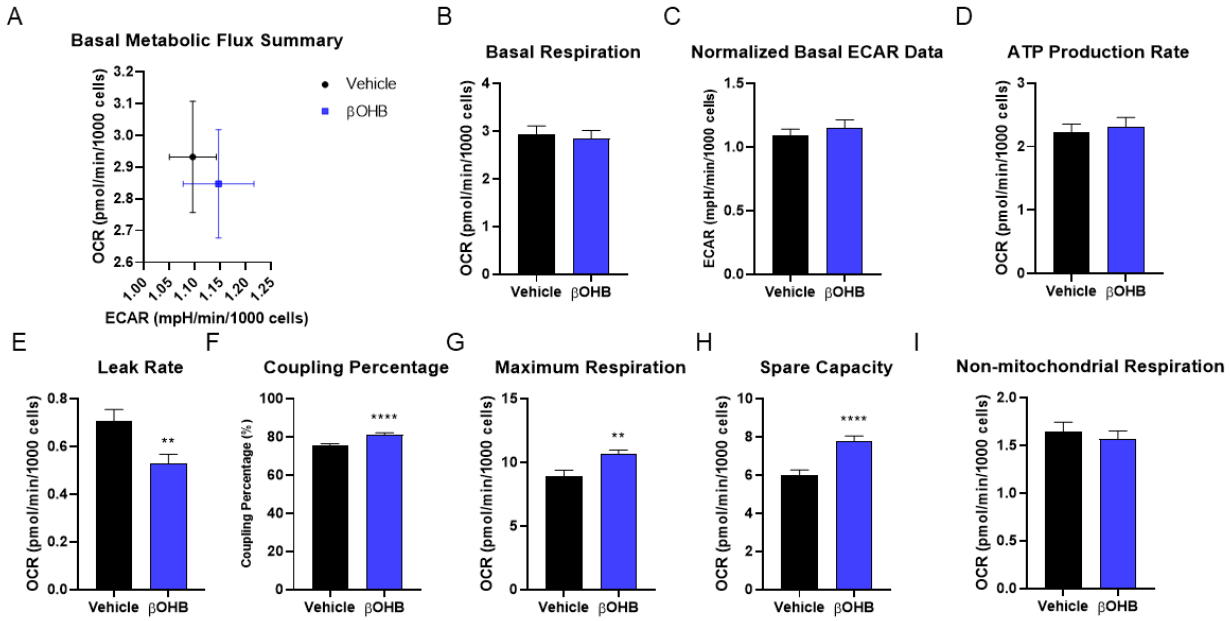
A
Basal Metabolic Flux Summary
OCR (pmol/min/1000 cells)
ECAR (mpH/min/1000 cells)
Vehicle
βOHB
B
Basal Respiration
OCR (pmol/min/1000 cells)
Vehicle βOHB
C
Normalized Basal ECAR Data
ECAR (mpH/min/1000 cells)
Vehicle βOHB
D
ATP Production Rate
OCR (pmol/min/1000 cells)
Vehicle βOHB
E
Leak Rate
OCR (pmol/min/1000 cells)
**
Vehicle βOHB
F
Coupling Percentage
Coupling Percentage (%)
****
Vehicle βOHB
G
Maximum Respiration
OCR (pmol/min/1000 cells)
**
Vehicle βOHB
H
Spare Capacity
OCR (pmol/min/1000 cells)
****
Vehicle βOHB
I
Non-mitochondrial Respiration
OCR (pmol/min/1000 cells)
Vehicle βOHB

Figure 2-23: β-hydroxybutyrate does not alter basal metabolic fluxes in primary astrocytes but does enhance spare capacity. A-C) βOHB did not alter either basal OCR or ECAR with chronic administration. D) βOHB did not alter OCR associated with ATP production in astrocytes. E-F) βOHB reduced leak rate while increasing coupling percentage in astrocytes. G-H) βOHB increased both maximal and spare respiratory capacity in astrocytes. I) βOHB did not alter astrocytic non-mitochondrial respiration rates. (n = 18 per group. *, **, ***, **** correspond to p-values < 0.05, 0.01, 0.001, and 0.0001 respectively. Error bars represent SEM).

Chapter 3: 90-Day Ketogenic Diet Intervention Has Differential Effects on Neuronal and Astrocytic Transcriptional Pathways Relevant to Alzheimer's Disease Pathogenesis in Mouse Brain.

Introduction

Alzheimer's disease (AD) is the most common form of dementia and neurodegenerative disease currently estimated to effect nearly 6 million people in the United States alone. Disease pathogenesis is marked by accumulation of extracellular plaques of amyloid beta (Aβ42), intracellular tangles of hyperphosphorylated tau, inflammation, neuronal loss, mitochondrial dysfunction, and glucose hypometabolism (Andrews et al., 2020; Frisoni et al., 2017; Jack et al., 2013; Menta & Swerdlow, 2019; Swerdlow, 2016; Weidling & Swerdlow, 2019; Wilkins & Swerdlow, 2016a). Many of these pathologic changes begin to occur during preclinical stages before a loss in cognitive ability is readily apparent indicating that early interventions to correct these deficits may have therapeutic benefit. One suggested therapy to correct the bioenergetic dysfunction observed in AD is the high-fat, low-carbohydrate ketogenic diet (KD) (S. J. Koppel & Swerdlow, 2018). A phase one retention and feasibility trial for the ketogenic diet in AD subjects have shown that a three-month KD intervention exhibited improved performance on the Alzheimer's Disease Cognitive Assessment Scale-cognitive subscale while being maintained on the diet (Matthew K. Taylor et al., 2017; M. K. Taylor, Swerdlow, Burns, et al., 2019).

The KD has been in use clinically for over a century to provide neurologic benefit to patients with epilepsy who are resistant to other forms of pharmacologic management (S. J. Koppel & Swerdlow, 2018; M. K. Taylor, Swerdlow, & Sullivan, 2019). Among other effects, it is known to reduce serum insulin and increase hepatic generation of ketone bodies derived from fatty acids for use as an energy substrate in extrahepatic tissues. In doing so, the KD provides a primary energy alternative to glucose in the central nervous system (CNS) as the brain does not derive hardly any energy from the β-oxidation of fats and is almost entirely reliant on glucose derived energy production under normal physiologic conditions. Ketone bodies are utilized

primarily by the brain, cardiac muscle, and testes to generate ATP through mitochondrial respiration and oxidative phosphorylation. Unlike glucose, the delivery of ketone bodies to the brain does not appear to be affected by age or dementia status (Castellano et al., 2015; Courchesne-Loyer et al., 2016; S. C. Cunnane, Courchesne-Loyer, Vandenberghe, et al., 2016).

The KD and the ketone bodies it produces also demonstrate an increasingly wide array of recognized molecular signaling effects. The most abundant ketone body, β-hydroxybutyrate (βOHB), is known to inhibit histone deacetylase activity leading to increased transcription in several cell types (Newman & Verdin, 2014a, 2014b; Rardin et al., 2013; Shimazu et al., 2013). The KD has been suggested to exhibit anti-inflammatory effects through the regulation of the NLRP3 inflammasome and G protein coupled receptor (GPCR) signaling (Kimura et al., 2011; Rahman et al., 2014; Stilling et al., 2016; Won et al., 2013). The KD or other neuroketotherapeutics may also increase neurotrophic factor expression such as brain derived neurotrophic factor (BDNF) to support brain function (Marosi et al., 2016; Sleiman et al., 2016; Swerdlow, 2014b). The KD could be beneficial in aging as its been shown to increase lifespan in mice while βOHB reduces the accumulation of senescent cells in mouse vasculature (Han et al., 2018; Newman et al., 2017).

Regardless of what may be the precise mechanism of benefit the KD acts through to improve function in subjects with dementia, to fully understand the effects of the KD on the brain we must consider the multiple cell populations that make up the CNS, neurons and glia. It is already well known that neurons and astrocytes are specialized to their management of the availability of glucose in what is known as the astrocyte-neuron lactate shuttle (ANLS) (Aubert & Costalat, 2007; Bouzier-Sore et al., 2003). In this proposed phenomenon, astrocytes process glucose to pyruvate via glycolysis that is then delivered to neurons for energy production via

mitochondrial oxidative phosphorylation. Additionally, it has been shown that neurons will export oxidized lipid to astrocytes as a means of waste removal for neuroprotection (L. Liu et al., 2017). Previously, we have shown that βOHB enhanced mitochondrial respiration for energy production while simultaneously inducing cellular quiescence in SH-SY5Y cells and primary rat neurons through the modulation of PI3K-Akt-mTOR and Yamanaka factor signaling with limited effects on these pathways observed in primary rat astrocytes (See Chapter 2).

We hypothesize that the KD will exhibit differential effects on neurons and astrocytes *in vivo* similar to our findings that we observed *in vitro*. To test this, we compared the transcriptomes via RNAseq KEGG pathway analysis of neurons and astrocytes isolated from adult, male C57Bl6/N mice maintained on either standard chow or ketogenic diet for a period of 90 days (Minoru Kanehisa et al., 2008; M. Kanehisa & Goto, 2000). We found that manipulating bioenergetic pathways via the KD modulated transcriptional patterns of several phenomena central to AD pathogenesis in a differential pattern between neurons and astrocytes. Not only do these findings further suggest the KD directly affects AD relevant pathways, it further improves and underscores the need to better understand the multicellular biology of the brain to better refine and target relevant molecular pathways for the treatment of neurodegenerative disease.

Materials and Methods

Maintenance and Monitoring of Mice During Dietary Intervention

All experimental protocols involving vertebrate animals were submitted to and approved by the University of Kansas Medical Center Institutional Animal Care and Use Committee prior to any experimentation. Power calculations were performed using the PROPER method by the KUMC Biostatistics and Data Sciences Department to determine needed number of mice (Wu,

Wang, & Wu, 2014). For power calculations we assumed a sampling of approximately 20,000 genes, primary comparison of diet effect within cell-type (comparison of 2 groups), 5% of genes being differentially expressed, with a magnitude of effect defined from a normal distribution with standard deviation equal to 1 on a $\log_2$ scale. From this we determined that groups of n = 8, 10, and 12 would provide marginal power of 0.72, 0.75, and 0.77, respectively with a nominal false discovery rate of 0.1. Based upon preliminary data on our brain separation protocol to provide adequate gene enrichment and preserve RNA quality to an acceptable degree for RNAseq experiments we elected to purchase and utilize a total of 30 C57Bl6/N mice (Charles River Laboratories) with the goal of obtaining 12 viable samples per group for analysis.

Mice were purchased and arrived at 16-weeks of age and allowed to acclimate for one week before being assessed for baseline values of mass, blood glucose, and blood ketone levels. Blood was obtained by facial vein phlebotomy and metabolites were measured using the Precision Xtra meter (Abbott Diabetes Care, Inc. #9881465) with blood glucose (Abbott #9972865) and ketone test strips (Abbott #7074565) at the time of blood draw. Mice were stratified into dietary treatment groups by body mass to obtain equal mean initial body masses prior to dietary intervention. Two mice (one per group) began dietary intervention with standard chow (LabDiet #5053) or ketogenic diet (Bioserve #F3666) per day for 15 days and were maintained on the diet for 90 days before sacrifice for organ harvest (**Fig. 3-1**). Mouse mass and blood parameters were monitored periodically throughout dietary intervention. Food intake was measured by weighing food prior to and following a 24-hour feeding cycle per mouse for three days with a mean intake value per mouse (g) being determined and multiplied by the associated diet kcal/g to determine if there was a difference in daily kcal consumed by diet group. One mouse in the ketogenic diet fed group was euthanized before study endpoint for humane reasons

due to the development of cancer after consultation with KUMC veterinary staff. An additional five mice (3 chow, 2 keto diet) were euthanized after sustaining moderate to severe fight wounds under the advisement of veterinary staff.

Generation of Cell Type Enriched Isolates for RNA Isolation

At the end of the 90-day intervention period one pair of mice was euthanized per day for brain separation and RNA isolation. Mice were rapidly euthanized by guillotine decapitation and brains were removed from the skull and placed in digestion buffer within 30 seconds of decapitation. Digestion buffer was composed of 2 parts Neurobasal medium (gibco #21103-049) to 1-part Accutase (gibco #A11105-01) supplemented with DNAse I (Sigma #DN25) to a final concentration of 0.3 mg/mL. Brains were incubated in digestion buffer at 37°C for 20 minutes. Brains were supplemented with an additional 10 mL of neurobasal medium then triturated via 10x passages through 10 mL serological pipettes, followed by 10x passages through 5 mL serological pipettes, and a final 20x passages through 1,000 µL pipette tips in a 50 mL conical. Large debris was allowed to settle to the bottom of the tube. Upper media layer was collected and passed through a 70 µm cell strainer (Fisher #22-363-549) pre-hydrated with 5 mL neurobasal media. Pass through was collected and again strained through a 40 µm cell strainer (Fisher #22-363-547) pre-hydrated with 5 mL neurobasal media.

Final pass through was collected and centrifuged at 300 rcf for 10 minutes at 4°C to pellet cells. Supernatant was discarded. Cells were resuspended in 1.8 mL of ice-cold cell stain buffer composed of low-fluorescence Hibernate A (BrainBits, LLC), 0.5% bovine serum albumin (Boston Bioproducts #P-753), and SuperaseIn RNAse inhibitor (ThermoFisher #AM2696) and sterile filtered. 200 µL of myelin removal beads (Miltenyi Biotec #130-096-433)

were added and cells were incubated for 15 minutes at 4°C on a rocking shaker. 10 mL of fresh ice-cold cell stain buffer was added per sample and cells were again centrifuged as done previously. Supernatant was discarded and the cell pellet was resuspended in 4 mL of cell stain buffer. Cell suspension was evenly distributed by 1 mL volumes into clean, autoclaved microcentrifuge tubes. Tubes were placed into magnetic tube rack (ThermoFisher #12321D) at 4°C for 10 minutes. Unbound supernatant was carefully removed through pipetting and transferred to a new, clean 15 mL conical tube. Collections were centrifuged under prior conditions and supernatant was discarded. Cell pellets were resuspended in 720 µL of cell stain buffer and evenly distributed into two new, clean microcentrifuge tubes for cell-type specific enrichment protocols.

For neuronal enrichment, 80 µL of biotinylated antibody cocktail targeting non-neuronal cell types was added to cell suspension (Miltenyi Biotec #130-115-389) as per manufacturer instructions. Samples were incubated at 4°C for 10 minutes on a rotating tube rack (Fisher #05-450-127). Samples were centrifuged at 300 g for 10 minutes at 4°C and supernatant was carefully removed. Pellets were resuspended in 360 µL of cell stain buffer and 80 µL of anti-biotin magnetic beads were added. Cells were again incubated at 4°C for 10 minutes on a rotating tube rack. Samples were diluted with 1 mL of ice-cold cell stain buffer and placed in the magnetic stand for 10 minutes at 4°C. Unbound supernatant containing neuronal cells was carefully collected so as not to disturb the sedimented layer along the magnet containing glia and endothelium and transferred to a new, clean microcentrifuge tube. Collections were centrifuged as described above and supernatant was discarded. Cell pellets were dissolved in 1 mL of TRI reagent (ThermoFisher #15596018) and allowed to stand for ten minutes before proceeding to RNA isolation. RNA was isolated via phenol-chloroform extraction with TRI reagent with RNA

purity and content measured by A260/280 ratio before being transferred to core services for quality assessment and library generation.

For astrocyte enrichment, 80 µL of biotinylated antibody targeting glutamate aspartate transporter 1 (GLAST) was added to cell suspension (Miltenyi Biotec #130-095-826) as per manufacturer instructions. Samples were incubated at 4°C for 10 minutes on a rotating tube rack. Samples were centrifuged at 300 g for 10 minutes at 4°C and supernatant was carefully removed. Pellets were resuspended in 360 µL of cell stain buffer and 80 µL of anti-biotin magnetic beads were added. Cells were again incubated at 4°C for 15 minutes on a rotating tube rack. Samples were centrifuged as described previously and supernatant was discarded. Pellets were resuspended in 1 mL of ice-cold cell stain buffer and placed in the magnetic stand for 10 minutes at 4°C. Unbound supernatant containing non-astrocytic cells was carefully removed so as not to disturb the sedimented layer along the magnet containing astrocytes and discarded. Sedimented magnetized cells were washed in 1 mL of cell stain buffer and centrifuged to pellet as done previously. Supernatant was removed and pellets were dissolved in 1 mL of TRI reagent and allowed to stand for ten minutes before proceeding to RNA isolation. RNA was isolated via phenol-chloroform extraction with TRI reagent with RNA purity and content measured by A260/280 ratio before being transferred to core services for quality assessment and library generation. Completion of protocol from sacrifice to application of TRI reagent was accomplished routinely in just under 3 hours.

Assessment of Cell Enrichment by FACS Analysis

We performed immunostaining of a preliminary set of cell suspensions with fluorescent antibodies for FACS analysis to verify our ability to enrich for target populations. Following cell

enrichment protocols cell count was determined and adjusted to 1 x 10^6 cells/mL with cell stain buffer and aliquoted into new, clean microcentrifuge tubes for labeling of negative controls, single channel positive controls, and combined labeling for analysis. Included stains/antibodies were as follows: anti-GLAST-PE antibody for astrocytes (Miltenyi Biotec #130-118-344), anti-CD11b-PE/Cy7 antibody (Miltenyi Biotec #101216) for microglia, anti-O4-APC (Miltenyi Biotec #130-099-211) for oligodendrocyte precursors, and DAPI (1 µg/mL) for live/dead discrimination. Live dead discrimination was also performed using Ghost Dye 450 (TONBO Biosciences #13-0863-T100). Verification of nucleated events was performed using Vybrant DyeCycle Green stain (ThermoFisher #V35004). All antibodies were added at a 1 µL per 1 x 10^6 cells concentration. Staining occurred for 30 minutes on ice in the dark. Samples were then centrifuged as before and washed 3x in cell stain buffer. Following the final spin cells were resuspended in 500 µL and taken to the flow cytometry core for analysis. Samples were processed and analyzed by FACS on a BD FACSAria II cytometer (BD Biosciences, San Jose, CA). Cells were initially gated by forward scatter and side scatter (FSC and SSC respectively) to exclude most debris and multicellular events. Events that were DAPI negative but positive in more than one color channel were considered to be due to multicellular events or non-specific labeling of antibodies. Astrocytic events were considered as singly positive for GLAST-PE and neuronal events were considered as negative for all glial markers.

Generation of Total Stranded RNA Library and Performance of RNA-Seq

The Stranded Total RNA-Seq is performed using the Illumina NovaSeq 6000 Sequencing System at the University of Kansas Medical Center – Genomics Core (Kansas City, KS). Total RNA (input range: 315 ng – 1417 ng) was used to initiate the Stranded Total RNA-Seq library preparation protocol. The total RNA fraction underwent ribosomal reduction, size fragmentation

(6, 4, 3 or 2 minutes based on $\%DV_{200}$ calculation), reverse transcription into cDNA and ligation with the appropriate indexed adaptors using the TruSeq Stranded Total RNA HT Sample Preparation Kit (Illumina #RS-122-2203). Of the 48 samples generated from 24 mice, 32 samples (8 per group) were selected for further analysis based upon $\%DV_{200}$ quality $\geq 30\%$ (Hester et al., 2016; Illumina, 2015). Following Agilent Bioanalyzer QC of the library preparation and library quantification using the Roche Lightcycler96 with FastStart Essential DNA Green Master (Roche #06402712001), the RNA-Seq libraries are adjusted to a 2 nM concentration and pooled for multiplexed sequencing on the NovaSeq 6000. Two samples did not meet QC criteria for library generation and were excluded from further processing and analysis (n = 7,7,8,8 for CN, KN, CA, and KA respectively). The onboard clonal clustering procedure is automated during the NovaSeq 6000 sequencing run. The 100-cycle paired end sequencing is performed using the NovaSeq 6000 S1 Reagent Kit - 200 cycle (Illumina #20012864). Following collection, sequence data is converted from .bcl file format to fastQ files and de-multiplexed into individual sequences for further downstream analysis.

RNA-Seq Data Quality and Pathway Analysis

To assess RNA-Seq data quality, the FastQC tool (http://www.bioinformatics.babraham.ac.uk/projects/fastqc) was used. The QC report suggested high sequence duplication level in the samples. RSEM [PMID: 21816040] was then used to map sequences to mouse mm10 genome assembly. Following sequencing mapping, bowtie2 [PMID: 22388286] was selected as aligner within RSEM. RSEM produced low alignment rate as the unique alignment rates were observed to be <10 % for most samples. Both the high sequence duplication and the low alignment rate could be attributed to an RNA quality issue from the biological samples.

After the gene counts were obtained from RSEM, the correlation between samples was calculated to detect any potential mislabeling. The correlation analysis revealed that three samples were potentially mislabeled or otherwise significantly distinct from other samples within their group. These three samples were excluded prior to any subsequent statistical analyses. This resulted in a final cohort of n = 7,7,7,6 for CN, KN, CA, and KA respectively.

Following sample exclusions, the raw gene counts were normalized with library size and genes with non/low transcription of less than 1 cpm (count per million) in at least 2 out of 27 samples were filtered out. After filter non/low expressed genes, a total of ~23,000 genes were retained for downstream statistical analyses. The Bioconductor package “edgeR” [PMID: 19910308] was used for pair-wise comparisons of gene expression. Pathway analysis and visualization were performed using the R Bioconductor package “gage” [PMID: 19473525] and “pathview” [PMID: 23740750].

Table 3-1: List of antibodies used in experiments

Antibody	Dilution	Source	Catalog #
Non-neuronal antibody cocktail	20 µL/1 x 10^7 cells	Miltenyi Biotec	130-115-389
Anti-GLAST-biotin	20 µL/1 x 10^7 cells	Miltenyi Biotec	130-095-826
Anti-GLAST-PE	1 µL/1 x 10^6 cells	Miltenyi Biotec	130-118-344
Anti-CD11b-PE/Cy7	1 µL/1 x 10^6 cells	Miltenyi Biotec	#101216
Anti-O4-APC	1 µL/1 x 10^6 cells	Miltenyi Biotec	#130-099-211

Results

Physiologic Effects of Ketogenic Diet on Mice

Mice maintained on the ketogenic diet (KD) were found to exhibit increased ketosis for the duration of the intervention period (Initial: Chow 0.32 ± 0.10 mM, KD 0.29 ± 0.10 mM; Final: Chow 0.33 ± 0.11 mM, KD 0.82 ± 0.19 mM, mean ± SD, $p = 0.44$ and < 0.000001 respectively, **Fig. 3-2**). KD fed mice were observed to have reduced blood glucose compared to chow mice with the most pronounced difference occurring at the end of the intervention period (Chow 135.58 ± 37.02 mg/dL, KD 75.23 ± 35.37 mg/dL, mean ± SD, $p = 0.00037$, **Fig. 3-2**). Chow fed mice gained weight during the course of the study from an initial weight of 31.16 ± 4.07g to a final weight of 38.49 ± 4.80 g. KD fed mice lost weight initially from 29.10 ± 3.06g to a low of 26.40 ± 5.36g before gaining weight back to a final of 28.68 ± 6.67g (**Fig. 3-3**). KD fed mice ate significantly less food in terms of mass intake (Chow 5.29 ± 0.89 g/day, KD 2.34 ± 0.43 g/day; mean ± SD, $p < 0.0001$, **Fig. 3-4**) but consumed the same amount of daily kcal regardless of diet (Chow 18.03 ± 3.02 kcal/day, KD 16.96 ± 3.09 kcal/day; mean ± SD, $p = 0.36$, **Fig. 3-4**).

Evidence of Enrichment of Target Cell Populations and RNA Quality

To validate enrichment for target cell populations we first performed analysis sorting by FACS to verify enrichment by antibody labeling for cell-type specific surface antigens on a preliminary cohort of 3 mice. DAPI negative events made up 92.86 ± 1.66% of all events following gating on forward and side scatter across all separation protocols (**Fig. 3-5**). To determine what percentage of DAPI negative events represent live cells and not subcellular debris we made use of two separate dyes, Ghost Dye eFluor 450 and Dye Cycle Green, to identify viable cells and nucleated cells respectively. Dye Cycle Green labeling indicated that, of DAPI negative events, 85.45 ± 3.00% events were nucleated across all samples. Ghost Dye

labeling indicated cellular viability of 68.03 ± 2.69% of events post-gating on forward and side scatter plots. Following neuronal enrichment protocols, we observed an increase of events free of all glial markers to 95.85 ± 2.10% of events compared to 37.93 ± 6.88% in unsorted brains (**Fig. 3-5**). Following astrocyte enrichment protocols, we observed an increase of singly positive GLAST-PE labeled events from 38.23 ± 15.23% in unsorted brains to 56.58 ± 23.83% with an associated reduction in the non-astrocyte fraction to 8.34 ± 8.31% (**Fig. 3-5**).

Following isolation of target populations and RNA extraction we performed RNA quality control and quantitation using the Agilent Bioanalyzer. We found no difference in RNA quality across separation protocols or dietary interventions by DV_{200}% (Chow Neuron 42.69 ± 16.76%, Keto Neuron 45.81 ± 17.95%, Chow Astrocyte 47.25 ± 14.31%, Keto Astrocyte 49.72 ± 15.36%; mean ± SD, p = 0.9586 by two-way ANOVA, **Fig. 3-6**). We did however obtain greater RNA yields via neuronal isolation protocol compared to the astrocyte protocol but did not observe an effect of diet on RNA yield (Chow Neuron 2,964 ± 2,497 ng, Chow Astrocyte 1,160 ± 432 ng, Keto Neuron 2,857 ± 1,592 ng, Keto Astrocyte 1,004 ± 301 ng; mean ± SD, p = 0.0052 for cell type by two-way ANOVA, **Fig. 3-6**).

As we used the entirety of samples generated from the diet cohort to generate RNA to maximize yield, we did not perform post-sorting FACS analysis on those samples. Instead, we utilized transcript counts of known cell type specific transcripts within the data set to verify enrichment. For astrocytes, we examined expression of *Gfap*, *Aldh1l1*, *Slc1a3*, and *S100b*. Expression of each of these genes were increased in astrocyte enriched data sets relative to neuronally enriched data sets (*Gfap*: Astrocytes 82.02 ± 13.44, Neurons 16.42 ± 13.76, *Slc1a3*: Astrocytes 222.0 ± 46.32, Neurons 39.18 ± 33.34, *Aldh1l1*: Astrocytes 23.66 ± 5.24, Neurons 4.53 ± 4.27, *S100b*: Astrocytes 92.05 ± 23.07, Neurons 11.01 ± 10.23; mean ± SD, units are

CpM, **Fig. 3-7**). For neurons we looked at expression of mature neuronal markers *Rbfox3*, *Syp*, *Nefm*, and *Nefh*. We observed expression of these genes in both neuron and astrocyte enriched fractions with astrocytically enriched samples often demonstrating higher gene counts (*Rbfox3*: Neurons 19.33 ± 16.42, Astrocytes 33.48 ± 8.08, *Syp*: Neurons 16.58 ± 22.85, Astrocytes 36.63 ± 14.11, *Nefm*: Neurons 14.82 ± 8.59, Astrocytes 25.63 ± 6.66, *Nefh*: Neurons 8.24 ± 5.46, Astrocytes 22.28 ± 4.79; mean ± SD, units are CpM, **Fig. 3-7**). Given higher raw neuronal gene count in astrocyte samples than expected, we further verified enrichment of neuronal genes in neuron isolation preparations by ratioing the summated neuronal gene counts mentioned above to summated astrocyte gene counts within individual samples. In doing so, we found that all but one sample generated from neuron isolations demonstrated a higher neuron:astrocyte gene ratio compared to samples generated by astrocyte enrichment protocol (Neurons 0.9926 ± 0.302, Astrocytes 0.292 ± 0.102; mean ± SD, $p < 0.0001$, **Fig. 3-7**). Correlation analysis of samples that underwent statistical analysis are shown in **Figure 3-8**.

We further assessed the presence of microglial, oligodendrocytic, and endothelial genes to determine if either protocol demonstrated robust contamination of other cell types. We did not observe substantial expression of most of these other lineage specific transcripts compared to neuronal or astrocytic transcripts as demonstrated in **Figure 3-7**.

Changes in Individual Gene Expression

No genes were identified as differentially expressed to a statistically significant degree following adjustment of raw p-values for multiple hypothesis testing. For transparency, we have included a table of the top genes by lowest raw p-value for each dietary comparison within cell types and direction of change in expression for the reader's consideration **Table 3-4**. From here

forward any data regarding individual genes or discussions of such genes is done with an understanding that no statistical significance has been found.

KEGG Pathway Analysis

A total of 96 molecular signaling pathways and 30 pathology associated pathways were found to be upregulated in KD fed mouse neurons compared to chow fed neurons to a statistically significant degree. No pathways were found to be downregulated in neurons of KD fed mice compared to chow. Within astrocytes, KD fed mice were found to have 5 activated and 67 suppressed molecular signaling pathways by KEGG analysis. One pathology associated pathway was activated in KD fed astrocytes while 14 were suppressed as compared to chow astrocytes. 58 molecular pathways and 14 pathology pathways were found to be commonly significant between both KD fed neurons and astrocytes, all of which differed in the direction of effect with increases observed in neurons and decreases observed in astrocytes.

Of pathology transcriptional pathways activated by KD, 11 were cancer associated, 5 involved neurodegenerative disease, 5 involved infection, 3 involved metabolic disorders, 4 dealt with addiction, and 2 were cardiovascular disease associated. The three pathologies with the lowest q-values were all neurodegenerative disorders: Alzheimer's disease, Parkinson's disease, and Huntington's disease. Within astrocytes, the only upregulated pathology pathway involved response to *S. aureus* infection. Of the remaining suppressed pathways, 7 involved cancer, 3 were associated with addiction, two involved metabolic disorders, 1 involved infection, and 1 was cardiovascular disease associated.

Molecular pathways with lowest q-value and complete pathological pathways for each cell type are shown in **Tables 3-2 and 3-3** respectively.

Transcriptional Changes of Alzheimer's Disease Associated Transcripts

Given the three lowest q-value pathologies implicated were all neurodegenerative and our own hypothesis that the KD can be used as an effective treatment for age associated neurodegenerative disease, we have chosen to focus on the data associated with Alzheimer's disease pathogenesis for the remainder of the present manuscript. Transcripts that makeup the curated KEGG pathway analysis and the influence KD had in neurons may be viewed in **Figure 3-9**. From these data it appears the pathway was implicated primarily due to increased transcription of mitochondrial electron transport chain complexes for oxidative phosphorylation (**Fig. 3-10**), amyloid precursor protein, apolipoprotein E and its receptor LRP1, tau and its kinase GSK3β, and multiple proteins involved in modulating intracellular calcium levels in neurons of mice fed a KD.

As the KEGG pathway does not involve all known proteins and interactions that influence different pathogenic species involved in AD, we first expanded our study by examining expression changes in genes that have been implicated in AD by genome wide association studies as seen in **Figure 3-11**. From this it appears that the KD increases transcription of genes associated with APP metabolism, cholesterol metabolism, endocytosis, and cytoskeleton/axon development while downregulating the inflammatory mediator Ms4a superfamily. Astrocytic response is generally more inert except for increased transcription of Ms4a family members.

Expanding our investigation to include APP secretases and genes with known protein interactions with different APP products we observed a moderate increase in γ-secretase subunits, the α-secretase ADAM10, and β-secretase BACE1 (**Fig. 3-12**). Aβ42 has been shown to disrupt Notch signaling. We observed no changes in neuronal Notch family transcripts but an upregulation in the Notch inhibitor Numb. No differences were observed in levels of

mitochondrial Tomm40 or Timm23 which APP has been shown to interact with intracellularly. Astrocytes demonstrated reductions to BACE1, Numb, and extracellular matrix encoding genes that bind APP products.

Investigating transcript levels of the other major aggregating protein in AD revealed increased transcription of tau (*MAPT)* in neurons (**Fig. 3-13**). Additionally, neurons exhibited increased transcription of several tau kinases and phosphatases with the greatest differential effect observed in the phosphatase *Ppp3cb*. Again, astrocytes exhibited generally reduced transcription of these genes when mice were maintained on a ketogenic diet.

Of genes that interact with ApoE, neurons showed increased expression of ApoJ (*Clu*), with alternating patterns of upregulation and downregulation of apolipoprotein receptors with the greatest change being an increase in the ApoE receptor *Sorl1* (**Fig. 3-14**). Lipoprotein lipase (*Lpl*) was downregulated in neurons. Astrocytes demonstrated the opposite pattern in regulating levels of ApoE receptor transcripts and *Lpl*.

To evaluate metabolic pathways and insulin sensitivity we have chosen to compare those pathways in neurons and astrocytes as both were found to be significant in both populations. As seen in **Figures 3-15 and 3-16**, the directionality of gene expression is opposed as in other phenomena we've shown. The differences seem to be most pronounced for JNK, PI3K, Ras/Raf, ERK1/2 and PKA with lesser changes in intermediates of associated pathways.

Discussion

In our current study we investigated how a dietary intervention modulates transcriptional response in the brain as a function of cell type. The ketogenic diet largely increased transcriptional pathway activation and neurons while suppressing transcriptional responses in

astrocytes as determined by KEGG pathway analysis. The stark contrast of these responses may indicate that the KD fundamentally enhances neuronal function while suppressing glial function leading to glial quiescence in times of nutritional scarcity.

Of the top pathology pathways implicated, the top three pathologies implicated by neuron transcriptome changes were all neurodegenerative diseases. When we investigated further into AD relevant gene changes, we consistently observed a general increase in gene transcription in neurons with opposite effects observed in astrocytes. While it may be difficult to appreciate how increases in some of these genes, such as APP and tau kinases, would be beneficial in the treatment of AD we feel it is important to consider two points. First, the levels of individual mRNAs do not necessarily reflect protein level or pathway activation status as this does not consider rates of protein degradation or post-translational modifications. Secondly, we would make the point that all therapeutic strategies centered on reducing the amounts of variants of amyloid and tau species have not, as of yet, led to proven clinical improvement in AD subjects. Regardless of how exactly KD is altering AD relevant pathways, these data suggest that manipulating bioenergetics sit squarely at the crossroads of all relevant AD phenomena and have the capacity to alter them, potentially for therapeutic benefit.

Previously it has been shown that oligomeric Aβ42 suppresses mitochondrial respiration while ketone bodies prevent mitochondrial entry of Aβ42 (Yin et al., 2016). Similarly, declining mitochondrial function has been shown to increase APP processing to pathogenic Aβ42 (Wilkins & Swerdlow, 2016a). Therefore, it may be that neuroketotherapeutics both reduce the formation of Aβ42 oligomers and prevent mitochondrial entry by enhancing neuronal oxidative phosphorylation transcription and mitochondrial respiration as we have observed here *in vivo* and previously *in vitro* (See Chapter 2). The KD may also help prevent the accumulation of

misfolded proteins through the activation of ER protein folding pathways in neurons as indicated by KEGG analysis (**Table 3-2**) or by upregulating multiple heat shock proteins to act as chaperones (**Figure 3-18**). Increasingly, both systemic and brain insulin resistance is being implicated as part of the pathophysiology of AD that contributes to glucose hypometabolism and mitochondrial dysfunction. It has been shown that some AD relevant genes such as APP demonstrate low spatial correlation to insulin signaling pathway intermediates such as Akt and IRS1 (Diehl, Mullins, & Kapogiannis, 2017). Our present study has shown the ability of KD to modify the insulin signaling pathway at key regulatory steps including Akt, JNK, ERK1/2, PI3K, and IRS. It would make logical sense that KD would improve insulin sensitivity and has been shown to do so in diabetics although understanding how it specifically influences brain insulin resistance could benefit from further study (Bolla, Caretto, Laurenzi, Scavini, & Piemonti, 2019; Kinzig, Honors, & Hargrave, 2010). For instance, it is not well understood if brain insulin resistance is more a consequence of astrocytic dysfunction at the blood brain barrier or neuronal dysfunction determining fuel utilization.

While we did not observe any significantly altered individual genes following multiple hypothesis testing, we do feel it is appropriate to comment on a selection of a series of genes that appeared to share functional similarities or belonged to the same familial domain as their inclusion on lists of lowest raw p-values or magnitude of differential expression at random does not seem likely. Beginning with neuronal expression, three of the top ten implicated genes as ordered by ascending raw p-value were all involved in ubiquitin signaling pathways: *Rnf115*, *Ubac2*, and *Rnf14* (**Table 3-4**). *Rnf115* (ring finger protein 115/Rabring7) just barely missed significance with a false discovery rate of 0.16. *Rnf115* and *Rnf14* both function as E3 ubiquitin ligases that are thought to play a role in membrane receptor internalization, ubiquitination, and

trafficking content between the endosome and lysosome (Smith, Berry, & McGlade, 2013). We noted that three of the top 20 genes as ordered by magnitude of increased differential expression centered around histone biology: *Hist1h4m*, *Hist1h4f*, and *Hist1h3a* (**Table 3-5**). This is of interest as it supports earlier studies indicating a role for ketone bodies to modulate gene transcription through histone regulation by acting as histone deacetylase inhibitors (Marosi et al., 2016; Shimazu et al., 2013; Xie et al., 2016). Finally, when examining astrocytic genes ordered by greatest levels of suppression of transcription, we notice that three of the six most suppressed genes are all members of the protocadherin α family (**Table 3-6**).

When considering limitations of the current study we would like to first acknowledge the difficulty in producing high quality RNA through this experimental protocol that is completely free of contamination from other cell types. We cannot preclude the disproportionate loss of transcripts with short poly-A tails leading to a possible 3'-UTR bias in our current transcriptome dataset. We also feel it is important to underscore that changes in transcriptional pathways alone may not reflect the activation status of these pathways as these data do not consider translational rates nor the status of regulatory post translational modifications. As such, our present data solely implicate these phenomena as being affected by KD without being determinant as to how the KD specifically alters such pathways for a functional outcome. Further, we enriched for CNS cell type irrespective of brain region from which they were derived. Therefore, it is important to consider that not all pathway activations we detected may apply to these cell types in all brain regions as neuronal heterogeneity varies greatly from brain region to brain region.

Regarding the ketogenic diet utilized in this study, greater than 90% of the daily kcals are derived from fat, 10% from protein, and almost no kcals from carbohydrate which is roughly equivalent with a 4:1 classic ketogenic diet (M. K. Taylor, Swerdlow, & Sullivan, 2019). While

this proportion is often necessary to produce reliable, robust ketosis in rodents, it is not particularly feasible to translate to humans as a long-term diet. Ketogenic diets consumed by humans are more commonly 1:1 ketogenic diet where 70% of kcals are derived from fats, 20% from protein, and the remainder from carbohydrates. The extreme proportion of macronutrients used to induce ketosis in rodents may have important consequences and lead to pathway activation/suppression that may not be recapitulated by a more balanced diet or across organisms. Additionally, we noted that blood glucose levels of our KD cohort began to trend into hypoglycemia near the end of our 90-day intervention. It becomes difficult to attribute what portion of the diet induced specific pathway activations in the present study between induction by ketosis, insulin reduction, low blood glucose, or some combination of the aforementioned changes or other currently unrecognized mechanism. Identification of specific mechanisms of action would require a return to simpler interventions or the development of models of sustained ketosis without the need for dietary interventions that feature multiple confounding effects in addition to changes in ketonemia.

Nevertheless, the present study marks the first time to our knowledge the effects of a dietary intervention on the brain transcriptome have been assessed across multiple cell types *in vivo*. In doing so, we have found that the responses between neurons and astrocytes are distinctly specialized and often in opposition to each other in regard to specific molecular pathways. The current study suggests the ketogenic diet affects systems involved in neurodegenerative disease and may improve function in these diseases by enhancing neuronal oxidative phosphorylation while altering dynamics of insulin signaling and protein processing among other effects in neurons and astrocytes. Further improving our understanding of what pathways and which features of the diet regulate these transcriptional changes will improve our mechanistic

understanding of the effects of the ketogenic diet and could lead to the development of an effective dietary mimetic for the treatment of neurodegenerative disease and dementia.

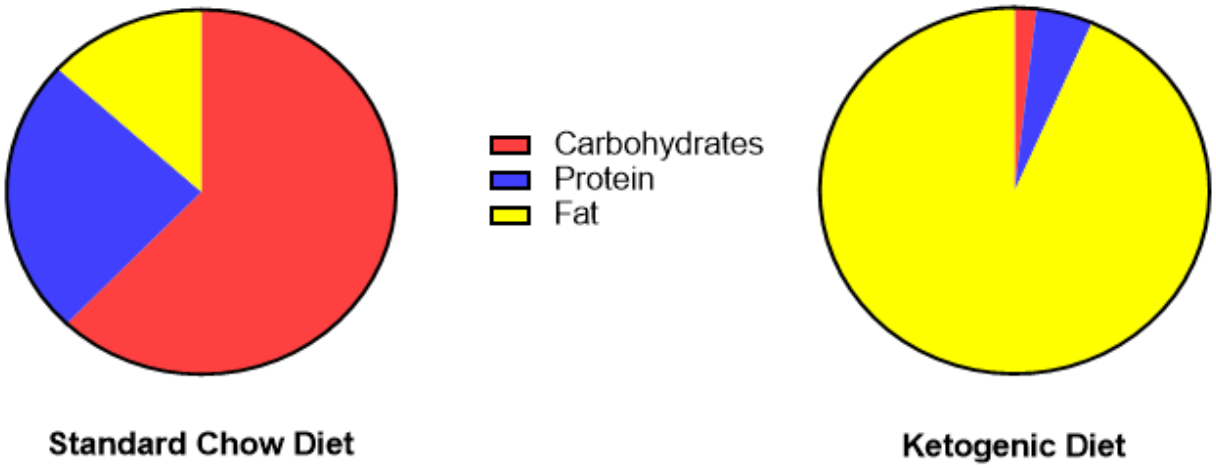

Standard Chow Diet

Ketogenic Diet

Figure 3-1: Macronutrient breakdown of diets by macronutrients as sources of kcal. Chow diet kcals come from 62.14% carbohydrate, 24.65% protein, and 13.21% fat. Ketogenic diet kcals come from 93.37% fat, 4.70% protein, and 1.80% carbohydrate.

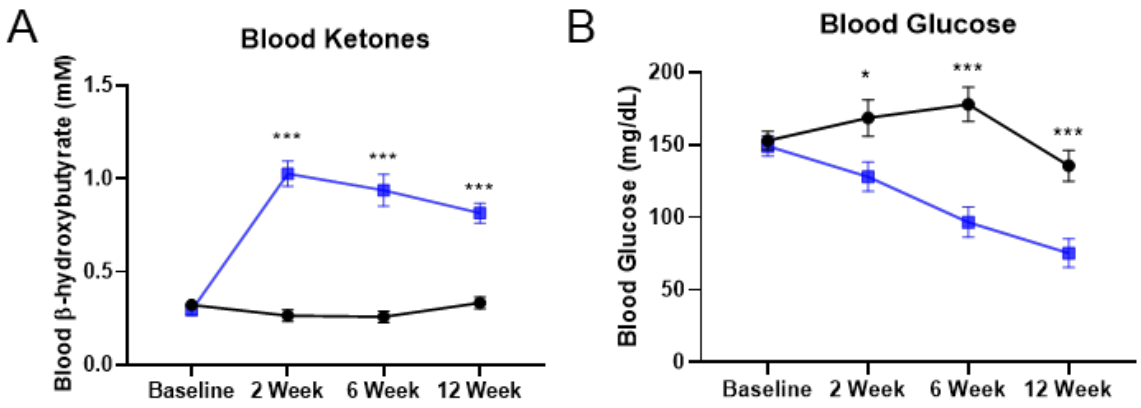
A
Blood Ketones
Blood β-hydroxybutyrate (mM)
1.5
1.0
0.5
0.0
***
***
***
Baseline
2 Week
6 Week
12 Week
B
Blood Glucose
Blood Glucose (mg/dL)
200
150
100
50
0
*
***
***
Baseline
2 Week
6 Week
12 Week

Figure 3-2: Ketogenic diet induces ketosis while reducing blood glucose. A) KD induces ketosis that was maintained throughout the duration of the dietary intervention. B) KD reduced blood glucose progressively throughout the study. Error bars represent standard error of the mean. *, **, ***, **** correspond to p-values < 0.05, 0.01, 0.001, and 0.0001 respectively. Ns indicates not significant.

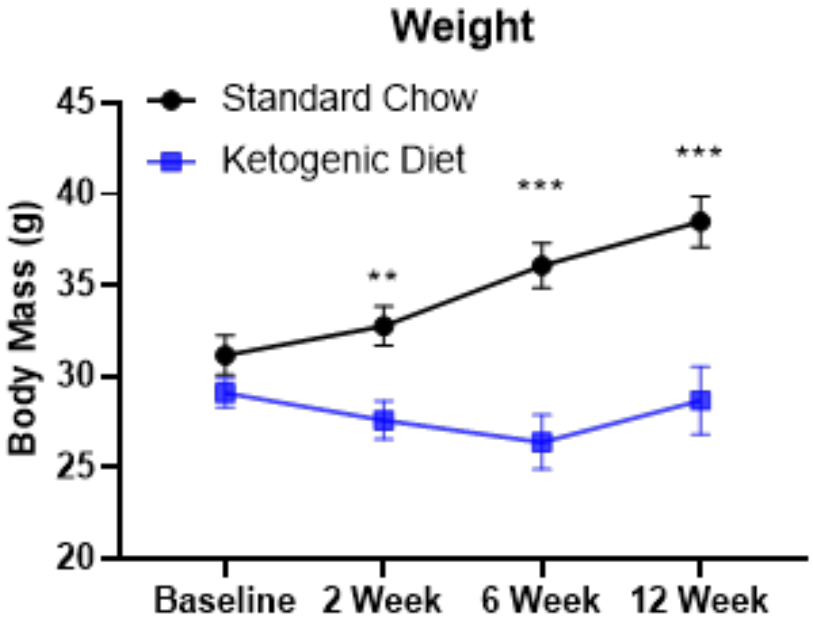
Weight
Standard Chow
Ketogenic Diet
Body Mass (g)
45
40
35
30
25
20
**
***
***
Baseline
2 Week
6 Week
12 Week

Figure 3-3: Ketogenic diet prevents weight gain in a 90-day intervention in adult mice. KD prevented weight gain that chow fed mice experienced. Error bars represent standard error of the mean. *, **, ***, **** correspond to p-values < 0.05, 0.01, 0.001, and 0.0001 respectively. Ns indicates not significant.

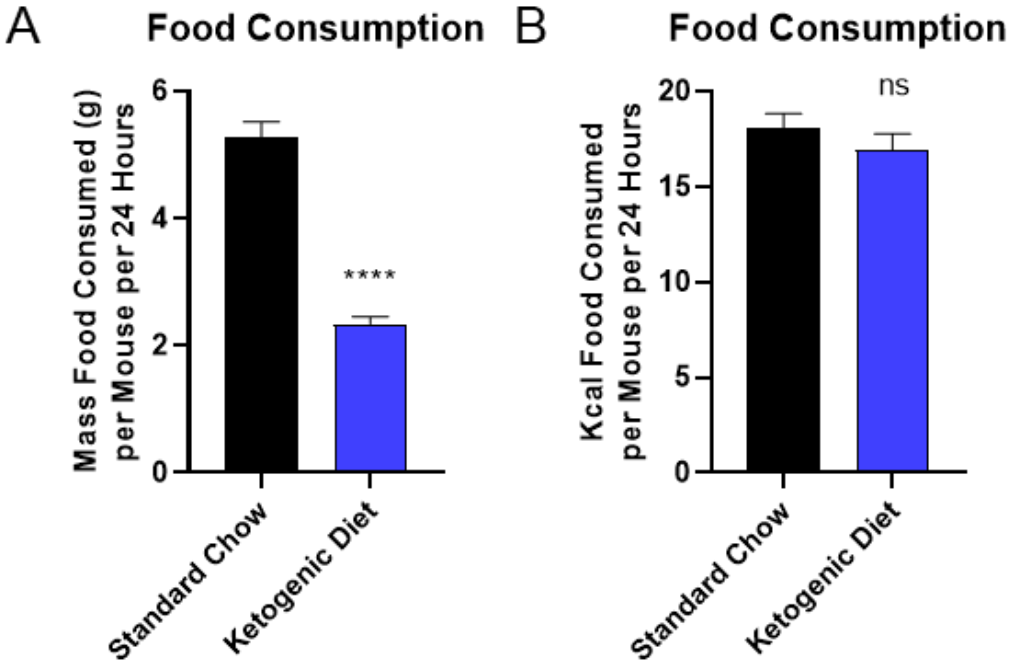
A
Food Consumption
Mass Food Consumed (g) per Mouse per 24 Hours
6
4
2
0
****
Standard Chow
Ketogenic Diet
B
Food Consumption
Kcal Food Consumed per Mouse per 24 Hours
20
15
10
5
0
ns
Standard Chow
Ketogenic Diet

Figure 3-4: Mice maintained on ketogenic diet ate less total food by mass but consumed the same amount of total calories. A) Mice maintained on KD ate less food by mass during the diet period. B) There was no difference in daily food intake by kcal. Error bars represent standard error of the mean. *, **, ***, **** correspond to p-values < 0.05, 0.01, 0.001, and 0.0001 respectively. Ns indicates not significant.

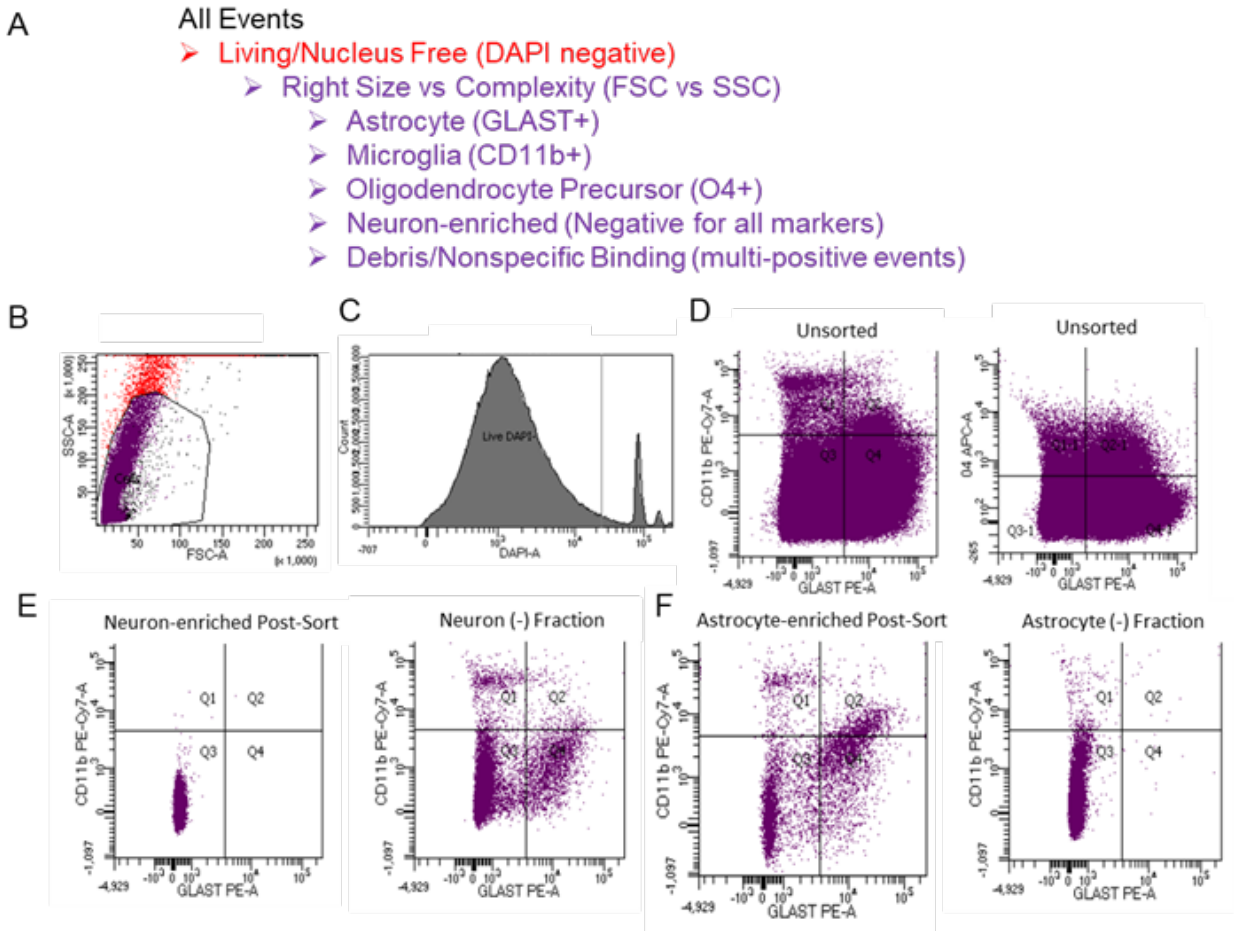
A
All Events
Living/Nucleus Free (DAPI negative)
Right Size vs Complexity (FSC vs SSC)
Astrocyte (GLAST+)
Microglia (CD11b+)
Oligodendrocyte Precursor (O4+)
Neuron-enriched (Negative for all markers)
Debris/Nonspecific Binding (multi-positive events)
B
SSC-A
FSC-A
C
Count
DAPI-A
Live DAPI-
D
Unsorted
CD11b PE-Cy7-A
GLAST PE-A
Unsorted
O4 APC-A
GLAST PE-A
E
Neuron-enriched Post-Sort
CD11b PE-Cy7-A
GLAST PE-A
Neuron (-) Fraction
CD11b PE-Cy7-A
GLAST PE-A
F
Astrocyte-enriched Post-Sort
CD11b PE-Cy7-A
GLAST PE-A
Astrocyte (-) Fraction
CD11b PE-Cy7-A
GLAST PE-A

Figure 3-5: FACS Analysis shows enrichment of target populations in preliminary studies. A) Schematic of gating and definition of target populations by antibody labeling. Color of schematic matches event colors in below charts. B) Initial gating was done by forward and side scatter to reduce the amount of total debris factored into final analysis. C) DAPI staining was included to identify apoptotic cells (DAPI-positive). D) Unsorted cells demonstrated large numbers of events in all quadrants/staining combinations. E) Neuron enrichment protocols provided a neuron enriched fraction where most events were found in the 3rd quadrant and negative for glial antibodies. The neuron negative fraction showed large amounts of events positively labeled with glial antibodies. F) Astrocyte enrichment protocol increased the proportion of singly positive GLAST labeled events (quadrant 4) compared to unsorted events. The astrocyte negative fraction generated by the protocol displayed a greatly reduced number of GLAST-positive events.

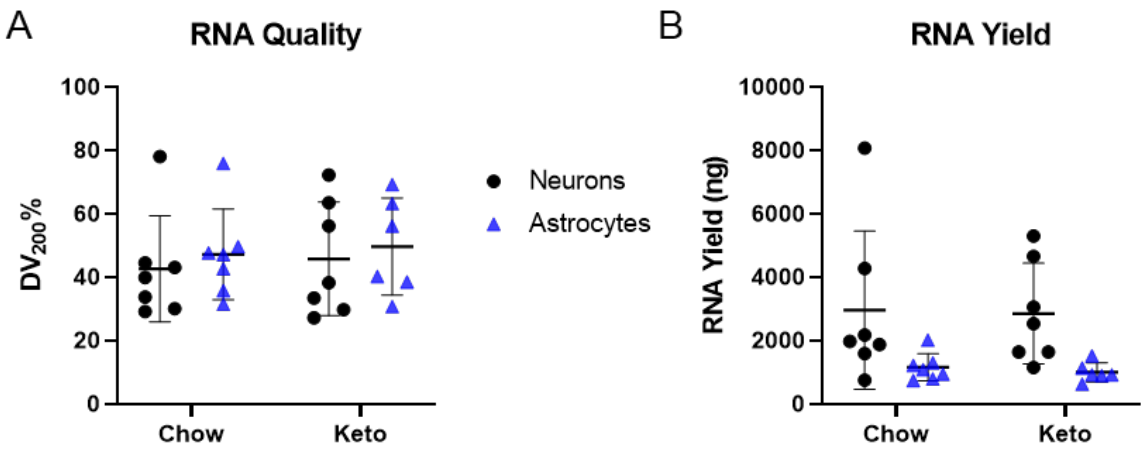
A
RNA Quality
100
80
60
40
20
0
DV200%
Chow
Keto
Neurons
Astrocytes
B
RNA Yield
10000
8000
6000
4000
2000
0
RNA Yield (ng)
Chow
Keto

Figure 3-6: RNA quality and yields by diet and enrichment protocol. A) RNA quality did not differ by diet or enrichment protocol. B) RNA yield was not affected by diet but was lower in astrocytes comparatively to neurons. Bars indicate means ± standard deviation. **** indicates p-value < 0.0001.

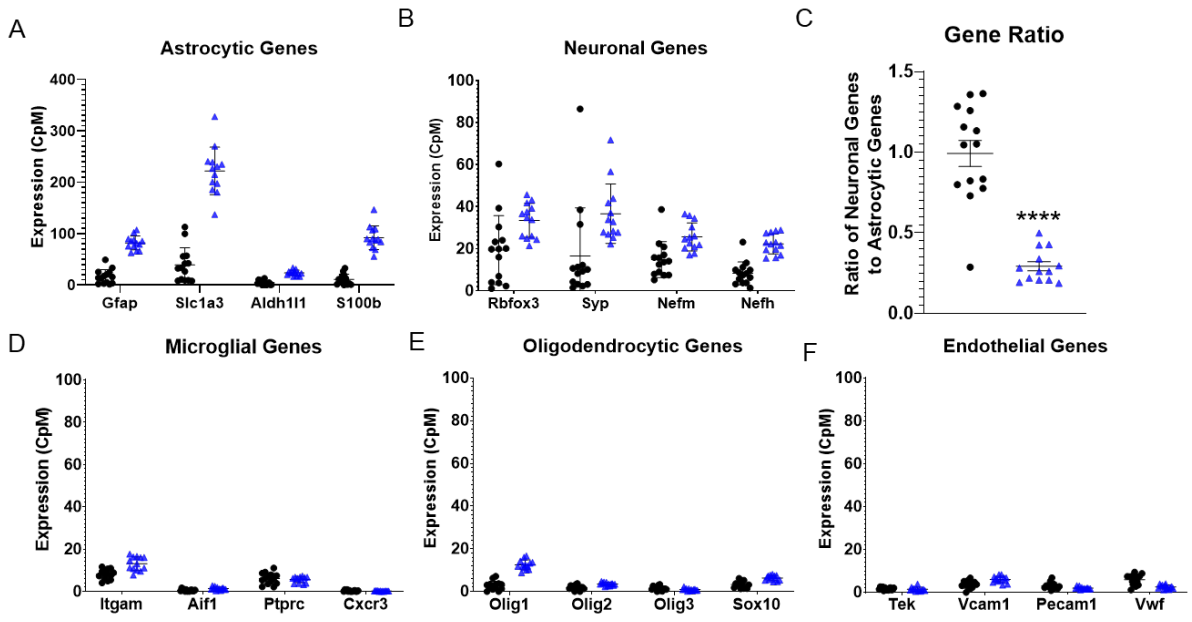
A
Astrocytic Genes
Expression (CpM)
400
300
200
100
0
Gfap
Slc1a3
Aldh1l1
S100b
B
Neuronal Genes
Expression (CpM)
100
80
60
40
20
0
Rbfox3
Syp
Nefm
Nefh
C
Gene Ratio
Ratio of Neuronal Genes to Astrocytic Genes
1.5
1.0
0.5
0.0
****
D
Microglial Genes
Expression (CpM)
100
80
60
40
20
0
Itgam
Aif1
Ptprc
Cxcr3
E
Oligodendrocytic Genes
Expression (CpM)
100
80
60
40
20
0
Olig1
Olig2
Olig3
Sox10
F
Endothelial Genes
Expression (CpM)
100
80
60
40
20
0
Tek
Vcam1
Pecam1
Vwf

Figure 3-7: Transcriptome libraries generated for RNAseq showed relative enrichment of genes specific to target populations. A) Astrocyte enriched libraries demonstrated higher CpMs of astrocyte specific genes *Gfap, Slc1a3, Aldh1l1,* and *S100b* relative to neuronally enriched samples. B) Neuronally enriched samples demonstrated expression of neuron specific genes *Rbfox3, Syp, Nefm,* and *Nefh*. Astrocyte samples also demonstrated expression of neuronal genes although at lower CpMs than astrocytic genes. C) Ratioing the aggregate CpMs of neuron specific genes to astrocyte specific genes within individual samples demonstrated a general enrichment for genes in accordance with their cell enrichment protocol. 13 of 14 neuronal samples had substantially higher ratios than those observed in astrocyte samples. D) We investigated levels of *Itgam*, *Aif1*, *Ptprc*, and *Cxcr3* to verify depletion of microglia. E) We utilized *Olig1*, *Olig2*, *Olig3*, and *Sox10* to verify depletion of oligodendrocytes. F) We examined amounts of *Tek, Vcam1, Pecam1*, and *Vwf* to verify depletion of endothelial cells. Bars indicate means ± standard deviation. **** indicates p-value < 0.0001.

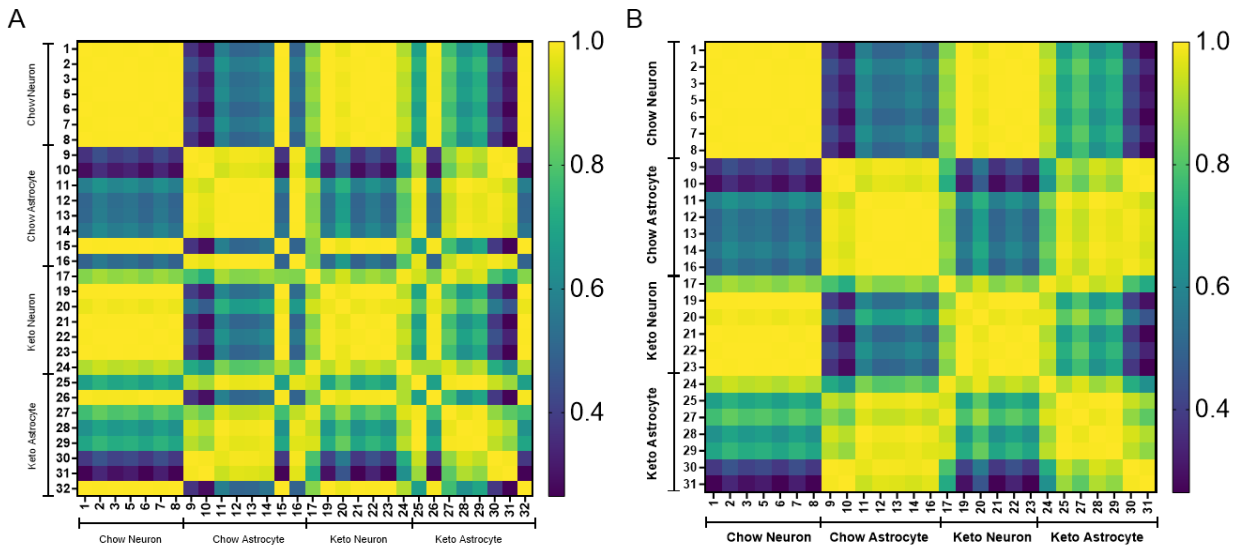
A
Chow Neuron
Chow Astrocyte
Keto Neuron
Keto Astrocyte
1.0
0.8
0.6
0.4
B
Chow Neuron
Chow Astrocyte
Keto Neuron
Keto Astrocyte
1.0
0.8
0.6
0.4

Figure 3-8: Intrasample correlation analysis of all samples that underwent cDNA library generation. A) Expanded heatmap of intrasample correlation analysis. Samples 15, 26, and 32 diverged from other samples within their groups and were excluded prior to downstream gene enrichment and pathway analysis. B) Intrasample transcriptome correlation analysis for samples that underwent downstream processing. Yellow indicates perfect correlation of 1.00. Navy blue indicates no correlation of 0.00.

Table 3-2: Complete table of molecular pathway changes found to be significantly altered by ketogenic diet.

Activated by KD in Neurons	q-value	Activated by KD in neurons (continued)	q-value	Activated by KD in Astrocytes	q-value	Suppressed by KD in Astrocytes	q-value
Protein processing in endoplasmic reticulum	0.000655132	Apoptosis	0.046919013	Hematopoietic cell lineage	0.00783	Axon guidance	2.82E-05
Insulin signaling pathway	0.001221279	Various types of N-glycan biosynthesis	0.051371288	Cytokine-cytokine receptor interaction	0.0096	Glutamatergic synapse	2.82E-05
Oxidative phosphorylation	0.001221279	Prolactin signaling pathway	0.051962248	Retinol metabolism	0.03534	Circadian entrainment	1.22E-04
Adrenergic signaling in cardiomyocytes	0.001221279	Signaling pathways regulating pluripotency of stem cells	0.052210388	Steroid hormone biosynthesis	0.04085	Spliceosome	1.51E-04
Dopaminergic synapse	0.001221279	Thyroid hormone synthesis	0.053805821	Complement and coagulation cascades	0.04085	Long-term potentiation	3.54E-04
cAMP signaling pathway	0.001221279	Inflammatory mediator regulation of TRP channels	0.058050713			Phosphatidylinositol signaling system	4.20E-04
Autophagy - animal	0.001221279	Long-term depression	0.058050713			GABAergic synapse	4.20E-04
MAPK signaling pathway	0.001221279	Collecting duct acid secretion	0.062766729			Oxytocin signaling pathway	4.20E-04
ErbB signaling pathway	0.001221279	Pancreatic secretion	0.062766729			Retrograde endocannabinoid signaling	4.97E-04
Oocyte meiosis	0.001246883	Mineral absorption	0.069200623			Insulin secretion	5.91E-04
Ras signaling pathway	0.001559926	Platelet activation	0.070280918			Dopaminergic synapse	5.91E-04
Ribosome	0.001667042	T cell receptor signaling pathway	0.070280918			GnRH signaling pathway	8.44E-04
Long-term potentiation	0.001686365	Cell cycle	0.07140136			Cholinergic synapse	8.44E-04
Retrograde endocannabinoid signaling	0.001745341	Circadian rhythm	0.077681213			mRNA surveillance pathway	8.44E-04
Oxytocin signaling pathway	0.001839688	VEGF signaling pathway	0.079879205			Protein processing in endoplasmic reticulum	1.38E-03
Glutamatergic synapse	0.001948751	SNARE interactions in vesicular transport	0.079879205			ErbB signaling pathway	3.14E-03
GABAergic synapse	0.001948751	Leukocyte transendothelial migration	0.081864502			Thyroid hormone signaling pathway	3.19E-03
Endocytosis	0.002273079	Fc epsilon RI signaling pathway	0.082962634			Autophagy - animal	3.19E-03
Neurotrophin signaling pathway	0.002273079	N-Glycan biosynthesis	0.082962634			Adrenergic signaling in cardiomyocytes	4.11E-03
Circadian entrainment	0.002351848	PI3K-Akt signaling pathway	0.084185286			Gap junction	5.33E-03
Axon guidance	0.002351848	Adipocytokine signaling pathway	0.084185286			MAPK signaling pathway	5.33E-03
Estrogen signaling pathway	0.002715537	B cell receptor signaling pathway	0.087405129			Endocytosis	5.33E-03
Gap junction	0.002801536	Serotonergic synapse	0.089972706			cAMP signaling pathway	5.76E-03
Rap1 signaling pathway	0.002857003	Inositol phosphate metabolism	0.092283132			Inositol phosphate metabolism	5.78E-03
Apelin signaling pathway	0.00405118	Glycosphingolipid biosynthesis - lacto and neolacto series	0.095714989			RNA transport	5.78E-03
GnRH signaling pathway	0.00405118	RNA transport	0.096699991			Insulin signaling pathway	8.63E-03
Regulation of actin cytoskeleton	0.00405118	Cellular senescence	0.096699991			Ubiquitin mediated proteolysis	8.63E-03
Cholinergic synapse	0.004176082					Endocrine and other factor-regulated calcium reabsorption	8.63E-03
Thyroid hormone signaling pathway	0.005284868					Calcium signaling pathway	8.63E-03
Longevity regulating pathway - multiple species	0.005410776					Neurotrophin signaling pathway	8.80E-03
Phospholipase D signaling pathway	0.005410776					Phospholipase D signaling pathway	1.03E-02
Insulin secretion	0.005410776					Aldosterone synthesis and secretion	1.03E-02
mTOR signaling pathway	0.005636697					Ribosome biogenesis in eukaryotes	1.03E-02
cGMP-PKG signaling pathway	0.006200815					Progesterone-mediated oocyte maturation	1.03E-02
Cardiac muscle contraction	0.006300348					Focal adhesion	1.08E-02
Longevity regulating pathway	0.007804526					RNA degradation	1.16E-02
Mitophagy - animal	0.007863903					Synaptic vesicle cycle	1.26E-02
Gastric acid secretion	0.008532551					Long-term depression	1.41E-02
Progesterone-mediated oocyte maturation	0.009023482					Bacterial invasion of epithelial cells	1.49E-02
Fc gamma R-mediated phagocytosis	0.009801314					cGMP-PKG signaling pathway	1.88E-02
Synaptic vesicle cycle	0.010141554					VEGF signaling pathway	1.91E-02
Tight junction	0.010230985					Aminoacyl-tRNA biosynthesis	2.07E-02
EGFR tyrosine kinase inhibitor resistance	0.01107239					Lysine degradation	2.44E-02
Glucagon signaling pathway	0.011455177					Endocrine resistance	2.45E-02
HIF-1 signaling pathway	0.012502468					Longevity regulating pathway	2.53E-02
Sphingolipid signaling pathway	0.012547859					Oocyte meiosis	2.86E-02
Adherens junction	0.013219241					Vasopressin-regulated water reabsorption	2.91E-02
Aldosterone synthesis and secretion	0.013424029					Sphingolipid signaling pathway	2.95E-02
Phosphatidylinositol signaling system	0.016081058					Cardiac muscle contraction	3.65E-02
Endocrine resistance	0.016522123					Tight junction	3.65E-02
Ubiquitin mediated proteolysis	0.016522123					Ras signaling pathway	3.77E-02
Salivary secretion	0.017046446					Aldosterone-regulated sodium reabsorption	4.37E-02
Focal adhesion	0.017063526					Apelin signaling pathway	5.05E-02
Endocrine and other factor-regulated calcium reabsorption	0.017063526					mTOR signaling pathway	5.19E-02
Melanogenesis	0.018110157					Mannose type O-glycan biosynthesis	5.46E-02
Carbon metabolism	0.019007126					Rap1 signaling pathway	5.50E-02
Vasopressin-regulated water reabsorption	0.01956765					Estrogen signaling pathway	5.85E-02
AMPK signaling pathway	0.022385969					Circadian rhythm	6.21E-02
Hippo signaling pathway	0.022385969					Gastric acid secretion	6.35E-02
Lysosome	0.024283797					EGFR tyrosine kinase inhibitor resistance	7.11E-02
FoxO signaling pathway	0.030660946					Glucagon signaling pathway	7.25E-02
Spliceosome	0.0330317					Proteoglycans in cancer	7.60E-02
Calcium signaling pathway	0.039873991					Autophagy - other	8.01E-02
Wnt signaling pathway	0.040626783					Glycerophospholipid metabolism	8.64E-02
Fatty acid metabolism	0.041965132					Other types of O-glycan biosynthesis	8.64E-02
Chemokine signaling pathway	0.043084574					Serotonergic synapse	8.64E-02
Aldosterone-regulated sodium reabsorption	0.043193037					Fc gamma R-mediated phagocytosis	9.66E-02
Renin secretion	0.046048287					HIF-1 signaling pathway	9.67E-02
Regulation of lipolysis in adipocytes	0.046672424					Adherens junction	9.67E-02

Table 3-3: Complete listing of pathology associated pathways found to be significantly influenced by ketogenic diet sorted by cell type and direction of effect.

Activated by KD in Neurons	q-value	Activated by KD in Astrocytes	q-value	Suppressed by KD in Astrocytes	q-value
Alzheimer's disease	0.000655132	Staphylococcus aureus infection	0.033983162	Bacterial invasion of epithelial cells	1.49E-02
Parkinson's disease	0.001667042			Morphine addiction	0.00309
Huntington's disease	0.002016036			Choline metabolism in cancer	0.00309
Renal cell carcinoma	0.002158549			Type II diabetes mellitus	0.00319
Non-alcoholic fatty liver disease (NAFLD)	0.002715537			Nicotine addiction	0.0108
Proteoglycans in cancer	0.00405118			Amphetamine addiction	0.01164
Alcoholism	0.004716036			Central carbon metabolism in cancer	0.01947
Morphine addiction	0.006020527			Renal cell carcinoma	0.02431
Amphetamine addiction	0.009695652			Glioma	0.05505
Bacterial invasion of epithelial cells	0.010793315			Dilated cardiomyopathy	0.05851
Fluid shear stress and atherosclerosis	0.011455177			Endometrial cancer	0.06348
Prostate cancer	0.011447938			MicroRNAs in cancer	0.07043
Endometrial cancer	0.016090616			Insulin resistance	0.08874
Colorectal cancer	0.017046446				
Type II diabetes mellitus	0.017063526				
Choline metabolism in cancer	0.020426807				
MicroRNAs in cancer	0.021320745				
Glioma	0.024955821				
Insulin resistance	0.024973282				
Chagas disease (American trypanosomiasis)	0.035017864				
Central carbon metabolism in cancer	0.040626783				
Pancreatic cancer	0.0587737				
Chronic myeloid leukemia	0.061346286				
Salmonella infection	0.06957064				
Prion diseases	0.07140136				
Tuberculosis	0.073387089				
Dilated cardiomyopathy	0.073387089				
HTLV-I infection	0.084185286				
Amyotrophic lateral sclerosis (ALS)	0.09834874				
Nicotine addiction	0.09834874				

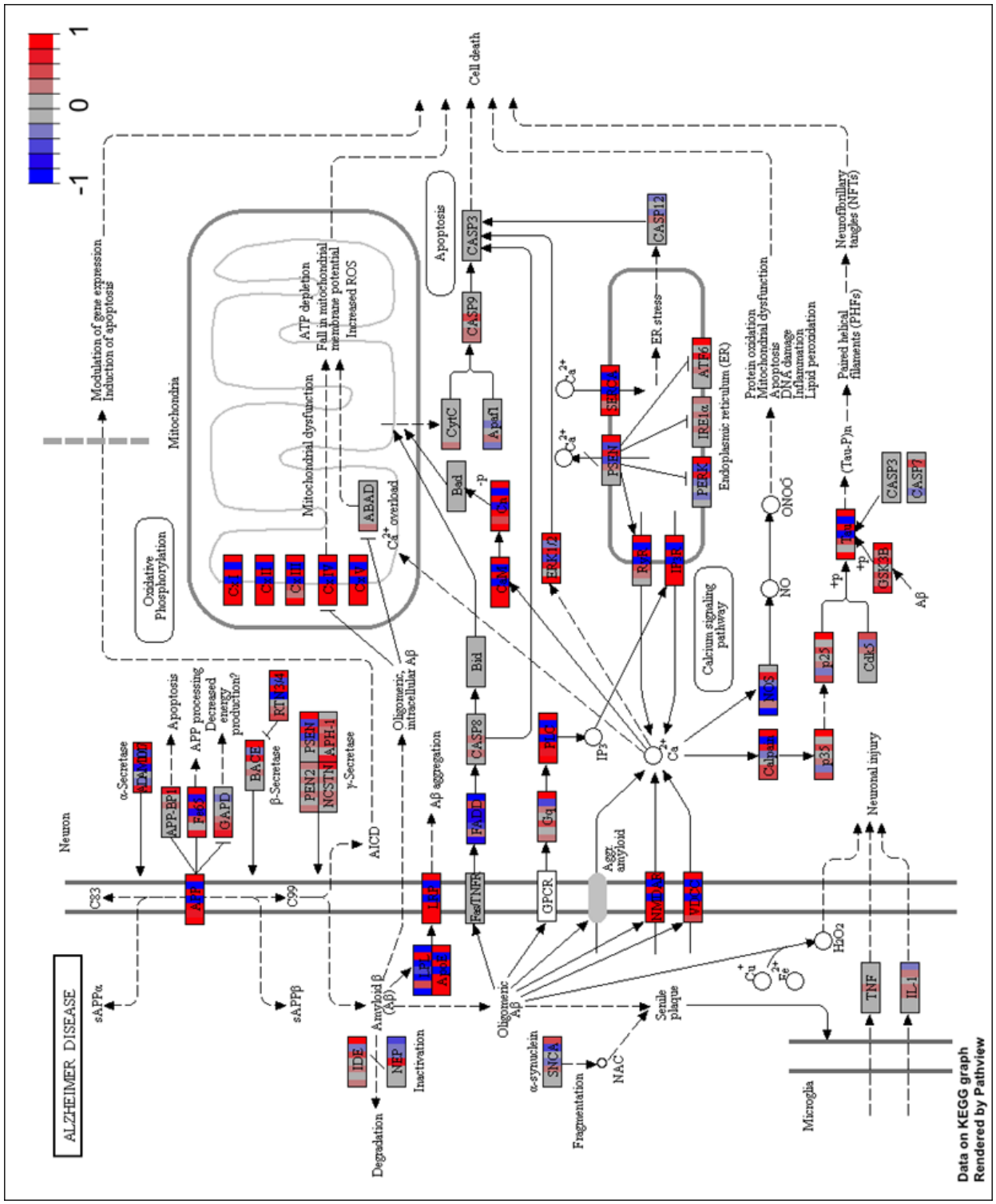
ALZHEIMER DISEASE
Neuron
Mitochondria
Oxidative Phosphorylation
Cell death
Apoptosis
Modulation of gene expression
Induction of apoptosis
ATP depletion
Fall in mitochondrial membrane potential
Increased ROS
Mitochondrial dysfunction
Ca2+ overload
α-Secretase
β-Secretase
γ-Secretase
APP processing
Decreased energy production?
Oligomeric, intracellular Aβ
AICD
Aβ aggregation
Aggr. amyloid
Calcium signaling pathway
Endoplasmic reticulum (ER)
ER stress
Protein oxidation
Mitochondrial dysfunction
Apoptosis
DNA damage
Inflammation
Lipid peroxidation
Paired helical filaments (PHFs)
Neurofibrillary tangles (NFTs)
Neuronal injury
Microglia
sAPPα
sAPPβ
Amyloid β (Aβ)
Degradation
Inactivation
Oligomeric Aβ
Senile plaque
α-synuclein
Fragmentation
NAC
Data on KEGG graph
Rendered by Pathview

Figure 3-9: Generated KEGG pathway of Alzheimer's disease transcripts affected by ketogenic diet in mouse neurons. For each gene transcript displayed, individual mice fed a ketogenic diet are represented by vertical color bars placed over the gene name to indicate relative expression compared to the mean of the chow cohort for the same gene. Blue reflects a decrease in relative expression, red represents increased relative expression, and grey indicates no change. The color scheme ranges from -1 to +1 indicating a $\log_2$ fold change.

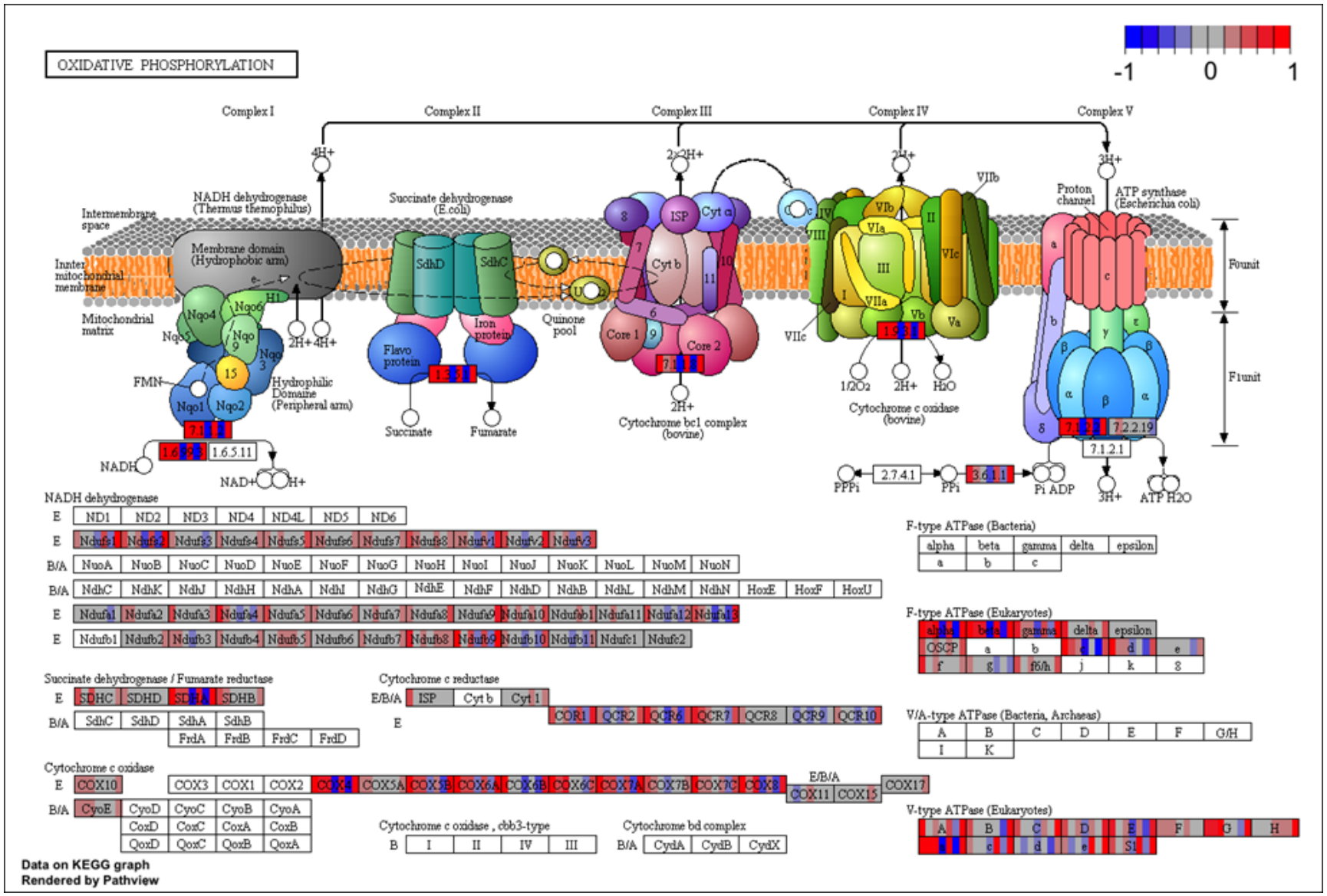
OXIDATIVE PHOSPHORYLATION
-1
0
1
Complex I
Complex II
Complex III
Complex IV
Complex V
NADH dehydrogenase (Thermus thermophilus)
Succinate dehydrogenase (E.coli)
Intermembrane space
Inner mitochondrial membrane
Mitochondrial matrix
Membrane domain (Hydrophobic arm)
Hydrophilic Domaine (Peripheral arm)
Flavo protein
Iron protein
Quinone pool
Cytochrome bc1 complex (bovine)
Cytochrome c oxidase (bovine)
Proton channel
ATP synthase (Escherichia coli)
Fo unit
F1 unit
NADH
NAD+
Succinate
Fumarate
FMN
PPPi
PPi
Pi ADP
ATP H2O
NADH dehydrogenase
Succinate dehydrogenase / Fumarate reductase
Cytochrome c reductase
Cytochrome c oxidase
Cytochrome c oxidase , cbb3-type
Cytochrome bd complex
F-type ATPase (Bacteria)
F-type ATPase (Eukaryotes)
V/A-type ATPase (Bacteria, Archaeas)
V-type ATPase (Eukaryotes)
Data on KEGG graph
Rendered by Pathview

Figure 3-10: Generated KEGG pathway of oxidative phosphorylation subunit transcripts affected by ketogenic diet in mouse CNS neurons. Subunits of all ETC complexes show varying degrees of increased expression in most samples. The color scheme ranges from -1 to +1 indicating a $\log_2$ fold change.

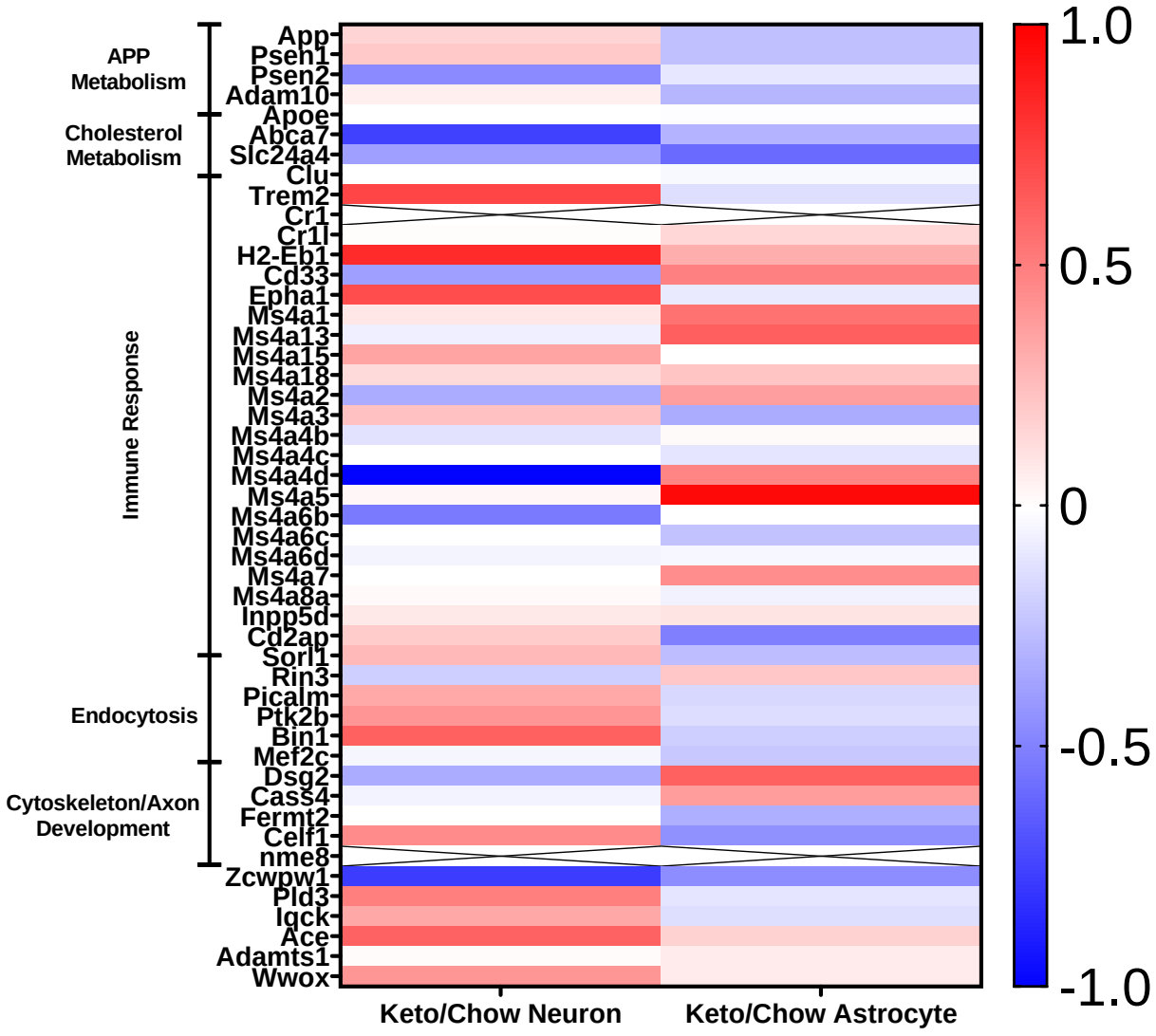
APP Metabolism
Cholesterol Metabolism
Immune Response
Endocytosis
Cytoskeleton/Axon Development
App
Psen1
Psen2
Adam10
Apoe
Abca7
Slc24a4
Clu
Trem2
Cr1
Cr1l
H2-Eb1
Cd33
Epha1
Ms4a1
Ms4a13
Ms4a15
Ms4a18
Ms4a2
Ms4a3
Ms4a4b
Ms4a4c
Ms4a4d
Ms4a5
Ms4a6b
Ms4a6c
Ms4a6d
Ms4a7
Ms4a8a
Inpp5d
Cd2ap
Sorl1
Rin3
Picalm
Ptk2b
Bin1
Mef2c
Dsg2
Cass4
Fermt2
Celf1
nme8
Zcwpw1
Pld3
Iqck
Ace
Adamts1
Wwox
Keto/Chow Neuron
Keto/Chow Astrocyte
1.0
0.5
0
-0.5
-1.0

Figure 3-11: Heat map indicating changes in mRNA expression of genes implicated to influence risk of developing AD as found by genome wide association studies (GWAS). Each row corresponds to a single gene with gene response of neurons and astrocytes to ketogenic diet intervention are organized in the left and right columns respectively. The color of each cell indicates the relative median change of KD samples compared to the normalized mean of chow fed samples. Increased expression is represented by red, decreases by blue, and no change by white. Saturation of color indicates the magnitude of the associated change in expression on a log-base-2 scale.

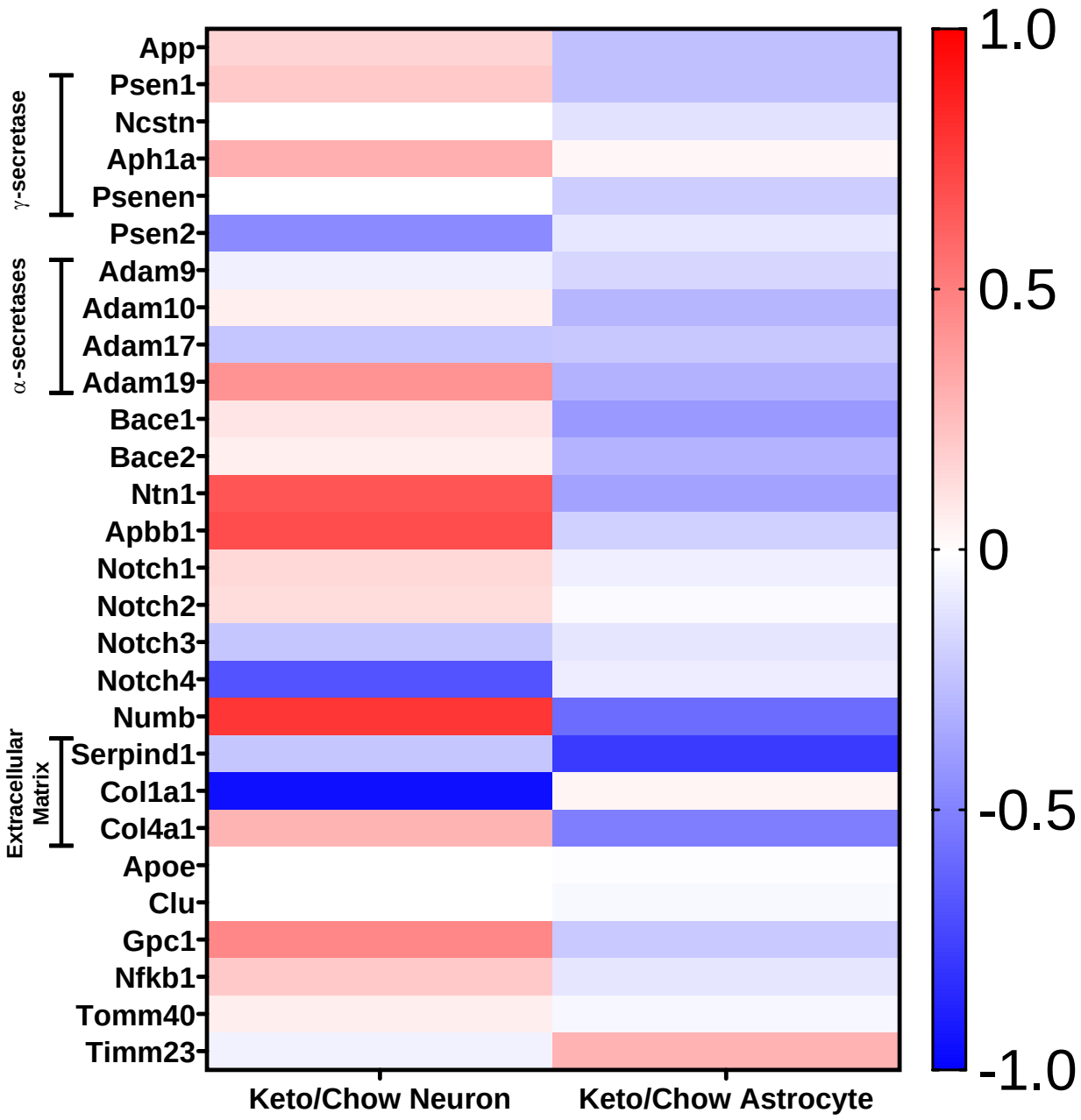
App
Psen1
Ncstn
Aph1a
Psenen
Psen2
Adam9
Adam10
Adam17
Adam19
Bace1
Bace2
Ntn1
Apbb1
Notch1
Notch2
Notch3
Notch4
Numb
Serpind1
Col1a1
Col4a1
Apoe
Clu
Gpc1
Nfkb1
Tomm40
Timm23
γ-secretase
α-secretases
Extracellular Matrix
Keto/Chow Neuron
Keto/Chow Astrocyte
1.0
0.5
0
-0.5
-1.0

Figure 3-12: Heat map of genes found to interact with amyloid precursor protein or its derivatives. Each row corresponds to a single gene with gene response of neurons and astrocytes to ketogenic diet intervention are organized in the left and right columns respectively. The color of each cell indicates the relative median change of KD samples compared to the normalized mean of chow fed samples. Increased expression is represented by red, decreases by blue, and no change by white. Saturation of color indicates the magnitude of the associated change in expression on a log-base-2 scale.

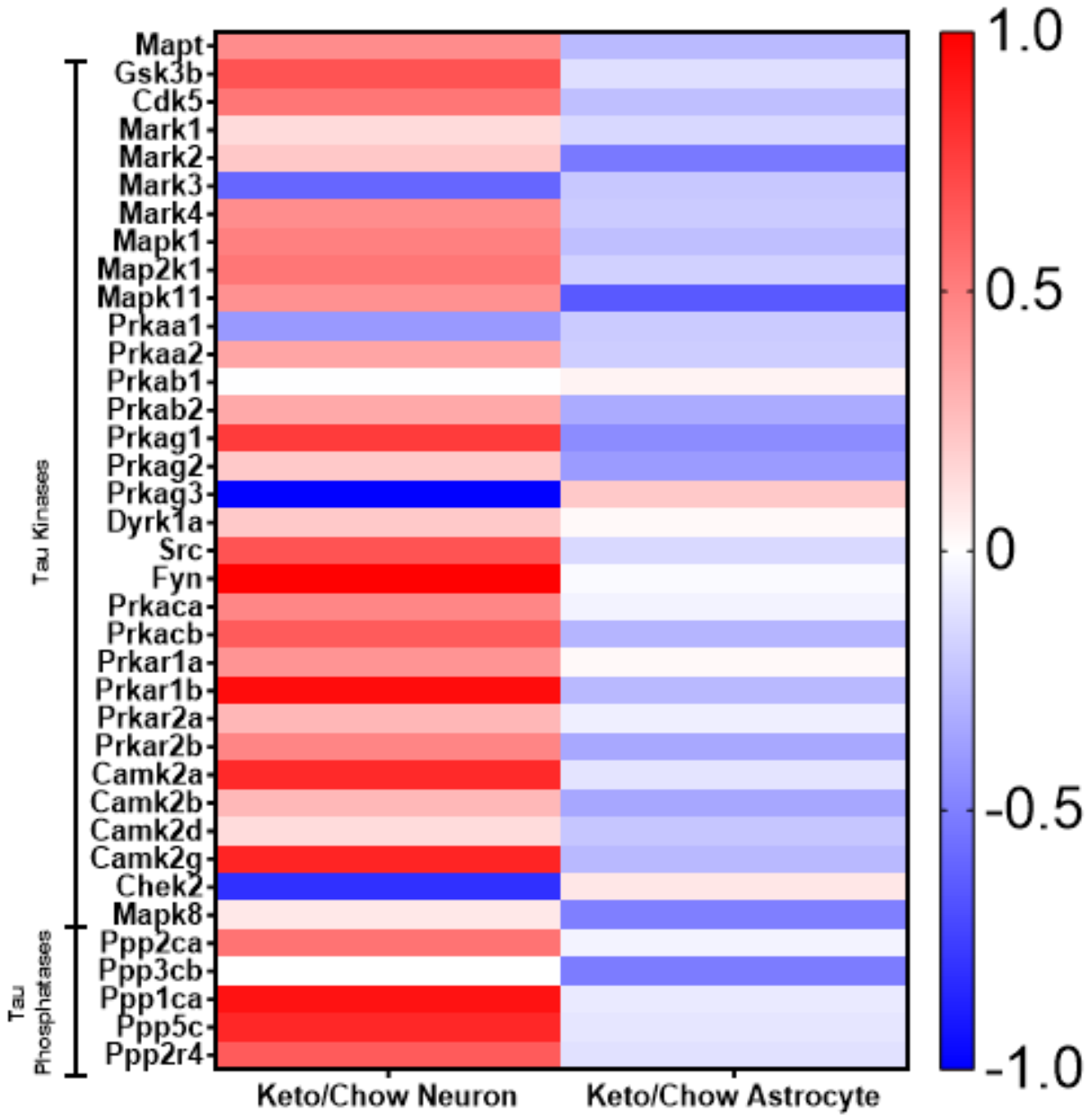
Mapt
Gsk3b
Cdk5
Mark1
Mark2
Mark3
Mark4
Mapk1
Map2k1
Mapk11
Prkaa1
Prkaa2
Prkab1
Prkab2
Prkag1
Prkag2
Prkag3
Dyrk1a
Src
Fyn
Prkaca
Prkacb
Prkar1a
Prkar1b
Prkar2a
Prkar2b
Camk2a
Camk2b
Camk2d
Camk2g
Chek2
Mapk8
Ppp2ca
Ppp3cb
Ppp1ca
Ppp5c
Ppp2r4
Tau Kinases
Tau Phosphatases
Keto/Chow Neuron
Keto/Chow Astrocyte
1.0
0.5
0
-0.5
-1.0

Figure 3-13: Heat map of tau (*Mapt*) and its known kinases and phosphatases. Each row corresponds to a single gene with gene response of neurons and astrocytes to ketogenic diet intervention are organized in the left and right columns respectively. The color of each cell indicates the relative median change of KD samples compared to the normalized mean of chow fed samples. Increased expression is represented by red, decreases by blue, and no change by white. Saturation of color indicates the magnitude of the associated change in expression on a log-base-2 scale.

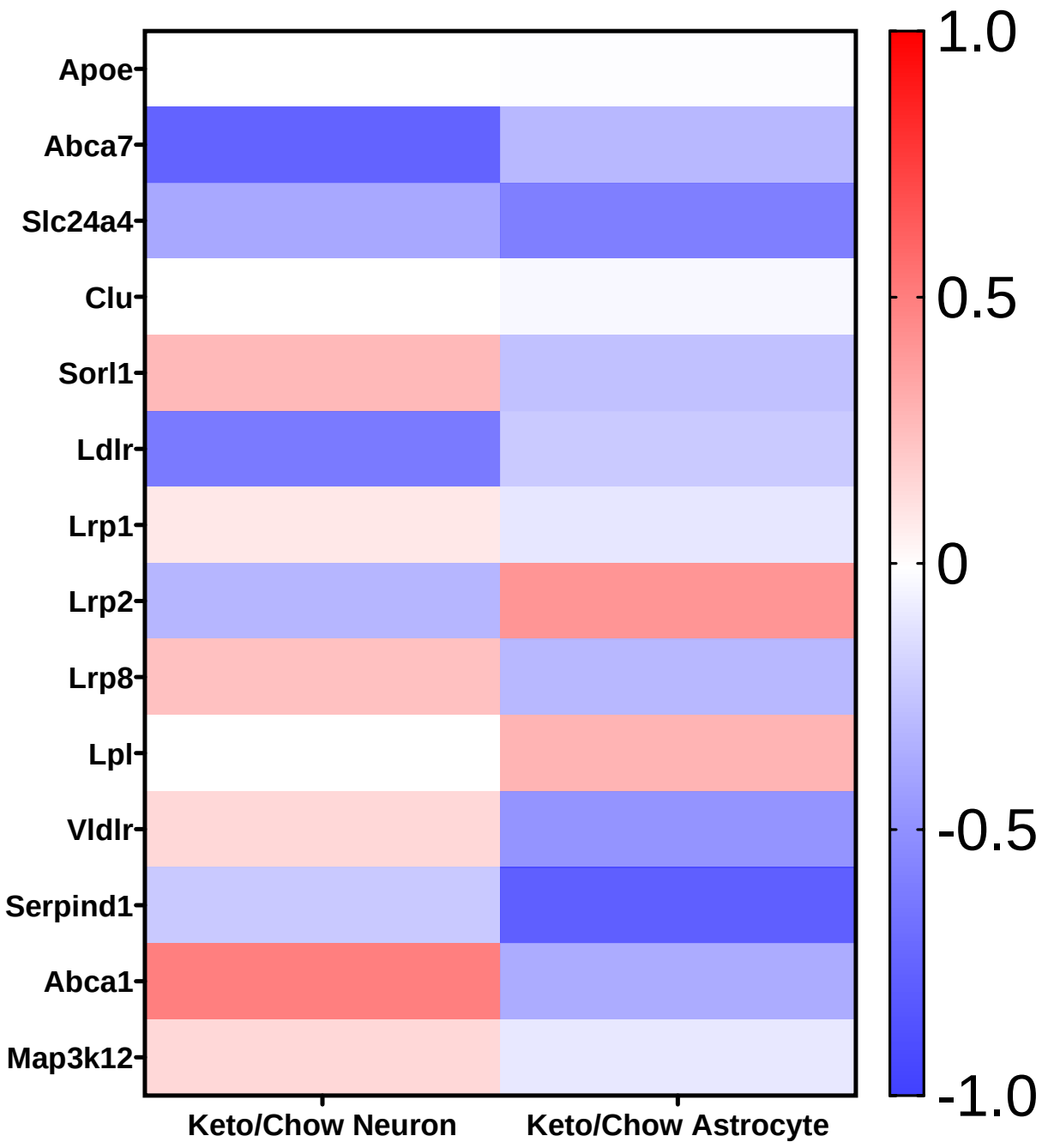
Apoe
Abca7
Slc24a4
Clu
Sorl1
Ldlr
Lrp1
Lrp2
Lrp8
Lpl
Vldlr
Serpind1
Abca1
Map3k12
Keto/Chow Neuron
Keto/Chow Astrocyte
1.0
0.5
0
-0.5
-1.0

Figure 3-14: Heat map of gene expression for apolipoprotein E (ApoE) and its known interacting genes. Each row corresponds to a single gene with gene response of neurons and astrocytes to ketogenic diet intervention are organized in the left and right columns respectively. The color of each cell indicates the relative median change of KD samples compared to the normalized mean of chow fed samples. Increased expression is represented by red, decreases by blue, and no change by white. Saturation of color indicates the magnitude of the associated change in expression on a log-base-2 scale.

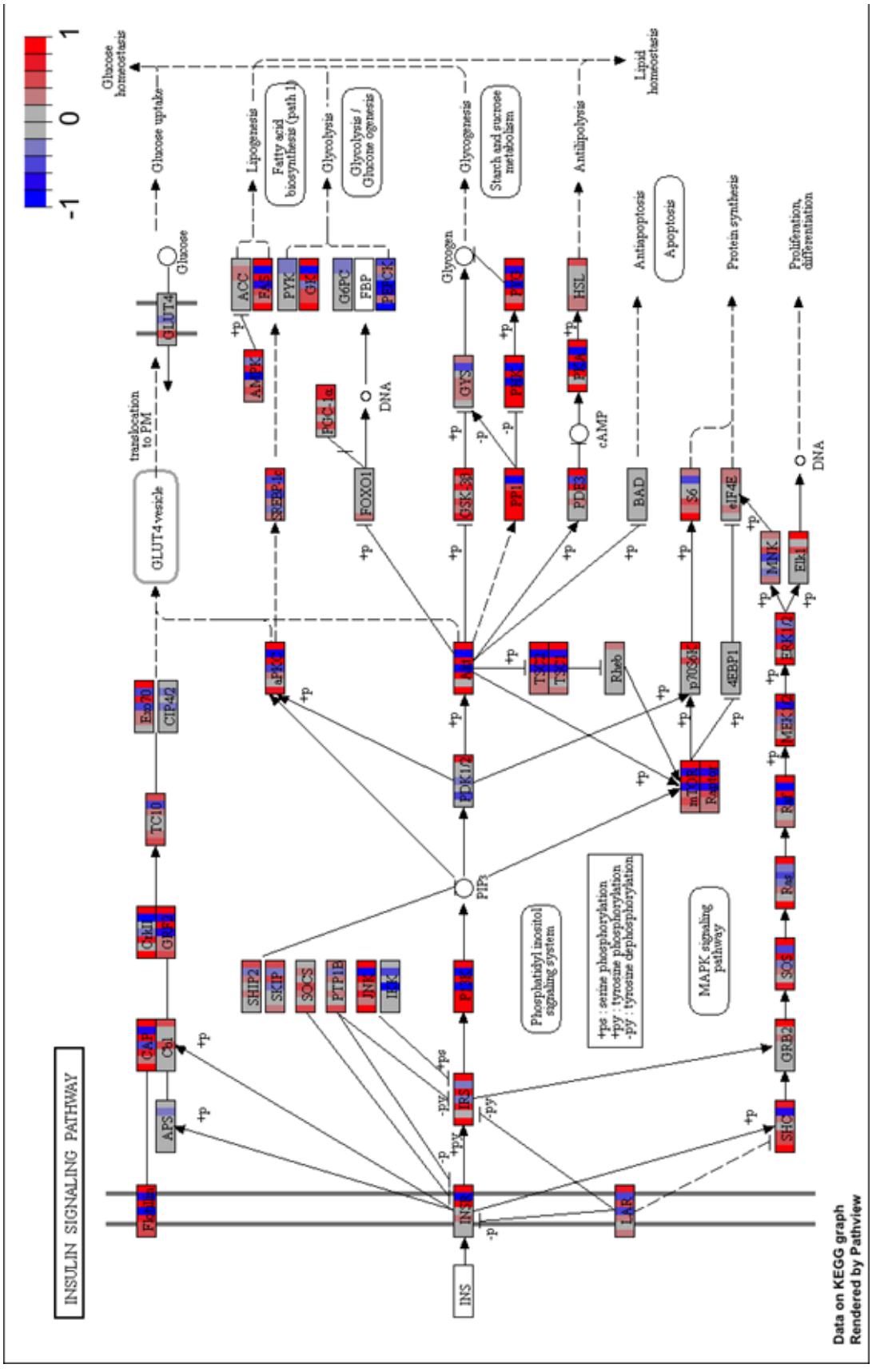
INSULIN SIGNALING PATHWAY
-1
0
1
Glucose homeostasis
Glucose uptake
Glucose
GLUT4
translocation to PM
GLUT4 vesicle
Lipogenesis
Fatty acid biosynthesis (path 1)
Glycolysis
Glycolysis / Gluconeogenesis
Glycogen
Glycogenesis
Starch and sucrose metabolism
Antilipolysis
Lipid homeostasis
Antiapoptosis
Apoptosis
Protein synthesis
Proliferation, differentiation
cAMP
DNA
INS
INSR
IRS
PI3K
PIP3
AKT
PDK1/2
mTOR
Rheb
TSC1
TSC2
p70S6K
4EBP1
S6
eIF4E
GRB2
SOS
Ras
RAF
MEK1/2
ERK1/2
MNK
Elk1
SHC
LAR
APS
CAP
Cbl
CBL
CRK
GRB2
TC10
Exo70
CIP4/2
SHIP2
SKIP
SOCS
PTP1B
JNK
IKK
PKC
Phosphatidyl inositol signaling system
MAPK signaling pathway
+ps : serine phosphorylation
+py : tyrosine phosphorylation
-py : tyrosine dephosphorylation
AMPK
ACC
FAS
PYK
G6PC
FBP
PEPCK
PGC-1α
FOXO1
SREBP1c
GYS
PHK
PYG
GSK3β
PP1
PDE3
HSL
BAD
Data on KEGG graph
Rendered by Pathview

Figure 3-15: Generated KEGG pathway of insulin signaling pathway transcriptional changes in neurons induced by ketogenic diet. Neuronal transcription of the insulin signaling pathway is generally increased. Differences appear clustered around JNK, PI3K, Akt, Ras, Raf, ERK1/2, and PKA. PEPCK displays the inversed pattern where its expression appears suppressed in neurons and increased in astrocytes.

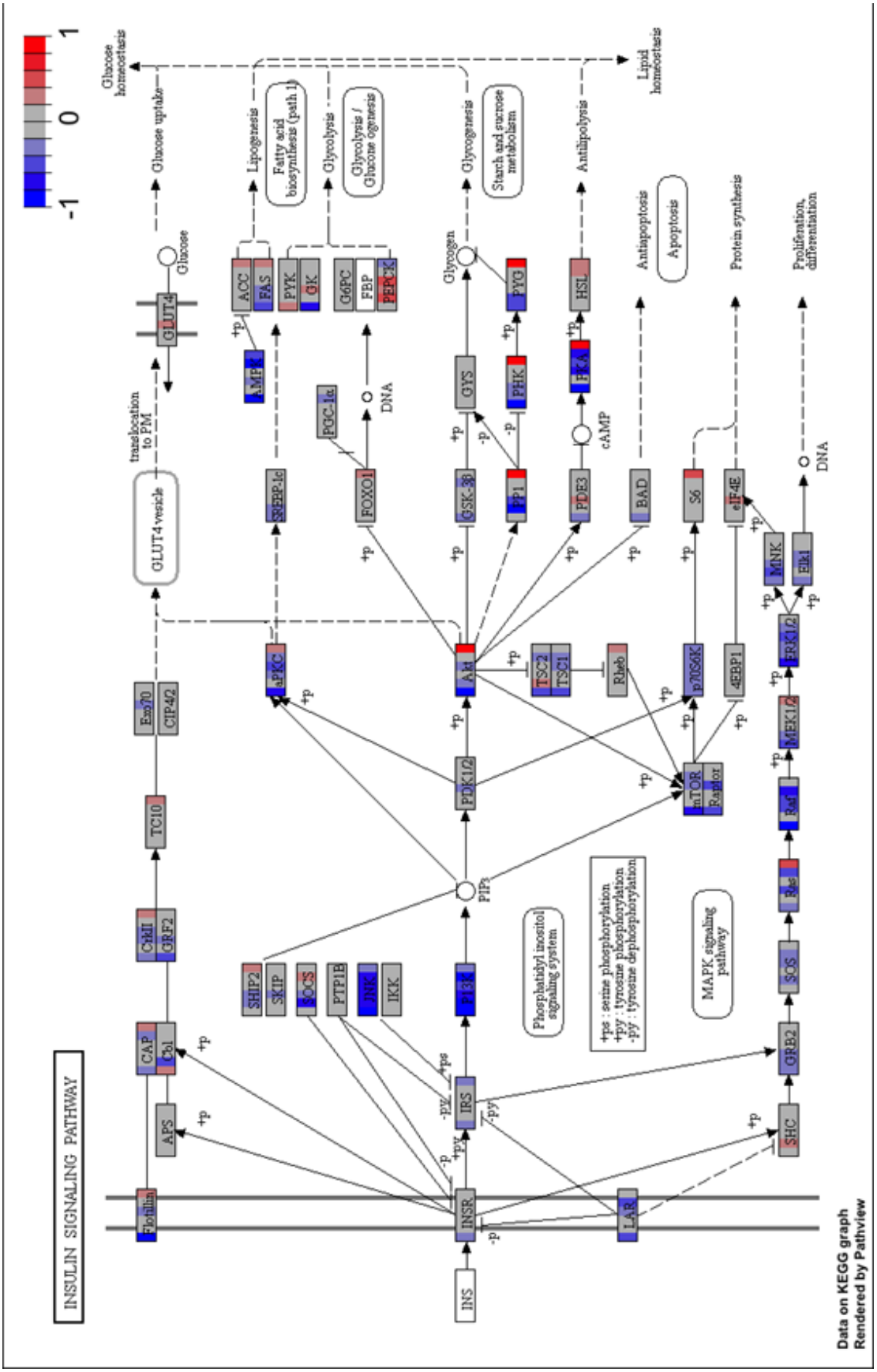
INSULIN SIGNALING PATHWAY
-1
0
1
Glucose homeostasis
Glucose uptake
Glucose
GLUT4
translocation to PM
GLUT4 vesicle
Lipogenesis
Fatty acid biosynthesis (path 1)
Glycolysis
Glycolysis / Gluconeogenesis
Glycogenesis
Glycogen
Starch and sucrose metabolism
Antilipolysis
Lipid homeostasis
Antiapoptosis
Apoptosis
Protein synthesis
Proliferation, differentiation
ACC
FAS
PYK
GK
G6PC
FBP
PEPCK
PYG
HSL
LMP1
PGC-1α
DNA
GYS
PHK
HKA
cAMP
SREBP-1c
FOXO1
GSK-3β
PP1
PDE3
BAD
S6
eIF4E
MNK
Elk1
aPKC
Akt
TSC2
TSC1
Rheb
p70S6K
4EBP1
ERK1/2
MEK1/2
PDK1/2
mTOR
Raptor
Raf
Ras
SOS
GRB2
SHC
Eps70
CIP4/2
TC10
CrkII
GRF2
CAP
Cbl
APS
Flotillin
INSR
IRS
PI3K
PIP3
LAR
INS
SHIP2
SKIP
SOCS
PTP1B
JNK
IKK
Phosphatidyl inositol signaling system
+ps : serine phosphorylation
+py : tyrosine phosphorylation
-py : tyrosine dephosphorylation
MAPK signaling pathway
Data on KEGG graph
Rendered by Pathview

Figure 3-16: Generated KEGG pathway of insulin signaling pathway transcriptional changes in astrocytes induced by ketogenic diet. Astrocytic response is largely suppressed. Differences appear clustered around JNK, PI3K, Akt, Ras, Raf, ERK1/2, and PKA. PEPCK displays the inversed pattern where its expression appears suppressed in neurons and increased in astrocytes.

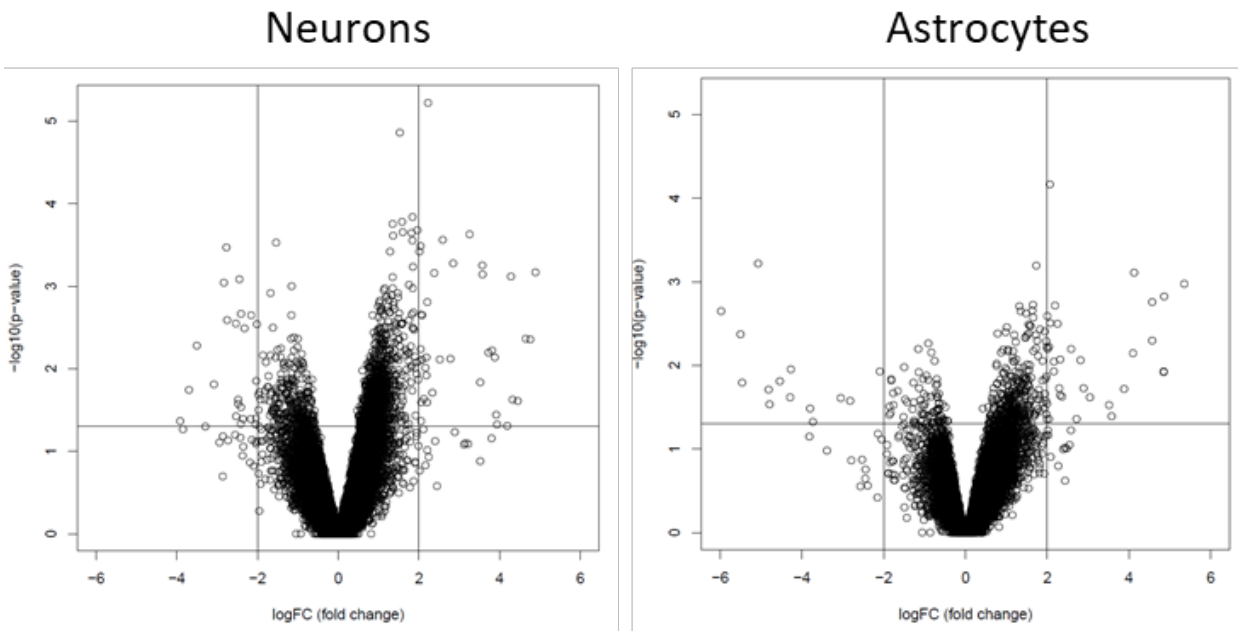
Neurons
Astrocytes
−log10(p−value)
logFC (fold change)
0
1
2
3
4
5
−6
−4
−2
0
2
4
6

Figure 3-17: Volcano plots of differentially expressed genes. A) Volcano plot demonstrating distribution of gene expression data of KD neurons compared to chow neurons. B) Volcano plot demonstrating distribution of gene expression data of KD astrocytes compared to chow astrocytes. X-axis demonstrates differential expression on a log(Fold Change) scale with vertical bars serving as the delineation for genes that are "differentially expressed." Y-axis corresponds to $\log_{10}$(p-value) with genes above the horizontal black line being considered significant by raw p-value. No genes were found to be significant following multiple hypothesis testing. Each circle represents a single gene.

Table 3-4: Differentially expressed genes in neurons and astrocytes organized by ascending raw p-value. No individual genes were found to be significant after multiple hypothesis testing. Top panel are neuronal genes organized by ascending raw p-value. Top neuronal genes include a mitochondrial complex I subunit and genes involved in E3 ubiquitin ligase activity among others. Bottom panel are astrocytic genes. No consistent pattern is evident other than multiple olfactory receptor genes.

Gene	logFC	logCPM	PValue	Encodes
Ndufb5	2.225381264	1.877515228	6.00E-06	NADH:ubiquinone oxidoreductase subunit B5
Rnf115	1.52709865	2.136617527	1.39E-05	E3 ubiquitin protein ligase ring finger protein 115
1700020I14Rik	1.839627723	3.565015028	0.00014723	Opa interacting protein 5, opposite strand 1
Ctxn1	1.581929119	2.97128811	0.000168726	cortexin 1
Ubac2	1.345515682	1.856780184	0.000176338	ubiquitin associated domain containing 2
Gfra4	1.959718259	1.34197156	0.000210059	glial cell line derived neurotrophic factor family receptor alpha 4
B4galt3	1.59821715	1.533429249	0.000224228	UDP-Gal:betaGlcNAc beta 1,4-galactosyltransferase, polypeptide 3
Rpusd1	1.816874097	0.914260157	0.000227457	RNA pseudouridylate synthase domain containing 1
AK155692	3.257311838	8.83485587	0.00023801	
Rnf14	1.359387848	3.53301341	0.000246002	E3 ubiquitin ligase ring finger protein 14
Olfr1431	2.587730325	-0.265027719	0.000275828	olfactory receptor 1431
Tst	1.842553606	1.744770532	0.000282924	thiosulfate sulfurtransferase, mitochondrial
Gene	**logFC**	**logCPM**	**PValue**	**Encodes**
Olfr1173	2.06359	0.275846	6.83E-05	olfactory receptor 1173
Gm9833	-5.07338	-0.84472	0.000609743	predicted gene 9833
Olfr1281	1.732922	0.892128	0.00064395	olfactory receptor 1281
Mup10	4.127457	-0.73484	0.00078149	major urinary protein 10
Gm4340	5.352636	0.892857	0.001066191	predicted gene 4340
AK004434	4.858772	-0.98017	0.00149721	
BC060616	4.566287	-0.91653	0.001754201	
Olfr612	1.650096	0.632264	0.00189627	olfactory receptor 612
Azgp1	2.19179	-0.05477	0.001945021	alpha-2-glycoprotein 1, zinc
AK161373	1.318604	0.821006	0.001956496	
Serpina10	1.633761	0.228275	0.002214632	serine (or cysteine) peptidase inhibitor, clade A (alpha-1 antiproteinase, antitrypsin), member 10
Pcdha4	-5.97547	0.204799	0.002240494	protocadherin alpha 4
Cabp4	1.347845	0.068265	0.002257912	calcium binding protein 4
Cilp	1.476974	0.990341	0.002389504	cartilage intermediate layer protein, nucleotide pyrophosphohydrolase
Vmn1r68	1.99795	0.355469	0.00257838	vomeronasal 1 receptor 68
Olfr1447	1.654429	0.429855	0.00270419	olfactory receptor 1447
Mfsd6l	2.075944	-0.10842	0.003151691	major facilitator superfamily domain containing 6-like
Oca2	2.249891	-0.07859	0.003205539	oculocutaneous albinism II
Srpx2	1.541896	-0.05799	0.003285461	sushi-repeat-containing protein, X-linked 2
Olfr1079	1.591969	0.555849	0.003368619	olfactory receptor 1079
Ntf3	1.571966	-0.05722	0.003388646	neurotrophin 3

Table 3-5: Differentially expressed genes in neurons organized by magnitude and direction of changes in expression. Upper panel are genes exhibiting increased expression on ketogenic diet. Three genes demonstrating the greatest magnitude of increased expression are involved in histone biology. Lower panel lists genes most suppressed by ketogenic diet.

Gene	logFC	logCPM	PValue	Encodes
Gm13769	4.887181052	-0.32966001	0.000689679	olfactory receptor 1565
Gm21693	4.757027355	-0.589979963	0.004451215	predicted gene 21693
BC099577	4.646347773	-0.740510017	0.004319167	RIKEN cDNA D830044I16 gene
BC099611	4.446431035	-0.632928632	0.024531925	human immunodeficiency virus type I enhancer binding protein 3
AK015096	4.317314283	0.561650689	0.023692685	predicted gene 26782
Hist1h4m	4.278381888	0.452483132	0.000763382	histone cluster 1, H4m
6430411K18Rik	4.186302551	-0.339768775	0.049912945	
AK164389	3.935381655	0.162214325	0.047488691	
Gm20604	3.913110793	-0.140135283	0.036069339	
AK044848	3.881221725	-0.94174677	0.007290992	
Hist1h4f	3.80934429	-0.52074203	0.00604827	Histone H4
AK195420	3.796480365	-0.203678224	0.070561994	
Scrn2	3.726965078	-0.344424992	0.00646881	Secernin 2
Lars2	3.575173916	7.990991695	0.000723554	leucyl-tRNA synthetase, mitochondrial
AK048085	3.571704849	0.345745282	0.000560823	
BC054394	3.51709465	0.337009757	0.014663266	
AK155692	3.257311838	8.83485587	0.00023801	
AB347309	2.889373213	-0.225404212	0.058820591	
Phpt1	2.848356054	0.490248903	0.000536413	phosphohistidine phosphatase 1
Hist1h3a	2.779661013	-0.629368037	0.007622204	histone H3
Olfr1431	2.587730325	-0.265027719	0.000275828	olfactory receptor 1431
Angptl4	2.515931264	-0.099656581	0.00779669	Angiopoietin-like 4
Pyroxd1	2.381033116	0.742193398	0.000693242	pyridine nucleotide-disulphide oxidoreductase domain 1
Deb1	2.333724073	0.190815363	0.019582217	differentially expressed in B16F10 1
Ndufb5	2.225381264	1.877515228	6.00E-06	NADH:ubiquinone oxidoreductase subunit B5

Gene	logFC	logCPM	PValue	Encodes
Tcrg	-3.917862458	-1.022906318	0.043144047	T Cell Receptor Gamma Locus
AK143933	-3.84868964	-0.837901969	0.054938761	
AK037822	-3.699004335	-1.118671863	0.018220364	
Fthl17-ps1	-3.500133538	-0.513953091	0.005293875	ferritin, heavy polypeptide-like 17, pseudogene 1
AK075572	-3.292132885	-0.763578369	0.050340771	
Ifna7	-3.077930953	-0.761689232	0.015710984	Interferon Alpha 7
AK209947	-2.854556202	-0.893748782	0.065885744	
Dupd1	-2.835019144	-0.585264916	0.000904344	dual specificity phosphatase and pro isomerase domain containing 1
4930413M19 Rik	-2.768010381	-0.301928161	0.000339662	
AK196308	-2.754327401	0.280788103	0.002607941	
Gm10941	-2.55050704	-0.903400094	0.063144728	Uncharacterized Protein
Myo7b	-2.537455998	-0.216089599	0.002830038	Myosin VIIB
AK038197	-2.532087113	-0.401183786	0.037655738	
Gm21671	-2.479759389	-0.818737653	0.026876738	predicted gene 21671
Gngt2	-2.477192212	-0.524766771	0.023701432	G Protein Subunit Gamma Transducin 2
Lipc	-2.448849646	-0.286180906	0.000836519	lipase, hepatic

Table 3-6: Differentially expressed genes in astrocytes organized by magnitude and direction of changes in expression. Upper panel are genes exhibiting increased expression on ketogenic diet. Bottom panel lists genes with greatest suppression by ketogenic diet. Three of the six most suppressed genes in astrocytes are all members of the protocadherin α family.

Gene	logFC	logCPM	PValue	Encodes
Gm4340	5.352636	0.892857	0.001066191	predicted gene 4340
AK004434	4.858772	-0.98017	0.00149721	
BC099611	4.84777	-0.63293	0.012028496	
mKIAA0217	4.845608	-0.01493	0.011970413	
BC060616	4.566287	-0.91653	0.001754201	
Gm13290	4.564359	-0.50714	0.00505247	predicted gene 13290
Mup10	4.127457	-0.73484	0.00078149	major urinary protein 10
AK183756	4.096607	-0.9086	0.007182291	
Gm4567	3.876475	1.018568	0.019160406	Predicted gene 10668
AK038197	3.575784	-0.40118	0.041170544	
Olfr27	3.510013	-0.02144	0.030041682	olfactory receptor 27
Guca1a	3.043139	-0.7802	0.02409671	Guanylate Cyclase Activator 1A

Gene	logFC	logCPM	PValue	Encodes
Pcdha4	-5.97547	0.204799	0.002240494	Protocadherin alpha 4
AK157947	-5.50068	-0.65575	0.004295523	
6430411K18Rik	-5.46279	-0.33977	0.016295783	
Gm9833	-5.07338	-0.84472	0.000609743	predicted gene 9833
Pcdha6	-4.8144	0.220271	0.019456482	Protocadherin Alpha 6
Pcdha7	-4.78927	-0.04967	0.029429494	Protocadherin Alpha 7
AK166469	-4.54032	-0.67981	0.015600632	
Zfp91Cntf	-4.28701	-0.66989	0.024322131	Zinc Finger Protein 91 Homolog, Ciliary Neurotrophic Factor Transcription Unit

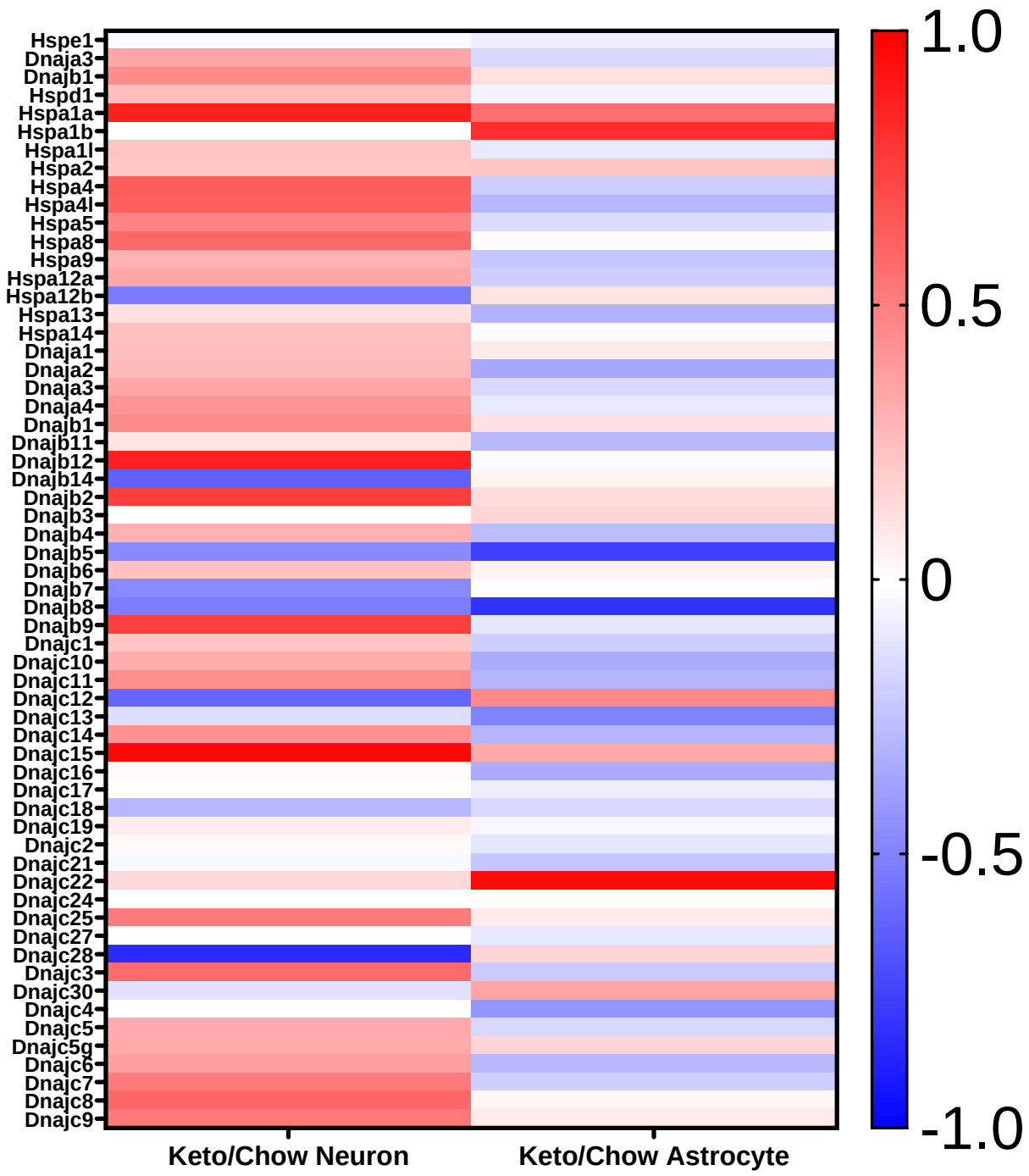
Hspe1
Dnaja3
Dnajb1
Hspd1
Hspa1a
Hspa1b
Hspa1l
Hspa2
Hspa4
Hspa4l
Hspa5
Hspa8
Hspa9
Hspa12a
Hspa12b
Hspa13
Hspa14
Dnaja1
Dnaja2
Dnaja3
Dnaja4
Dnajb1
Dnajb11
Dnajb12
Dnajb14
Dnajb2
Dnajb3
Dnajb4
Dnajb5
Dnajb6
Dnajb7
Dnajb8
Dnajb9
Dnajc1
Dnajc10
Dnajc11
Dnajc12
Dnajc13
Dnajc14
Dnajc15
Dnajc16
Dnajc17
Dnajc18
Dnajc19
Dnajc2
Dnajc21
Dnajc22
Dnajc24
Dnajc25
Dnajc27
Dnajc28
Dnajc3
Dnajc30
Dnajc4
Dnajc5
Dnajc5g
Dnajc6
Dnajc7
Dnajc8
Dnajc9
Keto/Chow Neuron
Keto/Chow Astrocyte
1.0
0.5
0
-0.5
-1.0

Figure 3-18: Heat map of changes in heat shock protein gene expression induced by ketogenic diet in neurons and astrocytes. Each row corresponds to a single gene with gene response of neurons and astrocytes to ketogenic diet intervention are organized in the left and right columns respectively. The color of each cell indicates the relative median change of KD samples compared to the normalized mean of chow fed samples. Increased expression is represented by red, decreases by blue, and no change by white. Saturation of color indicates the magnitude of the associated change in expression on a log-base-2 scale.

Chapter 4: Generation and Initial Characterization of the Conditionally Expressing Malonyl-CoA Insensitive CPT1A^{M593S} Mouse

Introduction

Metabolic dysfunction including glucose hypometabolism and mitochondrial failure are featured of Alzheimer's disease and other neurodegenerative disorders (Andrews et al., 2020; Menta & Swerdlow, 2019; Swerdlow, 2016, 2020; Watts, Wilkins, Michaelis, & Swerdlow, 2019; Weidling & Swerdlow, 2019; Wilkins & Swerdlow, 2016a). Correcting glucose hypometabolism through the supplementation of ketone bodies through the use of high-fat, low-carbohydrate ketogenic diets may be therapeutic in this setting by correcting bioenergetic failure or through another, unknown, mechanism (Courchesne-Loyer et al., 2016; S. Cunnane et al., 2011; S. C. Cunnane, Courchesne-Loyer, St-Pierre, et al., 2016; S. C. Cunnane, Courchesne-Loyer, Vandenberghe, et al., 2016; Han et al., 2018; S. J. Koppel & Swerdlow, 2018; Newman et al., 2017; M. K. Taylor, Swerdlow, & Sullivan, 2019). Early evidence suggests that ketogenic diet may indeed support cognitive function in Alzheimer's disease subjects (Matthew K. Taylor et al., 2017; M. K. Taylor, Swerdlow, Burns, et al., 2019). One considerable barrier to implementing ketogenic diets for clinical use is that the diet is generally difficult to maintain and found by many patients to be generally unpalatable (M. K. Taylor, Swerdlow, & Sullivan, 2019). Due to this, identification of specific underlying therapeutic mechanisms could be valuable to the development of a ketogenic diet dietary mimetic for the treatment of neurologic disease.

Previous studies have made efforts to characterize the molecular effects of ketotherapeutics either via dietary intervention in animals or direct application of ketone bodies *in vitro* (Hennebelle et al., 2016; Kashiwaya et al., 2010; Newport et al., 2015; Yao, Chen, et al., 2011). These studies become limited as complete dietary interventions make it difficult to identify the causative agent of the diet responsible for observed downstream effects due to a large number of confounding physiologic changes. These changes include, but are not limited to,

induction of ketonemia, reductions in serum insulin, increases in serum glucagon, increases in lipolysis of white adipose, and changes in circulating lipid profile (S. J. Koppel & Swerdlow, 2018). Meanwhile *in vitro* studies are limited due to their artificial nature that does not take into account the multicellular environment of the central nervous system.

To overcome these limitations, it becomes necessary to deliver reliable sustained ketone delivery to the brain *in vivo* without the accompanying confounding variables introduced through complex dietary interventions. Previous studies have sought to overcome this barrier through the use of feed supplementation with novel ketone ester supplements, medium chain triglyceride supplements, or through the use of subcutaneous osmotic pumps to deliver ketone bodies exogenously (Hennebelle et al., 2016; Kashiwaya et al., 2010; Newport et al., 2015; Yao, Chen, et al., 2011). While effective to a degree, they are limited as either being labor intensive, vulnerable to confounding effects due to differences in feed consumption or rely on surgical techniques that are invasive to research animals.

To address this pitfall, we have created a transgenic mouse model capable of constitutive fatty acid import into the mitochondria under conditional cre-lox expression control. In doing so, we hypothesize that constitutive fat trafficking will lead to enhanced β-oxidation of fats and successive constitutive ketogenesis even in the absence of carbohydrate restriction or excess fat supplementation in the diet.

To accomplish this, we have made use of a plasmid generously provided by Michael Wolfgang, PhD, of Johns Hopkins University. This plasmid encodes carnitine palmitoyl transferase 1A (CPT1A) mutated to produce a substitution of methionine for serine at amino acid 593 ($CPT1A^{M593S}$). Normally, CPT1A serves as the rate limiting enzyme in mitochondrial β-

oxidation of fats as it catalyzes the conjugation of long chain acyl groups to L-carnitine forming acyl-carnitines. These acyl-carnitines are able to be transported across the mitochondrial outer and inner membranes to gain access to the mitochondrial matrix. There, they serve as substrate for β-oxidation, energy production, and, in select tissues, for ketogenesis. In times of nutrient excess, excessive amounts of acetyl-CoA exit the mitochondria and are converted by acetyl-CoA carboxylase 1 (ACC1) to malonyl-CoA. Malonyl-CoA serves to inhibit CPT1A to allow cytosolic carbons to be utilized for *de novo* lipogenesis, steroidogenesis, and prevent futile cycling of fatty acyls (Akkaoui et al., 2009). The CPT1A^{M593S} has been previously demonstrated to abolish negative feedback inhibition of malonyl-CoA on CPT1A enzymatic activity leading to constitutive activity of the enzyme (Lopez-Vinas et al., 2007).

As the liver performs the majority of ketogenesis in mammals, we have targeted expression of the transgene initially to hepatocytes via crossbreeding to Albumin-Cre mice in order to achieve systemic elevated ketosis in the absence of dietary interventions (Garber et al., 1974). Neurons do not perform β-oxidation to an appreciable degree due to the localization of CPT1C to endoplasmic reticulum and not mitochondria in brain regions including the hypothalamus, amygdala, and hippocampus (Sierra et al., 2008; Virmani et al., 2015). CPT1C instead is thought to play a role in regulation of feeding behavior, autophagy signaling, modulation of oxidative metabolism, and generation of ceramides (Lee & Wolfgang, 2012; Palomo-Guerrero et al., 2019; Wolfgang et al., 2006). Unlike neurons, however, astrocytes are known to express CPT1A and have been shown to perform not only β-oxidation of fatty acids *in vitro*, but ketogenesis as well (Blazquez, Sanchez, Velasco, & Guzman, 1998; Fukao et al., 1997; Guzman & Blazquez, 2001; Nehlig & Pereira de Vasconcelos, 1993). To study the effects of

localized increased β-oxidation within the CNS and astrocytic ketogenesis *in situ*, CPT1A^{M593S} mice were further crossed to Gfap-Cre mice.

In the present writing we detail preliminary findings characterizing the effects of CPT1Amut transgene expression in hepatocytes. CPT1Amut expressing mice do not demonstrate systemic elevated ketosis whether maintained on standard chow diet, ketogenic diet, or under fasting conditions compared to non-carrier (NCAR) littermates. Intrahepatic levels of ketone bodies are higher in transgenic mice, especially in female mice. Early molecular signaling studies indicate that hepatocytes may adapt to increased fatty acid flux to the mitochondria through the export of excess carbon as citrate to the cytosol and the downregulation of mitochondrial fatty acid synthesis (mtFAS). Response of extrahepatic tissues and the effects of astrocytic expression are still subjects of and require further investigation.

Materials and Methods

All protocols described herein pertaining to the use of animals were reviewed and approved by the University of Kansas Medical Center Institutional Animal Care and Use Committee (KUMC-IACUC) prior to any experimentation or acquisition of animals.

Plasmid Source and Design

The plasmid construct that served as the basis for this work was generously provided by Dr. Michael Wolfgang, Ph.D. of Johns Hopkins University (**Fig. 4-1**). The total plasmid size was 10,822 bp in length and featured an ampicillin resistance gene for bacterial colony selection. Once linearized, the plasmid features an insert for mCherry followed by a stop codon flanked by two *loxp* sites. Downstream of mCherry lies a sequence for carnitine-palmitoyl transferase A

(CPT1A) conjugated to cerulean fluorescent protein (CFP). The CPT1A sequence is mutated for a substitution of amino acid 593 from methionine to serine which has been shown to prevent negative feedback inhibition of malonyl-CoA on CPT1A enzymatic activity. Both mCherry and CPT1Amut-CFP expression is regulated by the cytomegalovirus CAG promoter sequence which lies 5' to mCherry. The insert sequence is flanked on both the 5' and 3' end by fragments of genetic material matching the Rosa-26 safe harbor locus.

Generation of Founders and Confirmation of Transgene Incorporation

The transgenic insert was targeted to the Rosa-26 locus via guide RNA (gRNA) mediated recruitment of CRISPR/Cas9 to induce double strand breaks and allow for homologous end repair and incorporation of linearized plasmid sequence. Successful incorporation of novel genetic material into the Rosa-26 locus was verified through isolation of genetic DNA from tail snip or earhole punch. Tissue was first digested overnight at 60°C in buffer containing 0.4% sodium dodecyl sulfate, 200 mM NaCl, 5 mM EDTA, and 0.5 mg/mL Proteinase K (ThermoFisher Cat # 25530-015) at a pH of 8.00. Samples were retrieved and 1 mL of phenol:chloroform:isoamyl alcohol (Sigma #77617) was added. Samples were inverted to mix and allowed to stand for 10 minutes at room temperature before being centrifuged at 12,000 rcf for 10 minutes at 4°C. The upper aqueous layer was retrieved and transferred to a clean, new microcentrifuge tube and 1 mL of 100% isopropanol was added followed by 3 M sodium acetate to a final concentration of 0.3 M. Samples were stored overnight at -20°C to precipitate DNA. Samples were centrifuged at previous conditions to pellet DNA. Supernatant was aspirated and 1 mL of 70% ethanol was added. Tubes were pulse vortexed to wash pellets in ethanol before centrifugation at 7,500 rcf for 5 minutes at 4°C. Ethanol was carefully removed and pellets were briefly air dried before being resuspended in 40 µL of nuclease-free water. DNA concentration

and purity were determined spectrophotometrically by measuring A260/280 ratios and concentration was adjusted to 250 ng/µL.

Genotyping PCR was performed with primer sets designed to recognize either 5' or 3' ends of the genetic insert sequence. The primer sets are as follows: 5' Upper 5' – AAA GAA GAG GCT GTG CTT TGG – 3', 5' Lower 5' – ATT ATT GAC GTC AAT GGG CGG – 3', 3' Upper 5' - TAT GAA GAT CCC TCG ACC TGC – 3', and 3' lower 5' – AGT CAA GCC AGT CCA AGA GAA – 3'. Wild-type Rosa-26 locus was identified using the following primers: WT Primer 1: 5' – CTC TGC TGC CTC CTG GCT TC -3' and WT Primer 2: 5' – CGA GGC GGA TCA CAA GCA ATA – 3'.

Genotyping PCR reactions were performed using 2 µL of template and 23 µL of master mix comprised of 16.94 µL nuclease-free water, 5.0 µL 5x Advantage Buffer (Takara Cat # 639241), 0.25 µL Advantage HD polymerase, 0.2 µL dNTP (Takara Cat #630125), 0.33 µL of 100 µM Primer 1, and 0.33 µL of 100 µM Primer 2. Cycling conditions for all reactions were performed as follows:

Denaturation at 95°C for 2 minutes

35 cycles: Denaturation at 95 °C for 15 seconds

Anneal at 62 °C for 30 seconds

Extension at 72 °C for 75 seconds

Final Extension at 72 °C for 5 minutes.

PCR reaction products were resolved on an ethidium bromide 1% agarose-TAE gel to resolve size of band products. The 5' reaction, 3' reaction, and WT reactions were predicted to produce bands sizing 1.3 kb, 1.1 kb, and 322 bp respectively. Bands were visualized under UV light using the BioRad Chemidoc XRS+ Imaging System.

Crosses of F0 R26-CPT1A^{M593S} mice were performed to male or female Speer6-ps1$^{Tg(Alb-cre)21Mgn}$ mice (Albumin-Cre; Jackson Laboratories Strain #003574) for hepatic expression of CPT1A^{M593S}. Genotyping of Albumin-Cre breeding offspring to identify Cre-Recombinase were performed according to directions for the strain from Jackson Laboratories. Astrocytic expression was achieved through crosses of F0 R26-CPT1A^{M593S} males to hemizygous Gfap-Cre females (B6.Cg-Tg(Gfap-cre)73.12Mvs/J, Jackson Laboratories, Strain #012886). Again, genotyping to identify Cre-Recombinase carriers were performed according to recommendations from the Jackson Laboratories available on their website.

Backcrossing and Congenic Monitoring

As founder mice were generated on hybrid C67BL6/J:FVBn background we performed backcrossing to C57BL6/J mice over 5 generations with single nucleotide polymorphism tracking through Jackson Laboratories. Each generation, the transgenic offspring with the highest percentage of C57BL6/J specific SNPs was selected for further backcrossing until animals were measured to be over 99% C57BL6/J. At this point, the N5 generation was considered congenic to the Jackson inbred strain and was considered the F0 generation for future crosses/experiments.

Dietary Interventions and Phlebotomy

Mice were maintained *ad libitum* on either standard chow (LabDiet #5053) or high-fat, low-carbohydrate ketogenic diet (Bioserve #F3666) for variable portions of time. During fasting periods, mice had *ad libitum* access to water at all times. Routine blood draws were performed by facial vein puncture no more than once every two weeks with no more than 150 µL of blood collected at any given time. Blood metabolites were measured using the Precision Xtra meter (Abbott Diabetes Care, Inc. #9881465) with blood glucose (Abbott #9972865) and ketone test strips (Abbott #7074565) at the time of blood draw.

Glucose tolerance testing was performed on mice following an 8-hour fast. Initial blood draws were sampled by tail cut and read immediately. Following initial readings, mice received intraperitoneal injections of 2 g glucose dissolved in sterile PBS/kg body weight. Repeated measures were performed at 15, 30, 60, and 120 minutes.

Indirect Calorimetry

To study the effects of CPT1Amut expression on animal behavior and energy metabolism we made use of indirect calorimetry caging. Indirect calorimetry was performed at the University of Kansas Medical Center Metabolic Obesity Phenotyping Facility using the Promethion continuous indirect calorimetry system (Sable Systems International, Las Vegas, NV). Animals were moved to single animal housing at least one day prior to being relocated into metabolic cages where they were housed for three days. Manufacturer developed macros were used to calculate resting, active, mean, and total energy expenditure. Gas exchange metrics included volume of respired O_2, CO_2, H_2O, and respiratory quotient (RQ). Consumption of food and water, walking behavior, and sleep behavior were also measured during the housing period

utilizing feed and water hoppers and XYZ Beambreak Activity Monitor (Sable Systems, Las Vegas, NV). Data was obtained separately for light and dark cycles and averaged for the last two days of the housing period. Animals were housed on a 14:10 hour light:dark cycle.

Intrahepatic Ketone Measurements

To measure intrahepatic ketone levels approximately 100 mg of frozen liver was placed into 500 µL of ice-cold homogenization buffer (220 mM mannitol, 70 mM sucrose, 1mM EDTA, and 5 mM HEPES, pH = 7.40) and homogenized for 30 strokes on ice using a glass-on-glass Dounce homogenizer. Samples were placed into new, clean 1.5 mL microcentrifuge tubes and centrifuged at 1,000 rcf for 5 minutes at 4°C. 10 µL of supernatant was collected and ketone body content was measured using the Precision Xtra meter with ketone test strips. Measured concentration was multiplied by volume of supernatant to determine total ketone content and normalized to mg of input material.

Generation of Cell Lysates and Western Blotting

Approximately 50 mg of frozen liver was placed in 500 µL of RIPA lysis buffer containing Thermo Halt Protease and Phosphate inhibitor cocktail (Thermo #1861284). RIPA buffer contained 10 mM Tris-HCl (pH 8.0), 1 mM EDTA, 0.5 mM EGTA, 1% Triton X-100, 0.1% sodium deoxycholate, 0.1% SDS, and 140 mM NaCl. Livers were homogenized for 30 strokes on ice using a glass-on-glass Dounce homogenizer. Homogenized sample was collected and placed into a new, clean microcentrifuge tube.

Lysates were then centrifuged for 5 minutes at 1,000 rcf at 4°C. Supernatant was transferred to a clean tube and stored at -80°C until ready for protein quantification. 10 µL of

concentrated lysate was diluted with 100 µL of fresh cold RIPA supplemented with PPI prior to protein concentration determination. Protein concentration was determined via BCA Assay (Pierce #23225). Diluted lysate and albumin standards were measured in duplicate in clear, flat bottom 96 well plates. Following addition of BCA working reagent plates were incubated for 30 minutes at 37°C. Absorbance was measured at λ = 562 nm. Lysates were diluted in laemmli buffer and water and subsequently boiled for 10 minutes at 95°C. Samples were stored at -20°C until use.

Lysates were resolved by SDS-PAGE using pre-cast 4-12% criterion gels run at constant voltage of 100V in Tris/glycine/SDS running buffer (BioRad #1610772). 50 µg of protein was loaded per lane along with 5 µL protein ladder. Following SDS-PAGE protein was transferred to PVDF membrane activated by methanol (GE Amersham Hybond #10600023) in Tris/glycine buffer (BioRad #1610771) with 20% methanol. Protein transfer occurred at 400 mA for 1 hour on ice. Following transfer membranes were washed in Tris buffered saline with 0.1% tween (TBST) prior to blocking for 1 hour with 5% bovine serum albumin (BSA) in TBST (Boston BioProducts P-753). Blocked membranes were incubated at 4°C overnight on an orbital shaker incubating in primary antibody diluted in 5% BSA in TBST (pT308 Akt CST #2965 1:1000, pS473 Akt LifeTechnologies #700392 1:1000, Total Akt CST #4685 1:1000, pS455 ACLY CST #4331 1:2000, Total ACLY CST #13390 1:2000, pS79 ACC1 CST #3661 1:1000, Total ACC1 CST #3676 1:1000, β-tubulin CST #2146 1:1000, CPT1A abcam #ab128568 1:2000, Cre-Recombinase abcam #ab190177 1:2000, GAPDH CST #2118 1:5000, GFP abcam #ab6556 1:1000, Total HMGCR abcam ab#174830 1:3000, Total LIAS Sigma HPA018842 1:1000, Lipoic Acid abcam #ab58724 1:5000). The following day membranes were washed 3 times for 5 minutes in TBST followed by a 1-hour incubation at room temperature in appropriate secondary

(Invitrogen Superclonal Secondary Antibody, HRP Conjugate #A28177 or #A27036), diluted 1:4000 in 5% condensed milk in TBST. Membranes were washed an additional 3 times for 5 minutes each prior to visualization of bands using Supersignal West Femto Maximum Sensitivity Substrate (Thermo #34096) on a BioRad Chemidoc XRS+ imager. Densitometry was performed using Image Lab software (BioRad) with protein levels normalized to either β-tubulin or total protein content determined by amido black stain (Sigma #A8181).

Statistical Analysis

Direct comparisons between genotypes were performed via unpaired two-tailed student's t-test. When assessing statistical significance between genotypes when factoring in sex we employed two-way analysis of variance (ANOVA) testing with Tukey's post-hoc analysis. When examining the effects of diet on behavioral outcomes from indirect calorimetry we performed paired two-tailed student's t-tests. Results were considered to be statistically significant for p-values less than 0.05.

Table 4-1: List of antibodies used in experiments.

Antibody	Dilution	Source	Catalog #
pT308 Akt	1:1000	Cell Signaling Technologies	#2965
pS473 Akt	1:1000	LifeTechnologies	#700392
Total Akt	1:1000	Cell Signaling Technologies	#4685
pS455 ACLY	1:2000	Cell Signaling Technologies	#4331
Total ACLY	1:2000	Cell Signaling Technologies	#13390
pS79 ACC1	1:1000	Cell Signaling Technologies	#3661
Total ACC1	1:1000	Cell Signaling Technologies	#3676
β-tubulin	1:1000	Cell Signaling Technologies	#2147
CPT1A	1:2000	abcam	#ab128568
Cre-Recombinase	1:2000	abcam	#ab190177
GAPDH	1:5000	Cell Signaling Technologies	#2118
GFP	1:1000	abcam	#ab6556
HMGCR	1:3000	abcam	#ab174830
LIAS	1:1000	Sigma	# HPA018842
Lipoic Acid	1:5000	abcam	#ab58724

Table 4-2: List of primers used in experiments.

Primer	Sequence
WT-Rosa26 Forward	5’ – CTC TGC TGC CTC CTG GCT TC -3’
WT-Rosa26 Reverse	5’ – CGA GGC GGA TCA CAA GCA ATA – 3’
5’ R26-CPT1A^{M593S} Transgene Forward	5’ – AAA GAA GAG GCT GTG CTT TGG – 3’
5’ R26-CPT1A^{M593S} Transgene Reverse	5’ – ATT ATT GAC GTC AAT GGG CGG – 3’
3’ R26-CPT1A^{M593S} Transgene Forward	5’ - TAT GAA GAT CCC TCG ACC TGC – 3’
3’ R26-CPT1A^{M593S} Transgene Reverse	5’ – AGT CAA GCC AGT CCA AGA GAA – 3’
Albumin-Cre WT Ms Chromosome 13	5’ – TGC AAA CAT CAC ATG CAC AC – 3’
Common Albumin-Cre Primer	5’ – TTG GCC CCT TAC CAT AAC TG – 3’
Mutant Forward Albumin-Cre Primer	5’ – GAA GCA GAA GCT TAG GAA GAT GG – 3’
Gfap-Cre Transgene Forward	5’ – TCC ATA AAG GCC CTG ACA TC – 3’
Gfap-Cre Transgene Reverse	5’ – TGC GAA CCT CAT CAC TCG T – 3’
Gfap-Cre Internal Positive Control	5’ – CAA ATG TTG CTT GTC TGG TG – 3’
Gfap-Cre Internal Positive Control	5’ – GTC AGT CGA GTG CAC AGT TT – 3’

Results

Generation of Founders and Confirmation of Germline Transmission

Transgenic founders were created through the use of CRISPR-Cas9 technology to insert our linearized plasmid sequence to the mouse Rosa-26 safe harbor locus (**Fig. 4-2**). Targeting to the R26 locus was done to ensure single copy incorporation into the mouse genome without interrupting known protein coding gene sequences. The incorporated plasmid sequence encodes mcherry followed by a stop codon flanked by two *loxp* sites. Our construct of interest, mutated aa 593 M>S carnitine palmitoyl transferase 1A conjugated to cerulean fluorescent protein ($CPT1A^{M593S}$-CFP), is contained in the sequence downstream to the mcherry-STOP sequence. Both constructs are reliant on the cytomegalovirus CAG promoter sequence which lies upstream to both previously described sequences. Our transgene of interest would therefore only be expressed when crossed with mouse strains expressing Cre-recombinase allowing for organ targeting or timed expression studies in strains where Cre expression is regulated by drug interventions. Incorporation of novel genetic material in the founding litter was confirmed through PCR with primer sets recognizing endogenous R26 locus and unique insert genetic code at 5' end, 3' end, and internal to the genetic insert.

Founders were created using C57BL6/J:FVBn hybrid mice. Prior to experimentation, we performed genetic backcrossing to C57BL6/J mice for five generations (N1-N5 generations) with single nucleotide polymorphism tracking to achieve congenic C57BL6/J transgenic mice. Our novel genetic insert was identified in the N1 generation by PCR reaction as performed in the founders indicating germline transmission of the transgene. Once the N5 generation was created they were from there forward considered the F0 population of transgenic mice and used to cross

with Albumin-Cre or Gfap-Cre expressing lines to generate CPT1A^{M593S}-CFP expressing mice for experimental investigation in hepatocytes and astrocytes respectively.

Confirmation of transgene expression in Albumin-Cre x CPT1A^{M593S} mouse livers

Expression of the CPT1A^{M593S}-CFP conjugate gene product in Cre-expressing tissues was first investigated by crossing our transgenic line into an albumin-cre line for hepatocyte targeted expression. Upon sacrifice livers were removed and whole cell protein was isolated for Western blot (**Fig. 4-3**). Labeling for CPT1A produced a band at the predicted weight near 110 kDa in non-cre expressing mouse livers while producing a doublet with a band at 110 kDa and another around 135 kDa in albumin-cre x CPT1A^{M593S} mice. We next blotted for CFP to verify expression of the unique identifying tag following Cre-flox. CFP labeling produced a band around 135 kDa in Alb-Cre x CPT1A^{M593S} mice but not in transgene negative litter mates.

Measurement of Blood Glucose, Ketone Bodies, and Body Weight

No difference has been observed in body weight in male or female mice at any point between birth and extending out to 8 months of age (**Fig. 4-5**). Similarly, no significant difference was observed in blood glucose or ketonemia between albumin-cre and albumin-cre x CPT1A^{M593S} mice when (**Fig. 4-6**) maintained on chow diet (Glucose: NCAR 202.4 ± 69.94 mg/dL, CPT1A^{M593S} 231.0 ± 69.30 mg/dL; p-value = 0.5236; Ketones: NCAR 0.392 ± 0.088 mM; CPT1A^{M593S} 0.422 ± 0.112 mM; p-value = 0.6264), ketogenic diet (Glucose: NCAR 163.60 ± 35.43 mg/dL; CPT1A^{M593S} 145.00 ± 41.01 mg/dL; p-value = 0.4346; Ketones: NCAR 2.80 ± 0.52 mM; CPT1A^{M593S} 3.10 ± 0.141 mM; p-value = 0.4007), or under fasting conditions (Glucose: NCAR 179.25 ± 89.47 mg/dL; CPT1A^{M593S} 166.50 ± 118.09 mg/dL; p-value = 0.4590; Ketones: NCAR 1.10 ± 0.47 mM, CPT1A^{M593S} 0.95 ± 0.21 mM; p-value = 0.9507). We

further performed glucose tolerance testing to determine if expression of the transgene effected systemic insulin resistance. We did not observe a significant difference in response to glucose tolerance testing between transgenic animals and non-transgenic animals regardless of sex (Area under the curve: NCAR 42,283 ± 13,619, CPT1A^{M593S} 38,126 ± 6,404; mean ± 95% CI) as shown in **Figure 4-7**.

Indirect Calorimetry and Mouse Behavior

Transgenic and non-transgenic litter mates were housed for several days to assess if there were differences in mouse respiratory exchange, feeding behavior, drinking behaviors, or activity. No difference was observed in mouse energy expenditure during either light or dark cycles (**Fig. 4-8,** Light Total EE: NCAR 5.733 ± 0.351 kcal, CPT1A^{M593S} 5.701 ± 0.182 kcal; p-value = 0.8837; Dark Total EE: NCAR 5.114 ± 0.494, CPT1A^{M593S} 5.123 ± 0.099 kcal; p-value = 0.9273). No difference was measured in gas exchange of O_2 (NCAR 1.43 ± 0.09 mL/min, CPT1A^{M593S} 1.41 ± 0.05 mL/min) CO_2 (NCAR 1.09 ± 0.10 mL/min, CPT1A^{M593S} 1.11 ± 0.01 mL/min), or H_2O (NCAR 0.17 ± 0.01 mL/min, CPT1A^{M593S} 0.18 ± 0.03 mL/min; p-value = 0.9233). Secondary to that, no difference was observed in respiratory quotient between genotypes (**Fig 4-9,** Light RQ: NCAR 0.757 ± 0.065, CPT1A^{M593S} 0.776 ± 0.019; p-value = 0.0059 by 2-way ANOVA; no significant interactions on Tukey's post-hoc analysis; Dark RQ: NCAR 0.825 ± 0.043, CPT1A^{M593S} 0.857 ± 0.019; p-value = 0.1502). No significant difference was found between rates or amounts of food (**Fig. 4-10,** Light Total Food Consumed: NCAR 1.63 ± 0.97g, CPT1A^{M593S} 1.71 ± 1.20 g; p-value = 0.4925; Dark Total Food Consumed: NCAR 2.42 ± 1.05 g, CPT1A^{M593S} 2.515 ± 0.526 g; p-value = 0.6038) or water consumption (**Fig. 4-11,** Light Total Water: NCAR 1.76 ± 0.56 g, CPT1A^{M593S} 1.61 ± 0.41 g; p-value = 0.4180; Dark Total Water: NCAR 3.49 ± 0.73 g, CPT1A^{M593S} 3.11 ± 0.57 g; p-value = 0.1333). No significant

difference was found in total distance traveled in either light or dark cycle as a function of genotype (**Fig. 4-12,** Light Total Walking Distance: NCAR 83.56 ± 32.18 g, CPT1A^{M593S} 89.13 ± 43.41 m; p-value = 0.2685; Dark Total Walking Distance: NCAR 159.27 ± 73.90 m, CPT1A^{M593S} 193.16 ± 20.81 m; p-value = 0.0495 by 2-way ANOVA, no significant interactions on Tukey's post-hoc analysis). Finally, no difference in sleep behavior was observed during the caging period (**Fig. 4-13,** Light Sleep Hours: NCAR 10.78 ± 0.43 h, CPT1A^{M593S} 10.72 ± 0.95 h; p-value = 0.6906; Dark Sleep Hours: NCAR 4.26 ± 1.41 h, CPT1A^{M593S} 4.17 ± 1.34 h; p-value = 0.0141 by 2-way ANOVA; no significant interactions on Tukey's post-hoc analysis).

In order to determine if changes in mouse behavior would become more pronounced with increased availability of dietary fats, we repeated our measurements using indirect calorimetry while performing daily feedings with ketogenic diet in place of chow. We again did not find an effect of genotype in response to these parameters while animals were maintained on ketogenic diet in either sex. We did observe several effects of diet on animal behavior irrespective of genotype that were significant by two-way ANOVA. Maintaining animals on KD significantly reduced mean (Chow 0.512 ± 0.038 kcal, Keto 0.497 ± 0.039 kcal; p-value = 0.2500) and total animal energy expenditure (Chow 5.118 ± 0.377 kcal, Keto 4.967 ± 0.390 kcal; p-value = 0.2500) during the active dark cycle in both sexes (**Fig. 4-8**). KD feed increased mean (Chow 0.409 ± 0.020 kcal, Keto 0.489 ± 0.028 kcal; p-value = 0.0078) and total energy expenditure (Chow 5.721 ± 0.283 kcal, Keto 3.949 ± 0.229 kcal; p-value = 0.0078) during the light cycle for both sexes. KD feed reduced animal respiratory quotient (RQ) in both sexes (**Fig. 4-9,** Light RQ: Chow 0.76 ± 0.05, Keto 0.67 ± 0.02; p-value = 0.0078; Dark RQ: Chow 0.84 ± 0.04, Keto 0.68 ± 0.03; p-value = 0.0078). Animals performed more feeding bouts (**Fig. 4-10,** Chow 14.25 ± 5.94 bouts, Keto 23.48 ± 6.56 bouts; $p < 0.0001$) but ate overall less food by mass (Chow 2.46 ± 0.84

g, Keto 1.21 ± 0.36 g; $p < 0.0001$) during the dark cycle when provided KD in place of chow. Animals maintained on KD exhibited reduced number of drinking bouts (Chow 64.8 ± 18.9 bouts, Keto 54.51 ± 14.8 bouts; p-value = 0.0744) reduced mean uptake of water per bout (Chow 0.057 ± 0.026 mL/min, Keto 0.029 ± 0.007 mL/min; $p < 0.0001$), and reduced total water uptake (Chow 3.32 ± 0.67 mL, Keto 1.53 ± 0.49 mL; $p < 0.0001$) as seen in **Figure 4-11**. KD had no significant effect on total distance traveled or on mean walking speed (**Fig. 4-12**). Animals maintained on KD had no significant difference in their sleep behavior during the dark cycle but did sleep significantly more during the light cycle (**Fig. 4-13,** Light Cycle: Chow 10.75 ± 0.68 h, Keto 11.36 ± 1.01 h; p-value = 0.0182; Dark Cycle: Chow 4.22 ± 1.33 h, Keto 4.69 ± 0.71 h; p-value = 0.1928).

Measuring Hepatic Changes and Intrahepatic Ketone Levels

Failing to observe increased systemic ketonemia or other physiologic phenotypes in hepatocyte expressing transgenic mice we explored the possibility that transgene expression was modulating liver physiology that was not overtly manifest at the level of the whole organism or in the blood. To begin, we compared gross weights of liver at necropsy to total body weight. Livers were found to be significantly larger in $CPT1A^{M593S}$ hepatocyte expressing mice, especially among female mice by mixed-effects analysis (**Fig. 4-14,** p-value of mixed effects analysis on effect of genotype $p = 0.0113$, post-hoc comparison of NCARs to $CPT1A^{M593S}$ females p-value = 0.0438).

We next measured to ketone body content within the liver by measuring ketone content in liver homogenates normalized to input mass of organ prior to homogenization. We found that ketone bodies were significantly elevated in $CPT1A^{M593S}$ livers compared to NCAR livers across

all animals (**Fig. 4-14,** NCAR 1.3 ± 0.6 µmol βOHB/mg Liver, CPT1A^{M593S} 1.8 ± 0.4 µmol βOHB/mg Liver; p-value = 0.0265; n = 14,8; mean ± SD). No significant difference has been observed in male mice (NCAR 1.2 ±, CPT1AM^{593S} 1.6 ± 0.5; p-value 0.2778; n = 10, 3; mean ± SD). Female mice nearly reached significance on a limited number of animals (NCAR 1.5 ± 0.3; CPT1A^{M593S} 2.0 ± 0.3; p-value = 0.0601; n = 4,5; mean ± SD).

Hepatic Mitochondrial Enzyme Kinetics

To assess if CPT1A^{M593S} expression influenced mitochondria TCA cycle or ETC enzyme kinetics we performed citrate synthase, complex 1, and cytochrome oxidase enzymatic Vmax assays (**Fig. 4-15**). We did not detect a significant difference in V_{max} of any of these enzyme complexes. Citrate synthase was close to achieving significance across all animals when transgenic mice were normalized to NCAR littermates (NCAR 100 ± 30.1%, CPT1A^{M593S} 126.3 ± 62.9%, p-value = 0.196; n = 14,8; mean ± SD). Male CPT1A^{M593S} mice displayed a near-significant increase in CS Vmax when normalized to NCAR male littermates (NCAR Males 100 ± 20.5%, CPT1A^{M593S} Males 131.4 ± 41.5%; p-value = 0.0892; n = 10, 3; mean ± SD). Female CPT1A^{M593S} mice did not even remotely approach a significant difference in CS Vmax (NCAR Females 100 ± 27.1%, CPT1A^{M593S} Females 102.0 ± 60.0%; p-value = 0.954; n = 4,5; mean ± SD).

COX V_{max} exhibited non-significant increases in V_{max} across all CPT1A^{M593S} mice (All NCAR 100 ± 24.2%, All CPT1A^{M593S} 138.9 ± 86.6%; p-value 0.125; n = 14,8; mean ± SD) and female mice (NCAR Females 100 ± 6.1%, CPT1A^{M593S} 174.9 ± 99.7%; p-value 0.183; n = 4,5; mean ± SD), but a non-significant reduction in male CPT1A^{M593S} mice (NCAR Males 100 ± 28.6%, CPT1A^{M593S} Males 84.8 ± 21.5%; p-value = 0.4187; n = 10,3; mean ± SD).

Complex 1 V_{max} displayed higher variance than either CS or COX assays. As such, Rout outlier testing was performed with q = 1%. Two female samples, one in each genotype, were identified as outliers and excluded from downstream analysis. We detected no significant difference in Complex 1 across all animals (NCAR All 100 ± 97.9%, CPT1A^{M593S} All 167.9 ± 140.1%; p-value 0.219; n = 13,7; mean ± SD). No difference was found across males (NCAR Males 100 ± 98.1%, CPT1A^{M593S} Males 123.2 ± 132%; p-value = 0.7436; n = 10,3; mean ± SD). Nor was a difference detected amongst females (NCAR Females 100 ± 80.4%, CPT1A^{M593S} Females 288.5 ± 229.2%; p-value = 0.239; n = 3,4; mean ± SD).

Hepatic Molecular Signaling Changes

Although we did not observe statistically significant CS Vmax increases, we considered that it was possible increased ketonemia was not observed as some of the Acetyl-CoA generated from the β-oxidation of fats may be escaping the mitochondrial matrix, not as ketone bodies, but as citrate. We began to assess this possibility at a molecular signaling level via Western blotting (**Fig. 4-16**). We examined levels of activating phosphorylation of ATP Citrate Lyase (ACLY) which is responsible for converting citrate to acetyl-CoA in the cytosol. We found that CPT1A^{M593S} expressing mice had significantly increased levels of ACLY phosphorylation compared to NCAR littermates (pS455 ACLY: NCAR 100 ± 26.25%, CPT1A^{M593S} 198.1 ± 102.8%; p-value = 0.0380; n = 14,8; mean ± SD). Total ACLY levels did not differ significantly (Total ACLY: NCAR 100 ± 24.3%, CPT1A^{M593S} 130.1 ± 47.7%; p-value = 0.2413; n = 14,8; mean ± SD). We next assessed activation status of the upstream regulatory kinase for ACLY, protein kinase B (Akt). Phosphorylation of Akt at Ser473 was non-significantly elevated in CPT1A^{M593S} mice (NCAR 100 ± 62.19%, CPT1A^{M593S} 150.3 ± 74.13%; p-value = 0.1298; n =

14,8; mean ± SD). No difference was observed in levels of total Akt protein (NCAR 100 ± 22.43%, CPT1A^{M593S} 118.90 ± 34.21%; p-value = 0.3069; n = 10,5; mean ± SD).

Upon conversion of citrate to acetyl-CoA in the cytosol it can be used as substrate for *de novo* lipogenesis or cholesterol anabolism which is performed by acetyl-CoA carboxylase 1 (ACC1) and hydroxymethylglutrayl-CoA reductase (HMGCR) respectively. Phosphorylation at the inhibitory regulatory site Ser79 was increased in CPT1A^{M593S} mice (pS79 ACC1: NCAR 100 ± 30.77%, CPT1A^{M593S} 206.3 ± 708.42%; p-value = 0.0107; n = 14,8; mean ± SD). HMGCR exhibited no significant difference between NCARs and CPT1A^{M593S} littermates (NCAR 100 ± 61.14%, CPT1A^{M593S} 141.60 ± 54.72%; p-value = 0.1585; n = 14,7; mean ± SD).

As cytoplasmic *de novo* lipogenesis appeared inhibited by increased ACC1 phosphorylation, we hypothesized that mitochondrial fatty acid synthesis (mtFAS) would be similarly inhibited. We evaluated this by probing for lipoic acid synthase (LIAS) via western (**Fig. 4-17**). We found a non-significant reduction in total amounts of LIAS in CPT1A^{M593S} mice (NCAR 100 ± 52.42%, CPT1A^{M593S} 70.18 ± 45.45%; p-value = 0.1803; n = 14,8; mean ± SD). We next assessed if lipoic acid production was reduced by probing for lipoic acid which binds as a co-factor to four enzymatic complexes: glycine cleavage system H protein (GCSH), pyruvate dehydrogenase complex (PDHC), branched chain ketoacid dehydrogenase (BCKDH), and α-ketoglutarate dehydrogenase (KGDH). We detected no significant difference in lipoylation of GCSH or KGDH (GCSH: NCAR 100 ± 50.49%, CPT1A^{M593S} 62.63 ± 57.14%; p-value = 0.1476; KGDH: NCAR 100 ± 40.76%, CPT1A^{M593S} 76.76 ± 32.62%; p-value = 0.1606; n = (14,8); mean ± SD). Lipoylation of PDHC and BCKDH complexes was significantly reduced in CPT1A^{M593S} expressing mice (PDHC: NCAR 100 ± 40.73%, CPT1A^{M593S} 47.79 ± 18.88%; p-

value = 0.0006; BCKDH: NCAR 100 ± 37.94%, CPT1A^{M593S} 56.23 ± 27.02%; p-value = 0.0054; n = 14,8; mean ± SD).

Discussion

Prior to any further discussion of our findings we find it imperative to express that these early results are derived from an initial collection of litters comparing non-carriers to Albumin-Cre x CPT1A^{M593S} hemizygotes. To fully determine the effects, or lack thereof, of CPT1A^{M593S} expression would require a larger sampling of mice of all genotypes and sexes. As such, as work on this project moves forward the immediate task should be the generation of homozygous CPT1A^{M593S} breeders to accelerate colony expansion and overcome the limitations of prolonged breeding times and small sample sizes. This is especially true regarding colony expansion and crossings to Gfap-Cre strains as the Gfap-Cre breeding scheme requires solely the use of Gfap-Cre female hemizygous breeders due to the transient expression of Cre-Recombinase in spermatozoa of male breeders as identified by the Jackson Laboratories. This effect excludes the possibility of generating colonies with such male breeders as whole body expression becomes a distinct possibility and concern.

Preliminary findings of the study of the newly generated conditionally expressing CPT1A^{M593S} mouse suggests that hepatic expression of the transgene may alter carbon fluxes in and out of the mitochondria in an attempt to maintain homeostasis of trafficked fats. Hepatic expressing CPT1A^{M593S} mice exhibited increased intrahepatic ketone body content that was not observed systemically in the blood. Additionally, enzymatic citrate synthase V_{max} indicated possibly increases of CS activity in CPT1A^{M593S} mice. This coupled with increased ACLY phosphorylation suggests that acetyl-CoA derived from increased β-oxidation of fats is exported

from the mitochondrial matrix as both β-hydroxybutyrate and citrate. Downstream inhibition of ACC1 activity through its phosphorylation at serine 79 may indicate that cytosolic acetyl-CoA is being diverted away from further malonyl-CoA generation and *de novo* lipogenesis. To fully elucidate the fate of mitochondrially trafficked fatty acyl groups it would be critical to expand upon these findings by performing radiolabeled palmitate tracing experiments. Doing so would allow for a more comprehensive examination of the fate of carbon derived from fatty acids and provide a stronger indication for further targeted molecular signaling studies.

Similarly, preliminary investigations into mitochondrial fatty acid synthesis pathways demonstrated reductions in lipoic acid synthase and reduced incorporation of lipoic acid into pyruvate dehydrogenase complex and branched chain ketoacid dehydrogenase complex with a further non-significant reduction in lipoylation of glycine cleavage system H protein. As lipoic acid serves as an integral cofactor for these multimeric complexes, a downregulation of lipoic acid could be an adaptive response to reduce further entry of carbon derived from glucose into the TCA cycle and to modulate forward progression of the TCA cycle by destabilizing α-ketoglutarate dehydrogenase complex. Reduced lipoylation of BCKDH is an intriguing finding as the branched chain amino acids leucine, isoleucine, and valine are recognized as ketogenic amino acids. It is even being suggested that supplementation with these amino acids may serve as a potential adjunct therapy to the treatment of pediatric epilepsy given their ketogenic qualities (Evangeliou et al., 2009). It would be interesting to expand upon this avenue and investigate if CPT1A^{M593S} expressing mice have altered levels of branched chain amino acids in the liver or in systemic circulation.

While these effects would be valuable paths to follow regarding the effects of transgene expression within the liver, it is also necessary to evaluate extrahepatic tissues for changes in

ketolytic pathways. It is possible that no increase in blood ketones is observed in CPT1A^{M593S} expressing mice because expression of the transgene begins during embryonic development. This may allow for extrahepatic adaptation to increased ketosis through the upregulation of ketolytic enzymes to accelerate catabolic flux to compensate for increase hepatic ketogenesis. In doing so, it is possible that there is increased ketone delivery in CPT1A^{M593S} mice but static levels in the blood do not reflect the flux. This should be readily performed via western of the two primary ketolytic enzymes β-hydroxybutyrate dehydrogenase 1 (BDH1) and succinyl-CoA-3-oxaloacid transferase (SCOT) in brain, cardiac myocytes, and skeletal muscle. These tissues should be prioritized as they serve as the primary tissues to utilize ketone bodies for energy production in the case of brain and cardiac myocytes while skeletal muscle can serve as an internal control for non-ketolytic extrahepatic tissue.

While no behavioral difference was observed in mice via indirect calorimetry measurements at this stage it is important to note that group sizes, especially when stratified for sex, remain fairly low. As such, subtle changes in RQ, energy expenditure, or feeding behavior may not be appreciated at this stage. Further, histologic examination is warranted and necessary to determine correct compartmentalization of the transgene product. While expression of the CPT1A^{M593S}-CFP construct is appreciated via western blotting we currently have no spatial localization data. Further, it would be valuable to perform staining with Oil Red O and periodic acid Schiff staining to evaluate changes in hepatic lipid and glycogen content respectively. This would be especially true regarding content following intervention with high-fat, low carbohydrate or high-fat, high-carbohydrate diets as the effect of CPT1A^{M593S} expression may not be readily appreciated without the added stressor of extreme diets or other interventions.

This point is illustrated in previous studies that have utilized a similar construct to ours via delivery by adenovirus. In these studies, CPT1A^{M593S} mice failed to demonstrate robust phenotypes at baseline aside from mild activations of Akt phosphorylation at serine 473, a finding we ourselves have not replicated to a level of statistical significance, and Janus kinase (JNK) phosphorylation changes. However, when CPT1A^{M593S} were shown to be more resistant to obesity associated insulin resistance independent of rates of hepatic steatosis. This was associated with rescued activation of hepatic insulin signaling pathway intermediates IRS-1, IRS-2, Akt, and GSK3β, phenotypes that were not observed in normal weight, healthy mice (Monsenego et al., 2012). A similar study demonstrated that malonyl-CoA insensitive skeletal muscle isoform CPT1B was able to reduce high-fat, high-sucrose diet induced insulin resistance in muscle (Vavrova et al., 2016). Cultured rat hepatocytes overexpressing wild type CPT1A or CPT1A^{M593S} were shown to maintain β-oxidation of oleate even in the presence of glucose and insulin challenges while preventing the accumulation of intracellular triglycerides typically observed with such interventions with CPT1A^{M593S} mutants demonstrating greater efficacy in this regard (Akkaoui et al., 2009). It also remains possible that findings in these studies may be more a result of artifact than physiology as adenoviral mediated expression may lead to a large copy number of CPT1A^{M593S} with extreme expression levels that are not recapitulated by the single copy R26-CPT1A^{M593S} mouse we have generated.

It is also necessary to perform more fatty acid oxidation assays and CPT1A enzymatic activity assays to validate the effect of our expressed transgene although our collaborator Dr. Michael Wolfgang has validated its efficacy within his own lab and other groups have routinely demonstrated the efficacy of the mutation in abolishing malonyl-CoA inhibition. Early attempts to perform such studies on the oroboros-O2k system presented with technical issues including

mild response to ADP in enhancing state 3 respiration and extreme state 3S flux upon the addition of succinate. While concerns arose over the integrity of mitochondrial preparations, mild increases in oxygen consumption to the addition of exogenous reduced cytochrome C indicates that mitochondrial membranes were not likely to be ruptured. Nevertheless, returning to and addressing these experimental short comings will be critical moving forward.

Finally, even if increased systemic ketone trafficking is not a phenotype of the R26-CPT1A^{M593S} mouse, our findings of increased intrahepatic ketone body content may indicate that a similar intraorgan phenotype could be reproduced in brain via astrocyte targeted expression. Crossings are underway to Gfap-Cre breeders; however, this is a painstakingly slow process for reasons described above. While that is the case, increased fat utilization with or without enhanced ketogenesis would provide exciting opportunities to study the consequences of perturbed bioenergetic fluxes in astrocytes on brain health.

Taken together, there are intriguing threads as to believe that expression of CPT1A^{M593S} is having a phenotypic effect within these mice. The question remains, what effects exactly and what do they mean in regards not only to general mouse physiology but the utility of this model system in the study of brain bioenergetics and its relationship to brain health. Only time and further effort in these endeavors will we be able to definitively answer these questions.

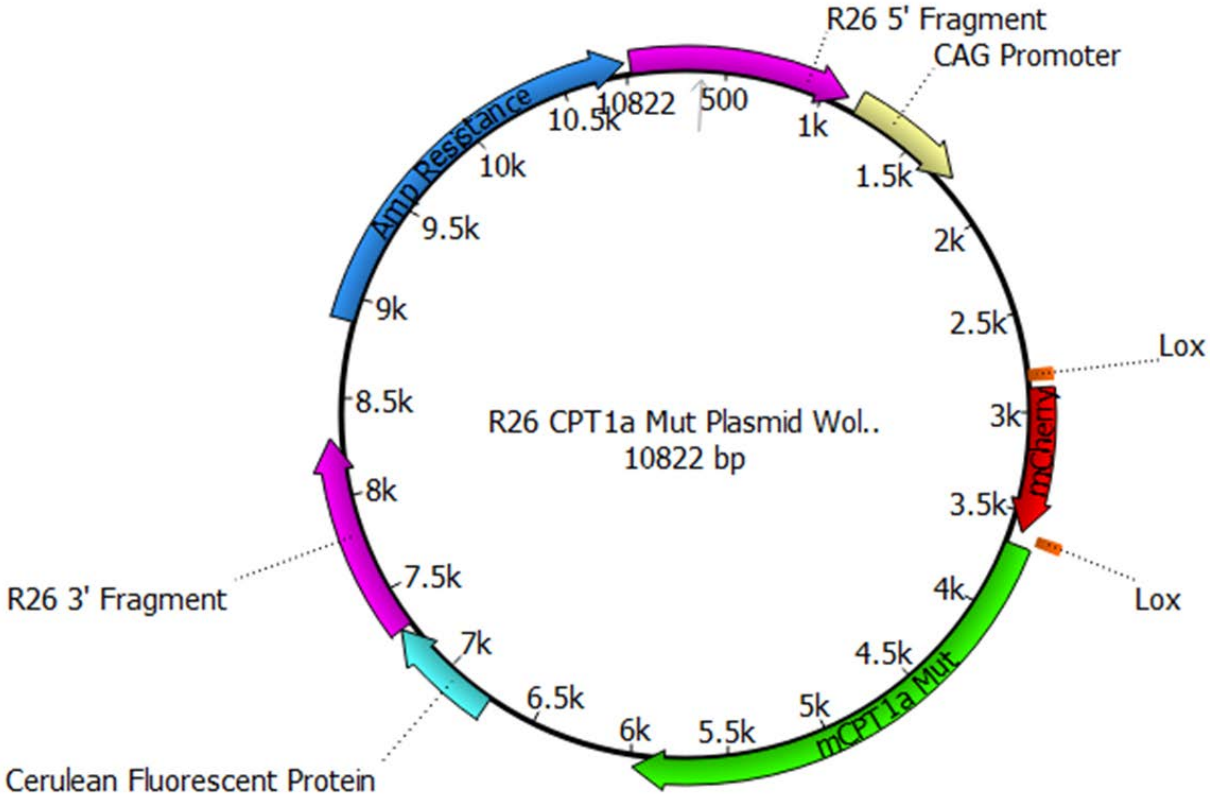
R26 5' Fragment
CAG Promoter
Lox
Lox
mCPT1a Mut
mCherry
Amp Resistance
R26 3' Fragment
Cerulean Fluorescent Protein
R26 CPT1a Mut Plasmid Wol..
10822 bp
10822
500
1k
1.5k
2k
2.5k
3k
3.5k
4k
4.5k
5k
5.5k
6k
6.5k
7k
7.5k
8k
8.5k
9k
9.5k
10k
10.5k

Figure 4-1: Schematic of plasmid provided by Michael Wolfgang, PhD.

A

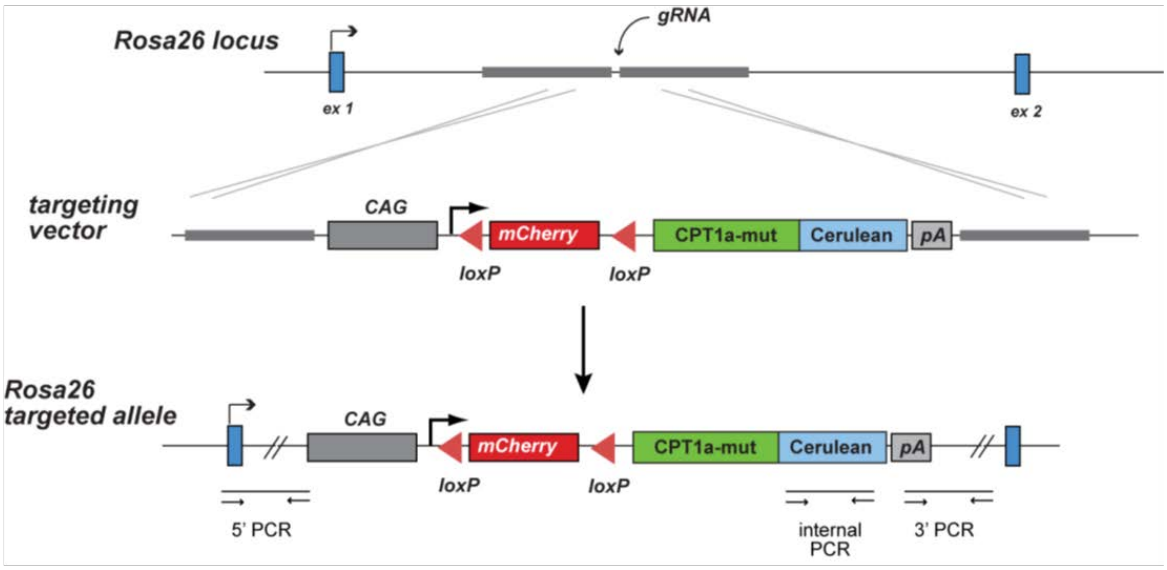
Rosa26 locus
gRNA
ex 1
ex 2
targeting vector
CAG
mCherry
CPT1a-mut
Cerulean
pA
loxP
loxP
Rosa26 targeted allele
CAG
mCherry
CPT1a-mut
Cerulean
pA
loxP
loxP
5' PCR
internal PCR
3' PCR

B

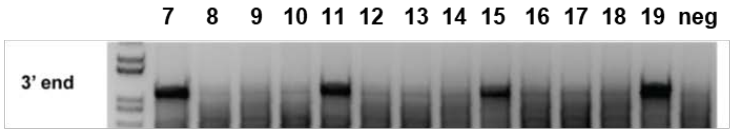
7 8 9 10 11 12 13 14 15 16 17 18 19 neg
3' end

C


14 15 16 17 18 19 20 21
3' end

Figure 4-2: Generation of CPT1A^{M593S} conditionally expressing founders. A) Schematic detailing insert strategy for linearized plasmid via CRISPR/Cas9 approach. B) Founders were identified via PCR identification of 5', internal, and 3' PCRs detailed in panel A. C) Germline transmission was confirmed via PCR identification of all three regions in the N1 backcross generation.

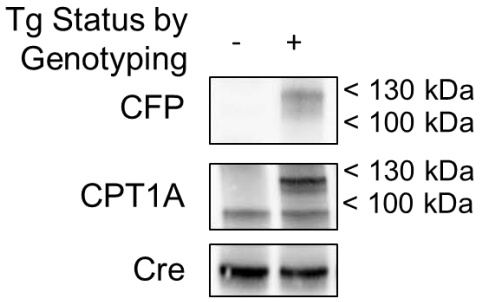
Tg Status by Genotyping
-
+
CFP
< 130 kDa
< 100 kDa
CPT1A
< 130 kDa
< 100 kDa
Cre

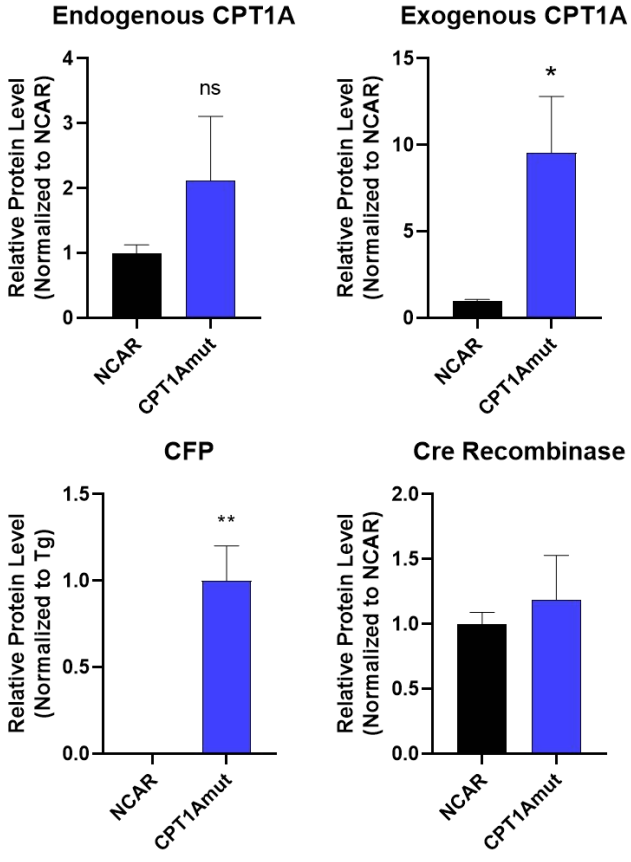
Endogenous CPT1A
Relative Protein Level (Normalized to NCAR)
ns
NCAR
CPT1Amut
Exogenous CPT1A
Relative Protein Level (Normalized to NCAR)
*
NCAR
CPT1Amut
CFP
Relative Protein Level (Normalized to Tg)
**
NCAR
CPT1Amut
Cre Recombinase
Relative Protein Level (Normalized to NCAR)
NCAR
CPT1Amut

Figure 4-3: Validation of transgene expression via Western Blot of liver whole cell lysate in Albumin-Cre x R26-CPT1A^{M593S} progeny. Endogenous CPT1A has a known molecular weight of 88 kDa. Mice identified as transgenic via PCR genotyping demonstrate a doublet when proved for CPT1A and an identifiable band when blotting for CFP.

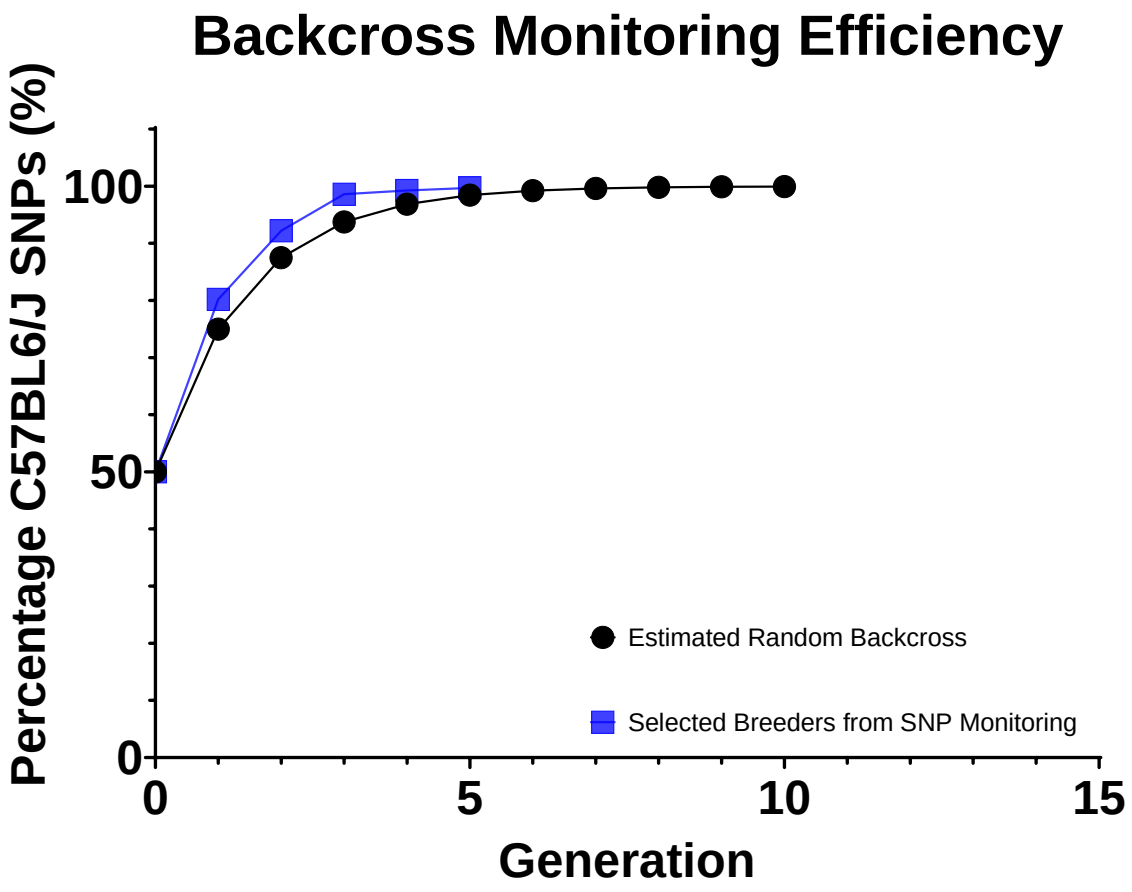
Backcross Monitoring Efficiency
Percentage C57BL6/J SNPs (%)
100
50
0
0
5
10
15
Generation
Estimated Random Backcross
Selected Breeders from SNP Monitoring

Figure 4-4: Backcrossing to C57BL6/J was performed with SNP monitoring to reach congenic status within five generations.

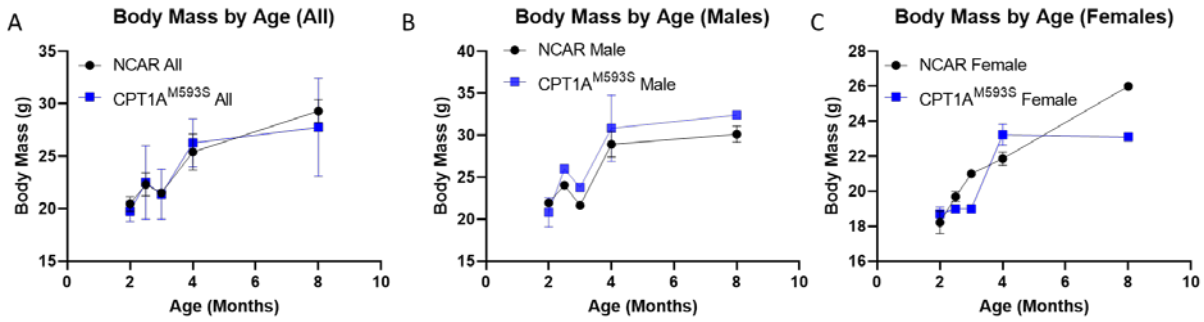
A
Body Mass by Age (All)
NCAR All
CPT1A M593S All
Body Mass (g)
Age (Months)
B
Body Mass by Age (Males)
NCAR Male
CPT1A M593S Male
Body Mass (g)
Age (Months)
C
Body Mass by Age (Females)
NCAR Female
CPT1A M593S Female
Body Mass (g)
Age (Months)

Figure 4-5: Body mass does not differ by genotype through the first eight months of life in either sex.

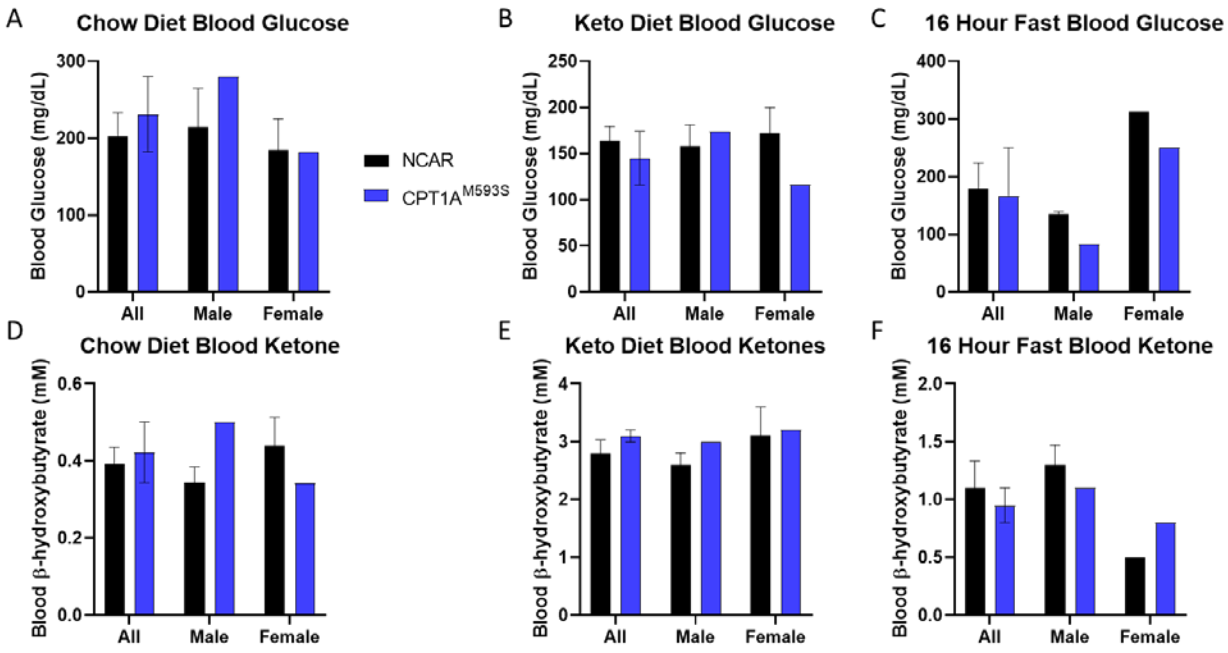
A
Chow Diet Blood Glucose
Blood Glucose (mg/dL)
300
200
100
0
All
Male
Female
NCAR
CPT1A M593S
B
Keto Diet Blood Glucose
Blood Glucose (mg/dL)
250
200
150
100
50
0
All
Male
Female
C
16 Hour Fast Blood Glucose
Blood Glucose (mg/dL)
400
300
200
100
0
All
Male
Female
D
Chow Diet Blood Ketone
Blood β-hydroxybutyrate (mM)
0.6
0.4
0.2
0.0
All
Male
Female
E
Keto Diet Blood Ketones
Blood β-hydroxybutyrate (mM)
4
3
2
1
0
All
Male
Female
F
16 Hour Fast Blood Ketone
Blood β-hydroxybutyrate (mM)
2.0
1.5
1.0
0.5
0.0
All
Male
Female

Figure 4-6: Blood glucose and ketone measurements under chow diet, and ketogenic diet, and fasting conditions. A) Blood glucose did not differ between genotypes on chow diet. B) Blood glucose did not differ between genotypes on ketogenic diet. C) Blood glucose did not differ between genotypes following 16-hour fast. D) Blood ketones did not differ between genotypes on chow diet. E) Blood ketones did not differ between genotypes on ketogenic diet. F) Blood ketones did not differ between genotypes following a 16-hour fast. Error bars represent standard error of the mean.

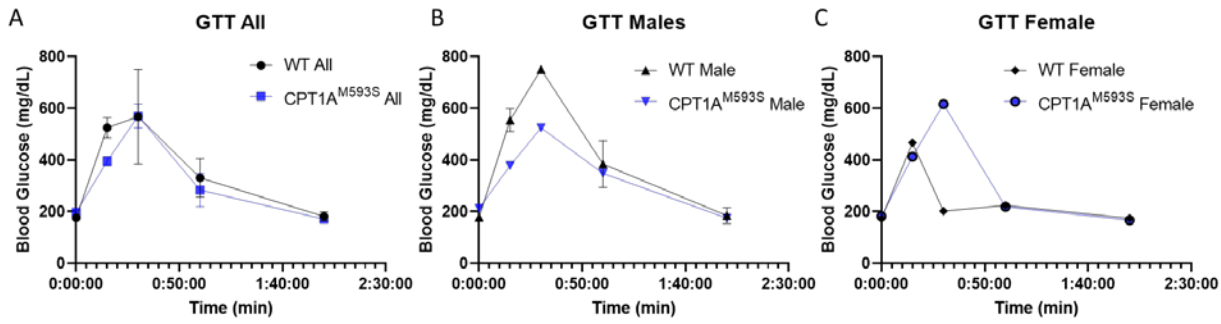
A
GTT All
WT All
CPT1A M593S All
Blood Glucose (mg/dL)
800
600
400
200
0
0:00:00
0:50:00
1:40:00
2:30:00
Time (min)
B
GTT Males
WT Male
CPT1A M593S Male
Blood Glucose (mg/dL)
Time (min)
C
GTT Female
WT Female
CPT1A M593S Female
Blood Glucose (mg/dL)
Time (min)

Figure 4-7: Glucose Tolerance Testing did not differ by genotype. A) Insulin sensitivity did not differ by genotypes across all animals. B) Insulin sensitivity did not differ by genotype in males. C) Insulin sensitivity did not differ by genotypes in females.

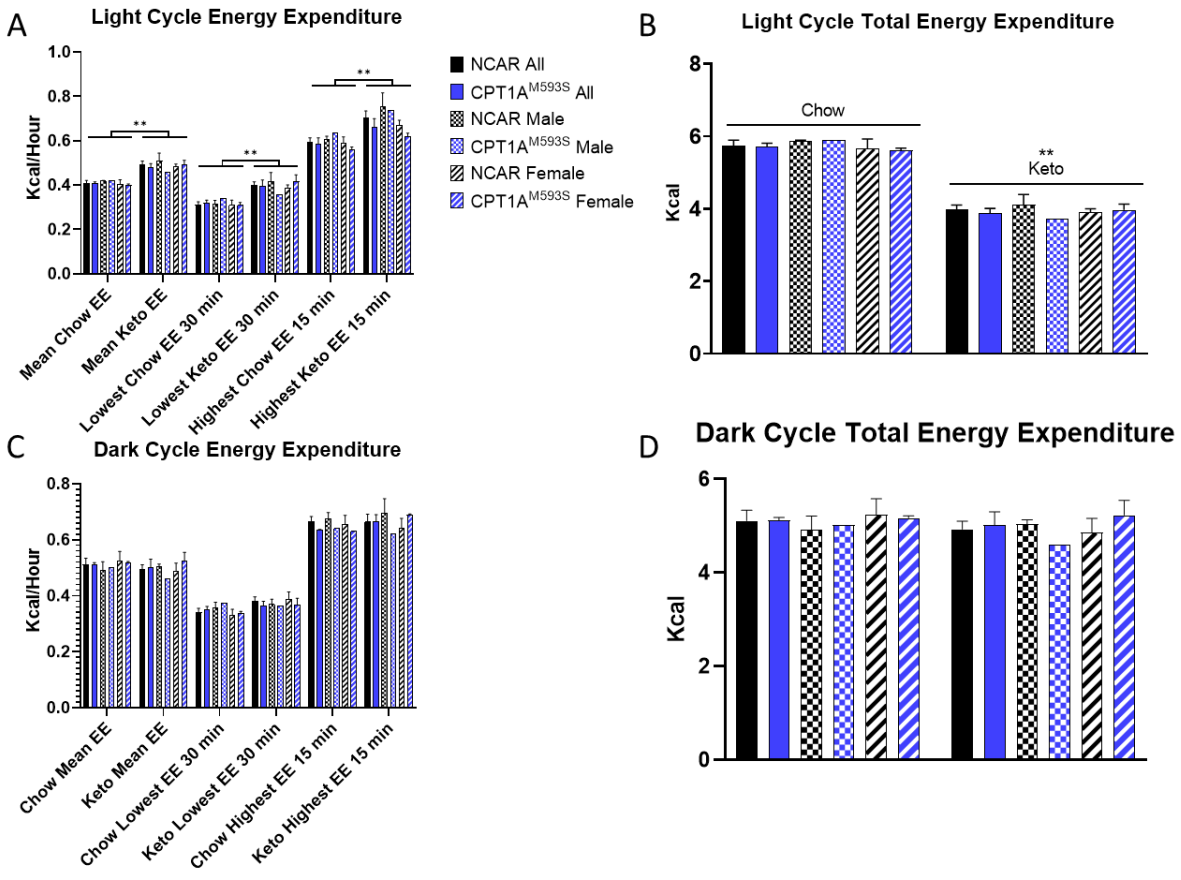
A
Light Cycle Energy Expenditure
Kcal/Hour
1.0
0.8
0.6
0.4
0.2
0.0
**
**
**
Mean Chow EE
Mean Keto EE
Lowest Chow EE 30 min
Lowest Keto EE 30 min
Highest Chow EE 15 min
Highest Keto EE 15 min
NCAR All
CPT1A M593S All
NCAR Male
CPT1A M593S Male
NCAR Female
CPT1A M593S Female
B
Light Cycle Total Energy Expenditure
Kcal
8
6
4
2
0
Chow
**
Keto
C
Dark Cycle Energy Expenditure
Kcal/Hour
0.8
0.6
0.4
0.2
0.0
Chow Mean EE
Keto Mean EE
Chow Lowest EE 30 min
Keto Lowest EE 30 min
Chow Highest EE 15 min
Keto Highest EE 15 min
D
Dark Cycle Total Energy Expenditure
Kcal
6
4
2
0

Figure 4-8: Indirect Calorimetry did not detect any differences in energy expenditure by genotype, but did identify reduced total energy expenditure for animals maintained on a ketogenic diet. A) Light cycle mean energy expenditure, lowest energy expenditure, and highest energy expenditure were elevated when animals were maintained on a ketogenic diet. B) Light cycle total energy expenditure was reduced in animals maintained on a ketogenic diet relative to chow fed animals. C) No difference was detected in mean energy expenditures during the dark cycle either by genotype or diet. D) No difference was measured in total energy expenditure during dark cycle by either genotype or diet. Error bars represent standard error of the mean. *, **, ***, and **** correspond to p-values < 0.05, 0.01, 0.001, and 0.0001 respectively.

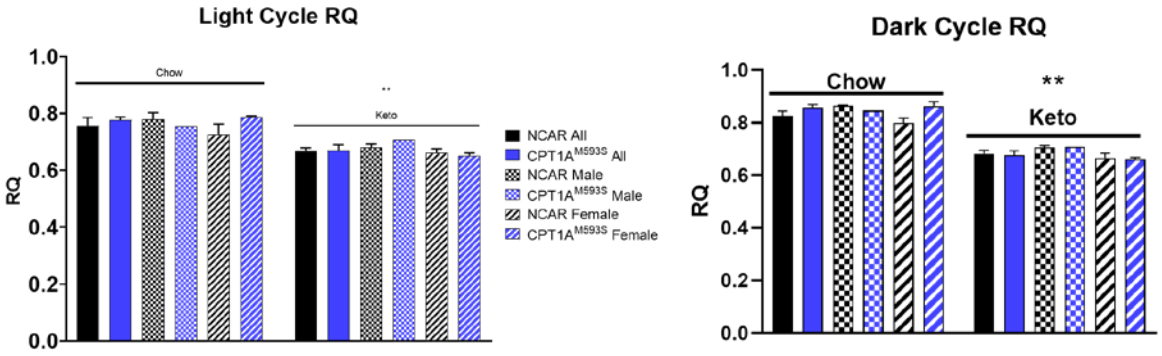
Light Cycle RQ
RQ
1.0
0.8
0.6
0.4
0.2
0.0
Chow
Keto
**
NCAR All
CPT1A M593S All
NCAR Male
CPT1A M593S Male
NCAR Female
CPT1A M593S Female
Dark Cycle RQ
RQ
1.0
0.8
0.6
0.4
0.2
0.0
Chow
Keto
**

Figure 4-9: Respiratory quotients are not influenced by genotype but are reduced by ketogenic diet. A) Light cycle. B) Dark Cycle. Error bars represent standard error of the mean. *, **, ***, and **** correspond to p-values < 0.05, 0.01, 0.001, and 0.0001 respectively.

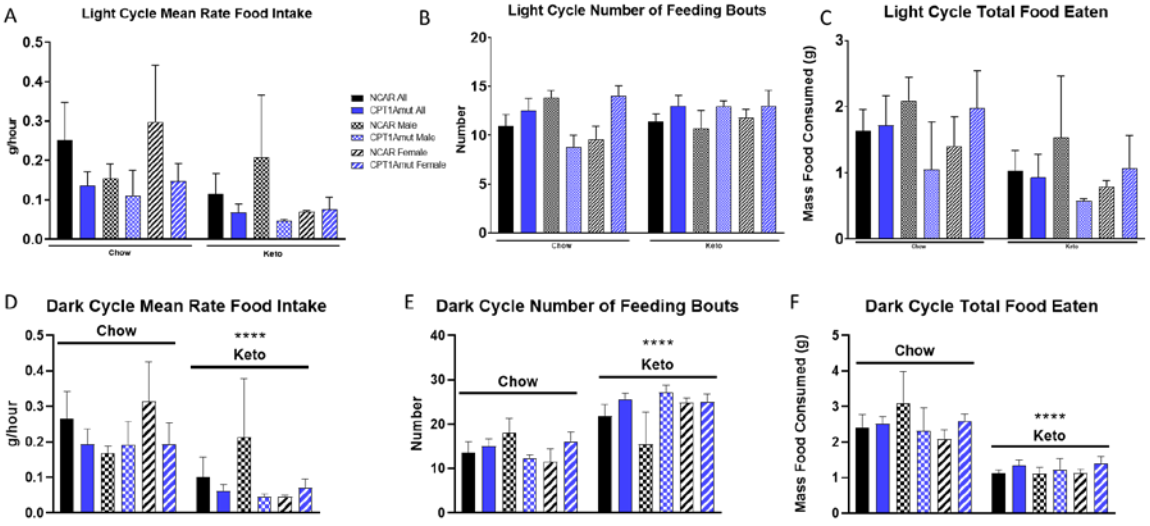
A
Light Cycle Mean Rate Food Intake
g/hour
0.5
0.4
0.3
0.2
0.1
0.0
Chow
Keto
NCAR All
CPT1Amut All
NCAR Male
CPT1Amut Male
NCAR Female
CPT1Amut Female
B
Light Cycle Number of Feeding Bouts
Number
20
15
10
5
0
Chow
Keto
C
Light Cycle Total Food Eaten
Mass Food Consumed (g)
3
2
1
0
Chow
Keto
D
Dark Cycle Mean Rate Food Intake
g/hour
0.5
0.4
0.3
0.2
0.1
0.0
Chow
****
Keto
E
Dark Cycle Number of Feeding Bouts
Number
40
30
20
10
0
Chow
****
Keto
F
Dark Cycle Total Food Eaten
Mass Food Consumed (g)
5
4
3
2
1
0
Chow
****
Keto

Figure 4-10: Feeding behavior was not influenced by genotype but altered by ketogenic diet. A-C) No difference measured in mean food intake, number of feeding bouts, or total food eaten were observed during the light cycle by genotype or diet. D-F) Ketogenic diet fed animals reduced their mean and total food eaten while increasing their number of feeding bouts during the dark cycle. No effect of genotype was observed. Error bars represent standard error of the mean. *, **, ***, and **** correspond to p-values < 0.05, 0.01, 0.001, and 0.0001 respectively.

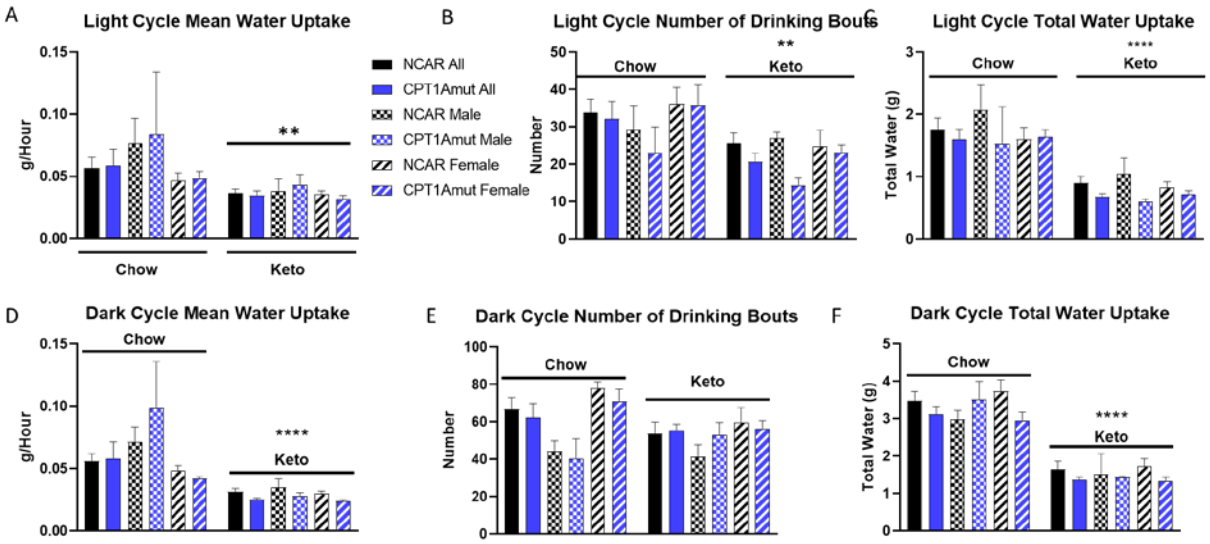
A
Light Cycle Mean Water Uptake
g/Hour
0.15
0.10
0.05
0.00
**
Chow
Keto
B
NCAR All
CPT1Amut All
NCAR Male
CPT1Amut Male
NCAR Female
CPT1Amut Female
Light Cycle Number of Drinking Bouts
Number
50
40
30
20
10
0
**
Chow
Keto
C
Light Cycle Total Water Uptake
Total Water (g)
3
2
1
0
****
Chow
Keto
D
Dark Cycle Mean Water Uptake
g/Hour
0.15
0.10
0.05
0.00
Chow
****
Keto
E
Dark Cycle Number of Drinking Bouts
Number
100
80
60
40
20
0
Chow
Keto
F
Dark Cycle Total Water Uptake
Total Water (g)
5
4
3
2
1
0
Chow
****
Keto

Figure 4-11: Drinking behavior was altered by ketogenic diet but not by genotype. A-C) Animals maintained on ketogenic diet exhibited reduced mean water uptake, number of drinking bouts, and total water consumed during the light cycle. D-F) Similarly, animals exhibited reductions in all measurements of drinking behavior when maintained on ketogenic diet during the dark cycle. Error bars represent standard error of the mean. *, **, ***, and **** correspond to p-values < 0.05, 0.01, 0.001, and 0.0001 respectively.

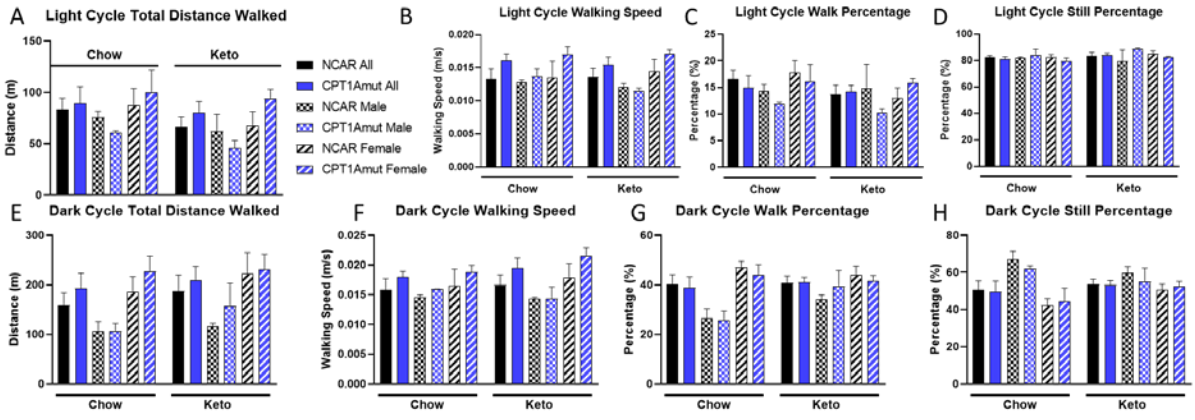
A
Light Cycle Total Distance Walked
Chow
Keto
Distance (m)
NCAR All
CPT1Amut All
NCAR Male
CPT1Amut Male
NCAR Female
CPT1Amut Female
B
Light Cycle Walking Speed
Walking Speed (m/s)
C
Light Cycle Walk Percentage
Percentage (%)
D
Light Cycle Still Percentage
E
Dark Cycle Total Distance Walked
F
Dark Cycle Walking Speed
G
Dark Cycle Walk Percentage
H
Dark Cycle Still Percentage

Figure 4-12: No differences were measured in mobility behavior or ability as a function of genotype or dietary intervention. A-D) No differences were noted during the light cycle. E-F) Behaviors remained static during the dark cycle as well. Error bars represent standard error of the mean. *, **, ***, and **** correspond to p-values < 0.05, 0.01, 0.001, and 0.0001 respectively.

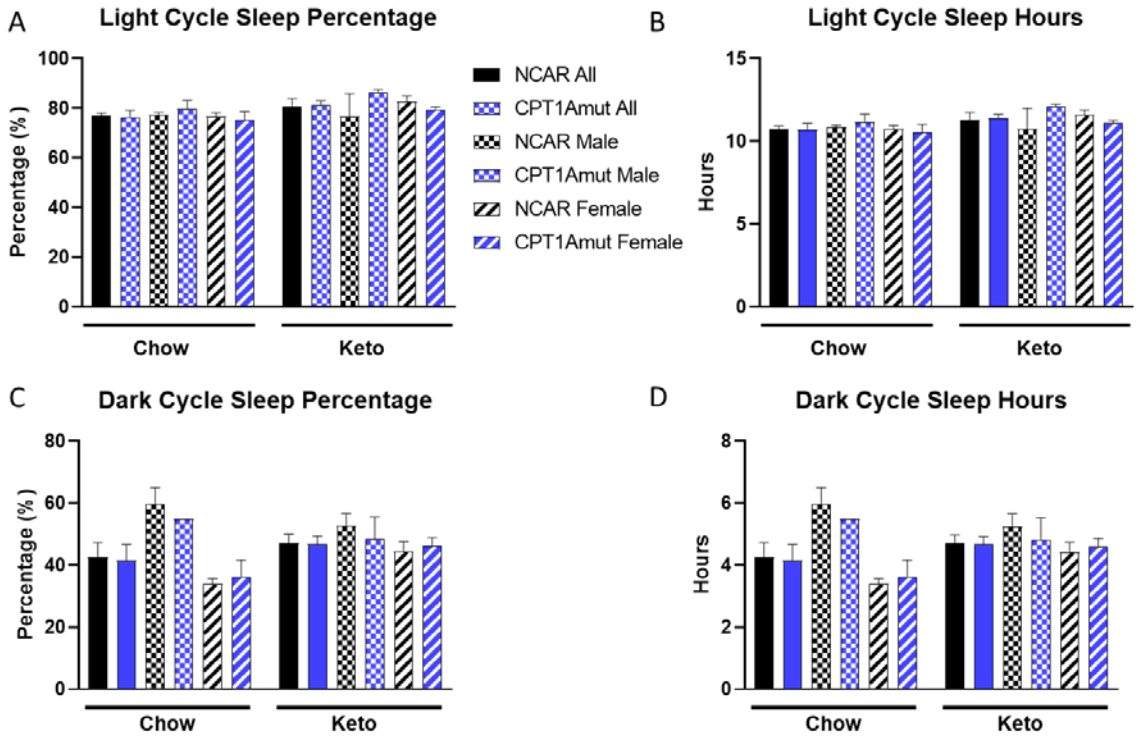
A
Light Cycle Sleep Percentage
Percentage (%)
100
80
60
40
20
0
Chow
Keto
NCAR All
CPT1Amut All
NCAR Male
CPT1Amut Male
NCAR Female
CPT1Amut Female
B
Light Cycle Sleep Hours
Hours
15
10
5
0
Chow
Keto
C
Dark Cycle Sleep Percentage
Percentage (%)
80
60
40
20
0
Chow
Keto
D
Dark Cycle Sleep Hours
Hours
8
6
4
2
0
Chow
Keto

Figure 4-13: Neither CPT1A^{M593S} genotype nor dietary intervention influenced sleep behavior. A-B) Animals spent the same amount of time asleep during the light cycle regardless of genotype or diet. C-D) Sleep behavior was not observed to differ during the dark cycle by genotype or diet. Error bars represent standard error of the mean. *, **, ***, and **** correspond to p-values < 0.05, 0.01, 0.001, and 0.0001 respectively.

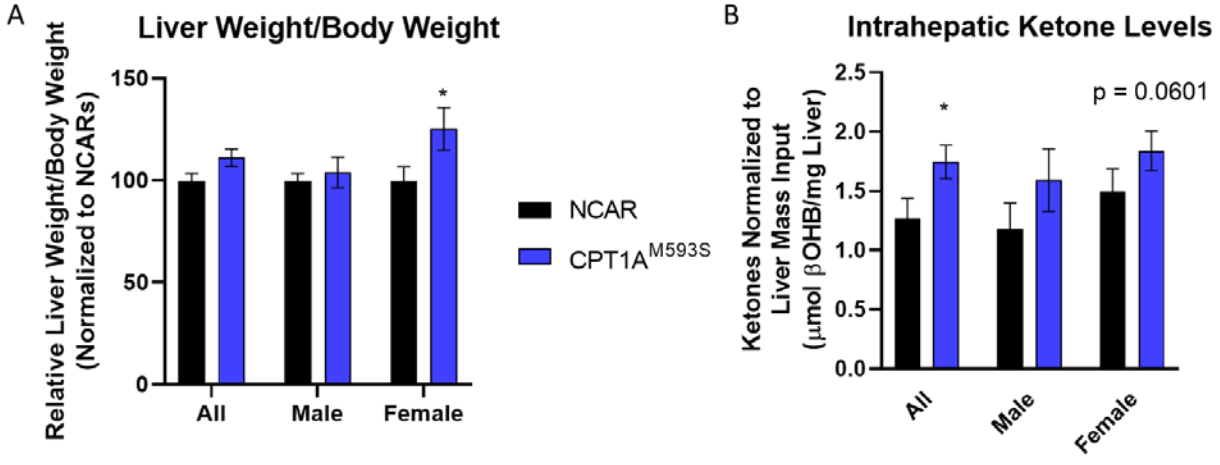
A
Liver Weight/Body Weight
Relative Liver Weight/Body Weight
(Normalized to NCARs)
150
100
50
0
*
All
Male
Female
NCAR
CPT1A M593S
B
Intrahepatic Ketone Levels
Ketones Normalized to
Liver Mass Input
(μmol βOHB/mg Liver)
2.5
2.0
1.5
1.0
0.5
0.0
*
p = 0.0601
All
Male
Female

Figure 4-14: CPT1A^{M593S} mice exhibit enlarged livers and increased intrahepatic ketone levels compared to NCAR litter mates. A) Female CPT1A^{M593S} exhibited significantly enlarged liver at necropsy when normalized to total body weight compared to NCAR females. B) Intrahepatic ketones were significantly elevated across all animals in CPT1AM^{593S} mice and nearly reached significance in females alone. Error bars represent standard error of the mean. *, **, ***, and **** correspond to p-values < 0.05, 0.01, 0.001, and 0.0001 respectively.

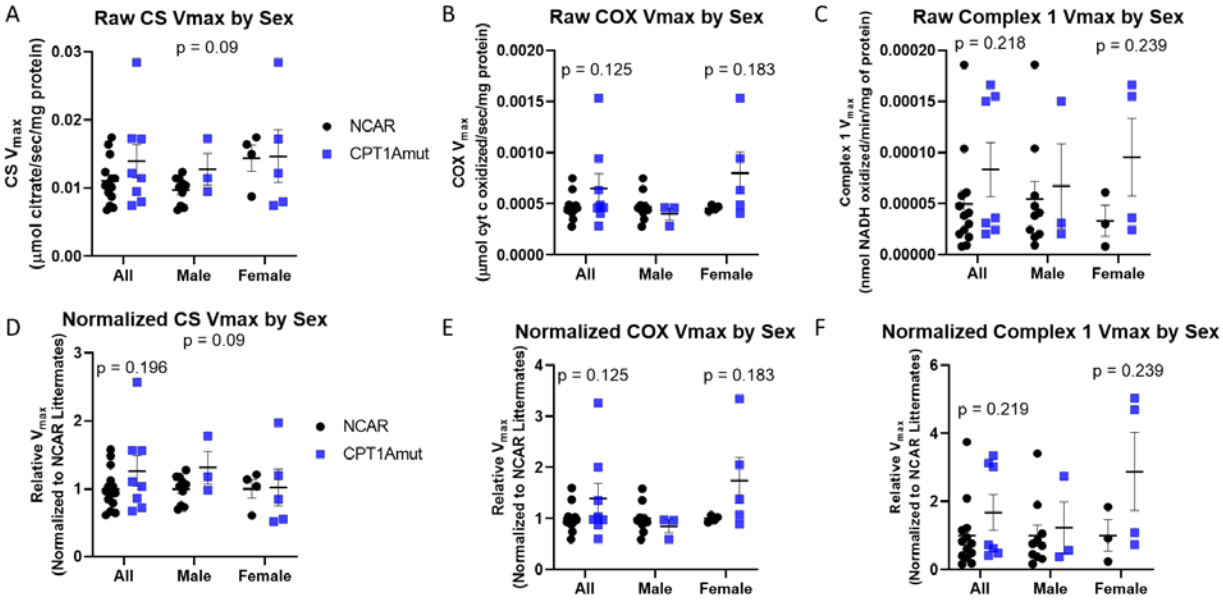
A
Raw CS Vmax by Sex
p = 0.09
CS Vmax
(µmol citrate/sec/mg protein)
0.03
0.02
0.01
0.00
All
Male
Female
NCAR
CPT1Amut
B
Raw COX Vmax by Sex
p = 0.125
p = 0.183
COX Vmax
(µmol cyt c oxidized/sec/mg protein)
0.0020
0.0015
0.0010
0.0005
0.0000
All
Male
Female
C
Raw Complex 1 Vmax by Sex
p = 0.218
p = 0.239
Complex 1 Vmax
(nmol NADH oxidized/min/mg of protein)
0.00020
0.00015
0.00010
0.00005
0.00000
All
Male
Female
D
Normalized CS Vmax by Sex
p = 0.09
p = 0.196
Relative Vmax
(Normalized to NCAR Littermates)
3
2
1
0
All
Male
Female
NCAR
CPT1Amut
E
Normalized COX Vmax by Sex
p = 0.125
p = 0.183
Relative Vmax
(Normalized to NCAR Littermates)
4
3
2
1
0
All
Male
Female
F
Normalized Complex 1 Vmax by Sex
p = 0.219
p = 0.239
Relative Vmax
(Normalized to NCAR Littermates)
6
4
2
0
All
Male
Female

Figure 4-15: No significant differences were found in mitochondrial enzymatic V_{max} assays between NCAR and CPT1A^{M593S} mice. A-C) No significant differences were observed in CS, COX, or complex 1 maximum enzymatic velocity between genotypes. D-F) No significant differences were observed when normalizing raw enzymatic rates to non-carrier litter mates. Error bars represent standard error of the mean. *, **, ***, and **** correspond to p-values < 0.05, 0.01, 0.001, and 0.0001 respectively.

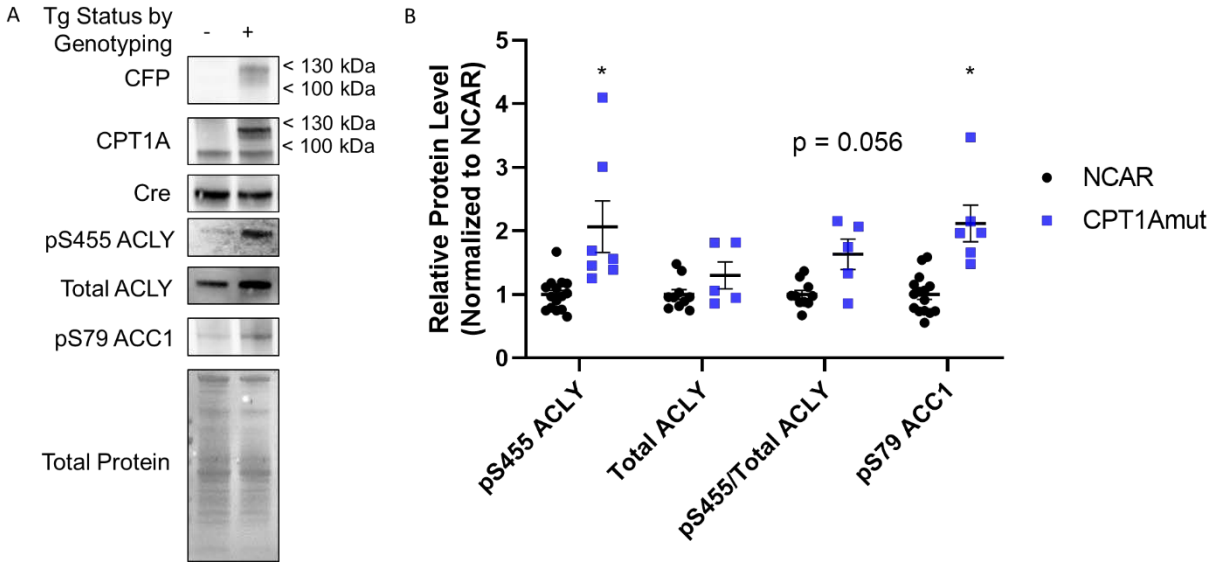
A
Tg Status by Genotyping
-
+
CFP
< 130 kDa
< 100 kDa
CPT1A
< 130 kDa
< 100 kDa
Cre
pS455 ACLY
Total ACLY
pS79 ACC1
Total Protein
B
Relative Protein Level (Normalized to NCAR)
0
1
2
3
4
5
*
*
p = 0.056
pS455 ACLY
Total ACLY
pS455/Total ACLY
pS79 ACC1
NCAR
CPT1Amut

Figure 4-16: CPT1A^{M593S} mice exhibited increased ACLY and ACC1 phosphorylation compared to NCAR littermates. A) Western blot representative images. B) Densitometry of antibody labeling normalized to NCAR littermates. Error bars represent standard error of the mean. *, **, ***, and **** correspond to p-values < 0.05, 0.01, 0.001, and 0.0001 respectively.

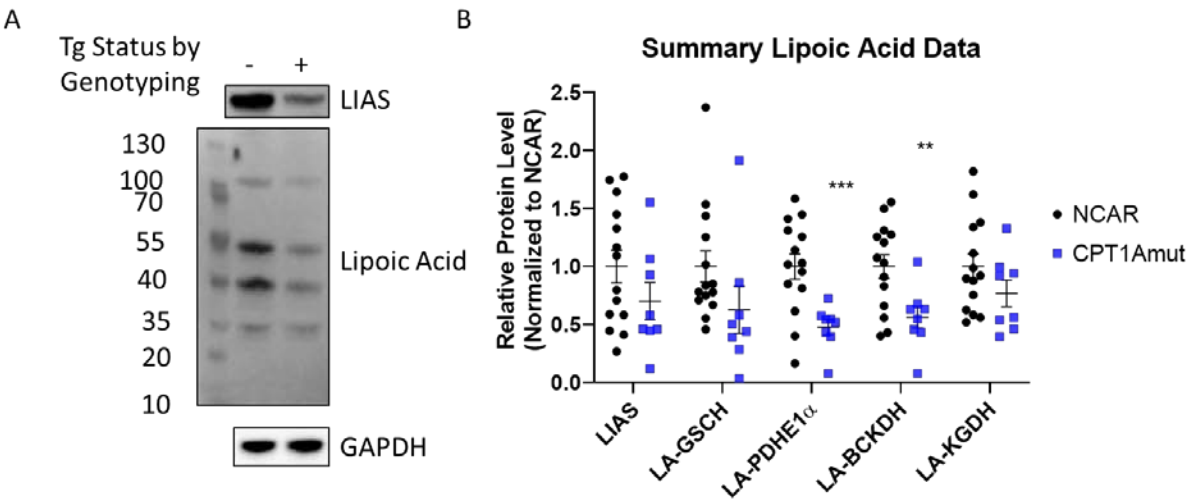
A
Tg Status by Genotyping
-
+
LIAS
130
100
70
55
40
35
20
10
Lipoic Acid
GAPDH
B
Summary Lipoic Acid Data
Relative Protein Level (Normalized to NCAR)
2.5
2.0
1.5
1.0
0.5
0.0
***
**
LIAS
LA-GSCH
LA-PDHE1α
LA-BCKDH
LA-KGDH
NCAR
CPT1Amut

Figure 4-17: CPT1A^{M593S} mice demonstrate reduced LIAS and lipoic acid incorporation into enzymatic complexes. A) Representative western blot images. B) Densitometry of associated westerns normalized to NCAR littermates. Error bars represent standard error of the mean. *, **, ***, and **** correspond to p-values < 0.05, 0.01, 0.001, and 0.0001 respectively.

Chapter 5: Conclusions

β-hydroxybutyrate supports respiration while signaling nutrient scarcity in SH-SY5Y cells and primary rat neurons.

The mechanism of benefit of neuroketotherapeutics remain largely unknown. In the setting of neurodegenerative diseases such as Alzheimer's disease, it has been suggested that bioenergetic support through increasing the availability of ketone bodies in the blood may be effective at treating dementia. Increasingly, it is becoming appreciated that the accumulation of senescent cells in the aged brain can have multiple deleterious consequences including increased inflammation as a result of the senescence associated secretory phenotype and the loss of renewal of replicative cells in the brain from resident stem cell populations such as neural progenitors in the hippocampus. Identifying strategies to delay the onset of irreversible cellular senescence through the activation of reversible cellular quiescence may similarly be beneficial in AD. Here, we provide evidence that supplementation with the ketone salt of β-hydroxybutyrate *in vitro* was able to support respiration in SH-SY5Y neuroblastoma cells and primary embryonic rat neurons.

First, we demonstrated that βOHB increased mitochondrial respiration and energy production in SH-SY5Y cells while simultaneously reducing the NAD^+/NADH ratio under chronic culturing conditions. This shift in respiration was associated with a reduction in mitochondrial membrane potential and an increase in protein level of mediators of autophagy and mitophagy and an increased *MT-ND1/β2M* gDNA ratio. As others have previously published, ketone bodies have been demonstrated to increase mitochondrial biogenesis signaling. These reports accompanied by our observations of increased mitophagy mediators appear to indicate that increased cycling of the mitochondrial organelle may be occurring under ketotic conditions. It would be interesting to expand upon these findings by making of use of mito-timer

and fluorescent mitophagy dyes to further assess the collective ages of mitochondria and observe mitophagic flux more directly.

Although energy production was elevated when the cells were provided with extra carbon in the form of βOHB, cell metabolic activity as assessed by MTT assay and cell growth rate were reduced. Reduced cellular growth appeared to correlate with a slowed transition through the G1-S checkpoint which is known to be regulated by mTOR signaling. Expanding upon this, we observed that culturing SH-SY5Y cells with βOHB reduced activation of the nutrition sensing pathway PI3K-Akt-mTOR despite the increased carbon availability and energy production. We also observed increased histone acetylation and transcription of the quiescence regulating Yamanaka factors *Oct4*, *Sox2*, and *myc* when cells were supplemented with βOHB.

Many of these findings observed in SH-SY5Y cells were recapitulated in primary rat embryonic neurons including increased mitochondrial respiration, reduced Akt phosphorylation, and increased histone acetylation and Oct4 protein level. These findings together indicate that ketone bodies support energy production while modulating cellular signaling pathways to induce quiescence in neuronal cells.

What remains unknown, but would be of interest to determine, is what about βOHB mechanistically induces these changes. First, are the molecular signaling effects occurring downstream of the bioenergetic effects or occur independently from them? To address this, it would be interesting to make use of mitochondrial DNA depleted SH-SY5Y cells, otherwise known as rho0 (ρ0) cells. These ρ0 cells do not have a functional mitochondrial electron transport chain and as such would be unable to respond bioenergetically to βOHB availability as all energy derived from ketolysis occurs through the generation of high energy electron carriers

that are dependent upon functional ETC flux. Therefore, one could surmise that if ρ0 cells continue to exhibit changes in growth rate, PI3K-Akt-mTOR signaling, and Yamanaka factor transcription that these changes are induced independent of the bioenergetic effects of βOHB. Secondly, it may be interesting to determine whether PI3K-Akt-mTOR lies upstream of Yamanaka factor transcription increases or vice versa. This may be addressed through the use of specific mTOR inhibitor rapamycin or one of its analogues. In doing so, these experiments may point to the value of the study of FDA approved mTOR inhibitors for the treatment of neurodegenerative disease through the induction of cellular quiescence signaling pathways.

Astrocytes do not respond bioenergetically to β-hydroxybutyrate supplementation *in vitro*.

Unlike neurons, primary rat astrocytes did not respond to chronic supplementation of βOHB by increasing mitochondrial respiration. Similarly, histone acetylation was not increased and consistent suppression of Akt phosphorylation was observed in astrocytes when treated with βOHB. This differential response to βOHB availability indicates that the brain may be specialized to spare βOHB from glial catabolism so as to maintain availability of this carbon source for neuronal consumption as an emergency reserve during times of nutrient scarcity. Although to be certain of this, expanded *in vivo* studies would be required. While this is of interest from a physiological and evolutionary perspective, it may also have important lessons for the treatment of neurologic disease. Providing ketones to the CNS *en masse* may reduce potency if therapeutic response is dependent on a specific response unique to a single CNS cell population subtype and the intervening agent distributes across all populations. This may especially be the case in regard to ketone-based therapies as transport of ketones into cells relies on monocarboxylate transporters that are ubiquitous in the CNS.

Further studies into the effects of ketone bodies on astrocytes are warranted to better appreciate if they induce an alternative, unrecognized effect on astrocytic biology or if they are largely inert in this population. A larger, more ambitious future direction for this line of study would be the development and validation of new drug delivery therapies not only to overcome the blood brain barrier, but to achieve CNS cell population targeting upon entry to the brain. Development of such technology could have profound impact on improving the potency and specificity of pharmaceutical effects on neurologic disease which could improve efficacy and reduce adverse secondary effects.

Mouse Neuronal and Astrocytic Transcriptional Response to 90-Day Ketogenic Diet Intervention Differs Greatly.

To expand upon our *in vitro* findings, we maintained two populations of adult, male C57BL6/N mice on standard chow and ketogenic diets for 90-days and isolated neuronally and astrocytically enriched cell fractions for transcriptomic profiling. KEGG pathway analysis of neurons indicated that ketogenic diet increased transcription of intermediates for such phenomena as mitochondrial oxidative phosphorylation, endoplasmic reticulum protein processing, and insulin signaling among many others. Amongst pathology associated pathways, the top three pathways altered in neurons included Alzheimer's disease, Parkinson's disease, and Huntington's disease indicating that ketogenic diet modulates phenomena relevant to neurodegenerative disease pathogenesis. Many of these pathways appeared to rely upon upregulation of mitochondrial electron transport chain subunits, PI3K-Akt-mTOR signaling, JNK signaling, and ERK 1/2 signaling pathways for pathway identification.

Meanwhile, astrocytic transcriptional response was largely suppressed in response to ketogenic diet compared to standard chow fed mice. Altered pathways in astrocytes included steroid hormone biosynthesis, axon guidance, and insulin signaling pathways. Pathology associated pathways included those pertaining to infectious disease, cancer, drug addiction, and type II diabetes mellitus. When investigated further, it appears that these pathway results stem from modulations in JNK signaling, Akt signaling, ERK 1/2, inflammatory cytokine signaling, and changes in enzymes involved in glucuronidation.

All of these purported changes require further investigation at the protein and histological level to confirm the exact nature of their response to ketogenic diet. Further, from a mechanistic perspective it would be valuable to return to *in vitro* studies in these cell types to determine which exact pathway activations are responding as a part of ketone supplementation, increased fat availability in the diet, changes in insulin, changes in glucagon, or other facets of the ketogenic diet. Of these findings, it is gratifying that neurodegenerative disease were returned as such highly significant results on the KEGG pathway analysis to lend credence to the hypothesis of the utility in treating these disorders. As far as newly recognized molecular pathways and potential mechanisms are concerned, alterations in ER protein processing and endocytosis seem to be the most intriguing as translatable effects that could have AD modulating properties. Improved ER protein processing may alter the manner in which APP or tau is processed via glycosylation or alternative protein processing mechanisms that may divert them away from pathogenic forms that could initiate or accelerate disease progression. It is also increasingly recognized that endocytosis is disrupted in AD and understanding the effects of KD on endocytosis may provide insight on how to modulate this behavior to prevent the accumulation of extracellular amyloid plaques.

Even more novel from a purely biological perspective is the alteration in glucuronidation pathways in astrocytes. Glucuronidation is best understood for its role in phase II drug metabolism for the excretion of xenobiotics. While it has been previously established that astrocytes perform the majority of glucuronidation in the brain, its purpose is unclear. Currently it is understood to increase that sex steroids, dopamine, and serotonin serve as substrates for glucuronidation in the brain although the physiological consequences of such modulation are poorly understood. Ketogenic diet would be a useful intervention to expand upon this understudied aspect of mammalian biology that could have important ramifications in the fields of psychological disorders, parkinsonian disorders, and neuropharmacology.

Initial findings and future directions for the utilization and study of the CPT1A^{M593S} mouse model.

Here, we will briefly summarize the conclusions found in the discussion of Chapter 4 that are written in greater detail. Preliminary findings into the characterization of the CPT1A^{M593S} indicate that hepatic expression of the transgene does not manifest in increased ketonemia under standard chow diet, ketogenic diet, or prolonged fasting conditions relative to non-carrier littermates. However, there is evidence to suggest that hepatic ketogenesis is elevated and that export of acetyl-CoA from the mitochondrial matrix as citrate may be elevated while mitochondrial fatty acid synthesis is suppressed. As such, the immediate future of this project should accomplish the following goals.

Firstly, histologic examination of the transgenic livers should be performed to confirm correct subcellular localization of the transgene to the mitochondria and not the peroxisome as CPT1A is known to traffic to both organelles. While this is performed histologic examination of

lipid and glycogen content could also be performed to assess changes in carbon accumulation in the liver that may account for observations of increased liver weight relative to total body weight. Second, more mice are needed to confirm or refute initial findings regarding alterations in mitochondrial enzymatic activity and molecular signaling changes within both sexes. To address the issue of slow pace of progress secondary to limited numbers of transgenic pups, it should be an immediate goal to generate homozygous CPT1A^{M593S} breeders so that the investigator is not at the mercy of chance for the number of transgenic pups per litter. The other immediate advantage of generating homozygous breeders would be the ability to produce homozygous CPT1A^{M593S} mice on a Cre background to observe the effects of increased copy number on phenotype. It remains possible that constitutively increased ketosis is a phenotype of the CPT1A^{M593S} mouse model but only on ketogenic conditions. Additionally, it would be interesting to know what the physiologic consequences are of changes in ACLY, ACC1, and LIAS protein status. To address this, it would be valuable to perform radiolabeled fat tracing to understand the fate of radiolabeled palmitate and how carbons derived from fat are trafficked between non-carriers and transgenic mice. Finally, and perhaps most critically, examination of the consequences of transgene expression in astrocytes would be imperative to the study of the effects of transgene expression on the CNS, especially if intraorgan increases in ketone body content are also a phenotype of astrocytic CPT1A^{M593S} expression.

Summary

Metabolic dysfunction is an early and important feature of brain aging and Alzheimer's disease. Addressing metabolic dysfunction either through bioenergetic support or the activation of cellular quiescence may have important therapeutic effects on these neurologic states. Ketogenic therapies, either the ketogenic diet or use of a ketone salt, appear to support

bioenergetics and signal cellular quiescence in a cell population specific manner. As such, further study into the application of neuroketotherapeutics to promote healthy brain aging or treat neurodegenerative disease are indicated. However, it should be done with ample consideration as to the metabolic compartmentalization of the CNS and differential response to interventions with respect to cell type.

References

Adam, P. A., Raiha, N., Rahiala, E. L., & Kekomaki, M. (1975). Oxidation of glucose and D-B-OH-butyrate by the early human fetal brain. *Acta Paediatr Scand, 64*(1), 17-24.

Akkaoui, M., Cohen, I., Esnous, C., Lenoir, V., Sournac, M., Girard, J., & Prip-Buus, C. (2009). Modulation of the hepatic malonyl-CoA-carnitine palmitoyltransferase 1A partnership creates a metabolic switch allowing oxidation of de novo fatty acids. *Biochem J, 420*(3), 429-438. doi:10.1042/bj20081932

Al-Mudallal, A. S., LaManna, J. C., Lust, W. D., & Harik, S. I. (1996). Diet-induced ketosis does not cause cerebral acidosis. *Epilepsia, 37*(3), 258-261.

Andrews, S. J., Fulton-Howard, B., Patterson, C., McFall, G. P., Gross, A., Michaelis, E. K., . . . Pa, J. (2020). Mitonuclear interactions influence Alzheimer's disease risk. *Neurobiol Aging, 87*, 138.e137-138.e114. doi:10.1016/j.neurobiolaging.2019.09.007

Apfelbaum, M., Lacatis, D., Reinberg, A., & Assan, R. (1972). Persisting circadian rhythm in insulin, glucagon, cortisol etc. of healthy young women during caloric restriction (protein diet). *Rev Med Chir Soc Med Nat Iasi, 76*(1), 123-130.

Aubert, A., & Costalat, R. (2007). Compartmentalization of brain energy metabolism between glia and neurons: insights from mathematical modeling. *Glia, 55*(12), 1272-1279. doi:10.1002/glia.20360

Baird, G. D., Heitzman, R. J., & Hibbitt, K. G. (1972). Effects of starvation on intermediary metabolism in the lactating cow. A comparison with metabolic changes occurring during bovine ketosis. *Biochem J, 128*(5), 1311-1318.

Barborka, C. J. (1928). Ketogenic diet treatment of epilepsy in adults. *Journal of the American Medical Association, 91*(2), 73-78. doi:10.1001/jama.1928.02700020007003

Bartzokis, G., Lu, P. H., & Mintz, J. (2004). Quantifying age-related myelin breakdown with MRI: novel therapeutic targets for preventing cognitive decline and Alzheimer's disease. *J Alzheimers Dis, 6*(6 Suppl), S53-59.

Bartzokis, G., Sultzer, D., Lu, P. H., Nuechterlein, K. H., Mintz, J., & Cummings, J. L. (2004). Heterogeneous age-related breakdown of white matter structural integrity: implications for cortical "disconnection" in aging and Alzheimer's disease. *Neurobiol Aging, 25*(7), 843-851. doi:10.1016/j.neurobiolaging.2003.09.005

Baydyuk, M., & Xu, B. (2014). BDNF signaling and survival of striatal neurons. *Frontiers in Cellular Neuroscience, 8*, 254. doi:10.3389/fncel.2014.00254

Bekesi, A., & Williamson, D. H. (1990). An explanation for ketogenesis by the intestine of the suckling rat: the presence of an active hydroxymethylglutaryl-coenzyme A pathway. *Biol Neonate, 58*(3), 160-165.

Blazquez, C., Sanchez, C., Velasco, G., & Guzman, M. (1998). Role of carnitine palmitoyltransferase I in the control of ketogenesis in primary cultures of rat astrocytes. *J Neurochem, 71*(4), 1597-1606.

Blomqvist, G., Alvarsson, M., Grill, V., Von Heijne, G., Ingvar, M., Thorell, J. O., . . . Ekberg, K. (2002). Effect of acute hyperketonemia on the cerebral uptake of ketone bodies in nondiabetic subjects and IDDM patients. *Am J Physiol Endocrinol Metab, 283*(1), E20-28. doi:10.1152/ajpendo.00294.2001

Blomqvist, G., Thorell, J. O., Ingvar, M., Grill, V., Widen, L., & Stone-Elander, S. (1995). Use of R-beta-[1-11C]hydroxybutyrate in PET studies of regional cerebral uptake of ketone bodies in humans. *Am J Physiol, 269*(5 Pt 1), E948-959.

Bolla, A. M., Caretto, A., Laurenzi, A., Scavini, M., & Piemonti, L. (2019). Low-Carb and Ketogenic Diets in Type 1 and Type 2 Diabetes. *Nutrients, 11*(5), 962. doi:10.3390/nu11050962

Bough, K. J., Wetherington, J., Hassel, B., Pare, J. F., Gawryluk, J. W., Greene, J. G., . . . Dingledine, R. J. (2006). Mitochondrial biogenesis in the anticonvulsant mechanism of the ketogenic diet. *Ann Neurol, 60*(2), 223-235. doi:10.1002/ana.20899

Bouzier-Sore, A. K., Serres, S., Canioni, P., & Merle, M. (2003). Lactate involvement in neuron-glia metabolic interaction: (13)C-NMR spectroscopy contribution. *Biochimie, 85*(9), 841-848.

Breckenridge, W. C., & Kuksis, A. (1967). Molecular weight distributions of milk fat triglycerides from seven species. *J Lipid Res, 8*(5), 473-478.

Brinton, R. D. (2008). Estrogen regulation of glucose metabolism and mitochondrial function: therapeutic implications for prevention of Alzheimer's disease. *Adv Drug Deliv Rev, 60*(13-14), 1504-1511. doi:10.1016/j.addr.2008.06.003

Bruce, E. D., Konda, S., Dean, D. D., Wang, E. W., Huang, J. H., & Little, D. M. (2015). Neuroimaging and traumatic brain injury: State of the field and voids in translational knowledge. *Mol Cell Neurosci, 66*(Pt B), 103-113. doi:10.1016/j.mcn.2015.03.017

Bussian, T. J., Aziz, A., Meyer, C. F., Swenson, B. L., van Deursen, J. M., & Baker, D. J. (2018). Clearance of senescent glial cells prevents tau-dependent pathology and cognitive decline. *Nature, 562*(7728), 578-582. doi:10.1038/s41586-018-0543-y

Carmichael, O., Schwarz, C., Drucker, D., Fletcher, E., Harvey, D., Beckett, L., . . . DeCarli, C. (2010). Longitudinal changes in white matter disease and cognition in the first year of the Alzheimer disease neuroimaging initiative. *Arch Neurol, 67*(11), 1370-1378. doi:10.1001/archneurol.2010.284

Castellano, C. A., Nugent, S., Paquet, N., Tremblay, S., Bocti, C., Lacombe, G., . . . Cunnane, S. C. (2015). Lower brain 18F-fluorodeoxyglucose uptake but normal 11C-acetoacetate metabolism in mild Alzheimer's disease dementia. *J Alzheimers Dis, 43*(4), 1343-1353. doi:10.3233/jad-141074

Cheng, B., Yang, X., An, L., Gao, B., Liu, X., & Liu, S. (2009). Ketogenic diet protects dopaminergic neurons against 6-OHDA neurotoxicity via up-regulating glutathione in a rat model of Parkinson's disease. *Brain Res, 1286*, 25-31. doi:10.1016/j.brainres.2009.06.060

Chong, Z. Z., Kang, J. Q., & Maiese, K. (2002). Erythropoietin is a novel vascular protectant through activation of Akt1 and mitochondrial modulation of cysteine proteases. *Circulation, 106*(23), 2973-2979.

Chong, Z. Z., Kang, J. Q., & Maiese, K. (2003). Erythropoietin fosters both intrinsic and extrinsic neuronal protection through modulation of microglia, Akt1, Bad, and caspase-mediated pathways. *Br J Pharmacol, 138*(6), 1107-1118. doi:10.1038/sj.bjp.0705161

Chong, Z. Z., Li, F., & Maiese, K. (2005). Activating Akt and the brain's resources to drive cellular survival and prevent inflammatory injury. *Histology and histopathology, 20*(1), 299-315.

Chu, A. C., Ho, P. W., Kwok, K. H., Ho, J. W., Chan, K. H., Liu, H. F., . . . Ho, S. L. (2009). Mitochondrial UCP4 attenuates MPP+ - and dopamine-induced oxidative stress,

mitochondrial depolarization, and ATP deficiency in neurons and is interlinked with UCP2 expression. *Free Radic Biol Med, 46*(6), 810-820. doi:10.1016/j.freeradbiomed.2008.12.015

Cotter, D. G., d'Avignon, D. A., Wentz, A. E., Weber, M. L., & Crawford, P. A. (2011). Obligate Role for Ketone Body Oxidation in Neonatal Metabolic Homeostasis. *The Journal of Biological Chemistry, 286*(9), 6902-6910. doi:10.1074/jbc.M110.192369

Courchesne-Loyer, A., Croteau, E., Castellano, C. A., St-Pierre, V., Hennebelle, M., & Cunnane, S. C. (2016). Inverse relationship between brain glucose and ketone metabolism in adults during short-term moderate dietary ketosis: A dual tracer quantitative positron emission tomography study. *J Cereb Blood Flow Metab*. doi:10.1177/0271678x16669366

Cunnane, S., Nugent, S., Roy, M., Courchesne-Loyer, A., Croteau, E., Tremblay, S., . . . Rapoport, S. I. (2011). Brain fuel metabolism, aging, and Alzheimer's disease. *Nutrition, 27*(1), 3-20. doi:10.1016/j.nut.2010.07.021

Cunnane, S. C., Courchesne-Loyer, A., St-Pierre, V., Vandenberghe, C., Pierotti, T., Fortier, M., . . . Castellano, C. A. (2016). Can ketones compensate for deteriorating brain glucose uptake during aging? Implications for the risk and treatment of Alzheimer's disease. *Ann N Y Acad Sci, 1367*(1), 12-20. doi:10.1111/nyas.12999

Cunnane, S. C., Courchesne-Loyer, A., Vandenberghe, C., St-Pierre, V., Fortier, M., Hennebelle, M., . . . Castellano, C. A. (2016). Can Ketones Help Rescue Brain Fuel Supply in Later Life? Implications for Cognitive Health during Aging and the Treatment of Alzheimer's Disease. *Front Mol Neurosci, 9*, 53. doi:10.3389/fnmol.2016.00053

Cunnane, S. C., & Crawford, M. A. (2003). Survival of the fattest: fat babies were the key to evolution of the large human brain. *Comp Biochem Physiol A Mol Integr Physiol, 136*(1), 17-26.

de la Monte, S. M. (2009). Insulin resistance and Alzheimer's disease. *BMB Rep, 42*(8), 475-481.

de Leon, M. J., Convit, A., Wolf, O. T., Tarshish, C. Y., DeSanti, S., Rusinek, H., . . . Fowler, J. (2001). Prediction of cognitive decline in normal elderly subjects with 2-[(18)F]fluoro-2-deoxy-D-glucose/poitron-emission tomography (FDG/PET). *Proc Natl Acad Sci U S A, 98*(19), 10966-10971. doi:10.1073/pnas.191044198

Deransart, C., Hellwig, B., Heupel-Reuter, M., Leger, J. F., Heck, D., & Lucking, C. H. (2003). Single-unit analysis of substantia nigra pars reticulata neurons in freely behaving rats with genetic absence epilepsy. *Epilepsia, 44*(12), 1513-1520.

Devi, L., Prabhu, B. M., Galati, D. F., Avadhani, N. G., & Anandatheerthavarada, H. K. (2006). Accumulation of amyloid precursor protein in the mitochondrial import channels of human Alzheimer's disease brain is associated with mitochondrial dysfunction. *J Neurosci, 26*(35), 9057-9068. doi:10.1523/jneurosci.1469-06.2006

Diehl, T., Mullins, R., & Kapogiannis, D. (2017). Insulin resistance in Alzheimer's disease. *Transl Res, 183*, 26-40. doi:10.1016/j.trsl.2016.12.005

Dienel, G. A. (2013). Astrocytic energetics during excitatory neurotransmission: What are contributions of glutamate oxidation and glycolysis? *Neurochem Int, 63*(4), 244-258. doi:10.1016/j.neuint.2013.06.015

Drysdale, G. R., & Lardy, H. A. (1953). Fatty acid oxidation by a soluble enzyme system from mitochondria. *J Biol Chem, 202*(1), 119-136.

Echtay, K. S. (2007). Mitochondrial uncoupling proteins--what is their physiological role? *Free Radic Biol Med, 43*(10), 1351-1371. doi:10.1016/j.freeradbiomed.2007.08.011

Erecinska, M., Nelson, D., Daikhin, Y., & Yudkoff, M. (1996). Regulation of GABA level in rat brain synaptosomes: fluxes through enzymes of the GABA shunt and effects of glutamate, calcium, and ketone bodies. *J Neurochem, 67*(6), 2325-2334.

Evangeliou, A., Spilioti, M., Doulioglou, V., Kalaidopoulou, P., Ilias, A., Skarpalezou, A., . . . Nikolaidis, N. (2009). Branched chain amino acids as adjunctive therapy to ketogenic diet in epilepsy: pilot study and hypothesis. *J Child Neurol, 24*(10), 1268-1272. doi:10.1177/0883073809336295

Fernandes, C. G., da Rosa, M. S., Seminotti, B., Pierozan, P., Martell, R. W., Lagranha, V. L., . . . Wajner, M. (2013). In vivo experimental evidence that the major metabolites accumulating in 3-hydroxy-3-methylglutaryl-CoA lyase deficiency induce oxidative stress in striatum of developing rats: a potential pathophysiological mechanism of striatal damage in this disorder. *Mol Genet Metab, 109*(2), 144-153. doi:10.1016/j.ymgme.2013.03.017

Fernandes, C. G., Pierozan, P., Soares, G. M., Ferreira, F., Zanatta, A., Amaral, A. U., . . . Pessoa-Pureur, R. (2015). NMDA Receptors and Oxidative Stress Induced by the Major Metabolites Accumulating in HMG Lyase Deficiency Mediate Hypophosphorylation of Cytoskeletal Proteins in Brain From Adolescent Rats: Potential Mechanisms Contributing to the Neuropathology of This Disease. *Neurotox Res, 28*(3), 239-252. doi:10.1007/s12640-015-9542-z

Freemantle, E., Vandal, M., Tremblay-Mercier, J., Tremblay, S., Blachere, J. C., Begin, M. E., . . . Cunnane, S. C. (2006). Omega-3 fatty acids, energy substrates, and brain function during aging. *Prostaglandins Leukot Essent Fatty Acids, 75*(3), 213-220. doi:10.1016/j.plefa.2006.05.011

Frisoni, G. B., Boccardi, M., Barkhof, F., Blennow, K., Cappa, S., Chiotis, K., . . . Winblad, B. (2017). Strategic roadmap for an early diagnosis of Alzheimer's disease based on biomarkers. *Lancet Neurol, 16*(8), 661-676. doi:10.1016/s1474-4422(17)30159-x

Fukao, T., Song, X. Q., Mitchell, G. A., Yamaguchi, S., Sukegawa, K., Orii, T., & Kondo, N. (1997). Enzymes of ketone body utilization in human tissues: protein and messenger RNA levels of succinyl-coenzyme A (CoA):3-ketoacid CoA transferase and mitochondrial and cytosolic acetoacetyl-CoA thiolases. *Pediatr Res, 42*(4), 498-502. doi:10.1203/00006450-199710000-00013

Gano, L. B., Patel, M., & Rho, J. M. (2014). Ketogenic diets, mitochondria, and neurological diseases. *J Lipid Res, 55*(11), 2211-2228. doi:10.1194/jlr.R048975

Garber, A. J., Menzel, P. H., Boden, G., & Owen, O. E. (1974). Hepatic ketogenesis and gluconeogenesis in humans. *J Clin Invest, 54*(4), 981-989. doi:10.1172/jci107839

Geyelin, H. R. (1921). Fasting as a method for treating epilepsy. *Med Rec, 99*, 1037-1039.

Gibbs, M. E., Gibbs, Z., & Hertz, L. (2009). Rescue of Abeta(1-42)-induced memory impairment in day-old chick by facilitation of astrocytic oxidative metabolism: implications for Alzheimer's disease. *J Neurochem, 109 Suppl 1*, 230-236. doi:10.1111/j.1471-4159.2009.05800.x

Gibson, C. L., Murphy, A. N., & Murphy, S. P. (2012). Stroke outcome in the ketogenic state--a systematic review of the animal data. *J Neurochem, 123 Suppl 2*, 52-57. doi:10.1111/j.1471-4159.2012.07943.x

Gibson, G. E., Xu, H., Chen, H. L., Chen, W., Denton, T. T., & Zhang, S. (2015). Alpha-ketoglutarate dehydrogenase complex-dependent succinylation of proteins in neurons and neuronal cell lines. *J Neurochem, 134*(1), 86-96. doi:10.1111/jnc.13096

Gu, Z., Jiang, Q., Fu, A. K., Ip, N. Y., & Yan, Z. (2005). Regulation of NMDA receptors by neuregulin signaling in prefrontal cortex. *J Neurosci, 25*(20), 4974-4984. doi:10.1523/jneurosci.1086-05.2005

Guelpa, G. M., A. (1911). La lutte contre l'e'pilepsie par la de' sintoxication et par la re'e'ducation alimentaire. *Rev Ther Medico-Chirurgicale, 78*, 8–13.

Guerreiro, R., & Bras, J. (2015). The age factor in Alzheimer's disease. *Genome medicine, 7*, 106-106. doi:10.1186/s13073-015-0232-5

Guzman, M., & Blazquez, C. (2001). Is there an astrocyte-neuron ketone body shuttle? *Trends Endocrinol Metab, 12*(4), 169-173.

Han, Y.-m., Bedarida, T., Ding, Y., Somba, B. K., Lu, Q., Wang, Q., . . . Zou, M.-H. (2018). β-Hydroxybutyrate Prevents Vascular Senescence through hnRNP A1-Mediated Upregulation of Oct4. *Molecular Cell, 71*(6), 1064-1078.e1065. doi:https://doi.org/10.1016/j.molcel.2018.07.036

Hansford, R. G., Hogue, B. A., & Mildaziene, V. (1997). Dependence of H2O2 formation by rat heart mitochondria on substrate availability and donor age. *J Bioenerg Biomembr, 29*(1), 89-95.

Hansson Petersen, C. A., Alikhani, N., Behbahani, H., Wiehager, B., Pavlov, P. F., Alafuzoff, I., . . . Ankarcrona, M. (2008). The amyloid beta-peptide is imported into mitochondria via the TOM import machinery and localized to mitochondrial cristae. *Proc Natl Acad Sci U S A, 105*(35), 13145-13150. doi:10.1073/pnas.0806192105

Hasebe, N., Fujita, Y., Ueno, M., Yoshimura, K., Fujino, Y., & Yamashita, T. (2013). Soluble beta-amyloid Precursor Protein Alpha binds to p75 neurotrophin receptor to promote neurite outgrowth. *PLoS One, 8*(12), e82321. doi:10.1371/journal.pone.0082321

Hegardt, F. G. (1999). Mitochondrial 3-hydroxy-3-methylglutaryl-CoA synthase: a control enzyme in ketogenesis. *Biochem J, 338 (Pt 3)*, 569-582.

Henderson, S. T. (2008). Ketone bodies as a therapeutic for Alzheimer's disease. *Neurotherapeutics, 5*(3), 470-480. doi:10.1016/j.nurt.2008.05.004

Hennebelle, M., Courchesne-Loyer, A., St-Pierre, V., Vandenberghe, C., Castellano, C. A., Fortier, M., . . . Cunnane, S. C. (2016). Preliminary evaluation of a differential effect of an alpha-linolenate-rich supplement on ketogenesis and plasma omega-3 fatty acids in young and older adults. *Nutrition, 32*(11-12), 1211-1216. doi:10.1016/j.nut.2016.03.025

Henry, M. K., Lynch, J. T., Eapen, A. K., & Quelle, F. W. (2001). DNA damage-induced cell-cycle arrest of hematopoietic cells is overridden by activation of the PI-3 kinase/Akt signaling pathway. *Blood, 98*(3), 834-841.

Hester, S. D., Bhat, V., Chorley, B. N., Carswell, G., Jones, W., Wehmas, L. C., & Wood, C. E. (2016). Editor's Highlight: Dose-Response Analysis of RNA-Seq Profiles in Archival Formalin-Fixed Paraffin-Embedded Samples. *Toxicol Sci, 154*(2), 202-213. doi:10.1093/toxsci/kfw161

Hilditch, T. P. (1944). The component acids of milk fats of the goat, ewe and mare. *Biochem J, 38*(5), 443-447.

Hirtz, D., Thurman, D. J., Gwinn-Hardy, K., Mohamed, M., Chaudhuri, A. R., & Zalutsky, R. (2007). How common are the "common" neurologic disorders? *Neurology, 68*(5), 326-337. doi:10.1212/01.wnl.0000252807.38124.a3

Ho, J. W., Ho, P. W., Liu, H. F., So, D. H., Chan, K. H., Tse, Z. H., . . . Ho, S. L. (2012). UCP4 is a target effector of the NF-kappaB c-Rel prosurvival pathway against oxidative stress. *Free Radic Biol Med, 53*(2), 383-394. doi:10.1016/j.freeradbiomed.2012.05.002

Ho, P. W., Chu, A. C., Kwok, K. H., Kung, M. H., Ramsden, D. B., & Ho, S. L. (2006). Knockdown of uncoupling protein-5 in neuronal SH-SY5Y cells: Effects on MPP+-induced mitochondrial membrane depolarization, ATP deficiency, and oxidative cytotoxicity. *J Neurosci Res, 84*(6), 1358-1366. doi:10.1002/jnr.21034

Ho, P. W., Ho, J. W., Tse, H. M., So, D. H., Yiu, D. C., Liu, H. F., . . . Ho, S. L. (2012). Uncoupling protein-4 (UCP4) increases ATP supply by interacting with mitochondrial Complex II in neuroblastoma cells. *PLoS One, 7*(2), e32810. doi:10.1371/journal.pone.0032810

Holtzman, D., & Ulrich, J. (2019). Senescent glia spell trouble in Alzheimer's disease. *Nature Neuroscience, 22*(5), 683-684. doi:10.1038/s41593-019-0395-2

Hugo, S. E., Cruz-Garcia, L., Karanth, S., Anderson, R. M., Stainier, D. Y. R., & Schlegel, A. (2012). A monocarboxylate transporter required for hepatocyte secretion of ketone bodies during fasting. *Genes & Development, 26*(3), 282-293. doi:10.1101/gad.180968.111

Illumina. (2015). Technical Note: Expression Analysis of FFPE Samples.

Insull, W., Jr., & Ahrens, E. H., Jr. (1959). The fatty acids of human milk from mothers on diets taken ad libitum. *Biochem J, 72*(1), 27-33.

Ishii, K., Sasaki, M., Kitagaki, H., Yamaji, S., Sakamoto, S., Matsuda, K., & Mori, E. (1997). Reduction of cerebellar glucose metabolism in advanced Alzheimer's disease. *J Nucl Med, 38*(6), 925-928.

Jack, C. R., Jr., Knopman, D. S., Jagust, W. J., Petersen, R. C., Weiner, M. W., Aisen, P. S., . . . Trojanowski, J. Q. (2013). Tracking pathophysiological processes in Alzheimer's disease: an updated hypothetical model of dynamic biomarkers. *Lancet Neurol, 12*(2), 207-216. doi:10.1016/s1474-4422(12)70291-0

Jang, H. J., Yang, Y. R., Kim, J. K., Choi, J. H., Seo, Y. K., Lee, Y. H., . . . Suh, P. G. (2013). Phospholipase C-gamma1 involved in brain disorders. *Adv Biol Regul, 53*(1), 51-62. doi:10.1016/j.jbior.2012.09.008

Jarrett, S. G., Milder, J. B., Liang, L. P., & Patel, M. (2008). The ketogenic diet increases mitochondrial glutathione levels. *J Neurochem, 106*(3), 1044-1051. doi:10.1111/j.1471-4159.2008.05460.x

Ji, A. L., Zhang, X., Chen, W. W., & Huang, W. J. (2017). Genetics insight into the amyotrophic lateral sclerosis/frontotemporal dementia spectrum. *J Med Genet*. doi:10.1136/jmedgenet-2016-104271

Johnson, S., & Imai, S.-I. (2018). NAD (+) biosynthesis, aging, and disease. *F1000Res, 7*, 132-132. doi:10.12688/f1000research.12120.1

Juge, N., Gray, J. A., Omote, H., Miyaji, T., Inoue, T., Hara, C., . . . Moriyama, Y. (2010). Metabolic control of vesicular glutamate transport and release. *Neuron, 68*(1), 99-112. doi:10.1016/j.neuron.2010.09.002

Julien, C., Tremblay, C., Emond, V., Lebbadi, M., Salem, N., Jr., Bennett, D. A., & Calon, F. (2009). Sirtuin 1 reduction parallels the accumulation of tau in Alzheimer disease. *J Neuropathol Exp Neurol, 68*(1), 48-58. doi:10.1097/NEN.0b013e3181922348

Kalapos, M. P. (2003). On the mammalian acetone metabolism: from chemistry to clinical implications. *Biochimica et Biophysica Acta (BBA) - General Subjects, 1621*(2), 122-139. doi:http://dx.doi.org/10.1016/S0304-4165(03)00051-5

Kalia, L. V., & Lang, A. E. (2015). Parkinson's disease. *The Lancet, 386*(9996), 896-912. doi:10.1016/S0140-6736(14)61393-3

Kandel, E. R. (2001). The molecular biology of memory storage: a dialogue between genes and synapses. *Science, 294*(5544), 1030-1038. doi:10.1126/science.1067020

Kanehisa, M., Araki, M., Goto, S., Hattori, M., Hirakawa, M., Itoh, M., . . . Yamanishi, Y. (2008). KEGG for linking genomes to life and the environment. *Nucleic acids research, 36*(Database issue), D480-D484. doi:10.1093/nar/gkm882

Kanehisa, M., & Goto, S. (2000). KEGG: kyoto encyclopedia of genes and genomes. *Nucleic acids research, 28*(1), 27-30. doi:10.1093/nar/28.1.27

Kang, J. Q., Chong, Z. Z., & Maiese, K. (2003). Akt1 protects against inflammatory microglial activation through maintenance of membrane asymmetry and modulation of cysteine protease activity. *J Neurosci Res, 74*(1), 37-51. doi:10.1002/jnr.10740

Kashiwaya, Y., Pawlosky, R., Markis, W., King, M. T., Bergman, C., Srivastava, S., . . . Veech, R. L. (2010). A ketone ester diet increases brain malonyl-CoA and Uncoupling proteins 4 and 5 while decreasing food intake in the normal Wistar Rat. *J Biol Chem, 285*(34), 25950-25956. doi:10.1074/jbc.M110.138198

Keith, H. (1935). Experimental convulsions induced by administration of thujone. *Archives Neurological Psychiatry, 34*, 1022-1040.

Kim, D. Y., Hao, J., Liu, R., Turner, G., Shi, F. D., & Rho, J. M. (2012). Inflammation-mediated memory dysfunction and effects of a ketogenic diet in a murine model of multiple sclerosis. *PLoS One, 7*(5), e35476. doi:10.1371/journal.pone.0035476

Kimura, I., Inoue, D., Maeda, T., Hara, T., Ichimura, A., Miyauchi, S., . . . Tsujimoto, G. (2011). Short-chain fatty acids and ketones directly regulate sympathetic nervous system via G protein-coupled receptor 41 (GPR41). *Proc Natl Acad Sci U S A, 108*(19), 8030-8035. doi:10.1073/pnas.1016088108

Kinzig, K. P., Honors, M. A., & Hargrave, S. L. (2010). Insulin sensitivity and glucose tolerance are altered by maintenance on a ketogenic diet. *Endocrinology, 151*(7), 3105-3114. doi:10.1210/en.2010-0175

Klosinski, L. P., Yao, J., Yin, F., Fonteh, A. N., Harrington, M. G., Christensen, T. A., . . . Brinton, R. D. (2015). White Matter Lipids as a Ketogenic Fuel Supply in Aging Female Brain: Implications for Alzheimer's Disease. *EBioMedicine, 2*(12), 1888-1904. doi:10.1016/j.ebiom.2015.11.002

Kobau, R., Zahran, H., Thurman, D. J., Zack, M. M., Henry, T. R., Schachter, S. C., & Price, P. H. (2008). Epilepsy surveillance among adults--19 States, Behavioral Risk Factor Surveillance System, 2005. *MMWR Surveill Summ, 57*(6), 1-20.

Kogan, J. H., Frankland, P. W., Blendy, J. A., Coblentz, J., Marowitz, Z., Schutz, G., & Silva, A. J. (1997). Spaced training induces normal long-term memory in CREB mutant mice. *Curr Biol, 7*(1), 1-11.

Koppel, I., & Timmusk, T. (2013). Differential regulation of Bdnf expression in cortical neurons by class-selective histone deacetylase inhibitors. *Neuropharmacology, 75*, 106-115. doi:10.1016/j.neuropharm.2013.07.015

Koppel, S. J., & Swerdlow, R. H. (2018). Neuroketotherapeutics: A modern review of a century-old therapy. *Neurochem Int, 117*, 114-125. doi:10.1016/j.neuint.2017.05.019

Kuczynski, B., Targan, E., Madison, C., Weiner, M., Zhang, Y., Reed, B., . . . Jagust, W. (2010). White matter integrity and cortical metabolic associations in aging and dementia. *Alzheimers Dement, 6*(1), 54-62. doi:10.1016/j.jalz.2009.04.1228

Kwok, K. H., Ho, P. W., Chu, A. C., Ho, J. W., Liu, H. F., Yiu, D. C., . . . Ho, S. L. (2010). Mitochondrial UCP5 is neuroprotective by preserving mitochondrial membrane potential,

ATP levels, and reducing oxidative stress in MPP+ and dopamine toxicity. *Free Radic Biol Med, 49*(6), 1023-1035. doi:10.1016/j.freeradbiomed.2010.06.017

LaManna, J. C., Salem, N., Puchowicz, M., Erokwu, B., Koppaka, S., Flask, C., & Lee, Z. (2009). KETONES SUPPRESS BRAIN GLUCOSE CONSUMPTION. *Adv Exp Med Biol, 645*, 301-306. doi:10.1007/978-0-387-85998-9_45

Lau, D., Bengtson, C. P., Buchthal, B., & Bading, H. (2015). BDNF Reduces Toxic Extrasynaptic NMDA Receptor Signaling via Synaptic NMDA Receptors and Nuclear-Calcium-Induced Transcription of inhba/Activin A. *Cell Reports, 12*(8), 1353-1366. doi:https://doi.org/10.1016/j.celrep.2015.07.038

Le Foll, C., Dunn-Meynell, A. A., & Levin, B. E. (2015). Role of FAT/CD36 in fatty acid sensing, energy, and glucose homeostasis regulation in DIO and DR rats. *Am J Physiol Regul Integr Comp Physiol, 308*(3), R188-198. doi:10.1152/ajpregu.00367.2014

Le Foll, C., Dunn-Meynell, A. A., Miziorko, H. M., & Levin, B. E. (2014). Regulation of hypothalamic neuronal sensing and food intake by ketone bodies and fatty acids. *Diabetes, 63*(4), 1259-1269. doi:10.2337/db13-1090

Le Foll, C., Dunn-Meynell, A. A., Miziorko, H. M., & Levin, B. E. (2015). Role of VMH ketone bodies in adjusting caloric intake to increased dietary fat content in DIO and DR rats. *Am J Physiol Regul Integr Comp Physiol, 308*(10), R872-878. doi:10.1152/ajpregu.00015.2015

Le Foll, C., & Levin, B. E. (2016). Fatty acid-induced astrocyte ketone production and the control of food intake. *Am J Physiol Regul Integr Comp Physiol, 310*(11), R1186-1192. doi:10.1152/ajpregu.00113.2016

Lee, J., & Wolfgang, M. J. (2012). Metabolomic profiling reveals a role for CPT1c in neuronal oxidative metabolism. *BMC Biochem, 13*, 23. doi:10.1186/1471-2091-13-23

Lehninger, A. L., Sudduth, H. C., & Wise, J. B. (1960). D-beta-Hydroxybutyric dehydrogenase of muitochondria. *J Biol Chem, 235*, 2450-2455.

Lezi, E., & Swerdlow, R. H. (2012). Mitochondria in neurodegeneration. *Adv Exp Med Biol, 942*, 269-286. doi:10.1007/978-94-007-2869-1_12

Lim, S., Chesser, A. S., Grima, J. C., Rappold, P. M., Blum, D., Przedborski, S., & Tieu, K. (2011). D-beta-hydroxybutyrate is protective in mouse models of Huntington's disease. *PLoS One, 6*(9), e24620. doi:10.1371/journal.pone.0024620

Lindblad, B. S., Settergren, G., Feychting, H., & Persson, B. (1977). Total parenteral nutrition in infants. Blood levels of glucose, lactate, pyruvate, free fatty acids, glycerol, d-beta-hydroxybutyrate, triglycerides, free amino acids and insulin. *Acta Paediatr Scand, 66*(4), 409-419.

Liu, D., Chan, S. L., de Souza-Pinto, N. C., Slevin, J. R., Wersto, R. P., Zhan, M., . . . Mattson, M. P. (2006). Mitochondrial UCP4 mediates an adaptive shift in energy metabolism and increases the resistance of neurons to metabolic and oxidative stress. *Neuromolecular Med, 8*(3), 389-414. doi:10.1385/nmm:8:3:389

Liu, L., MacKenzie, K. R., Putluri, N., Maletic-Savatic, M., & Bellen, H. J. (2017). The Glia-Neuron Lactate Shuttle and Elevated ROS Promote Lipid Synthesis in Neurons and Lipid Droplet Accumulation in Glia via APOE/D. *Cell Metab, 26*(5), 719-737.e716. doi:10.1016/j.cmet.2017.08.024

Lopez-Vinas, E., Bentebibel, A., Gurunathan, C., Morillas, M., de Arriaga, D., Serra, D., . . . Gomez-Puertas, P. (2007). Definition by functional and structural analysis of two

malonyl-CoA sites in carnitine palmitoyltransferase 1A. *J Biol Chem, 282*(25), 18212-18224. doi:10.1074/jbc.M700885200
Lutz, M. I., Milenkovic, I., Regelsberger, G., & Kovacs, G. G. (2014). Distinct patterns of sirtuin expression during progression of Alzheimer's disease. *Neuromolecular Med, 16*(2), 405-414. doi:10.1007/s12017-014-8288-8
Manning, B. D., & Cantley, L. C. (2007). AKT/PKB signaling: navigating downstream. *Cell, 129*(7), 1261-1274. doi:10.1016/j.cell.2007.06.009
Mantamadiotis, T., Lemberger, T., Bleckmann, S. C., Kern, H., Kretz, O., Martin Villalba, A., . . . Schutz, G. (2002). Disruption of CREB function in brain leads to neurodegeneration. *Nat Genet, 31*(1), 47-54. doi:10.1038/ng882
Marosi, K., Kim, S. W., Moehl, K., Scheibye-Knudsen, M., Cheng, A., Cutler, R., . . . Mattson, M. P. (2016). 3-Hydroxybutyrate regulates energy metabolism and induces BDNF expression in cerebral cortical neurons. *J Neurochem, 139*(5), 769-781. doi:10.1111/jnc.13868
Masaldan, S., Belaidi, A. A., Ayton, S., & Bush, A. I. (2019). Cellular Senescence and Iron Dyshomeostasis in Alzheimer's Disease. *Pharmaceuticals (Basel), 12*(2), 93. doi:10.3390/ph12020093
Matsuzaki, H., Tamatani, M., Mitsuda, N., Namikawa, K., Kiyama, H., Miyake, S., & Tohyama, M. (1999). Activation of Akt kinase inhibits apoptosis and changes in Bcl-2 and Bax expression induced by nitric oxide in primary hippocampal neurons. *J Neurochem, 73*(5), 2037-2046.
McNally, M. A., & Hartman, A. L. (2012). Ketone bodies in epilepsy. *J Neurochem, 121*(1), 28-35. doi:10.1111/j.1471-4159.2012.07670.x
Melo, T. M., Nehlig, A., & Sonnewald, U. (2006). Neuronal-glial interactions in rats fed a ketogenic diet. *Neurochem Int, 48*(6-7), 498-507. doi:10.1016/j.neuint.2005.12.037
Menta, B. W., & Swerdlow, R. H. (2019). An Integrative Overview of Non-Amyloid and Non-Tau Pathologies in Alzheimer's Disease. *Neurochem Res, 44*(1), 12-21. doi:10.1007/s11064-018-2603-y
Middleton, B. (1972). The existence of ketoacyl-CoA thiolases of differing properties and intracellular localization in ox liver. *Biochem Biophys Res Commun, 46*(2), 508-515.
Milder, J. B., Liang, L. P., & Patel, M. (2010). Acute oxidative stress and systemic Nrf2 activation by the ketogenic diet. *Neurobiol Dis, 40*(1), 238-244. doi:10.1016/j.nbd.2010.05.030
Minichiello, L., Calella, A. M., Medina, D. L., Bonhoeffer, T., Klein, R., & Korte, M. (2002). Mechanism of TrkB-mediated hippocampal long-term potentiation. *Neuron, 36*(1), 121-137.
Minlebaev, M., & Khazipov, R. (2011). Antiepileptic effects of endogenous beta-hydroxybutyrate in suckling infant rats. *Epilepsy Res, 95*(1-2), 100-109. doi:10.1016/j.eplepsyres.2011.03.003
Monsenego, J., Mansouri, A., Akkaoui, M., Lenoir, V., Esnous, C., Fauveau, V., . . . Prip-Buus, C. (2012). Enhancing liver mitochondrial fatty acid oxidation capacity in obese mice improves insulin sensitivity independently of hepatic steatosis. *J Hepatol, 56*(3), 632-639. doi:10.1016/j.jhep.2011.10.008
Morris, A. A. (2005). Cerebral ketone body metabolism. *J Inherit Metab Dis, 28*(2), 109-121. doi:10.1007/s10545-005-5518-0

Mosconi, L., de Leon, M., Murray, J., E, L., Lu, J., Javier, E., . . . Swerdlow, R. H. (2011). Reduced mitochondria cytochrome oxidase activity in adult children of mothers with Alzheimer's disease. *J Alzheimers Dis, 27*(3), 483-490. doi:10.3233/jad-2011-110866

Mosconi, L., De Santi, S., Brys, M., Tsui, W. H., Pirraglia, E., Glodzik-Sobanska, L., . . . de Leon, M. J. (2008). Hypometabolism and altered cerebrospinal fluid markers in normal apolipoprotein E E4 carriers with subjective memory complaints. *Biol Psychiatry, 63*(6), 609-618. doi:10.1016/j.biopsych.2007.05.030

Mosconi, L., De Santi, S., Li, J., Tsui, W. H., Li, Y., Boppana, M., . . . de Leon, M. J. (2008). Hippocampal hypometabolism predicts cognitive decline from normal aging. *Neurobiol Aging, 29*(5), 676-692. doi:10.1016/j.neurobiolaging.2006.12.008

Mosconi, L., Mistur, R., Switalski, R., Brys, M., Glodzik, L., Rich, K., . . . de Leon, M. J. (2009). Declining brain glucose metabolism in normal individuals with a maternal history of Alzheimer disease. *Neurology, 72*(6), 513-520. doi:10.1212/01.wnl.0000333247.51383.43

Mosconi, L., Tsui, W. H., Herholz, K., Pupi, A., Drzezga, A., Lucignani, G., . . . de Leon, M. J. (2008). Multicenter standardized 18F-FDG PET diagnosis of mild cognitive impairment, Alzheimer's disease, and other dementias. *J Nucl Med, 49*(3), 390-398. doi:10.2967/jnumed.107.045385

Musi, N., Valentine, J. M., Sickora, K. R., Baeuerle, E., Thompson, C. S., Shen, Q., & Orr, M. E. (2018). Tau protein aggregation is associated with cellular senescence in the brain. *Aging Cell, 17*(6), e12840. doi:10.1111/acel.12840

Neal, E. G., Chaffe, H., Schwartz, R. H., Lawson, M. S., Edwards, N., Fitzsimmons, G., . . . Cross, J. H. (2008). The ketogenic diet for the treatment of childhood epilepsy: a randomised controlled trial. *Lancet Neurol, 7*(6), 500-506. doi:10.1016/s1474-4422(08)70092-9

Nehlig, A. (1999). Age-dependent pathways of brain energy metabolism: the suckling rat, a natural model of the ketogenic diet. *Epilepsy Res, 37*(3), 211-221.

Nehlig, A., & Pereira de Vasconcelos, A. (1993). Glucose and ketone body utilization by the brain of neonatal rats. *Prog Neurobiol, 40*(2), 163-221.

Newman, J. C., Covarrubias, A. J., Zhao, M., Yu, X., Gut, P., Ng, C.-P., . . . Verdin, E. (2017). Ketogenic Diet Reduces Midlife Mortality and Improves Memory in Aging Mice. *Cell metabolism, 26*(3), 547-557.e548. doi:10.1016/j.cmet.2017.08.004

Newman, J. C., & Verdin, E. (2014a). Ketone bodies as signaling metabolites. *Trends in endocrinology and metabolism: TEM, 25*(1), 42-52. doi:10.1016/j.tem.2013.09.002

Newman, J. C., & Verdin, E. (2014b). β-hydroxybutyrate: Much more than a metabolite. *Diabetes research and clinical practice, 106*(2), 173-181. doi:10.1016/j.diabres.2014.08.009

Newport, M. T., VanItallie, T. B., Kashiwaya, Y., King, M. T., & Veech, R. L. (2015). A new way to produce hyperketonemia: use of ketone ester in a case of Alzheimer's disease. *Alzheimers Dement, 11*(1), 99-103. doi:10.1016/j.jalz.2014.01.006

Ng, F., Wijaya, L., & Tang, B. L. (2015). SIRT1 in the brain-connections with aging-associated disorders and lifespan. *Front Cell Neurosci, 9*, 64. doi:10.3389/fncel.2015.00064

Noseworthy, J. H., Lucchinetti, C., Rodriguez, M., & Weinshenker, B. G. (2000). Multiple sclerosis. *N Engl J Med, 343*(13), 938-952. doi:10.1056/nejm200009283431307

O'Dwyer, L., Lamberton, F., Bokde, A. L., Ewers, M., Faluyi, Y. O., Tanner, C., . . . Hampel, H. (2011). Multiple indices of diffusion identifies white matter damage in mild cognitive

impairment and Alzheimer's disease. *PLoS One, 6*(6), e21745. doi:10.1371/journal.pone.0021745
Offermanns, S., & Schwaninger, M. (2015). Nutritional or pharmacological activation of HCA(2) ameliorates neuroinflammation. *Trends Mol Med, 21*(4), 245-255. doi:10.1016/j.molmed.2015.02.002
Orhan, N., Ugur Yilmaz, C., Ekizoglu, O., Ahishali, B., Kucuk, M., Arican, N., . . . Kaya, M. (2016). Effects of beta-hydroxybutyrate on brain vascular permeability in rats with traumatic brain injury. *Brain Res, 1631*, 113-126. doi:10.1016/j.brainres.2015.11.038
Ovbiagele, B., & Nguyen-Huynh, M. N. (2011). Stroke Epidemiology: Advancing Our Understanding of Disease Mechanism and Therapy. *Neurotherapeutics, 8*(3), 319-329. doi:10.1007/s13311-011-0053-1
Owada, Y., Utsunomiya, A., Yoshimoto, T., & Kondo, H. (1997). Expression of mRNA for Akt, serine-threonine protein kinase, in the brain during development and its transient enhancement following axotomy of hypoglossal nerve. *J Mol Neurosci, 9*(1), 27-33. doi:10.1007/bf02789392
Owen, O. E., Kalhan, S. C., & Hanson, R. W. (2002). The key role of anaplerosis and cataplerosis for citric acid cycle function. *J Biol Chem, 277*(34), 30409-30412. doi:10.1074/jbc.R200006200
Palomo-Guerrero, M., Fado, R., Casas, M., Perez-Montero, M., Baena, M., Helmer, P. O., . . . Casals, N. (2019). Sensing of nutrients by CPT1C regulates late endosome/lysosome anterograde transport and axon growth. *Elife, 8*. doi:10.7554/eLife.51063
Prins, M. L., Fujima, L. S., & Hovda, D. A. (2005). Age-dependent reduction of cortical contusion volume by ketones after traumatic brain injury. *J Neurosci Res, 82*(3), 413-420. doi:10.1002/jnr.20633
Prins, M. L., Lee, S. M., Fujima, L. S., & Hovda, D. A. (2004). Increased cerebral uptake and oxidation of exogenous betaHB improves ATP following traumatic brain injury in adult rats. *J Neurochem, 90*(3), 666-672. doi:10.1111/j.1471-4159.2004.02542.x
Prins, M. L., & Matsumoto, J. H. (2014). The collective therapeutic potential of cerebral ketone metabolism in traumatic brain injury. *J Lipid Res, 55*(12), 2450-2457. doi:10.1194/jlr.R046706
Puchowicz, M. A., Zechel, J., Valerio, J., Emancipator, D., Xu, K., Pundik, S., . . . Lust, W. D. (2008). Neuroprotection in Diet Induced Ketotic Rat Brain Following Focal Ischemia. *Journal of cerebral blood flow and metabolism : official journal of the International Society of Cerebral Blood Flow and Metabolism, 28*(12), 1907-1916. doi:10.1038/jcbfm.2008.79
Puisac, B., Ramos, M., Arnedo, M., Menao, S., Gil-Rodriguez, M. C., Teresa-Rodrigo, M. E., . . . Pie, J. (2012). Characterization of splice variants of the genes encoding human mitochondrial HMG-CoA lyase and HMG-CoA synthase, the main enzymes of the ketogenesis pathway. *Mol Biol Rep, 39*(4), 4777-4785. doi:10.1007/s11033-011-1270-8
Rahman, M., Muhammad, S., Khan, M. A., Chen, H., Ridder, D. A., Muller-Fielitz, H., . . . Schwaninger, M. (2014). The beta-hydroxybutyrate receptor HCA2 activates a neuroprotective subset of macrophages. *Nat Commun, 5*, 3944. doi:10.1038/ncomms4944
Ramagopalan, S. V., & Sadovnick, A. D. (2011). Epidemiology of multiple sclerosis. *Neurol Clin, 29*(2), 207-217. doi:10.1016/j.ncl.2010.12.010
Ramsden, D. B., Ho, P. W., Ho, J. W., Liu, H. F., So, D. H., Tse, H. M., . . . Ho, S. L. (2012). Human neuronal uncoupling proteins 4 and 5 (UCP4 and UCP5): structural properties,

regulation, and physiological role in protection against oxidative stress and mitochondrial dysfunction. *Brain Behav, 2*(4), 468-478. doi:10.1002/brb3.55
Randle, P. J., Garland, P. B., Hales, C. N., & Newsholme, E. A. (1963). The glucose fatty-acid cycle. Its role in insulin sensitivity and the metabolic disturbances of diabetes mellitus. *Lancet, 1*(7285), 785-789.
Rardin, M. J., Newman, J. C., Held, J. M., Cusack, M. P., Sorensen, D. J., Li, B., . . . Gibson, B. W. (2013). Label-free quantitative proteomics of the lysine acetylome in mitochondria identifies substrates of SIRT3 in metabolic pathways. *Proc Natl Acad Sci U S A, 110*(16), 6601-6606. doi:10.1073/pnas.1302961110
Reger, M. A., Henderson, S. T., Hale, C., Cholerton, B., Baker, L. D., Watson, G. S., . . . Craft, S. (2004). Effects of beta-hydroxybutyrate on cognition in memory-impaired adults. *Neurobiol Aging, 25*(3), 311-314. doi:10.1016/s0197-4580(03)00087-3
Reiman, E. M., Chen, K., Alexander, G. E., Caselli, R. J., Bandy, D., Osborne, D., . . . Hardy, J. (2004). Functional brain abnormalities in young adults at genetic risk for late-onset Alzheimer's dementia. *Proc Natl Acad Sci U S A, 101*(1), 284-289. doi:10.1073/pnas.2635903100
Rodriguez-Perdigon, M., Solas, M., Moreno-Aliaga, M. J., & Ramirez, M. J. (2016). Lipoic acid improves neuronal insulin signalling and rescues cognitive function regulating VGlut1 expression in high-fat-fed rats: Implications for Alzheimer's disease. *Biochim Biophys Acta, 1862*(4), 511-517. doi:10.1016/j.bbadis.2016.01.004
Rodriguez, M. E., Azizuddin, K., Zhang, P., Chiu, S.-m., Lam, M., Kenney, M. E., . . . Oleinick, N. L. (2008). Targeting of mitochondria by 10-N-alkyl acridine orange analogues: role of alkyl chain length in determining cellular uptake and localization. *Mitochondrion, 8*(3), 237-246. doi:10.1016/j.mito.2008.04.003
Rosenbloom, M. H., Alkalay, A., Agarwal, N., Baker, S. L., O'Neil, J. P., Janabi, M., . . . Rabinovici, G. D. (2011). Distinct clinical and metabolic deficits in PCA and AD are not related to amyloid distribution. *Neurology, 76*(21), 1789-1796. doi:10.1212/WNL.0b013e31821cccad
Ross, C. A., & Tabrizi, S. J. (2011). Huntington's disease: from molecular pathogenesis to clinical treatment. *Lancet Neurol, 10*(1), 83-98. doi:10.1016/s1474-4422(10)70245-3
Rui, L. (2014). Energy metabolism in the liver. *Compr Physiol, 4*(1), 177-197. doi:10.1002/cphy.c130024
Samala, R., Klein, J., & Borges, K. (2011). The ketogenic diet changes metabolite levels in hippocampal extracellular fluid. *Neurochem Int, 58*(1), 5-8. doi:10.1016/j.neuint.2010.10.011
Selfridge, J. E., E, L., Lu, J., & Swerdlow, R. H. (2013). Role of mitochondrial homeostasis and dynamics in Alzheimer's disease. *Neurobiol Dis, 51*, 3-12. doi:10.1016/j.nbd.2011.12.057
Selfridge, J. E., Wilkins, H. M., E, L., Carl, S. M., Koppel, S., Funk, E., . . . Swerdlow, R. H. (2015). Effect of one month duration ketogenic and non-ketogenic high fat diets on mouse brain bioenergetic infrastructure. *J Bioenerg Biomembr, 47*(1-2), 1-11. doi:10.1007/s10863-014-9570-z
Shimazu, T., Hirschey, M. D., Newman, J., He, W., Shirakawa, K., Le Moan, N., . . . Verdin, E. (2013). Suppression of oxidative stress by beta-hydroxybutyrate, an endogenous histone deacetylase inhibitor. *Science, 339*(6116), 211-214. doi:10.1126/science.1227166
Sierra, A. Y., Gratacos, E., Carrasco, P., Clotet, J., Urena, J., Serra, D., . . . Casals, N. (2008). CPT1c is localized in endoplasmic reticulum of neurons and has carnitine

palmitoyltransferase activity. *J Biol Chem, 283*(11), 6878-6885. doi:10.1074/jbc.M707965200
Silva, A. J., Kogan, J. H., Frankland, P. W., & Kida, S. (1998). CREB and memory. *Annu Rev Neurosci, 21*, 127-148. doi:10.1146/annurev.neuro.21.1.127
Silva, D. F., Selfridge, J. E., Lu, J., E, L., Cardoso, S. M., & Swerdlow, R. H. (2012). Mitochondrial abnormalities in Alzheimer's disease: possible targets for therapeutic intervention. *Adv Pharmacol, 64*, 83-126. doi:10.1016/b978-0-12-394816-8.00003-9
Silva, D. F., Selfridge, J. E., Lu, J., E, L., Roy, N., Hutfles, L., . . . Swerdlow, R. H. (2013). Bioenergetic flux, mitochondrial mass and mitochondrial morphology dynamics in AD and MCI cybrid cell lines. *Hum Mol Genet, 22*(19), 3931-3946. doi:10.1093/hmg/ddt247
Simeone, T. A., Matthews, S. A., Samson, K. K., & Simeone, K. A. (2017). Regulation of brain PPARgamma2 contributes to ketogenic diet anti-seizure efficacy. *Exp Neurol, 287*(Pt 1), 54-64. doi:10.1016/j.expneurol.2016.08.006
Sleiman, S. F., Henry, J., Al-Haddad, R., El Hayek, L., Abou Haidar, E., Stringer, T., . . . Chao, M. V. (2016). Exercise promotes the expression of brain derived neurotrophic factor (BDNF) through the action of the ketone body beta-hydroxybutyrate. *Elife, 5*. doi:10.7554/eLife.15092
Smith, C. J., Berry, D. M., & McGlade, C. J. (2013). The E3 ubiquitin ligases RNF126 and Rabring7 regulate endosomal sorting of the epidermal growth factor receptor. *J Cell Sci, 126*(6), 1366. doi:10.1242/jcs.116129
Spulber, G., Niskanen, E., MacDonald, S., Smilovici, O., Chen, K., Reiman, E. M., . . . Soininen, H. (2010). Whole brain atrophy rate predicts progression from MCI to Alzheimer's disease. *Neurobiol Aging, 31*(9), 1601-1605. doi:10.1016/j.neurobiolaging.2008.08.018
Srivastava, S., Kashiwaya, Y., King, M. T., Baxa, U., Tam, J., Niu, G., . . . Veech, R. L. (2012). Mitochondrial biogenesis and increased uncoupling protein 1 in brown adipose tissue of mice fed a ketone ester diet. *Faseb j, 26*(6), 2351-2362. doi:10.1096/fj.11-200410
Stilling, R. M., van de Wouw, M., Clarke, G., Stanton, C., Dinan, T. G., & Cryan, J. F. (2016). The neuropharmacology of butyrate: The bread and butter of the microbiota-gut-brain axis? *Neurochem Int, 99*, 110-132. doi:10.1016/j.neuint.2016.06.011
Stobart, J. L., & Anderson, C. M. (2013). Multifunctional role of astrocytes as gatekeepers of neuronal energy supply. *Front Cell Neurosci, 7*, 38. doi:10.3389/fncel.2013.00038
Suh, P. G., Park, J. I., Manzoli, L., Cocco, L., Peak, J. C., Katan, M., . . . Ryu, S. H. (2008). Multiple roles of phosphoinositide-specific phospholipase C isozymes. *BMB Rep, 41*(6), 415-434.
Sullivan, P. G., Rippy, N. A., Dorenbos, K., Concepcion, R. C., Agarwal, A. K., & Rho, J. M. (2004). The ketogenic diet increases mitochondrial uncoupling protein levels and activity. *Ann Neurol, 55*(4), 576-580. doi:10.1002/ana.20062
Suzuki, M., Suzuki, M., Kitamura, Y., Mori, S., Sato, K., Dohi, S., . . . Hiraide, A. (2002). Beta-hydroxybutyrate, a cerebral function improving agent, protects rat brain against ischemic damage caused by permanent and transient focal cerebral ischemia. *Jpn J Pharmacol, 89*(1), 36-43.
Suzuki, M., Suzuki, M., Sato, K., Dohi, S., Sato, T., Matsuura, A., & Hiraide, A. (2001). Effect of beta-hydroxybutyrate, a cerebral function improving agent, on cerebral hypoxia, anoxia and ischemia in mice and rats. *Jpn J Pharmacol, 87*(2), 143-150.
Swerdlow, R. H. (2011). Brain aging, Alzheimer's disease, and mitochondria. *Biochim Biophys Acta, 1812*(12), 1630-1639. doi:10.1016/j.bbadis.2011.08.012

Swerdlow, R. H. (2012a). Alzheimer's disease pathologic cascades: who comes first, what drives what. *Neurotox Res, 22*(3), 182-194. doi:10.1007/s12640-011-9272-9
Swerdlow, R. H. (2012b). beta-Apptists and Tauists, it is time for a sermon from the book of biogenesis. *J Neurochem, 120*(3), 347-349. doi:10.1111/j.1471-4159.2011.07561.x
Swerdlow, R. H. (2012c). Mitochondria and cell bioenergetics: increasingly recognized components and a possible etiologic cause of Alzheimer's disease. *Antioxid Redox Signal, 16*(12), 1434-1455. doi:10.1089/ars.2011.4149
Swerdlow, R. H. (2014a). Bioenergetic medicine. *Br J Pharmacol, 171*(8), 1854-1869. doi:10.1111/bph.12394
Swerdlow, R. H. (2014b). Comment: BDNF, fitness, and the brain. *Neurology, 83*(15), 1351. doi:10.1212/wnl.0000000000000869
Swerdlow, R. H. (2016). Bioenergetics and metabolism: a bench to bedside perspective. *J Neurochem, 139 Suppl 2*, 126-135. doi:10.1111/jnc.13509
Swerdlow, R. H. (2020). Mitochondria in Alzheimer brains: A PET project shows complex changes. *Neurology*. doi:10.1212/wnl.0000000000009236
Tanner, G. R., Lutas, A., Martinez-Francois, J. R., & Yellen, G. (2011). Single K ATP channel opening in response to action potential firing in mouse dentate granule neurons. *J Neurosci, 31*(23), 8689-8696. doi:10.1523/jneurosci.5951-10.2011
Taylor, M. K., Sullivan, D. K., Mahnken, J. D., Burns, J. M., & Swerdlow, R. H. (2017). Feasibility and efficacy data from a ketogenic diet intervention in Alzheimer's disease. *Alzheimer's & dementia (New York, N. Y.), 4*, 28-36. doi:10.1016/j.trci.2017.11.002
Taylor, M. K., Swerdlow, R. H., Burns, J. M., & Sullivan, D. K. (2019). An Experimental Ketogenic Diet for Alzheimer Disease Was Nutritionally Dense and Rich in Vegetables and Avocado. *Curr Dev Nutr, 3*(4), nzz003. doi:10.1093/cdn/nzz003
Taylor, M. K., Swerdlow, R. H., & Sullivan, D. K. (2019). Dietary Neuroketotherapeutics for Alzheimer's Disease: An Evidence Update and the Potential Role for Diet Quality. *Nutrients, 11*(8). doi:10.3390/nu11081910
Temkin, O. (1994). *The Falling Sickness: A History of Epilepsy from the Greeks to the Beginnings of Modern Neurology*: Johns Hopkins University Press.
Tieu, K., Perier, C., Caspersen, C., Teismann, P., Wu, D. C., Yan, S. D., . . . Przedborski, S. (2003). D-beta-hydroxybutyrate rescues mitochondrial respiration and mitigates features of Parkinson disease. *J Clin Invest, 112*(6), 892-901. doi:10.1172/jci18797
Vanitallie, T. B., Nonas, C., Di Rocco, A., Boyar, K., Hyams, K., & Heymsfield, S. B. (2005). Treatment of Parkinson disease with diet-induced hyperketonemia: a feasibility study. *Neurology, 64*(4), 728-730. doi:10.1212/01.wnl.0000152046.11390.45
Vavrova, E., Lenoir, V., Alves-Guerra, M. C., Denis, R. G., Castel, J., Esnous, C., . . . Prip-Buus, C. (2016). Muscle expression of a malonyl-CoA-insensitive carnitine palmitoyltransferase-1 protects mice against high-fat/high-sucrose diet-induced insulin resistance. *Am J Physiol Endocrinol Metab, 311*(3), E649-660. doi:10.1152/ajpendo.00020.2016
Vazquez-Vela, M. E., Torres, N., & Tovar, A. R. (2008). White adipose tissue as endocrine organ and its role in obesity. *Arch Med Res, 39*(8), 715-728. doi:10.1016/j.arcmed.2008.09.005
Vijay, N., & Morris, M. E. (2014). Role of Monocarboxylate Transporters in Drug Delivery to the Brain. *Curr Pharm Des, 20*(10), 1487-1498.

Villain, N., Fouquet, M., Baron, J. C., Mezenge, F., Landeau, B., de La Sayette, V., . . . Chetelat, G. (2010). Sequential relationships between grey matter and white matter atrophy and brain metabolic abnormalities in early Alzheimer's disease. *Brain, 133*(11), 3301-3314. doi:10.1093/brain/awq203

Virmani, A., Pinto, L., Bauermann, O., Zerelli, S., Diedenhofen, A., Binienda, Z. K., . . . van der Leij, F. R. (2015). The Carnitine Palmitoyl Transferase (CPT) System and Possible Relevance for Neuropsychiatric and Neurological Conditions. *Mol Neurobiol, 52*(2), 826-836. doi:10.1007/s12035-015-9238-7

Vlassenko, A. G., Vaishnavi, S. N., Couture, L., Sacco, D., Shannon, B. J., Mach, R. H., . . . Mintun, M. A. (2010). Spatial correlation between brain aerobic glycolysis and amyloid-beta (Abeta) deposition. *Proc Natl Acad Sci U S A, 107*(41), 17763-17767. doi:10.1073/pnas.1010461107

Votyakova, T. V., & Reynolds, I. J. (2001). DeltaPsi(m)-Dependent and -independent production of reactive oxygen species by rat brain mitochondria. *J Neurochem, 79*(2), 266-277.

Wang, W., Wang, L., Lu, J., Siedlak, S. L., Fujioka, H., Liang, J., . . . Wang, X. (2016). The inhibition of TDP-43 mitochondrial localization blocks its neuronal toxicity. *Nat Med, 22*(8), 869-878. doi:10.1038/nm.4130

Wang, Z. J., Bergqvist, C., Hunter, J. V., Jin, D., Wang, D. J., Wehrli, S., & Zimmerman, R. A. (2003). In vivo measurement of brain metabolites using two-dimensional double-quantum MR spectroscopy--exploration of GABA levels in a ketogenic diet. *Magn Reson Med, 49*(4), 615-619. doi:10.1002/mrm.10429

Watts, A., Wilkins, H. M., Michaelis, E., & Swerdlow, R. H. (2019). TOMM40 '523 Associations with Baseline and Longitudinal Cognition in APOE varepsilon3 Homozygotes. *J Alzheimers Dis, 70*(4), 1059-1068. doi:10.3233/jad-190293

Wei, Z., Chigurupati, S., Bagsiyao, P., Henriquez, A., & Chan, S. L. (2009). The brain uncoupling protein UCP4 attenuates mitochondrial toxin-induced cell death: role of extracellular signal-regulated kinases in bioenergetics adaptation and cell survival. *Neurotox Res, 16*(1), 14-29. doi:10.1007/s12640-009-9039-8

Weidling, I., & Swerdlow, R. H. (2019). Mitochondrial Dysfunction and Stress Responses in Alzheimer's Disease. *Biology (Basel), 8*(2). doi:10.3390/biology8020039

Wheless, J. W. (2008). History of the ketogenic diet. *Epilepsia, 49 Suppl 8*, 3-5. doi:10.1111/j.1528-1167.2008.01821.x

Wilder, R. M. (1921). The effect of ketonemia on the course of epilepsy. *Mayo Clinic Bulletin, 2*, 307.

Wilkins, H. M., Carl, S. M., Greenlief, A. C., Festoff, B. W., & Swerdlow, R. H. (2014). Bioenergetic dysfunction and inflammation in Alzheimer's disease: a possible connection. *Front Aging Neurosci, 6*, 311. doi:10.3389/fnagi.2014.00311

Wilkins, H. M., & Swerdlow, R. H. (2016a). Amyloid precursor protein processing and bioenergetics. *Brain Res Bull*. doi:10.1016/j.brainresbull.2016.08.009

Wilkins, H. M., & Swerdlow, R. H. (2016b). Relationships Between Mitochondria and Neuroinflammation: Implications for Alzheimer's Disease. *Curr Top Med Chem, 16*(8), 849-857.

Winkler, E. A., Nishida, Y., Sagare, A. P., Rege, S. V., Bell, R. D., Perlmutter, D., . . . Zlokovic, B. V. (2015). GLUT1 reductions exacerbate Alzheimer's disease vasculo-neuronal dysfunction and degeneration. *Nat Neurosci, 18*(4), 521-530. doi:10.1038/nn.3966

Wolfgang, M. J., Kurama, T., Dai, Y., Suwa, A., Asaumi, M., Matsumoto, S., . . . Lane, M. D. (2006). The brain-specific carnitine palmitoyltransferase-1c regulates energy homeostasis. *Proc Natl Acad Sci U S A, 103*(19), 7282-7287. doi:10.1073/pnas.0602205103

Won, Y. J., Lu, V. B., Puhl, H. L., 3rd, & Ikeda, S. R. (2013). beta-Hydroxybutyrate modulates N-type calcium channels in rat sympathetic neurons by acting as an agonist for the G-protein-coupled receptor FFA3. *J Neurosci, 33*(49), 19314-19325. doi:10.1523/jneurosci.3102-13.2013

Woodyatt, R. T. (1921). Objects and method of diet adjustment in diabetes. *Archives of Internal Medicine, 28*(2), 125-141. doi:10.1001/archinte.1921.00100140002001

Wu, H., Wang, C., & Wu, Z. (2014). PROPER: comprehensive power evaluation for differential expression using RNA-seq. *Bioinformatics, 31*(2), 233-241. doi:10.1093/bioinformatics/btu640

Xie, Z., Zhang, D., Chung, D., Tang, Z., Huang, H., Dai, L., . . . Zhao, Y. (2016). Metabolic Regulation of Gene Expression by Histone Lysine beta-Hydroxybutyrylation. *Mol Cell, 62*(2), 194-206. doi:10.1016/j.molcel.2016.03.036

Yang, X., & Cheng, B. (2010). Neuroprotective and anti-inflammatory activities of ketogenic diet on MPTP-induced neurotoxicity. *J Mol Neurosci, 42*(2), 145-153. doi:10.1007/s12031-010-9336-y

Yao, J., Chen, S., Mao, Z., Cadenas, E., & Brinton, R. D. (2011). 2-Deoxy-D-glucose treatment induces ketogenesis, sustains mitochondrial function, and reduces pathology in female mouse model of Alzheimer's disease. *PLoS One, 6*(7), e21788. doi:10.1371/journal.pone.0021788

Yao, J., Rettberg, J. R., Klosinski, L. P., Cadenas, E., & Brinton, R. D. (2011). Shift in brain metabolism in late onset Alzheimer's disease: implications for biomarkers and therapeutic interventions. *Mol Aspects Med, 32*(4-6), 247-257. doi:10.1016/j.mam.2011.10.005

Yin, J. X., Maalouf, M., Han, P., Zhao, M., Gao, M., Dharshaun, T., . . . Shi, J. (2016). Ketones block amyloid entry and improve cognition in an Alzheimer's model. *Neurobiol Aging, 39*, 25-37. doi:10.1016/j.neurobiolaging.2015.11.018

Zhang, P., Kishimoto, Y., Grammatikakis, I., Gottimukkala, K., Cutler, R. G., Zhang, S., . . . Mattson, M. P. (2019). Senolytic therapy alleviates Aβ-associated oligodendrocyte progenitor cell senescence and cognitive deficits in an Alzheimer's disease model. *Nature Neuroscience, 22*(5), 719-728. doi:10.1038/s41593-019-0372-9

Zhao, S., Fu, J., Liu, X., Wang, T., Zhang, J., & Zhao, Y. (2012). Activation of Akt/GSK-3beta/beta-catenin signaling pathway is involved in survival of neurons after traumatic brain injury in rats. *Neurol Res, 34*(4), 400-407. doi:10.1179/1743132812y.0000000025

Zhao, W., Varghese, M., Vempati, P., Dzhun, A., Cheng, A., Wang, J., . . . Pasinetti, G. M. (2012). Caprylic triglyceride as a novel therapeutic approach to effectively improve the performance and attenuate the symptoms due to the motor neuron loss in ALS disease. *PLoS One, 7*(11), e49191. doi:10.1371/journal.pone.0049191

Zhao, Z., Lange, D. J., Voustianiouk, A., MacGrogan, D., Ho, L., Suh, J., . . . Pasinetti, G. M. (2006). A ketogenic diet as a potential novel therapeutic intervention in amyotrophic lateral sclerosis. *BMC Neurosci, 7*, 29. doi:10.1186/1471-2202-7-29

Appendix: Plasmid Genetic Sequence

5’-

GTCGACATTGATTATTGACTAGTCAATTGCCCCGCGGCAGGCCCTCCGAGCGTGGTG

GAGCCGTTCTGTGAGACAGCCGGGTACGAGTCGTGACGCTGGAAGGGGCAAGCGGG

TGGTGGGCAGGAATGCGGTCCGCCCTGCAGCAACCGGAGGGGGAGGGAGAAGGGA

GCGGAAAAGTCTCCACCGGACGCGGCCATGGCTCGGGGGGGGGGGGGCAGCGGAG

GANCGCTTCCGGCCGACGTCTCGTCGCTGATTGGCTTNTTTTCCTCCCGCCGTGTGTG

AAAACACAAATGGCGTGTTTTGGTTGGCGTAAGGCGCCTGTCAGTTAACGGCAGCC

GGAGTGCGCAGCCGCCGGCAGCCTCGCTCTGCCCACTGGGTGGGGCGGGAGGTAGG

TGGGGTGAGGCGAGCTGNACGTGCGGGCGCGGTCGGCCTCTGGCGGGGCGGGGGAG

GGGAGGGAGGGTCAGCGAAAGTAGCTCGCGCGCGAGCGGCCGCCCACCCTCCCCTT

CCTCTGGGGGAGTCGTTTTACCCGCCGCCGGCCGGGCCTCGTCGTCTGATTGGCTCT

CGGGGCCCAGAAAACTGGCCCTTGCCATTGGCTCGTGTTCGTGCAAGTTGAGTCCAT

CCGCCGGCCAGCGGGGGCGGCGAGGAGGCGCTCCCAGGTTCCGGCCCTCCCCTCGG

CCCCGCGCCGCAGAGTCTGGCCGCGCGCCCCTGCGCAACGTGGCAGGAAGCGCGCG

CTGGGGGCGGGGACGGGCAGTAGGGCTGAGCGGCTGCGGGGCGGGTGCAAGCACG

TTTCCGACTTGAGTTGCCTCAAGAGGGGCGTGCTGAGCCAGACCTCCATCGCGCACT

CCGGGGAGTGGAGGGAAGGAGCGAGGGCTCAGTTGGGCTGTTTTGGAGGCAGGAA

GCACTTGCTCTCCCAAAGTCGCTCTGAGTTGTTATCAGTAAGGGAGCTGCAGTGGAG

TAGGCGGGGAGAAGGCCGCACCCTTCTCCGGAGGGGGGAGGGGAGTGTTGCAATAC

CTTTCTGGGAGTTCTCTGCTGCCTCCTGGCTTCTGAGGACCGCCCTGGGCCTGGGAG

AATCCCTTGCCCCCTCTTCCCCTCGTGATCTGCAACTCCAGTCTTTACTAGTTATTAA

TAGTAATCAATTACGGGGTCATTAGTTCATAGCCCATATATGGAGTTCCGCGTTACA

TAACTTACGGTAAATGGCCCGCCTGGCTGACCGCCCAACGACCCCCGCCCATTGACG

TCAATAATGACGTATGTTCCCATAGTAACGCCAATAGGGACTTTCCATTGACGTCAA

TGGGTGGACTATTTACGGTAAACTGCCCACTTGGCAGTACATCAAGTGTATCATATG

CCAAGTACGCCCCCTATTGACGTCAATGACGGTAAATGGCCCGCCTGGCATTATGCC

CAGTACATGACCTTATGGGACTTTCCTACTTGGCAGTACATCTACGTATTAGTCATCG

CTATTACCATGGGTCGAGGTGAGCCCCACGTTCTGCTTCACTCTCCCCATCTCCCCCC

CCTCCCCACCCCCAATTTTGTATTTATTTATTTTTTAATTATTTTGTGCAGCGATGGGG

GCGGGGGGGGGGGGGGCGCGCGCCAGGCGGGGCGGGGCGGGGCGAGGGGCGGGG

CGGGGCGAGGCGGAGAGGTGCGGCGGCAGCCAATCAGAGCGGCGCGCTCCGAAAG

TTTCCTTTTATGGCGAGGCGGCGGCGGCGGCGGCCCTATAAAAAGCGAAGCGCGCG

GCGGGCGGGAGTCGCTGCGTTGCCTTCGCCCCGTGCCCCGCTCCGCGCCGCCTCGCG

CCGCCCGCCCCGGCTCTGACTGACCGCGTTACTCCCACAGGTGAGCGGGCGGGACG

GCCCTTCTCCTCCGGGCTGTAATTAGCGCTTGGTTTAATGACGGCTCGTTTCTTTTCT

GTGGCTGCGTGAAAGCCTTAAAGGGCTCCGGGAGGGCCCTTTGTGCGGGGGGGAGC

GGCTCGGGGGGTGCGTGCGTGTGTGTGTGCGTGGGGAGCGCCGCGTGCGGCCCGCG

CTGCCCGGCGGCTGTGAGCGCTGCGGGCGCGGCGCGGGGCTTTGTGCGCTCCGCGT

GTGCGCGAGGGGAGCGCGGCCGGGGGCGGTGCCCCGCGGTGCGGGGGGGCTGCGA

GGGGAACAAAGGCTGCGTGCGGGGTGTGTGCGTGGGGGGGTGAGCAGGGGGTGTG

GGCGCGGCGGTCGGGCTGTAACCCCCCCCTGCACCCCCCTCCCCGAGTTGCTGAGCA

CGGCCCGGCTTCGGGTGCGGGGCTCCGTGCGGGGCGTGGCGCGGGGCTCGCCGTGC

CGGGCGGGGGGTGGCGGCAGGTGGGGGTGCCGGGCGGGGCGGGGCCGCCTCGGGC

CGGGGAGGGCTCGGGGGAGGGGCGCGGCGGCCCCGGAGCGCCGGCGGCTGTCGAG

GCGCGGCGAGCCGCAGCCATTGCCTTTTATGGTAATCGTGCGAGAGGGCGCAGGGA

CTTCCTTTGTCCCAAATCTGGCGGAGCCGAAATCTGGGAGGCGCCGCCGCACCCCCT

CTAGCGGGCGCGGGCGAAGCGGTGCGGCGCCGGCAGGAAGGAAATGGGCGGGGAG

GGCCTTCGTGCGTCGCCGCGCCGCCGTCCCCTTCTCCATCTCCAGCCTCGGGGCTGC

CGCAGGGGGACGGCTGCCTTCGGGGGGGACGGGGCAGGGCGGGGTTCGGCTTCTGG

CGTGTGACCGGCGGCTCTAGAGCCTCTGCTAACCATGTTCATGCCTTCTTCTTTTTCC

TACAGCTCCTGGGCAACGTGCTGGTTATTGTGCTGTCTCATCATTTTGGCAAAGAATT

CGTGTGGTGGAATTGCCCTTATAACTTCGTATAGTATACATTATACGAAGTTATCAA

TGGTGAGCAAGGGCGAGGAGGATAACATGGCCATCATCAAGGAGTTCATGCGCTTC

AAGGTGCACATGGAGGGCTCCGTGAACGGCCACGAGTTCGAGATCGAGGGCGAGGG

CGAGGGCCGCCCCTACGAGGGCACCCAGACCGCCAAGCTGAAGGTGACCAAGGGTG

GCCCCCTGCCCTTCGCCTGGGACATCCTGTCCCCTCAGTTCATGTACGGCTCCAAGG

CCTACGTGAAGCACCCCGCCGACATCCCCGACTACTTGAAGCTGTCCTTCCCCGAGG

GCTTCAAGTGGGAGCGCGTGATGAACTTCGAGGACGGCGGCGTGGTGACCGTGACC

CAGGACTCCTCCCTGCAGGACGGCGAGTTCATCTACAAGGTGAAGCTGCGCGGCAC

CAACTTCCCCTCCGACGGCCCCGTAATGCAGAAGAAGACCATGGGCTGGGAGGCCT

CCTCCGAGCGGATGTACCCCGAGGACGGCGCCCTGAAGGGCGAGATCAAGCAGAGG

CTGAAGCTGAAGGACGGCGGCCACTACGACGCTGAGGTCAAGACCACCTACAAGGN

CAAGAAGCCCGTGCAGCTGCCCGGCGCCTACAACGTCAACATCAAGTTGGACATCA

CCTCCCACAACGAGGACTACACCATCGTGGAACAGTACGAACGCGCCGAGGGCCGC

CACTCCACCGGCGGCATGGACGAGCTGTACAAGTAAATAACTTCGTATAGTATACAT

TATACGAAGTTATAAGGGCAATTCTGCAGATGCTAGCGCCGCCACCATGGCAGAGG

CTCACCAAGCTGTGGCCTTCCAGTTCACAGTCACCCCTGATGGCATCGATCTCCGCC

TGAGCCATGAAGCCCTCAAACAGATCTGCCTGTCAGGGCTGCACTCCTGGAAGAAG

AAGTTCATCCGATTCAAGAATGGCATCATCACTGGTGTGTTCCCCGCGAGTCCCTCC

AGCTGGCTTATCGTGGTGGTGGGTGTGATATCATCCATGCATACCAAAGTGGACCCC

TCCCTGGGCATGATTGCAAAGATCAATCGGACCCTAGACACCACTGGCCGCATGTCA

AGCCAGACGAAGAACATCGTGAGTGGCGTCCTCTTTGGCACAGGGCTCTGGGTGGC

GATCATCATGACTATGCGCTACTCGCTGAAGGTGCTGCTCTCCTACCATGGCTGGAT

GTTTGCAGAGCACGGCAAAATGAGCCGCAGCACCAGAATCTGGATGGCTATGGTCA

AGGTCTTCTCGGGTCGAAAGCCCATGTTGTACAGCTTCCAGACGTCTCTGCCGCGCC

TGCCTGTCCCAGCTGTCAAAGATACCGTGAGCAGGTACCTGGAGTCTGTGAGGCCAC

TGATGAAGGAGGGAGACTTCCAACGCATGACAGCACTGGCCCAGGATTTTGCTGTC

AACCTTGGACCCAAATTGCAGTGGTATTTGAAGCTAAAATCCTGGTGGGCCACAAAT

TATGTGAGTGACTGGTGGGAGGAATACATCTACCTGCGGGGCCGAGGGCCGATCAT

GGTTAACAGCAACTACTACGCCATGGAGATGCTCTACATCACCCCAACCCATATTCA

GGCAGCGAGAGCTGGCAACACCATCCACGCCATACTGCTGTATCGTCGCACGGTAG

ACCGTGAGGAACTCAAACCTATTCGTCTTCTGGGATCTACAATTCCCCTCTGCTCTGC

TCAGTGGGAGCGACTCTTCAATACTTCCCGCATCCCTGGGGAGGAGACAGACACCA

TCCAACACGTCAAGGACAGCAGGCACATTGTCGTGTACCACAGAGGCCGTTACTTC

AAGGTCTGGCTCTACCATGACGGGAGGCTGCTGAGGCCCCGTGAGCTGGAGCAGCA

GATGCAGCAGATCCTGGATGACACCTCAGAGCCGCAGCCCGGGGAAGCCAAGCTTG

CCGCCCTCACTGCCGCAGACAGAGTGCCCTGGGCGAAGTGTCGGCAGACCTATTTTG

CACGAGGAAAAAATAAGCAATCTCTGGATGCGGTAGAAAAGGCAGCATTCTTCGTG

ACGTTGGACGAATCGGAACAGGGATATAGAGAGGAGGACCCTGAGGCATCTATTGA

CAGCTATGCCAAATCTCTGCTGCATGGTAGATGTTTCGACAGGTGGTTTGACAAGTC

CATCACCTTTGTTGTCTTCAAAAACAGCAAGATAGGCATAAACGCAGAGCATTCCTG

GGCGGACGCGCCCATCGTGGGCCATCTGTGGGAGTATGTCATGGCCACCGACGTCTT

CCAGCTGGGCTACTCAGAGGATGGACACTGTAAAGGAGACAAGAACCCCAACATCC

CCAAACCCACCAGGCTACAGTGGGACATTCCAGGAGAATGCCAGGAGGTCATAGAG

ACATCCCTAAGCAGTGCCAGTTTTTTGGCAAATGATGTGGACCTGCATTCCTTCCCAT

TTGACACCTTTGGCAAAGGCTTGATCAAGAAGTGCCGGACGAGTCCCGATGCCTTCA

TCCAGCTGGCACTGCAGCTCGCACATTACAAGGACATGGGCAAGTTCTGCCTCACGT

ATGAGGCTTCCTCGACTCGGCTCTTCCGAGAGGGGAGGACAGAGACTGTACGCTCCT

GCACTACGGAGTCCTGCAACTTTGTGCTGGCCATGATGGACCCCACAACAACGGCA

GAGCAGAGGTTCAAGCTGTTCAAGATAGCTTGTGAAAAGCACCAGCACCTGTACCG

CCTCGCCATGACGGGCGCTGGCATCGACCGCCACCTCTTCTGCCTCTATGTGGTGTC

CAAGTATCTGGCAGTCGACTCACCTTTCCTGAAGGAGGTACTGTCTGAGCCATGGAG

GTTGTCCACGAGCCAGACTCCTCAGCAGCAGGTGGAACTGTTTGACTTTGAGAAATA

CCCTGACTATGTGTCCTGTGGCGGGGGCTTTGGGCCGGTTGCTGATGACGGCTATGG

TGTTTCCTACATTATTGTGGGAGAGAATTTCATCCACTTCCATATTTCTTCCAAGTTC

TCTAGCCCTGAGACAGACTCACACCGCTTTGGGAAGCACTTGAGACAAGCCATGAT

GGACATTATCACCTTGTTTGGCCTCACCGCCAATTCCAAAAAGACGCGTGGATCCGG

AGTTAACGTGAGCAAGGGCGAGGAGCTGTTCACCGGGGTGGTGCCCATCCTGGTCG

AGCTGGACGGCGACGTAAACGGCCACAAGTTCAGCGTGTCCGGCGAGGGCGAGGGC

GATGCCACCTACGGCAAGCTGACCCTGAAGTTCATCTGCACCACCGGCAAGCTGCCC

GTGCCCTGGCCCACCCTCGTGACCACCCTGACCTGGGGCGTGCAGTGCTTCGCCCGC

TACCCCGACCACATGAAGCAGCACGACTTCTTCAAGTCCGCCATGCCCGAAGGCTAC

GTCCAGGAGCGCACCATCTTCTTCAAGGACGACGGCAACTACAAGACCCGCGCCGA

GGTGAAGTTCGAGGGCGACACCCTGGTGAACCGCATCGAGCTGAAGGGCATCGACT

TCAAGGAGGACGGCAACATCCTGGGGCACAAGCTGGAGTACAACGCCATCAGCGAC

AACGTCTATATCACCGCCGACAAGCAGAAGAACGGCATCAAGGCCAACTTCAAGAT

CCGCCACAACATCGAGGACGGCAGCGTGCAGCTCGCCGACCACTACCAGCAGAACA

CCCCCATCGGCGACGGCCCCGTGCTGCTGCCCGACAACCACTACCTGAGCACCCAGT

CCAAGCTGAGCAAAGACCCCAACGAGAAGCGCGATCACATGGTCCTGCTGGAGTTC

GTGACCGCCGCCGGGATCACTCTCGGCATGGACGAGCTGTACAAGTAAGCTAGCAA

GGGCAATTCTGCAGATATCCAGCACAGTGGCGGCCGCACTCCTCAGGTGCAGGCTG

CCTATCAGAAGGTGGTGGCTGGTGTGGCCAATGCCCTGGCTCACAAATACCACTGAG

ATCTTTTTCCCTCTGCCAAAAATTATGGGGACATCATGAAGCCCCTTGAGCATCTGA

CTTCTGGCTAATAAAGGAAATTTATTTTCATTGCAATAGTGTGTTGGAATTTTTTGTG

TCTCTCACTCGGAAGGACATATGGGAGGGCAAATCATTTAAAACATCAGAATGAGT

ATTTGGTTTAGAGTTTGGCAACATATGCCATATGCTGGCTGCCATGAACAAAGGTGG

CTATAAAGAGGTCATCAGTATATGAAACAGCCCCCTGCTGTCCATTCCTTATTCCAT

AGAAAAGCCTTGACTTGAGGTTAGATTTTTTTTATATTTTGTTTTGTGTTATTTTTTTC

TTTAACATCCCTAAAATTTTCCTTACATGTTTTACTAGCCAGATTTTTCCTCCTCTCCT

GACTACTCCCAGTCATAGCTGTCCCTCTTCTCTTATGAAGATCCCTCGACCTGCAGCC

CAAGCTTAGATGGGCGGGAGTCTTCTGGGCAGGCTTAAAGGCTAACCTGGTGTGTG

GGCGTTGTCCTGCAGGGGAATTGAACAGGTGTAAAATTGGAGGGACAAGACTTCCC

ACAGATTTTCGGTTTTGTCGGGAAGTTTTTTAATAGGGGCAAATAGGAAAATGGAGG

ATAGGAGTCATCTGGGGTTTATGCAGCAAAACTACAGGTATATTGCTTGTATCCGCC

TCGGAGATTTCCATGAGGAGATAAAGACATGTCACCCGAGTTTATACTCTCCTGCTT

AGATCCTACTACAGTATGAAATACAGTGTNGCGAGGTAGACTATGTAAGCAGATTT

AATCATTTTAAAGAGCCCAGTACTTCATATCCATTTCTCCCGCTCCTTCTGCAGCCTT

ATCAAAAGGTATTTAGAACACTCATTTTAGCCCCATTTTCATTTATTATACTGGCTTA

TCCAACCCCTAGACAGAGCATTGGCATTTTCCCTTTCCTGATCTTAGAAGTCTGATGA

CTCATGAAACCAGACAGATTAGTTACATACACCACAAATCGAGGCTGTAGCTGGGG

CCTCAACACTGCAGTTCTTTTATAACTCCTTAGTACACTTTTTGTTGATCCTTTGCCTT

GATCCTTAATTTTCAGTGTCTATCACCTCTCCCGTCAGGTGGTGTTCCACATTTGGGC

CTATTCTCAGTCCAGGGAGTTTTACAACAATAGATGTATTGAGAATCCAACCTAAAG

CTTAACTTTCCACTCCCATGAATGCCTCTCTCCTTTTTCTCCATTATAACTGAGCTATN

ACCATTAATGGTTTCAGGTGGATGTCTCCTCCCCCAATATACCTGATGTATCTACATA

TTGCCAGGCTGATATTTTAAGACATNAAAGGTATATTTCATTATTGAGCCACATGGT

ATTGATTACTGCTACTAAAATTTTGTCATTGTACACATCTGTAAAAGGTGGTTCCTTT

TGGAATGCAAAGTTCAGGTGTTTGTTGTCTTTCAATTGAAGCTTGGCGTAATCATGG

TCATAGCTGTTTCCTGTGTGAAATTGTTATCCGCTCACAATTCCACACAACATACGA

GCCGGAAGCATAAAGTGTAAAGCCTGGGGTGCCTAATGAGTGAGCTAACTCACATT

AATTGCGTTGCGCTCACTGCCCGCTTTCCAGTCGGGAAACCTGTCGTGCCAGCGGAT

CCGCATCTCAATTAGTCAGCAACCATAGTCCCGCCCCTAACTCCGCCCATCCCGCCC

CTAACTCCGCCCAGTTCCGCCCATTCTCCGCCCCATGGCTGACTAATTTTTTTTATTT

ATGCAGAGGCCGAGGCCGCCTCGGCCTCTGAGCTATTCCAGAAGTAGTGAGGAGGC

TTTTTTGGAGGCCTAGGCTTTTGCAAAAAGCTAACTTGTTTATTGCAGCTTATAATGG

TTACAAATAAAGCAATAGCATCACAAATTTCACAAATAAAGCATTTTTTTCACTGCA

TTCTAGTTGTGGTTTGTCCAAACTCATCAATGTATCTTATCATGTCTGGATCCGCTGC

ATTAATGAATCGGCCAACGCGCGGGGAGAGGCGGTTTGCGTATTGGGCGCTCTTCCG

CTTCCTCGCTCACTGACTCGCTGCGCTCGGTCGTTCGGCTGCGGCGAGCGGTATCAG

CTCACTCAAAGGCGGTAATACGGTTATCCACAGAATCAGGGGATAACGCAGGAAAG

AACATGTGAGCAAAAGGCCAGCAAAAGGCCAGGAACCGTAAAAAGGCCGCGTTGC

TGGCGTTTTTCCATAGGCTCCGCCCCCCTGACGAGCATCACAAAAATCGACGCTCAA

GTCAGAGGTGGCGAAACCCGACAGGACTATAAAGATACCAGGCGTTTCCCCCTGGA

AGCTCCCTCGTGCGCTCTCCTGTTCCGACCCTGCCGCTTACCGGATACCTGTCCGCCT

TTCTCCCTTCGGGAAGCGTGGCGCTTTCTCAATGCTCACGCTGTAGGTATCTCAGTTC

GGTGTAGGTCGTTCGCTCCAAGCTGGGCTGTGTGCACGAACCCCCCGTTCAGCCCGA

CCGCTGCGCCTTATCCGGTAACTATCGTCTTGAGTCCAACCCGGTAAGACACGACTT

ATCGCCACTGGCAGCAGCCACTGGTAACAGGATTAGCAGAGCGAGGTATGTAGGCG

GTGCTACAGAGTTCTTGAAGTGGTGGCCTAACTACGGCTACACTAGAAGGACAGTAT

TTGGTATCTGCGCTCTGCTGAAGCCAGTTACCTTCGGAAAAAGAGTTGGTAGCTCTT

GATCCGGCAAACAAACCACCGCTGGTAGCGGTGGTTTTTTTGTTTGCAAGCAGCAGA

TTACGCGCAGAAAAAAAGGATCTCAAGAAGATCCTTTGATCTTTTCTACGGGGTCTG

ACGCTCAGTGGAACGAAAACTCACGTTAAGGGATTTTGGTCATGAGATTATCAAAA

AGGATCTTCACCTAGATCCTTTTAAATTAAAAATGAAGTTTTAAATCAATCTAAAGT

ATATATGAGTAAACTTGGTCTGACAGTTACCAATGCTTAATCAGTGAGGCACCTATC

TCAGCGATCTGTCTATTTCGTTCATCCATAGTTGCCTGACTCCCCGTCGTGTAGATAA

CTACGATACGGGAGGGCTTACCATCTGGCCCCAGTGCTGCAATGATACCGCGAGAC

CCACGCTCACCGGCTCCAGATTTATCAGCAATAAACCAGCCAGCCGGAAGGGCCGA

GCGCAGAAGTGGTCCTGCAACTTTATCCGCCTCCATCCAGTCTATTAATTGTTGCCG

GGAAGCTAGAGTAAGTAGTTCGCCAGTTAATAGTTTGCGCAACGTTGTTGCCATTGC

TACAGGCATCGTGGTGTCACGCTCGTCGTTTGGTATGGCTTCATTCAGCTCCGGTTCC

CAACGATCAAGGCGAGTTACATGATCCCCCATGTTGTGCAAAAAAGCGGTTAGCTCC

TTCGGTCCTCCGATCGTTGTCAGAAGTAAGTTGGCCGCAGTGTTATCACTCATGGTT

ATGGCAGCACTGCATAATTCTCTTACTGTCATGCCATCCGTAAGATGCTTTTCTGTGA

CTGGTGAGTACTCAACCAAGTCATTCTGAGAATAGTGTATGCGGCGACCGAGTTGCT

CTTGCCCGGCGTCAATACGGGATAATACCGCGCCACATAGCAGAACTTTAAAAGTG

CTCATCATTGGAAAACGTTCTTCGGGGCGAAAACTCTCAAGGATCTTACCGCTGTTG

AGATCCAGTTCGATGTAACCCACTCGTGCACCCAACTGATCTTCAGCATCTTTTACTT

TCACCAGCGTTTCTGGGTGAGCAAAAACAGGAAGGCAAAATGCCGCAAAAAAGGG

AATAAGGGCGACACGGAAATGTTGAATACTCATACTCTTCCTTTTTCAATATTATTG

AAGCATTTATCAGGGTTATTGTCTCATGAGCGGATACATATTTGAATGTATTTAGAA

AAATAAACAAATAGGGGTTCCGCGCACATTTCCCCGAAAAGTGCCACCTG-3’